Regulation of Tumor-specific Immunity in

Human Clear Cell Renal Cell Carcinoma

Dissertation

zur
Erlangung der naturwissenschaftlichen Doktorwürde
(Dr. sc. nat.)

vorgelegt der
Mathematisch-naturwissenschaftlichen Fakultät
der
Universität Zürich
von

Stefanie R. Dannenmann

aus
Deutschland

Promotionskomitee

Prof. Dr. med. Christoph Renner (Vorsitz)
Prof. Dr. Maries van den Broek (Leitung der Dissertation)
Prof. Dr. Roland Wenger
Prof. Dr. med. Alexander Knuth
Prof. Dr. med. Alfred Zippelius

Zürich, 2013

TABLE OF CONTENTS

ZUSAMMENFASSUNG

Das Nierenzellkarzinom umfasst eine heterogene Gruppe von Tumoren, die zusammen ca. 90% aller Tumore der humanen Niere ausmachen. Die häufigste histologische Untergruppe stellt dabei das klarzellige Nierenzellkarzinom (ccRCC) dar. Zunehmend mehr Beweise zeigen, dass das Immunsystem ccRCC erkennt und auch kontrollieren kann. Aus diesem Grund werden immer mehr immuntherapeutische Strategien zur Behandlung dieser Patienten getestet. Immuntherapie mit immunstimulierenden Zytokinen, wie IL-2 und IFN-α, zeigen eine moderate therapeutische Wirkung in einigen Patienten, jedoch stellt die damit zusammenhängende schwerwiegende systemische Toxizität ein Problem dar.

Zellen des adaptiven Immunsystems erkennen so genannte Tumor-assoziierte Antigene (TAAs). Hierbei handelt es sich um Proteine, die mehr oder weniger selektiv (über)-exprimiert in transformierten Zellen vorliegen. Das Verstärken der spontanen TAA-spezifischen Immunität in Krebspatienten ist eine Strategie mit geringer Toxizität, mit der in manchen Patienten schon eine klinische Wirkung erreicht werden konnte. Aus diesem Grund haben wir die Expression von TAAs in Tumorgewebe von ccRCC Patienten analysiert und untersucht, ob eine spontane TAA-spezifische T Zellantwort in diesen Patienten detektierbar ist. Wir konnten feststellen, dass Cyclin D1 (CCND1) häufig in ccRCCs überexprimiert vorliegt und dass in den meisten Patienten auch eine CCND1-spezifische $CD8^+$ T Zellantwort existiert. Somit konnten wir zeigen, dass CCND1 ein potentielles therapeutisches Target für ccRCC darstellt.

Die Etablierung eines immunoregulatorischen Milieus in Tumoren, welches eine anti-Tumor Immunantwort supprimiert, ist sehr wahrscheinlich ein Grund, warum spontane und Therapie-induzierte Immunität oftmals nicht erfolgreich ist in der Eliminierung von Tumoren. Um Parameter zu identifizieren, die in der Immunregulierung des ccRCCs eine Rolle spielen, haben wir eine retrospektive Analyse für verschiedene Immunantwort-relevante Gene in Formalin-fixiertem, Paraffin-eingebettetem Tumormaterial von primären ccRCCs durchgeführt. Starke Expression von CD68 (Makrophagen) und FoxP3 (regulatorische T Zellen) korrelierten signifikant mit verkürztem Überleben. Wir konnten feststellen, dass Tumor-assoziierte Makrophagen (TAMs) in ccRCC Tumoren einen Phänotyp aufweisen, der charakteristisch ist für M2 (alternativ aktivierte) Makrophagen, welcher zum Teil durch die Tumorzellen induziert wird. Darauf folgende Experimente auf frischem Patientenmaterial zeigten, dass Tumor-infiltrierende T Zellen co-inhibitorische Moleküle und Zytokine stärker exprimieren als entsprechende T Zellen aus dem Blut. Zudem konnten wir beobachten, dass diese Veränderungen in Phänotyp und Funktion in autologen $CD4^+$ T Zellen aus dem Blut vom Tumor-assoziierten Milieu und von FACS-isolierten TAMs ausgelöst werden. Unsere Ergebnisse deuten darauf hin, dass ccRCCs zunehmend Makrophagen anziehen und eine Veränderung der Makrophagen in Richtung M2 TAMs bewirken. Diese M2 TAMs verändern Funktion und Phänotyp von Tumor-infiltrierenden T Zellen in der Hinsicht, dass regulatorische Funktionen auf Kosten von Effektorfunktionen zunehmen.

SUMMARY

Renal cell carcinoma is a heterogeneous group of tumors that encompass about 90% of all tumors of the human kidney, with clear cell renal cell carcinoma (ccRCC) as the major histological subgroup. There is growing evidence that the immune system recognizes and can control ccRCC and different immunotherapeutic strategies are being investigated as treatment for these patients. Immunotherapy using immunostimulatory cytokines such as IL-2 and IFN-α resulted in modest therapeutic efficacy in some patients, however, concomitant severe systemic toxicity is a problem.

Cells of the adaptive immune system recognize so-called tumor-associated antigens (TAAs), which are proteins that are more or less selectively (over)-expressed by transformed cells. Boosting spontaneous TAA-specific immunity in cancer patients is a strategy with low toxicity, which was shown to result in objective clinical responses in some patients. We therefore analyzed the expression of TAAs in tumor tissues of ccRCC patients and investigated whether spontaneous TAA-specific T cell responses were detectable in these patients. We found a frequent overexpression of Cyclin D1 (CCND1) in ccRCC tumor samples and in most of these patients also a CCND1-specific $CD8^+$ T cell response. Thus, we identified CCND1 as a potential therapeutic target.

The establishment of an immunoregulatory tumor microenvironment that suppresses anti-tumor immune responses may be a reason why spontaneous and therapy-induced immunity often is not successful in eradicating the tumor. To identify parameters involved in immunoregulation in ccRCC we performed a retrospective analysis on formalin-fixed paraffin-embedded tumor material of primary ccRCC for different immune response-related genes. High transcript levels of CD68 (macrophages) and FoxP3 (regulatory T cells) correlated significantly with reduced survival. We observed that tumor-associated macrophages (TAMs) in ccRCC tumors have a phenotype, which is characteristic for M2 (alternative activated) macrophages and which in part is induced by tumor cells. Prospective experiments on fresh patient material revealed that tumor-infiltrating T cells expressed higher levels of co-inhibitory molecules and cytokines than paired blood T cells. Furthermore, the tumor-associated milieu as well as FACS sorted TAMs induced deviation towards a more regulated phenotype and function of autologous, blood-derived $CD4^+$ T cells. Our results suggest that ccRCC progressively attracts macrophages and induces their skewing into M2 TAMs. These in turn subvert the function and phenotype of tumor-infiltrating T cells such that regulating functions are increased at the expense of effector functions.

1. INTRODUCTION

Immune response-related molecules that are relevant to the experiments presented in this thesis are highlighted in bold throughout the introduction, when mentioned and explained first time.

1.1 Immunosurveillance of cancer

A German surgeon, Wilhelm Busch of Bonn, described in 1866 the spontaneous remission of cancer after an attack of erysipelas, which is now known as a severe skin infection by *Streptococcus pyogenes*, a Gram-negative bacterium. Inspired by this observation, doctors tried to induce erysipelas in cancer patients of whom some were cured. Without being aware of these discoveries in Europe, William Coley, who worked as a surgeon in New York, noticed a similar correlation between the development of erysipelas and spontaneous cure of cancer in patients with sarcomas. In 1891, he deliberately infected the first patients with *S. pyogenes*, which resulted in complete and long-lasting remission of cancer. From 1893 onwards, William Coley used heat-killed *S. pyogenes*, which he later mixed with *Serratiamarcescens*, a Gram-negative bacterium, based on publications from a French scientist (G.H. Roger). This mix is known as Coley's Toxin or Coley's Fluid (1, 2). The mode of action of Coley's Toxin was not understood in the 19th century, but we now think that administration of agents that mimic an infection acted as a strong adjuvant and enabled proper induction of tumor-specific immunity in a proportion of cancer patients. In 1909, Paul Ehrlich was the first to suggest that cancers would arise more frequently in long-lived organisms if the immune system would not protect us from tumor outgrowth (3). Almost 50 years later, Frank Macfarlane Burnet and Lewis Thomas revised the hypothesis of immune protection against cancer based upon the enhanced understanding of immunity and the demonstration of the existence of tumor cell-specific neo-antigens (4, 5). They introduced the concept of cancer immunosurveillance, a hypothesis proposing that the immune system identifies and eliminates abnormal self-cells, including cells that are infected, transformed or carry genetic alterations. The cancer immunosurveillance hypothesis was seriously challenged by the fact that cancers develop in immunocompetent individuals and that immunodeficient, athymic nude mice were not more susceptible to chemically induced cancers (6, 7). The functional demonstration of tumor-associated antigens (TAAs) in mice further supported the cancer immunosurveillance theory (8) and finally in the 1990s improved mouse models of immunodeficiency clearly demonstrated a role of the adaptive and the innate immune system in tumor control (9, 10). The increased incidence of tumors found in immunosuppressed patients (11, 12), the detection of spontaneous immune responses in cancer patients (13, 14), and the favorable impact of tumor-infiltrating lymphocytes (TILs) on prognosis in some cancer types (15, 16) additionally supported the concept of cancer immunosurveillance.

1.2 Induction of an effective anti-tumor immune response

Based on our current knowledge three steps must take place for the induction of protective anti-tumor immunity, as illustrated in **Figure I-1**.

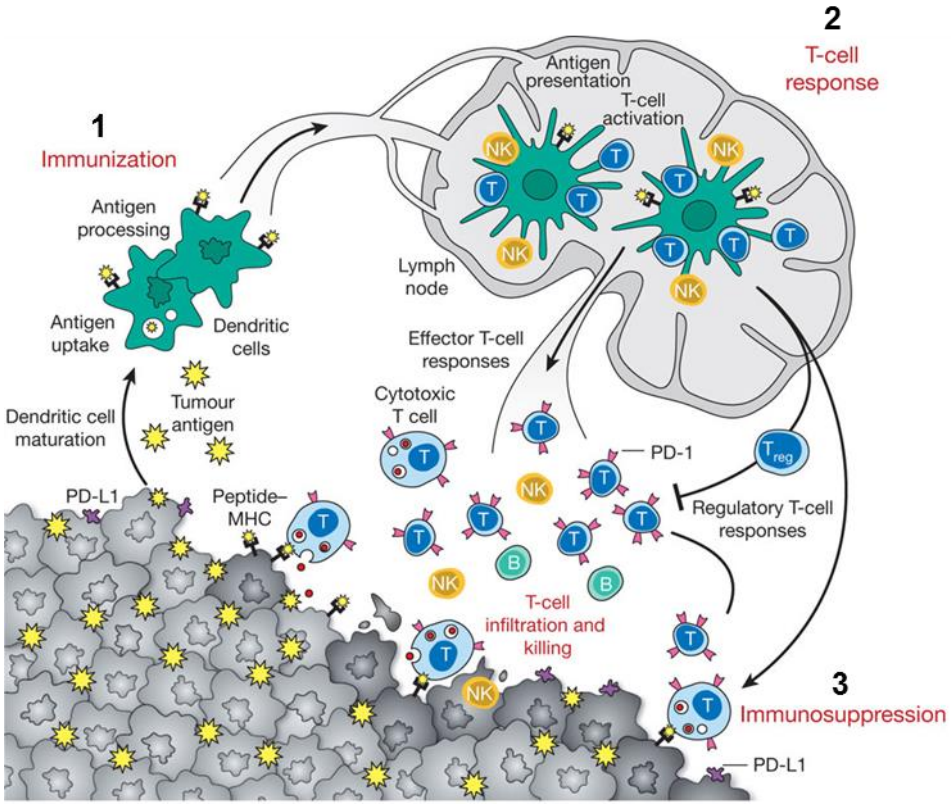

Figure I-1: Three steps are needed to enable an effective immune response

1) TAA-uptake and -processing of activated DCs, 2) production of protective T cell responses 3) overcoming local immunosuppression (figure from (17)).

1) To initiate a protective immune response, steady state or resting dendritic cells (DCs) must take up TAAs from dying tumor cells or a therapeutic vaccine. TAAs include cancer-testis (CT) antigens (e.g. MAGE, GAGE, and BAGE), overexpressed self-antigens (p53, HER2/neu), differentiation antigens (e.g. MART-1/Melan A, gp100, tyrosinase), point mutations of normal genes (altered self) (e.g. BCR-ABL, k-ras), and viral antigens (e.g. EBV, HPV) (18, 19). Subsequently, DCs process TAAs and present or cross-present TAA-derived peptides in the context of MHC class II or MHC class I molecules, respectively (20, 21). DCs then have to travel to the T cell zone of the tumor-draining lymph nodes, where they can activate naïve, tumor-specific T cells. For CCR7:CCL19/21-dependent migration into the T cell zone as well as for productive T cell activation, DCs must acquire an activated or mature phenotype, which includes the upregulation of co-stimulatory molecules such as CD40, CD70, CD80 and CD86, of certain cytokines such as IL-12 and of CCR7 (22). DC maturation usually occurs in the context of infections or inflammation, which can be mimicked by so-called adjuvants (23).

2) In the draining lymph node, mature DCs present the TAAs on **MHC-class I** and **-class II** molecules to **CD8$^+$** and **CD4$^+$** T cells, respectively. While **CD45**, known as the common leukocyte antigen, is expressed by all leukocytes and functions as a tyrosine phosphatase in leukocyte signaling, **CD3** is part of the T cell receptor (TCR)-complex and therefore specifically expressed by T cells. The CD3 molecule is crucial for signal transduction upon TCR ligation in $\alpha\beta$ T cells as well as in $\gamma\delta$ T cells. T cells with a TAA-specific TCR will be activated through interaction of the TCR with the peptide-bound MHC molecule presented by mature DCs. To mount an effective anti-tumor immune response, an additional stimulatory signal is needed provided by the interaction of T cell co-stimulatory molecules like CD28 with their surface receptors CD80/86 on DCs (24). It is crucial for the induction of protective adaptive immunity that antigens are presented to naïve T cells by mature DCs, whereas antigen presentation by steady state DCs results in robust peripheral T cell tolerance (anergy or deletion) (25, 26) or the generation of regulatory T cells (Tregs) (27, 28). It is questionable whether sufficient DC maturation occurs in the context of developing tumors and it therefore can't be excluded that the presentation of TAA results in insufficient T cell activation or even in tolerance. Another hurdle for the induction of protective adaptive immunity against cancer is the fact that most TAAs are self-molecules that induce central tolerance by negative selection of T cells in the thymus. It was shown that even tissue-specific antigens including melanocyte-specific antigens (Melan-A, tyrosinase, gp100) (29) and CT antigens (30) are expressed in the thymus of healthy individuals and thus presumably purge the T cell repertoire of high affinity T cells.

3) Activated TAA-specific T cells, will leave the lymph node and travel to the site of the tumor to execute an array of effector functions that aims to destroy cancer cells. Activated CD8$^+$ T cells differentiate into cytotoxic T lymphocytes (CTLs) and lyse tumor cells with the help of CD4$^+$ T cells and DCs (31). Memory CD4$^+$ and CD8$^+$ T cells and also components of the innate immune system such as heat-shock proteins (HSPs) and IFN-α are important to maintain protective immunity (32). In the tumor microenvironment many different immunosuppressive mechanisms can be operative, which prevent immune activation, trigger the "wrong" immune response or enable accumulation and expansion of regulatory immune cell types like Tregs and tumor-associated macrophages (TAMs) (see 1.3-1.5). These immunoregulatory mechanisms have to be overcome to mount an effective immune response.

1.3 The dual role of the immune system - Immunoediting

Immunosurveillance describes "the immunological protection of the host against the development of cancer, resulting from immune effector functions stimulated by immune recognition of either stress ligands or antigens expressed on transformed cells" (10). However, it is now well

established that immunosurveillance represents only one phase of a complex multistage interaction process between immune cells and tumor cells (33-35). The demonstration that tumors from immunocompetent hosts are less immunogenic than those from immunodeficient hosts suggested that tumors were sculpted by the immune response resulting in less immunogenic tumors (36). As a consequence, the immune system promotes the generation and outgrowth of tumor variants that escaped immune recognition and elimination. These results put forward the cancer immunoediting hypothesis, which considers that tumor-specific immunity plays a dual role - mediation of tumor destruction and promotion of tumor growth - during tumor development. As illustrated in **Figure I-2** immunoediting consists of three phases: elimination, equilibrium and escape. Those three phases are thought to proceed sequentially, but in some cases cells may directly enter either into equilibrium or escape phase (33).

Elimination

The elimination phase represents the host-protective cancer-immunosurveillance phase (described in 1.1) during which immune cells of the innate and adaptive immune system recognize and destroy tumor cells before cancer becomes clinically apparent. Mouse models of immunodeficiency provided first insights into the cell types and molecules of the immune system involved in this phase (9, 10).

Rag2-/- mice (deficient of $\alpha\beta$ and $\gamma\delta$ T cells, B cells and NKT cells) subcutaneously injected with the chemical carcinogen 3'-methylcholanthrene (MCA) developed sarcomas faster and with a higher incidence than wild type mice (36). In the same study the importance of lymphocytes in protection of tumor growth was also shown in a model of spontaneous tumor formation. Mice lacking either $\alpha\beta$ T cells or $\gamma\delta$ T cells were more susceptible to MCA-induced sarcomas than wild type mice revealing that both T cell subsets contribute to anti-tumor defense mechanisms (37).

Additionally, an increased incidence of MCA-induced sarcomas was observed in mice specifically deficient in NKT (38) or NK cells (39), indicative for a role of these cells in anti-tumor immunity. The reactions of NK and NKT cells are controlled by inhibitory and activating receptors (32). One stimulatory receptor that is of interest in regard to tumor immunology is the lectin-like **NKG2D** homo-dimer, which is expressed on NK cells, $\gamma\delta$ Tcells and CD8 $\alpha\beta$ T cells. The ligands for NKG2D are the MHC class I chain-related proteins A and B (**MICA** and **MICB**) (human) or Rae-1 (mouse) as well as the UL16 binding proteins (ULBPs) (40, 41). In steady state situations, NKG2D ligands are only expressed on the gastrointestinal epithelium of the stomach and large intestine, however, they are expressed by stressed epithelia (42) and many epithelium-derived tumors including kidney cancer (43-45).

Furthermore, effector cytokines and enzymes are required for tumor control, which was convincingly shown by increased susceptibility to carcinogen-induced tumors of mice deficient for **IFN-γ** (46), **perforin** (47, 48) and **IL-12** (49). In this line, there is evidence that also **granzyme B** (50) and **IL-2** (51) are needed for effective tumor elimination.

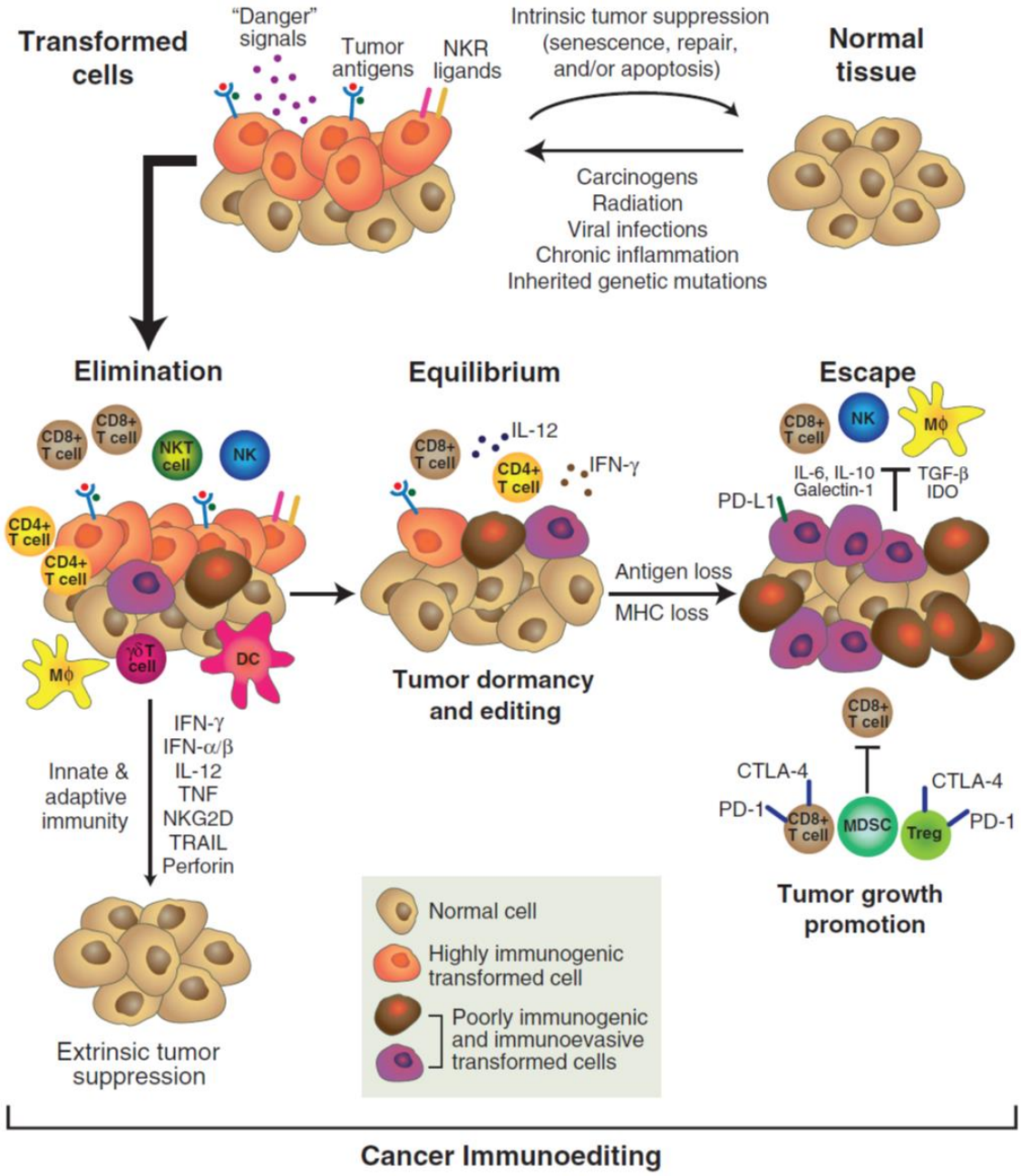

Figure I-2: The three phases of immunoediting

Immunoediting consists of the elimination, equilibrium and escape phase (figure from (33)).

Equilibrium

According to the immunoediting concept, the equilibrium phase may follow when the immune system fails to eliminate all cancer cells. During this phase, the adaptive immune system keeps the remaining tumor cells in check. Experimental proof was provided by a mouse model in which tumors were induced by low-dose MCA (52): Occult tumors rapidly grew out when cells of the adaptive immune system were depleted or when cytokines that promote adaptive immunity were blocked. A correlation of low levels of tumor cells in the bone marrow and protective immune memory was observed in a tumor mouse model (53), and similarly also in breast cancer patients

(54), which provided evidence for control of dormant tumors by $CD8^+$ T cells (55). Further clinical observations that can be explained by equilibrium are, for example a long period between successful treatment of the primary tumor and relapse (56), patients who remain free of disease despite micrometastasis (57) and development of donor-derived tumors in organ transplant recipients (58, 59).

Escape

When the balance between tumor growth and immunologic control tips in favor of the tumor, edited tumor cells that survived the equilibrium phase escape control and become clinically apparent. This implies that tumors develop in the face of (insufficient) anti-tumor immunity, which is illustrated by the fact that tumor-specific immunity can be measured in many patients with clinically apparent cancer (13, 14).

Tumors can escape the immune control by many different mechanisms (9, 60). The immunological pressure can lead to the escape of edited tumor variants with reduced immunogenicity. Downregulation of MHC class I molecules (61, 62), impaired TAA processing (63), or downregulation of TAA expression (64, 65) can lead to a reduced recognition of tumor cells by the adaptive immune system. Similarly, tumors can become unrecognizable for cells of the innate immune system through for example the loss of ligands for the NK cell effector molecule NKG2D (66). Upregulation of anti-apoptotic molecules or inactive forms of death receptors leads to an increased resistance of tumor cells to the lysis by immune cells (67, 68).

Besides these tumor-intrinsic alterations, subversion of anti-tumor immune responses by the establishment of an immunosuppressive tumor microenvironment is another escape mechanism (see below, **Figure I-3**).

1.4 Immunosuppressive tumor microenvironment

Tumor cells can acquire multiple mechanisms that lead to the establishment of an immunosuppressive microenvironment that hampers or even precludes protective anti-tumor immunity. Such mechanisms are for example the production of immunosuppressive factors (TGF-β, IL-10, VEGF, soluble MICA, IDO), the expression of co-inhibitory molecules (PD-L1, HVEM, Galectin-9) that interact with immunoregulatory molecules on T cells (PD-1, BTLA, Tim-3, CTLA-4, CD200), the recruitment of immunoregulatroy cell types (Tregs, TAMs, MDSCs), the generation of a shift in Th1/Th2 responses and the promotion of chronic inflammation.

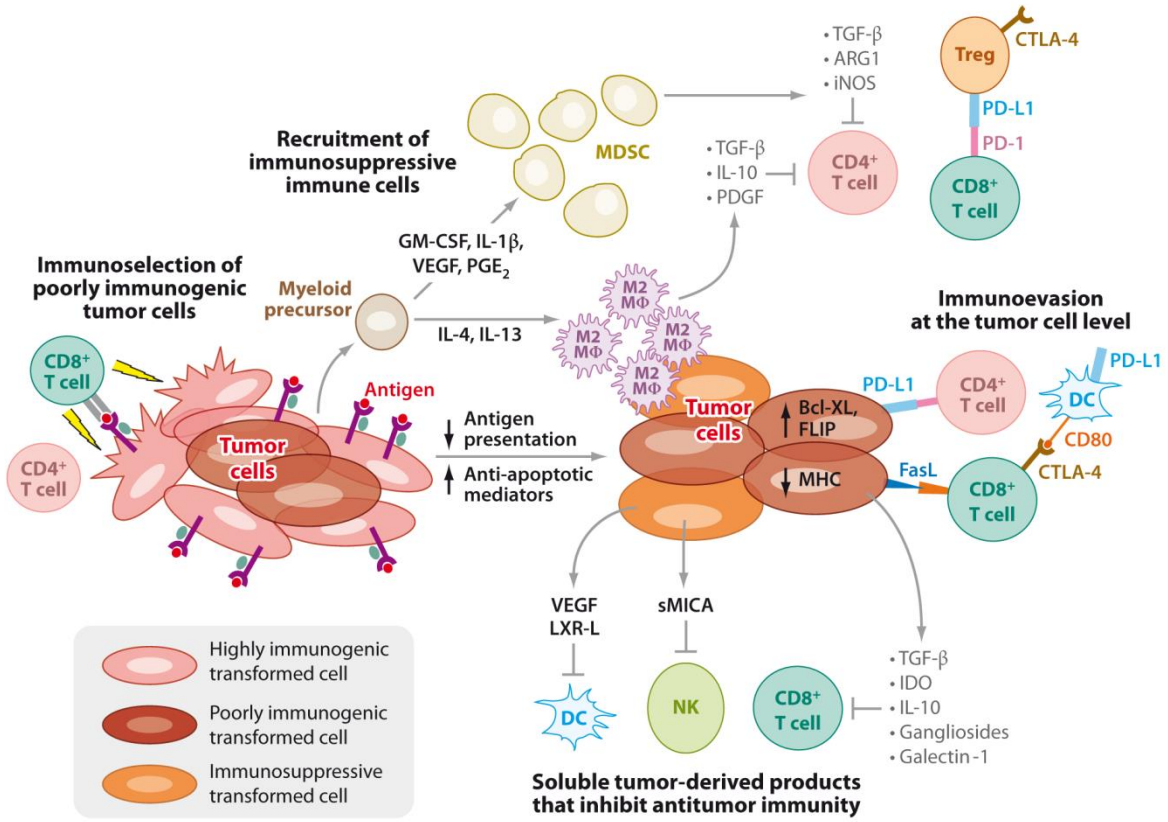

Figure I-3: Tumor escape mechanisms

Tumors acquire multiple intrinsic and extrinsic mechanisms to elude or inhibit anti-tumor immunity (figure from (9)).

Immunosuppressive factors released by tumor cells

Tumor cells can produce and release immunosuppressive soluble factors that inhibit immune effector functions or recruit regulatory cell types to generate an immunosuppressive microenvironment. Transforming growth factor-β (**TGF-β**) and **IL-10** are regulatory cytokines produced by tumor cells that interfere with the activation, maturation and differentiation of both innate and adaptive immune cells, leading to impaired anti-tumor immunity (69-71). Another regulatory factor released by tumor cells is the enzyme indoleamine 2,3-dioxygenase (**IDO**) that was shown to inhibit T cell proliferation and function by the induction of tryptophan deficiency in the tumor microenvironment (72).

Expression of immunosuppressive molecules on tumor cells

Tumor cells can inhibit the effector functions of immune cells in a cell-contact mediated manner by expression of inhibitory ligands on their surface.

As mentioned before, the activation of T cells requires a primary signal delivered through the engagement of the TCR with peptide-bound MHC molecules on antigen-presenting cells (APCs) and secondary signals transmitted through interactions of different co-stimulatory and -inhibitory

molecules. Co-stimulatory signals are for example delivered through CD28 on T cells with CD80/86 on APCs, while the interaction of cytotoxic T lymphocyte antigen 4 (**CTLA-4**) or programmed death 1 (**PD-1**) on activated T cells with CD80/86 or programmed death ligand 1 or 2 (**PD-L1**/PD-L2) on APCs and/or tumor cells inhibits T cell responses (73, 74). CTLA-4 is an inhibitory receptor expressed by a variety of immune cells, including activated T cells and Tregs. It binds CD80/86 with higher affinity than CD28 and thus can effectively outcompete co-stimulatory CD28 signaling (75). Furthermore, there is evidence that the engagement of B7 molecules on the surface of DCs with CTLA-4 on T cells leads to an upregulation of IDO in DCs (76) and by this to an activation of the immunoregulatory pathway of tryptophan metabolism often associated with increased IL-10 secretion and expansion of Tregs (77). It was shown that the expression of PD-L1 progressively increases on leukemic cells, which presumably results in progressive resistance to CTL-mediated killing (78). Besides PD-1, also T cell immunoglobulin and mucin-domain-containing molecule 3 (**Tim-3**) contributes to the loss of T effector cell function. The ligand for Tim-3, Galectin-9, is expressed by APCs. T cells that express both PD-1 and Tim-3 represent a cell population in TILs with an increased dysfunctional phenotype compared to T cells expressing just one of the molecules (79).

The role of the herpesvirus-entry mediator (**HVEM**) expressed on APCs is less clear: by binding to B- and T-lymphocyte attenuator (**BTLA**) the initiation and maintenance of ongoing T cell effector functions is inhibited. On the other hand, the engagement of HVEM with its endogenous ligand LIGHT can induce stimulatory signals in T cells (80). A recent study in melanoma patients showed that tumor-specific $CD8^+$ T cells are rendered dysfunctional by the tumor microenvironment through upregulation of the inhibitory receptors BTLA and PD-1. The combined blockage of PD-1, Tim-3 and BTLA enhanced the expansion, proliferation, and cytokine production of tumor–specific $CD8^+$ T cells (81).

CD200 has been detected on activated T cells within tumors (82). It is suggested that the interaction of CD200 with the CD200 receptor on myeloid cells transmits an inhibitory signal leading to a decreased production of Th1 cytokine production and increased IL-10 production (83). Furthermore, CD200 is also expressed by tumor cells of hematopoietic (84) and also some solid cancers (85) and was shown to be involved in the induction of Tregs (86).

Recruitment of regulatory immune cell types

Tumors promote the generation, activation and recruitment of immunosuppressive immune cells, thus changing the composition of the tumor infiltrate. Regulatory cells attenuate anti-tumor immunity through production of immunosuppressive cytokines and alterations in nutrient content of the microenvironment.

Myeloid-derived suppressor cells (MDSCs) are a heterogeneous population of cells of myeloid origin accumulating in some tumors. They were shown to inhibit both innate and adaptive immunity by suppressing $CD8^+$ and $CD4^+$ T cells, NK and NKT cells and by blocking DC

maturation (87). Many tumors also attract TAMs that contribute to tumor destruction or promote tumor growth depending on their phenotype (introduced in more detail in 1.5).

Tregs are a subpopulation of $CD4^+$ $CD25^{high}$ T cells that specifically express the transcription factor **FoxP3** (88). Suboptimal activation of DCs in the tumor microenvironment can lead to the generation of immunosuppressive Tregs (27, 28). Also MDSCs are involved in the induction of Tregs (89) and TGF-β production by tumor cells can convert effector T cells into Tregs (90). Tregs secrete the immunosuppressive cytokines IL-10 and TGF-β and are known to inhibit the effector functions of $CD8^+$ cytotoxic T cells and also NK cells, thereby downregulating cellular functions of both the adaptive and the innate immune system (91, 92). It is still not fully understood how Tregs block $CD8^+$ T cells, but the expression of CTLA-4 may be involved and also IL-2 consumption (90). An increased number of Tregs in the peripheral blood of patients and also a tumor infiltrate rich in Tregs showed a correlation with reduced survival of patients suffering from different cancer types like ovary, breast and liver cancer (93).

Promotion of a shift in Th1 and Th2 responses

Tumor progression can be associated with a general shift from Th1 to Th2 immune responses, particularly in the tumor microenvironment.

$CD4^+$ T cells can be divided into different subtypes based on cytokine secretion and chemokine expression patterns. While type 1 $CD4^+$ T cells (Th1) provide help to $CD8^+$ T cells and are considered to be effector cells with anti-tumor activity (94), type 2 $CD4^+$ T cells (Th2) are besides Tregs another subpopulation of $CD4^+$ T cells that polarize immunity away from a beneficial anti-tumor immunity (95).

Signal transducer and activator of transcription (STAT) proteins are central in regulating the cytokine profile of T cells. The STAT family consists of seven members, each responding to a defined set of cytokines and each also regulating the expression of a group of specific genes (96). Tyrosine phosphorylation is a critical step in the activation of STAT proteins, often mediated by cytokine-receptor associated Janus kinases (JAKs) (97). The development of Th1 and Th2 cells is induced by the cytokines IL-12 and **IL-4/IL-13** respectively. IL-12 can activate STAT-4 that leads to the differentiation of the Th1 subtype by inducing the production of Th1 cytokines like IFN-γ, whereas IL-4 and IL-13 activate STAT-6 that leads to the development of the Th2 subtype by inducing the secretion of Th2 cytokines like IL-4, IL-5 and IL-13 (98). STAT-3 is a STAT protein important for tumor immune evasion. Abnormal signaling of various growth factor receptors like epidermal growth factor (EGF) and vascular epidermal growth factor (VEGF) can lead to the persistent activation of STAT-3 in tumor cells. Subsequently STAT-3-driven tumor-derived factors, like IL-10, IL-6 and VEGF can enhance the activation of STAT-3 in tumor-associated immune cells (99). STAT-3 in immune cells promotes the development of an immunosuppressive environment by mediating the generation of immune suppressor cells, including MDSCs, Tregs and Th17 cells, inhibition of DC maturation, negative regulation of Th1-

type cytokines and enhanced production of immunosuppressive mediators like IL-10 and TGF-β (99).

Tumor-related chronic inflammation and immune regulation

There is evidence that chronic inflammation may result in malignant transformation (100) and it has been suggested that cancer immunoediting and tumor-promoting inflammation are not mutually exclusive processes, but may overlap instead (101).

A relationship between chronic inflammation and carcinogenesis is for example well established for the development of hepatocellular carcinoma in consequence of chronic hepatitis (HCC) (102) and that lymphotoxin beta receptor (**LT-βR**) signaling represents a pathway involved in inflammation-induced HCC (103). The proinflammatory cytokines lymphotoxin alpha (**LT-α**) and lymphotoxin beta (**LT-β**) are expressed by activated T-, B-, NK- and lymphoid tissue inducer cells and are under normal conditions crucial for organogenesis and maintenance of lymphoid tissues (104). Furthermore, lymphotoxin expression on T cells is required for DC maturation and for efficient priming, proliferation and cytokine secretion of T cells (105). LT-βR triggering by lymphotoxins induces the classical and alternative NF-κB signaling pathways which are linked to inflammation-induced carcinogenesis (106). The impact of the lymphotoxin signaling on tumor promotion still has to be defined for other tumor types.

Recent studies have shown that certain pro-inflammatory cytokines such as IL-23, **IL-17** and **TNF-α** can promote tumor development and growth, since experimental tumor growth is decreased in the absence of such cytokines (107-109). However, also a role in enhancing anti-tumor immunity was observed for IL-17 and it is still under debate whether Th17 cells exert more pro- or anti-tumorigenic functions (110). Besides its tumor-promoting role, also TNF-α was shown to protect the host against tumor formation by being important for priming, proliferation and recruitment of tumor-specific T cells (111).

1.5 Tumor-associated macrophages (TAMs)

Macrophages are part of the innate immune system and play an important role in many aspects of immunity (112).

Classical activation of macrophages occurs during acute inflammation and (bacterial) infections and is mediated by IFN-γ and LPS. Alternative activation frequently occurs in the context of chronic inflammation and is in part mediated by IL-4 and IL-13 (113-116). Because of the parallels in the cytokine profile of macrophages and $CD4^+$ T cells, Mills initiated the terminology M1/M2 macrophages for classically activated and alternatively activated macrophages in analogy to the Th1/Th2 paradigm (117).

M1 and M2 macrophages can be distinguished based on differential expression of transcription factors and surface molecules, as well as due to disparities in their cytokine profile and metabolism. A simplified picture that compares M1 and M2 macrophages is shown in **Figure I-4.**

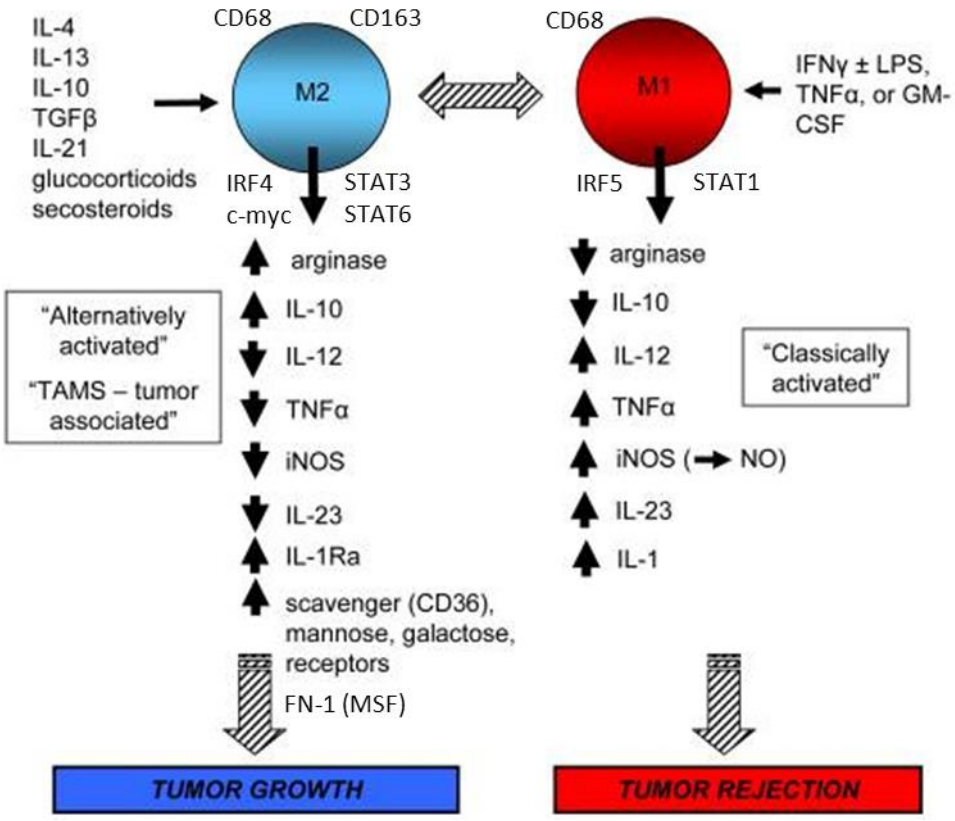

Figure I-4: Differences in M1 and M2 macrophages

Classical activation leads to the polarization of macrophages into tumoricidal M1 macrophages, while alternative activation leads to polarization of macrophages into tumor-promoting M2 macrophages and M2 TAMs (modified from (95)).

The classical M1 phenotype is promoted by IFN-γ mediated STAT-1 activation that promotes the expression of genes like IL-12, MHC-class II, and inducible nitric oxide synthase (**iNOS**) (118). IL-12 is a cytokine known to stimulate both the proliferation and cytotoxicity of T cells and NK cells (119). Besides IL-12, M1 macrophages also release large amounts of other proinflammatory cytokines such as IL-23 and TNF-α (120). Due to iNOS expression, M1 macrophages catalyze the production of anti-microbial nitric oxide (NO) from L-arginine that was shown to be important for macrophage-mediated tumor killing (121). Recently, it was observed that activation of the interferon regulatory factor-5 (**IRF-5**) also facilitates the M1-associated phenotype, and genome-wide expression analysis revealed that IRF-5 induces the expression of M1-signature genes and represses the M2-specific genes (122).

In contrast, signaling downstream of the IL-4 receptor leads to the activation of STAT-6 (123), a master regulator of M2 genes such as the mannose receptor (**MR**) and to a reduction of iNOS (124). In mice, M2 macrophages express increased levels of **Arginase-1**, which hydrolyses L-

Arginine into urea and L-ornithine. These products are further metabolized into polyamines and prolines, molecules involved in proliferation and tissue remodeling processes (125). IL-10, also involved in M2 polarization, induces activation of STAT-3 that leads to upregulation of SOCS3 an inhibitor of cytokine signaling leading to decreased secretion of Th1 type immune mediators thereby promoting T cell tolerance (126, 127). Recently it was shown that also **IRF-4** specifically regulates M2-signature genes and by this M2 macrophage polarization (128). M2 macrophages are known to mediate parasite clearance, suppress inflammation and support immunoregulation through for example the production of IL-10 and the promotion of Treg differentiation (120, 129).

Tumor-associated macrophages (TAMs) originate from blood monocytes that are recruited to the tumor already early during tumor development by tumor-derived signals, including CSF-1 and VEGF (130, 131). Due to the functional plasticity of macrophages, their phenotype can be influenced by factors of the tumor microenvironment, such as cytokines and hypoxia. In regard of cytokines and chronic state, established cancer resembles the situation of chronic inflammation. In this line, it was shown that tumor-conditioned media, as well as TGF-β and/or IL-10, major cytokines present in the tumor microenvironment, induce phonotypical changes in macrophages reminiscent of alternative activation (IL-4/IL-13) and M2 macrophages (132, 133). Such polarized TAMs, termed M2 TAMs hereafter, show an impaired expression of reactive nitrogen intermediates (NO) and high expression of angiogenic factors like VEGF and EGF (120). Furthermore, IL-12 is strongly reduced in M2 TAMs, while IL-10 production is markedly increased. While monocytes differentiated ex vivo to macrophages were able to lyse autologous tumor cells (134), neither macrophages from PBMCs of cancer patients (135) nor TAMs isolated from tumor ascites (136) showed anti-tumoricidal activity.

Whereas the pan-macrophage marker **CD68** is found on diverse subtypes of macrophages (137), M2 but not M1 TAMs express the hemoglobin scavenger receptor **CD163** (132, 138). Furthermore, M2 TAMs were shown to express higher levels of MR (139) and Fibronectin 1 (**FN-1**) (132, 140), and specifically express the migration-stimulating factor (MSF), a FN-1 isoform (132). Very recently **c-MYC** was identified as a marker for M2 TAMs (141). c-MYC is induced in human macrophages upon IL-4 and other M2-like stimuli, and is expressed in human $CD68^+$ TAMs in which it controls various M2-associated and protumoral genes (141).

M2 TAMs support the progression of cancer by many different aspects including the promotion of angiogenesis, matrix remodeling and metastasis (142-144). A positive paracrine feedback loop between tumor cells and TAMs promoting tumor cell invasiveness was shown in breast cancer (145). Tumor cells secrete colony stimulating factor 1 (**CSF-1**) and thereby recruit CSF-1 receptor (**CSF-1R**) positive TAMs to the tumor (**Figure I-5**). The interaction of CSF-1 and its receptor induces the secretion of epidermal growth factor (**EGF**) by TAMs that stimulates the production of CSF-1 by EGF receptor (**EGFR**) positive cancer cells. EGF promotes the formation of elongated protrusions and cell invasion. In humans CSF-1 not only impacts on TAMs, but also can bind to the CSF-1R on tumor cells and by this further amplifies the secretion of CSF-1 via an autocrine

loop (146). It was shown that the invasion of tumor cells can be blocked by either inhibiting the CSF-1R or the EGFR. Along this line, blockade of CSF-1 induced signaling reduced the number of macrophages in tumors and correlated with reduced mammary tumor metastasis (147). **Mena**, an actin regulatory protein, was found to be upregulated in human breast cancer as part of the tumor invasive signature (148). It was suggested to act downstream of the EGFR and enhances the sensitivity of cells towards EGF, leading to an increased metastatic potential of tumor cells (149). High Mena levels are associated with increased invasiveness and poor clinical outcome in breast cancer and melanoma patients (150, 151). Very recently it was suggested that the interaction of CSF-1 and CSF-1R induces M2 polarization in TAMs and that cytokines secreted by these TAMs activates STAT-3 in ccRCC tumor cells and consequently promotes cancer progression (152).

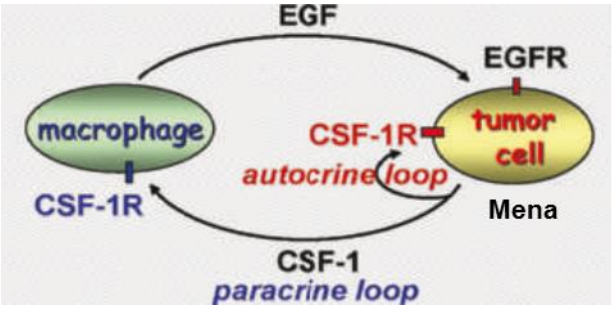

Figure I-5: EGF and CSF-1 dependent macrophage-mediated promotion of tumor invasion

A paracrine loop between macrophages, expressing CSF-1R and secreting EGF, and cancer cells, expressing EGFR and secreting CSF-1, leads to tumor invasion of breast cancer cells. This interaction is amplified by a CSF-1/CSF-1R autocrine loop of tumor cells and by Mena acting downstream of the EGFR (adapted from (146)).

TAMs promote tumor growth also in a tumor-extrinsic fashion, namely by suppressing local tumor-specific immunity (115, 133, 153). It is therefore not surprising that a high frequency of TAMs is often associated with an unfavorable prognosis (154). However, limited data are available on the correlation between prognosis and macrophage phenotype in human cancer. Furthermore, the nature and consequences of local interactions between TAMs and other components within the tumor, including T cells and tumor cells, are largely unknown.

1.6 Renal cell carcinoma

Renal cell carcinoma (RCC) encompasses a heterogeneous group of cancers deriving from the renal parenchyma (155). The majority of renal malignancies (85-95%) are classified as RCCs (156), which account for 3% of all adult neoplasms (157). According to the WHO classification RCC is divided in three major histological subtypes: clear cell RCC (ccRCC, 80-90%), papillary

RCC (10-15%) and chromophobe RCC (4-5%) (158). **Figure I-6** displays the macroscopic appearance of RCC and microscopic representations of the major subtypes.

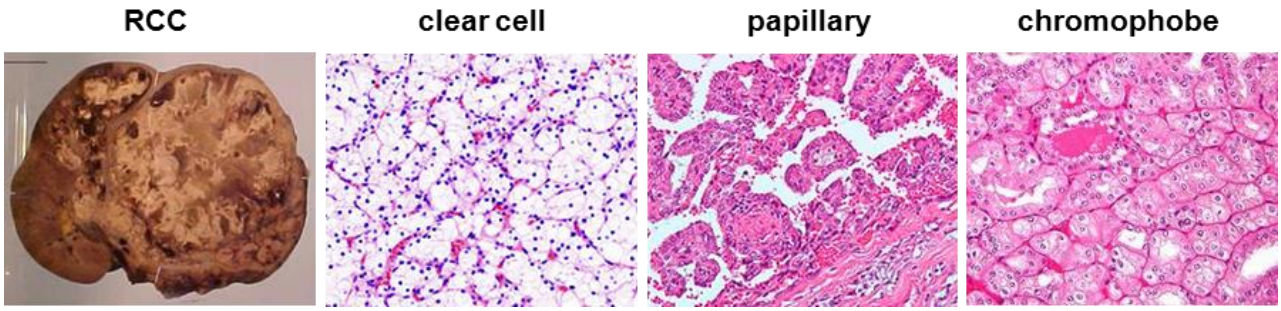

Figure I-6: RCC and its most common histological subtypes

Macroscopic and microscopic representations of RCC (http://health.act.gov.au/health-services/canberra-hospital/our-services/act-pathology/about-act-pathology/pathology-museum/urinary-system/left-kidney-renal-cell-carcinoma, http://en.wikipedia.org/wiki/Renal_cell_carcinoma).

An association between subtype and survival was observed in different studies, with ccRCC being the most aggressive tumor followed by papillary and chromophobe RCC (159, 160). Since RCC subtypes represent dissimilar diseases in morphology, genetics and clinical course (161), we restricted our analysis to the most common subtype - ccRCC - to minimize heterogeneity and because most established clinical data are available for ccRCC (162).

An elevated risk to develop RCC was observed with increased tobacco exposure, hypertension and obesity (163). Most RCCs are detected by chance when patients undergo medical examinations of the abdomen because of apparently unrelated symptoms. Less than 10% of RCC cases show the classic triad of symptoms that is hematuria (blood in the urine), abdominal or flank pain, and palpable mass on physical examination, usually a sign for a more advanced disease (164). The development of the clear cell subtype is closely linked to the loss of the von Hippel-Lindau (VHL) gene product (pVHL) and subsequent deregulation of the hypoxia inducible factor (HIF) family of transcription factors (165). Individuals with one defective copy of the VHL gene have an increased risk to develop ccRCC (166). Knockout studies, however, demonstrated that loss of VHL alone is not sufficient for ccRCC development and that thus additional events have to occur (167, 168).

Standard treatment of local disease is surgical resection of the tumor by radical or partial nephrectomy. RCC is curable by this treatment when detected sufficiently early, however, about one-third of patients already developed metastatic disease at time of diagnosis and about one-third develops metastases at a later time-point after surgery, which suggests the presence of undetected (micro)metastases at the time of surgery (169). Treatment of advanced and metastatic disease is challenging since RCC is highly resistant to chemo-, hormone- and radiotherapy (170) leading to poor prognosis for those patients with a 5-year survival rate of less than 10% (171).

Since deregulation of HIF is an important aspect of ccRCC development, agents blocking HIF target genes, especially vascular epithelial growth factor receptor (VEGFR) and platelet derived growth factor receptor (PDGFR), are currently evaluated in many clinical trials. The small molecule receptor-kinase inhibitors sunitinib and sorafenib, which target anti-angiogenesis, have been proven worldwide as second line standard treatments for metastatic RCC (172, 173). Clinical response was observed for sorafenib and sunitinib treatment (174, 175) however, complete responses were not observed after treatment with any of those inhibitors.

It is well established that RCC is an immunogenic tumor. For example, immunosuppressed patients have an increased incidence of RCC (33, 176), and RCC is more heavily infiltrated by immune cells than other cancers (177, 178). In addition, reports of long dormancy of metastatic lesions (179) and observations of spontaneous regression of RCC tumors in some cases (180, 181) support the thesis that RCC is controlled by the immune system.

1.7 Aims of this study

Basic research aimed at understanding the relations between RCC and immune cells has led to a complex network with many players (**Figure I-7**) (182, 183).

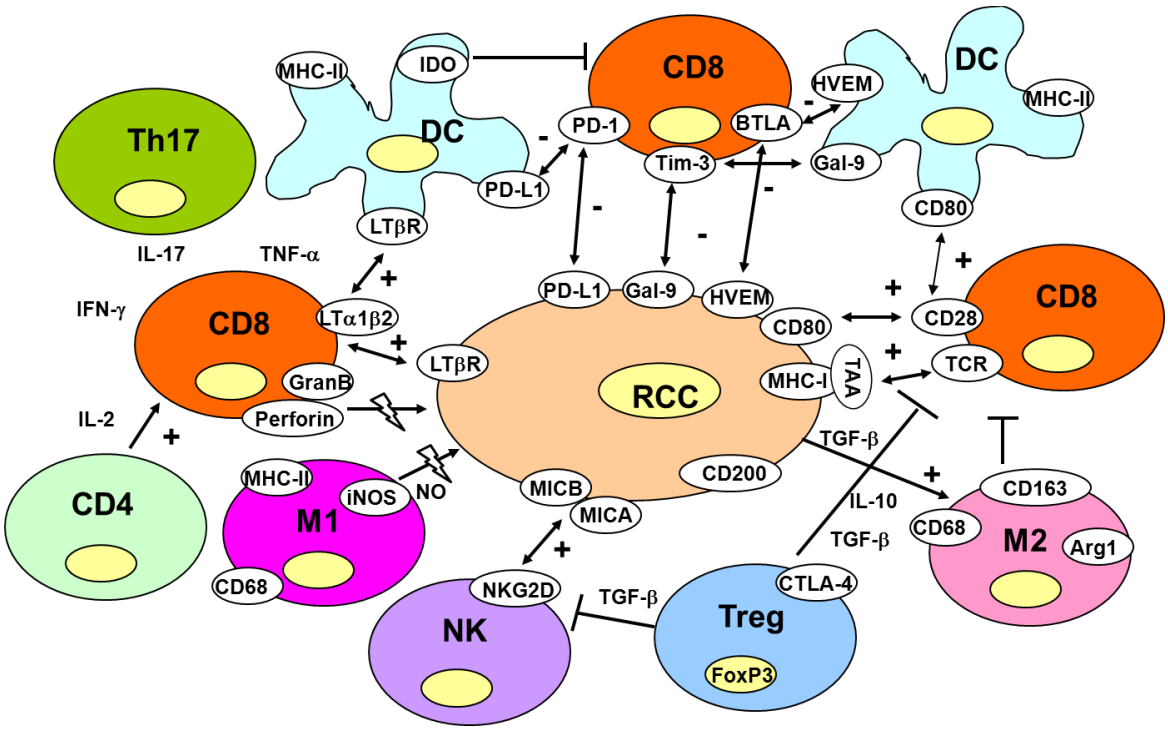

Figure I-7: Immunoregulation in ccRCC

Stimulatory interactions of immune cells and tumor cells are represented with **+**, inhibitory signals with **-**, and direct cytotoxic effects of immune cells with ↯ .

To identify which immunological parameters correlate with a favorable course of ccRCC, we correlated their expression with the most powerful and meaningful readout in humans: survival. Furthermore, we evaluated whether the local and peripheral immune responses differ phenotypically or functionally and if so, whether the tumor microenvironment contributes to the differences.

The specific aims of this study are

1) **To detect TAA-specific T cell responses in PBMCs and TILs of ccRCC patients**
2) **To identify an immunological signature that correlates with patient survival**
3) **To elucidate the impact of the tumor microenvironment and the identified immunological parameters on T cell phenotype and function**

For aims 1 and 3, I collected blood and fresh tumor material from 91 patients with kidney cancer, who underwent surgery as part of their treatment (summary **Table I-1**). Experiments were only performed on material from patients, who were newly diagnosed with the clear cell RCC subtype. I performed the experiments for aim 2 on formalin-fixed paraffin-embedded tumor material from 60 patients with primary ccRCC of whom information on tumor stage (pT) and survival was available (**Table S2** in results part 2.2).

Table I-1: Summary of fresh patient material collected in the scope of this thesis

all samples		
	#	**%**
patients	**91**	**100**
malignant samples	**71**	**78**
clear cell RCC	**36**	**50.7**
papillary RCC	**13**	**18.31**
chromophobe RCC	**9**	**12.68**
mixed forms of RCC	**4**	**5.63**
others	**6**	**8.45**
distant metastases	**3**	**4.23**

clear cell RCC		
	pT	**#**
tumor stage (pT)	**1**	**2**
	1a	**16**
	1b	**6**
	1c	**0**
	2	**4**
	3a	**3**
	3b	**5**
	3c	**0**
	4	**0**
HLA-A2 positive	**51.43%**	
HLA-A2 negative	**48.57%**	
patient age (years)	**average**	**63 ± 10**
	range	**37 - 84**

All patients underwent full or partial nephrectomy as part of their standard treatment at the Department of Urology, University Hospital Zurich, within the years 2008 to 2011. Clinical specimens (tumor samples and peripheral whole blood) were obtained following informed consent in accordance with the Declaration of Helsinki. The local ethics committee approved this study (EK-1017).

2. RESULTS

2.1 Spontaneous peripheral T cell response towards the tumor-associated antigen Cyclin D1 (CCND1) in patients with clear cell renal cell carcinoma

Manuscript in preparation

Authors: Stefanie Regine Dannenmann, Ali Bransi, Claudia Matter, Thomas Hermanns, Lotta von Boehmer, Stefan Stevanovic, Peter Hans Schraml, Holger Moch, Alexander Knuth and Maries van den Broek

Contributions: SRD and MvdB designed the experiments and wrote the manuscript. AB performed experiments for Cyclin D1 sequencing and Western blot analysis, CM and MvdB performed Cyclin D1 tetramer staining. SRD conducted and analyzed all remaining experiments.

Spontaneous peripheral T cell response towards the tumor-associated antigen Cyclin D1 (CCND1) in patients with clear cell renal cell carcinoma

Stefanie Regine Dannenmann[1], Ali Bransi[1], Claudia Matter[1], Thomas Hermanns[2], Lotta von Boehmer[1], Stefan Stevanovic[5], Peter Hans Schraml[3], Holger Moch[3], Alexander Knuth[1], Maries van den Broek[1,4]

University Hospital Zurich, Departments of [1]Oncology, [2]Urology, and [3]Pathology, Zurich, Switzerland; [5]University of Tubingen, Interfaculty Institute for Cell Biology, Department of Immunology, Tubingen, Germany

[4]Corresponding author: Maries van den Broek, University Hospital Zurich, Department of Oncology, Wagistrasse 14, CH-8592 Schlieren, Switzerland. Tel.: +41 44 556 3134, email: maries@van-den-broek.ch

ABSTRACT

Renal cell carcinoma (RCC) is a heterogeneous group of kidney cancers with clear cell RCC (ccRCC) as the major subgroup. We analyzed the expression and immunogenicity of different tumor-associated antigens (TAAs) in ccRCC patients. We found expression of MAGE-A9 and NY-ESO-1 and overexpression of PRAME, RAGE-1, G250, Cyclin D1, ADFP, C-MET and RGS-5 in many of the 23 primary ccRCC tumor samples tested. Subsequently, we investigated the presence of $CD8^+$ T cells specific for previously identified HLA-A2-restricted peptides derived from the relevant TAAs in the blood of HLA-$A2^+$ patients. We found spontaneous responses towards Cyclin D1 in 5 out of 6 patients with Cyclin D1-positive tumors. Cyclin D1-specific $CD8^+$ T cells secreted TNF-α, IFN-γ, and IL-2 and degranulated, suggesting the presence of polyfunctional tumor-specific $CD8^+$ T cells in the blood of patients with primary ccRCC.

The frequent occurrence of Cyclin D1 overexpression in ccRCC specimens (43%) and the frequent detection of functional Cyclin D1-specific T cells in those patients (83%) makes Cyclin D1 an interesting target for future immunotherapeutic strategies.

INTRODUCTION

The immune system recognizes and controls tumors through a process called cancer immune surveillance (1). In support of this, several studies found a correlation between the degree of tumor infiltration by T cells and survival in different cancer entities (2). In addition, spontaneous tumor-specific immunity can be detected in cancer patients (3), which is targeted to tumor-associated antigens (TAAs). TAAs include cancer-testis (CT) antigens, differentiation antigens, mutated proteins, overexpressed proteins and viral antigens (4). Boosting spontaneous TAA-specific immunity in cancer patients is a strategy with low toxicity, which resulted in objective clinical responses in some patients (5).

Renal cell carcinoma is a heterogeneous group of tumors that encompasses about 90% of all human kidney tumors, with ccRCC as the major histological subgroup (6). If detected early, patients can be cured by resection; however, about one-third of the tumors already metastasized at the time of diagnosis. Moreover, about 20-50% of patients will develop metastasis despite resection (7). Treatment of advanced and metastatic disease is challenging due to the relative chemo- and radiotherapy resistance of RCC (8).

Spontaneous regressions and the increased incidence of RCC in immunosuppressed patients, as well as the high density of tumor-infiltrating leukocytes (TILs) suggest immune recognition of this tumor type (9). For this reason, RCC patients are being treated with immunostimulatory compounds including IL-2 and/or IFN-α since the 1980s. Despite modest therapeutic efficacy observed in some patients, concomitant severe systemic toxicity is a problem (8). Although RCC is generally considered as an immunogenic cancer, data showing TAA-specific immunity in RCC patients are scarce.

We investigated tumor samples of 23 patients with primary ccRCC for the expression of genes encoding the CT antigens MAGE -A1 (CT1.1), -A3 (CT1.3), -A4 (CT1.4), -A9 (CT1.9), -A10 (CT1.10), synovial sarcoma X breakpoint 2 (SSX2/CT5.2), New York esophageal I (NY-ESO-1/CT6.1), L antigen 1 (LAGE-1/CT6.2) and MAGE-C1 (CT7), carbonic anhydrase IX (CA-IX/G250), renal antigen 1 (RAGE-1), preferentially expressed antigen of melanoma (PRAME), adipose differentiation-related protein (adipophilin/ADFP), C-MET proto-oncogene, Cyclin D1 (CCND1), and regulator of G-protein signaling 5 (RGS-5) via qRT-PCR. Furthermore, we investigated whether any of these antigens had induced spontaneous T cell responses in patients with primary diagnosed ccRCC.

RESULTS

Frequent expression of tumor-associated antigens in primary ccRCC tumor samples

We investigated the expression of 9 CT antigens and 7 additional antigens in 23 primary ccRCC specimens by qRT-PCR. We found expression of MAGE-A9 in 36% and of NY-ESO-1 in 55% of the samples, whereas the other 7 CT antigens were not expressed (**Figure 1A**). Although MAGE-A9 and NY-ESO-1 were frequently expressed, their expression levels were very low (**Figure 1B**). Furthermore, we observed overexpression of RAGE-1 in 13%, C-MET in 30%, PRAME in 39%, Cyclin D1 in 43%, ADFP in 65%, RGS-5 in 83% and CA-IX in 96% of ccRCCs (**Figure 1A, B**). More than 50% of the ccRCCs co-expressed 4-6 different TAAs (**Figure 1C**). We observed no evidence for preferred co-expression of particular TAAs (**Figure 1D**).

Spontaneous Cyclin D1-specific $CD8^+$ T cell responses in patients with primary ccRCC

Because limited material availability precluded the use of overlapping peptides derived from all overexpressed TAAs, we selected HLA-$A2^+$ patients and used previously described HLA-A2 restricted peptides for stimulation of PBMC (http://www.cancerimmunity.org/CTdatabase, (10-12), summarized in **Table 2**). After *in vitro* restimulation for 9 days with the relevant peptides, we performed a 5 h restimulation with the same peptides in the presence of brefeldin A and monensin, followed by intracellular staining (ICS) for the effector cytokines TNF-α, IFN-γ and IL-2 as well as staining for degranulation (surface CD107a). We found $CD8^+$ T cells specific for Cyclin D1-derived peptides in 5 out of 6 HLA-$A2^+$ patients, whose tumors overexpressed Cyclin D1 (**Figure 2A**), but not for any of the other peptides tested (data not shown). Due to limited material, the readout for patients Z-H-1144, Z-H-209, Z-H-929 and Z-H-1055 was performed with both Cyclin D1-derived peptides (Cyclin $D1_{101-109}$ and Cyclin $D1_{228-236}$) together. From patient Z-H-1184 and Z-H-1257, however, enough material was available for separate analysis of both Cyclin D1-derived epitopes and we found that the response in both patients was directed against Cyclin $D1_{101-109}$ as illustrated by a representative staining of patient Z-H-1184 (**Figure 2B**). Furthermore, the Cyclin D1-specific $CD8^+$ T cell response in all 5 patients had a polyfunctional character although only few cells secreted IL2 (**Figure 2C**).

To confirm the presence of Cyclin D1-specific T cells in ccRCC patients we additionally performed *ex-vivo* tetramer staining on PBMCs (**Supplementary Figure S1A**) and TILs (**Supplementary Figure S1B**) of ccRCC patients, when sufficient material was available. In PBMCs of patient Z-H-209, who did not show a Cyclin D1-specific response after *in vitro* stimulation, we also did not detect any tetramer-positive T cells. However, in the other patients tested, who responded to *in vitro* Cyclin D1-specific peptide stimulation (Z-H-903, Z-H-1055 and Z-H-1184), we detected Cyclin D1-specific T cells in PBMCs *ex vivo by tetramer staining* (**Supplementary Figure S1A**). While we could not find Cyclin D1-specific T cells in TILs of patient Z-H-929, whose PBMCs only responded weakly towards *in vitro* Cyclin D1-specific peptide stimulation, we detected tetramer-specific T cells in TILs of patient Z-H-1184 and Z-H-

1257, whose PBMCs clearly responded with cytokine secretion towards peptide stimulation (**Supplementary Figure S1B**).

To investigate whether Cyclin D1 induces a humoral immune response in ccRCC patients, we tested for Cyclin-D1 specific antibodies by Western blotting, however, we did not observe antibodies in serum of any of the 22 patients tested (**Supplementary Figure S2**).

DISCUSSION

To expand the number of clinically relevant TAAs that can be targeted by immunotherapy in patients with RCC, we investigated the expression of several CT antigens and some overexpressed antigens (13), in a panel of 23 primary ccRCC samples. We observed that most tumors expressed more than one TAA, which has been described for other tumor entities as well (14-16) and which enables therapeutic targeting of multiple antigens at the same time.

Except for MAGE-A9 and NY-ESO-1, we did not detect expression of any of the CT antigens analyzed in our patient cohort. Although some studies showed expression for MAGE-A3 and -A4 in RCC (17, 18) our results are in line with those of a previous review on CT antigens (19). The expression frequency of MAGE-A9 is in accordance with a previous study (10), however, we observed only very low levels of MAGE-A9 transcripts. Furthermore, as reported before (10), we also detected a signal for MAGE-A9 in the healthy kidney tissue control. The frequent expression of NY-ESO-1 was unexpected and is in discrepancy with published data (20-22). Using a highly sensitive qRT-PCR method we detected very low levels of NY-ESO-1, which may explain the discrepancy to other studies that mainly used immunohistochemistry. Although RAGE-1 was the first antigen recognized by autologous T cells on a human RCC cell line, it was only detected it in 1 out of 57 RCC samples (23). Our results are in agreement with other studies that observed higher expression frequencies, presumably due to more sensitive methods (10, 20). Furthermore, the frequency of PRAME-expression in ccRCC found here is in accordance with previously published reports (18, 20).

The von Hippel-Lindau protein (VHL) is mutated in most of ccRCC samples leading to a reduced proteolytic degradation of hypoxia inducible factor α (HIF-α) and as a result to upregulated HIF-α-mediated transcriptional programs (24). CA-IX is one of the HIF-α target genes that is frequently expressed in RCC but very rarely detected in normal kidney tissue (25). We observed an overexpression of CA-IX in all samples but one. CA-IX was described as a useful therapeutic target for RCC (11, 26, 27), which was evaluated in different clinical studies (28-30), but was so far not proven to induce a strong anti-tumor immune response. Besides CA-IX, ADFP, Cyclin D1, C-MET and RGS-5 are overexpressed in ccRCC (12). We found that ADFP was expressed more frequently than C-MET which is in contrast with published data (31, 32). Cyclin D1 is a cell cycle regulator that is crucial for G1-S transition (33) and is overexpressed in many cancers including

colorectal and breast carcinoma (34, 35). We found an overexpression in 43% of primary ccRCC samples, which is in the range of previously published data (36-38).

Although expression is a prerequisite for targeting, the amount of antigen, its expression pattern (homo- vs. heterogeneous) and its immunogenicity impact on the success of immunotherapy (20). Indeed, despite the frequent expression of NY-ESO-1, which is one of the most immunogenic CT antigens (22, 39) we did not find NY-ESO-1-specific $CD8^+$ T cell responses in any of the HLA-$A2^+$ ccRCC patients. We explain this finding by the low level of NY-ESO-1 expression. ADFP, C-MET and RSG-5 presumably are not very immunogenic in ccRCC patients, because we did not detect specific T cell responses towards these antigens, despite their frequent overexpression. This is in agreement with previously published data that described rare T cell responses in ccRCC patients (13), despite the fact that ADFP- and C-MET-specific T cells could be expanded from the blood of healthy donors (31, 32). We found no specific T cells to either of those antigens. Also RGS-5 overexpression did not result in detectable T cell responses in our cohort, although such responses were reported in blood of healthy donors and patients with acute myeloid leukemia (40).

In contrast, we detected Cyclin D1-specific $CD8^+$ T cells in the blood of 5/6 HLA-$A2^+$ patients, who overexpressed Cyclin D1 in the tumor, suggesting that overexpressed Cyclin D1 is immunogenic in patients with ccRCC. To test whether these T cell responses are directed towards a mutated epitope of Cyclin D1 in ccRCC, as observed before for the cyclin-dependent kinase 4 (CDK4) in melanoma (41), we sequenced the two Cyclin D1 epitopes. However, mutations of Cyclin D1 are very unlikely (42) and also here we did not find evidence for mutation (data not shown).

Ex vivo tetramer staining confirmed the presence of Cyclin D1-specific T cells in those patients who responded with cytokine secretion towards *in vitro* Cyclin D1-specific peptide stimulation. Although we detected a higher frequency of T cells specific for Cyclin $D1_{228\text{-}236}$ by tetramer in blood and TILs, we found a higher frequency of T cells specific for Cyclin $D1_{101\text{-}109}$ after *in vitro* restimulation followed by ICS. This observation may be explained by the possibility that Cyclin $D1_{228\text{-}236}$ is the immunodominant peptide and resulting in a more extensive *in vivo* proliferation of specific T cells, which may have compromised their ability to further expand *in vitro*. Alternatively, but not mutually exclusive, tetramer-positive T cells must not necessarily be functional, which may suggest a preferential functional exhaustion of T cells specific for Cyclin $D1_{228\text{-}236}$.

While in the case of ccRCC no association between Cyclin D1 expression and prognosis was observed (38) in most other cancers Cyclin D1 overexpression is associated with shorter patient survival and represents an interesting therapeutic target (42). However, since Cyclin D1 is intracellularly expressed and lacks intrinsic enzymatic activity it is difficult to target. One approach is to block the activity of Cyclin D1 indirectly by inhibiting associated kinases by specific kinase inhibitors (43), however, this strategy does not interfere with its kinase-independent tumor promoting effects.

Cyclin D1 induces immune responses in a variety of other cancers. For example Cyclin D1-specific $CD4^+$ and $CD8^+$ T cells can be expanded by prolonged *in vitro* restimulation from blood of healthy donors and patients with mantle cell lymphoma or colon cancer (44-46). Along this line, Cyclin D1 was identified before as a target for immunotherapy in mantel cell lymphoma (47). Whereas we did not find antibodies against Cyclin D1 in sera of ccRCC patients, such antibodies were detected in patients with prostate cancer (48).

To our knowledge this is the first study that describes naturally occurring Cyclin D1-specific $CD8^+$ T cell responses in cancer patients. Importantly, these responses had a polyfunctional effector character. We therefore propose Cyclin D1 as a target for immunotherapy in patients with ccRCC.

FIGURES AND TABLES

Table 1: Patient information

Histology	**clear cell renal cell carcinoma**	
Patient number	**n=23**	
Age (years)	**37-84 (64.1 ± 11)**	
Pathological Stage	**pT1**	**1**
	pT1a	**8**
	pT1b	**4**
	pT2	**3**
	pT3	**0**
	pT3a	**3**
	pT3b	**4**
	pT3c	**0**
	pT4	**0**

Table 2: Taq-Man Assays of TAAs and derived HLA-A2 restricted peptides

	TaqMan Assay ID	Position	Peptide Sequence	Peptide Source
MAGE-A1	Hs00607097_m1	278-286	KVLEYVIKV	not used
MAGE-A3	Hs00366532_m1	271-279	FLWGPRALV[d]	not used
MAGE-A4	Hs00365979_m1	230-239	GVYDGREHTV	not used
MAGE-A9	Hs00893224_m1	223-231	ALSVMGVYV	Thermo Scientific
MAGE-A10	Hs01560792_m1	254-262	GLYDGMEHL	not used
SSX2	Hs00817683_m1	41-49	KASEKIFYV	not used
NY-ESO-1	Hs00265824_m1	157-165	SLLMWITQC	Bio Synthesis
LAGE-1	Hs00535628_m1	41214	MLMAQEALAFL	not used
		157-165	SLLMWITQV	not used
MAGE-C1	Hs00193821_m1	959–968	ILFGISLREV	not used
		1083–1091	KVVEFLAML	not used
PRAME	Hs00196132_m1	425-433	SLLQHLIGL	Thermo Scientific
		100-108	VLDGLDVLL	Thermo Scientific
RAGE-1	Hs00179504_m1	32-40	PLPPARNGGL	Thermo Scientific
		352-360	LKLSGVVRL	Thermo Scientific
CA-IX	Hs00154208_m1	254-262	HLSTAFARV	Thermo Scientific
CCND1	Hs00765553_m1	101-109	LLGATCMFV	S. Stefanovic, Tuebingen
		228-236	RLTRFLSRV	S. Stefanovic, Tuebingen
ADFP	Hs00765634_m1	129-137	SVASTITGV	S. Stefanovic, Tuebingen
C-MET	Hs00179845_m1	654-662	YVDPVITSI	S. Stefanovic, Tuebingen
RGS-5	Hs00186212_m1	5-13	LAALPHSCL	S. Stefanovic, Tuebingen

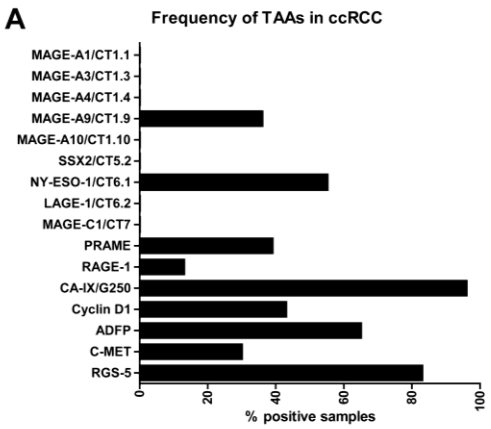

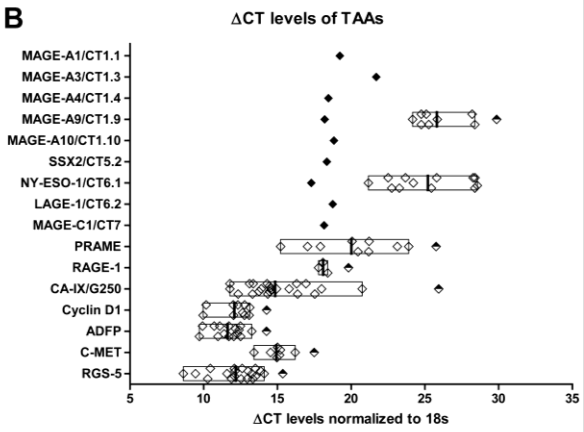

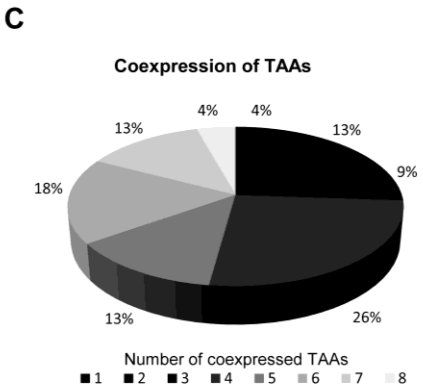

	1	2	3	4	5	6	7	8	9	10	11	12	13	14	15	16	17	18	19	20	21	22	23
MAGE-A1/CT1.1																							
MAGE-A3/CT1.3																							
MAGE-A4/CT1.4																							
MAGE-A9 /CT1.9	x	x	x			x	x				x		x		x								
MAGE-A10 /CT1.10																							
SSX2/CT5.2																							
NY-ESO-1/CT6.1	x	x	x	x		x	x	x		x	x				x	x	x						
LAGE-1/CT6.2																							
MAGE-C1/CT7																							
PRAME			x		x	x				x			x	x	x				x		x		
RAGE-1			x										x									x	
CA-IX/G250	x	x	x	x	x	x	x	x		x	x	x	x	x	x	x	x	x	x	x	x	x	x
CCND1	x		x			x		x					x	x					x	x		x	x
ADFP	x		x	x		x	x				x		x	x	x			x	x	x	x	x	x
C-MET	x								x					x				x	x			x	x
RGS-5	x	x	x	x		x	x	x		x	x	x	x	x	x	x			x	x	x	x	x

Figure 1: Expression of TAA transcripts in ccRCC specimens

RNA was isolated from 23 primary ccRCC samples, reverse transcribed and used as template for qRT-PCR analysis. (A) Frequency of expressed TAAs in primary ccRCC samples. (B) Detected ΔCT levels for the different TAA transcripts of the individual tumor samples after normalization to the endogenous control (18S rRNA). Results from tumor samples are represented as open, from testis as filled, and from healthy kidney as half-filled symbols. (C, D) Co-expression of TAAs in primary ccRCC samples.

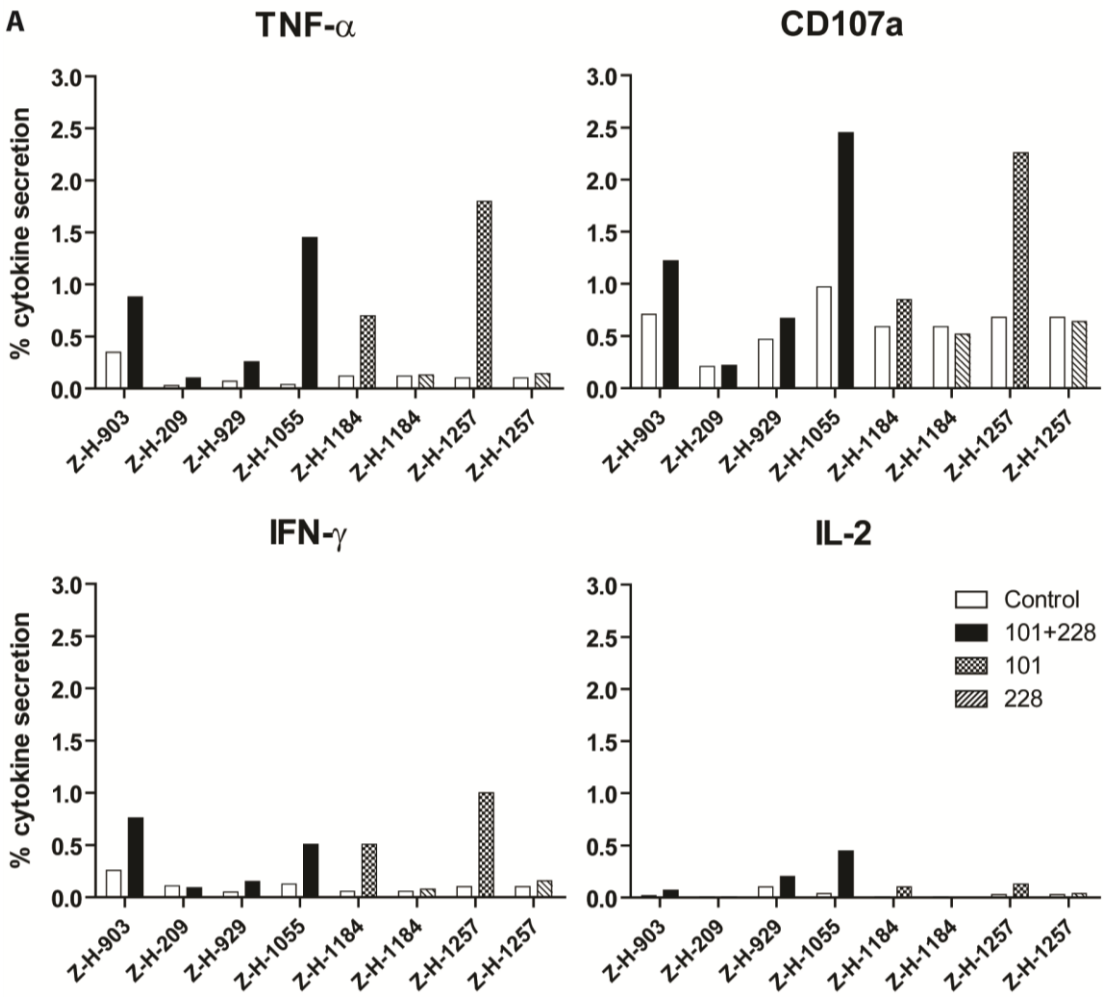
A
TNF-α
CD107a
IFN-γ
IL-2
% cytokine secretion
3.0
2.5
2.0
1.5
1.0
0.5
0.0
Z-H-903
Z-H-209
Z-H-929
Z-H-1055
Z-H-1184
Z-H-1184
Z-H-1257
Z-H-1257
Control
101+228
101
228

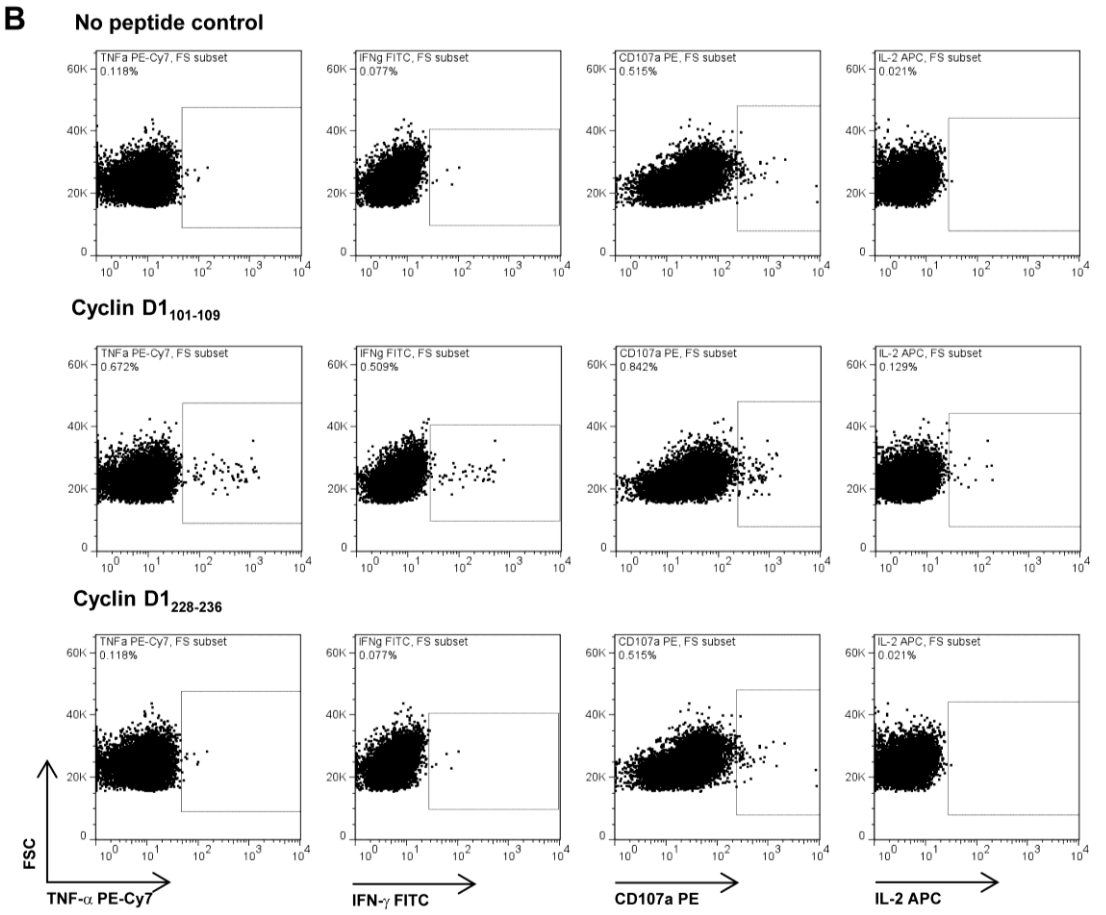
B
No peptide control
TNFa PE-Cy7, FS subset
0.118%
IFNg FITC, FS subset
0.077%
CD107a PE, FS subset
0.515%
IL-2 APC, FS subset
0.021%
Cyclin D1101-109
TNFa PE-Cy7, FS subset
0.672%
IFNg FITC, FS subset
0.509%
CD107a PE, FS subset
0.842%
IL-2 APC, FS subset
0.129%
Cyclin D1228-236
TNFa PE-Cy7, FS subset
0.118%
IFNg FITC, FS subset
0.077%
CD107a PE, FS subset
0.515%
IL-2 APC, FS subset
0.021%
FSC
TNF-α PE-Cy7
IFN-γ FITC
CD107a PE
IL-2 APC

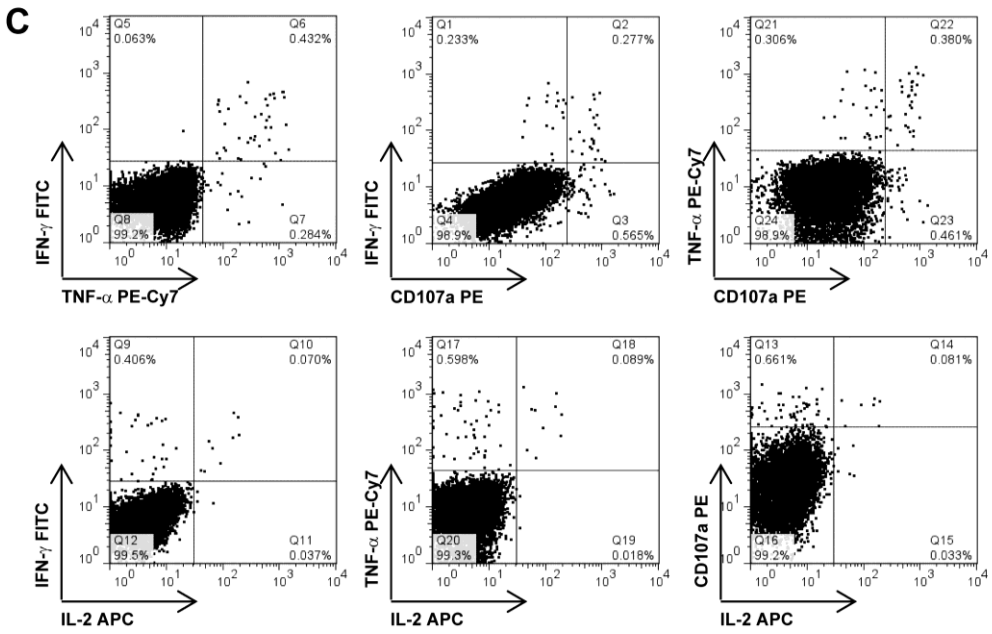

Figure 2: Cyclin D1-specific CD8$^+$ T cell response in PBMCs of ccRCC patients

CD8$^+$ T cells from PBMCs of HLA-A2$^+$ patients with Cyclin D1-overexpressing tumors were stimulated for 9 days with Cyclin D1-derived peptides in the presence of IL-2. Restimulation was performed using both Cyclin D1-derived epitopes (Cyclin D1$_{101-109}$ and Cyclin D1$_{228-236}$) together, separately or no peptide as highlighted in the figure, followed by surface staining for CD107a and intracellular staining for TNF-α, IFN-γ and IL-2. Cytokine production of CD8$^+$ T cells was measured after gating on live CD45$^+$, CD3$^+$, CD8$^+$, CD14$^-$, CD16$^-$, CD19$^-$ cells. (A) Summary of results from 6 individual patients. (B) Representative staining (patient P5) of single cytokine secretion. (C) Polyfunctional cytokine response.

SUPPLEMENTARY FIGURES

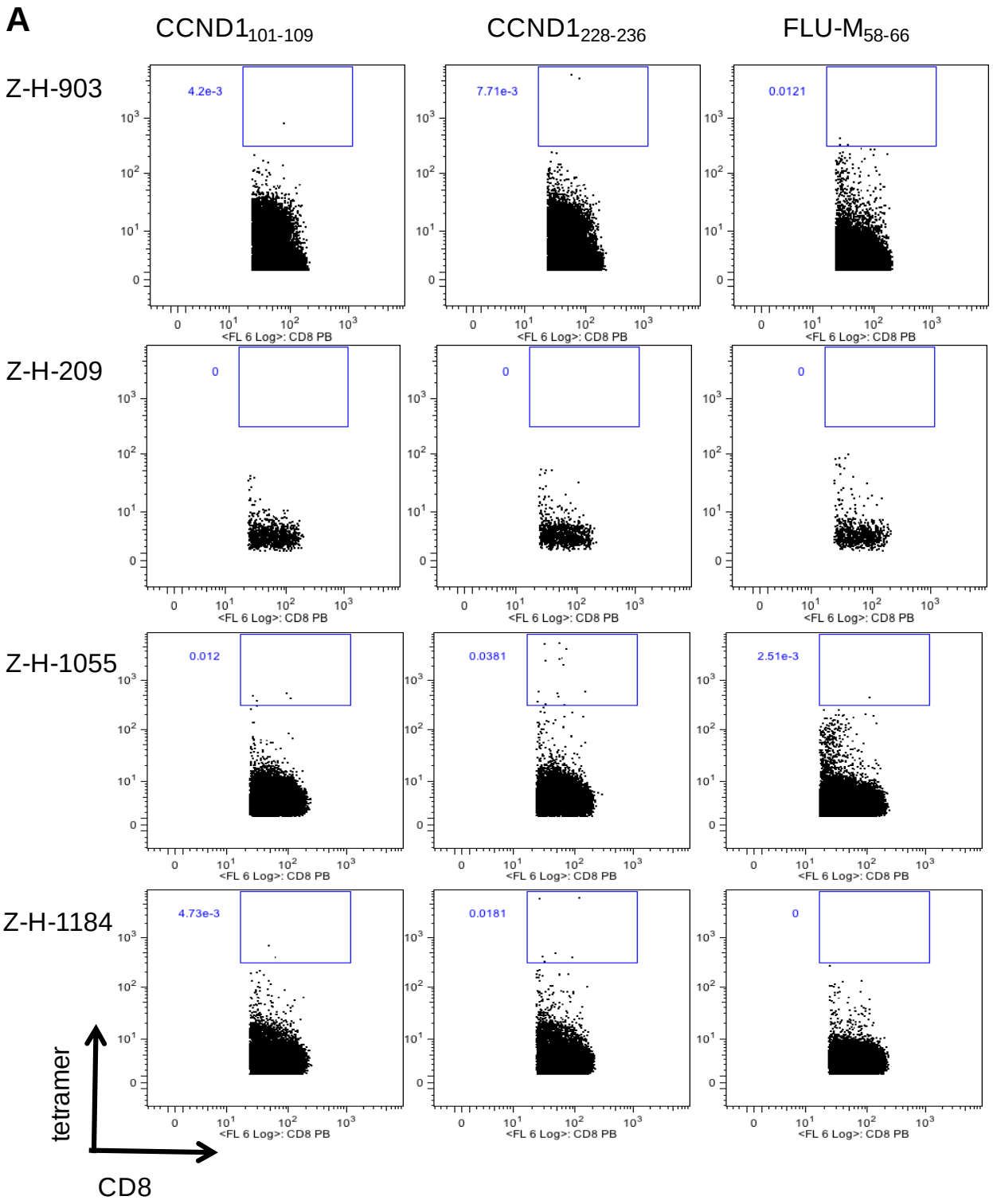

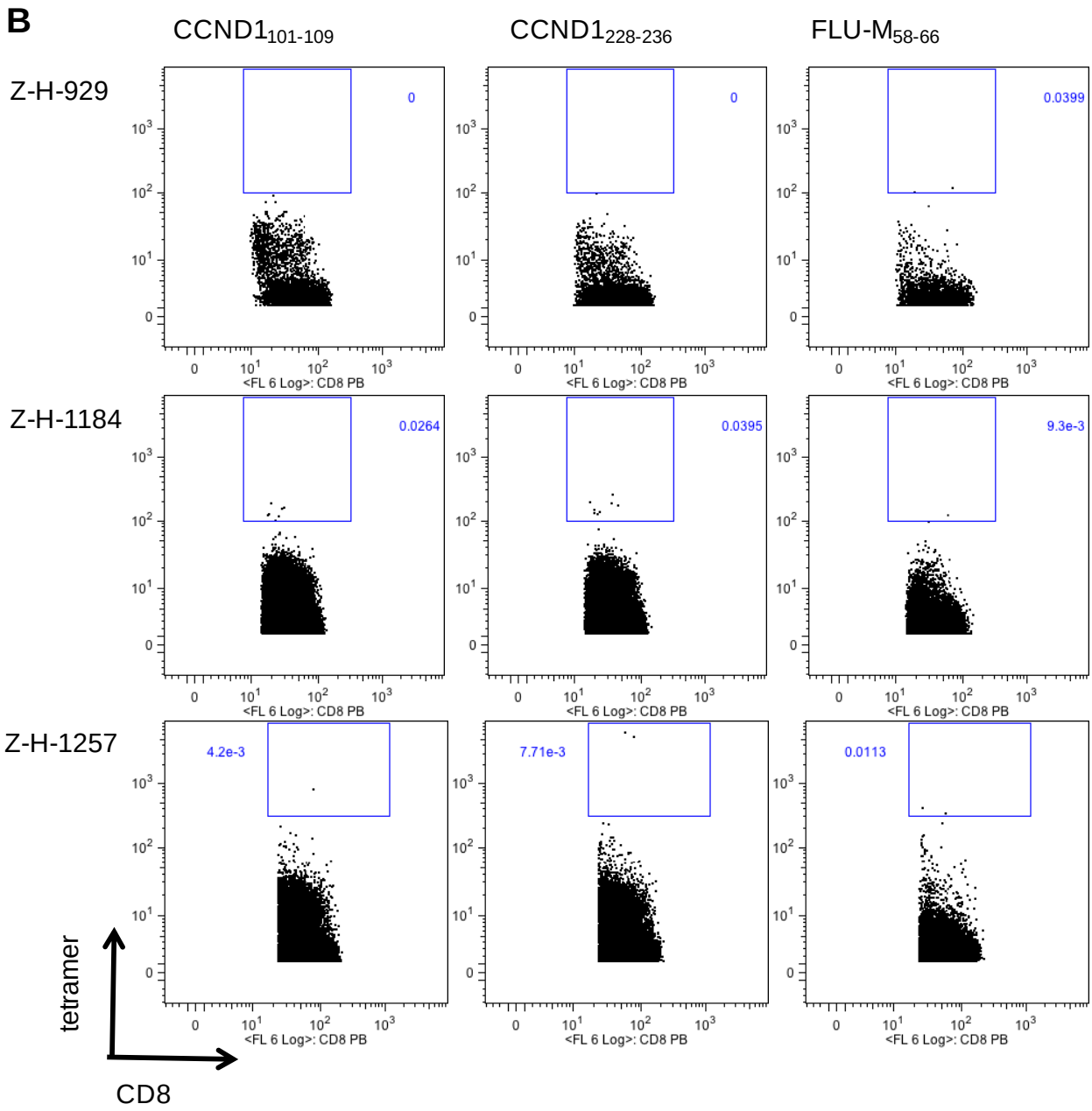

Supplementary Figure S1: Cyclin D1-specific tetramer staining in PBMCs and TILs of ccRCC patients

PBMCs (A) and TILs (B) were incubated with PE-conjugated Cyclin D1-specific tetramers and as a control with FLU-specific tetramers for 10 minutes at 37 °C, followed by incubation with CD45 APC, CD8 PasificBlue and live-dead stain (LIVE/DEAD® Fixable Aqua Dead Cell Stain Kit**,** Invitrogen) for 15 minutes at 4°C. Samples were measured with a CyAn ADP 9 (Beckman Coulter) and data were analyzed using the FlowJo software (TreeStar). Dot plots are shown after gating on live (aqua-) single CD45+ cells.

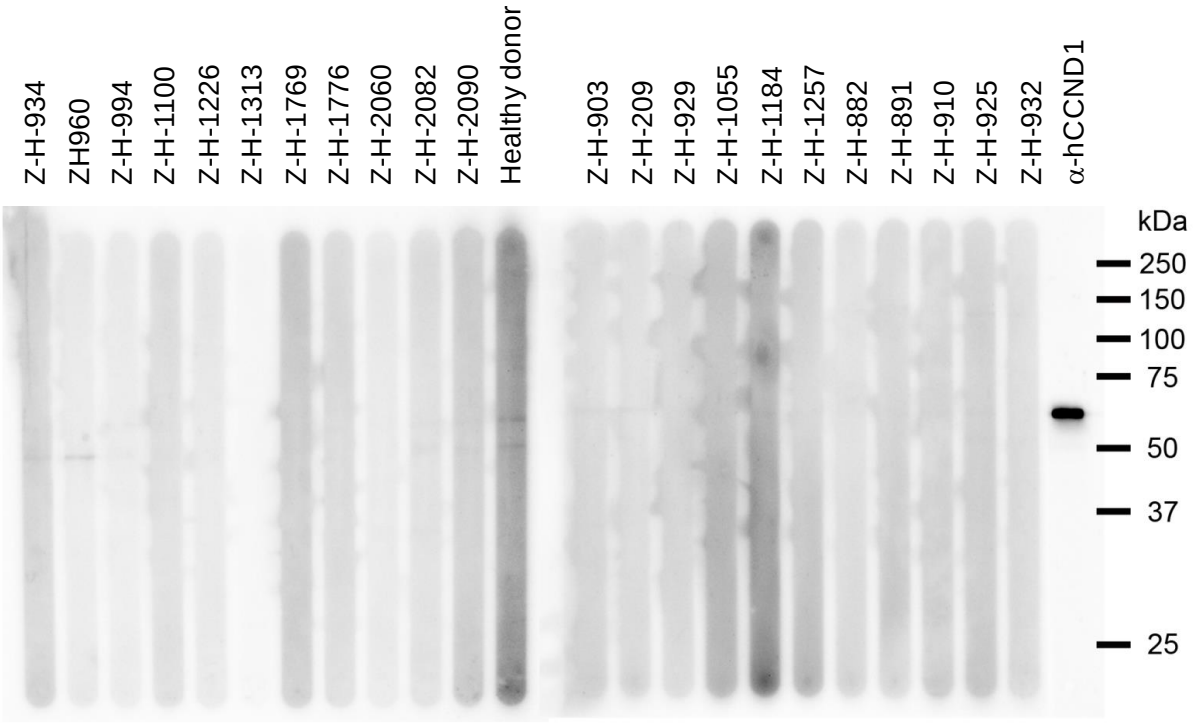

Supplementary Figure S2: Imunoblotting for Cyclin D1 in sera of ccRCC patients

Serum antibody response against the purified recombinant protein was tested by standard Western blot analysis using 3.6 mg of recombinant human Cyclin D1 (Abnova Cat.No. H00000595-PO1) and sera from 22 ccRCC patients at a 1:250 dilution. As positive control, purified MaxPab mouse polyclonal antibody anti-human CCND1 (Abnova Cat.No. H00000595-BO1P) was used at a 1:1000 dilution. As secondary reagents HRP-conjugated goat anti-mouse IgG (Jackson 115-035-008) was used for the positive control and HRP-conjugated goat anti-human IgG (Jackson 109-035-006) for the sera, both at a dilution of 1:25 000. Detection was done with Western Lightning Plus ECL reagents (Perkin Elmer Cat.No. NEL104001EA) on a Fusion FX7 machine (VILBER LOURMAT).

MATERIALS AND METHODS

Patients

Patients with ccRCC underwent full or partial nephrectomy as part of their standard treatment at the Department of Urology, University Hospital Zurich, within the years 2008 to 2011. Clinical specimens (tumor and peripheral whole blood) were obtained following informed consent in accordance with the Declaration of Helsinki. The local ethics committee approved the study (EK-1017, EK-1634). Detailed patients' characteristics are listed in **Table 1**. All patients were typed for HLA-A2 by flow cytometry using FITC-conjugated HLA-A2-specific or isotype control antibodies (BioLegend). Flow cytometry was performed on a CyAn ADP 9 (Beckman Coulter) and data were analyzed using the FlowJo software (TreeStar).

Processing of blood and tumor samples

PBMCs were isolated from peripheral blood by Ficoll (Ficoll-PaqueTM PLUS; GE Healthcare) density centrifugation and cryopreserved at -80°C until further analysis. Immediately after surgery one tumor tissue sample was snap-frozen in liquid nitrogen and another one was fixed in 4% buffered formalin and embedded in paraffin.

RNA isolation

Total RNA was extracted from snap-frozen ccRCC tumor samples using the RNeasy Mini Kit (Qiagen) and was subsequently digested with DNAse I (New England BioLabs) according to the manufacturer's instructions.

Real-time quantitative reverse transcription–polymerase chain reaction (qRT-PCR)

The concentration and purity of RNA was evaluated using the NanoDrop ND-1000 spectrophotometer (NanoDrop Technologies). Five hundred ng of RNA was reverse transcribed using the high-capacity cDNA Reverse Transcription Kit (Applied Biosystems) according to the manufacturer's instructions. The obtained cDNA was stored at -20 °C until qRT-PCR analysis. qRT-PCR was performed on a Rotor-Gene Q real-time PCR cycler (Qiagen) using commercially available predeveloped TaqMan reagents with optimized primer and probe concentrations (TaqMan® gene expression assays, Applied Biosystems) (**Table 2**). After an initial hold for 2 min at 50 °C and 10 min at 95 °C the probes were cycled 45 times at 95 °C for 15 sec and at 60 °C for 60 sec. All PCR reactions were performed in triplicates. Threshold cycle (CT) values were determined with the Rotor-Gene Q Series software 1.7. ΔCt values were calculated by normalizing the target mRNA levels to the endogenous control 18s-rRNA (Hs03928990_g1, Applied Biosystems). Testis cDNA served as a positive control for the expression analysis of CT antigens (human testes total RNA, Invitrogen). As qRT-PCR for MAGE-A9 suggested a low expression in the healthy kidney control (CT 35, ΔCT 30), expression in ccRCC specimens was only regarded positive at a CT < 35 and a ΔCt < 30. In the case of overexpressed antigens ΔCt

levels of tumors were compared to ΔCt levels of the healthy kidney control (human kidney total RNA, Invitrogen) using the $2^{-\Delta\Delta Ct}$ formula. Only changes ≥2 fold were considered as overexpression.

Genomic DNA extraction

Punch biopsies from paraffin-embedded ccRCC samples were incubated 10 min at 95 ºC with 300 µL of buffer containing 20 mM Tris pH 8.0, 20 mM EDTA pH 8.0 and 1% SDS. After cooling down, 3 µL of Proteinase K (18 +/- 4 mg/mL, Roche) were added to each sample and incubated at 55 ºC for 72 hours. Digested samples were centrifuged and 4 volumes of RLT buffer (AllPrep DNA/RNA Mini Kit, Qiagen) was added to the supernatant. Genomic DNA was then extracted following manufacturer's protocol.

Cyclin D1 sequencing

PCR amplification using purified genomic DNA was performed using the Phusion Hot Start High-Fidelity DNA Polymerase (Finnzymes) with the following PCR conditions: 10 min at 98 °C, followed by 34 cycles of 30 sec at 98 ºC, 30 sec at 68 ºC, 20 sec at 72 ºC with a final elongation of 5 min at 72 ºC. The sequences coding for the HLA-A2-restricted CTL epitope corresponding to Cyclin D1 amino acids 101-109 or 228-236 were amplified using forward primer 5'-TGCGAGGAACAGAAGTGCGA-3' / reverse primer 5'-TCCAGTGGTTACCAGCAGCTC-3' or forward primer 5'-TGCTCACAGCCTCCTTCCCT-3' / reverse primer 5'-TCGGCATTTCCGTGGCACTA-3' respectively. PCR products were purified using QIAquick Gel Extraction Kit (Qiagen) and sequenced using the same primers as those used for the amplification.

MACS sorting and *in vitro* stimulation

T cell stimulation was performed as previously described (49). Briefly, $CD8^+$ and $CD4^+$ T cells were sequentially isolated from PBMCs by positive selection using the MACS system (Miltenyi Biotech) according to manufacturer's instructions. The remaining $CD8^-CD4^-$ fraction was used as antigen presenting cells (APCs). APCs were loaded with relevant peptides at a concentration of 10^{-5} M for each peptide (**Table 2**). For *in vitro* stimulation 5×10^5 $CD8^+$ T cells were incubated with 5×10^5 loaded and irradiated (30 Gy) APCs in 96-well flatbottom plates. Cellswere cultured for 9 days in 200 µL TC-RPMI (*i.e*. RPMI (Gibco), supplemented with $NaHCO_3$ (2 g/L, Sigma), L-glutamine (2 mM, Sigma), penicillin and streptomycin (50 U/mL, Gibco), MEM nonessential amino acids (1X, Gibco), sodiumpyruvate (1 mM, Gibco), 10^{-4} M β-mercaptoethanol (Sigma) and 10% pooled human serum) plus DNaseI (6 U/mL, Sigma)). T-APCs were generated from purified autologous $CD4^+$ T cells by stimulation with 1 µg/mL phytohemagglutinin (PHA, Sigma) and 100 U/mL recombinant IL-2 (R&D Systems) during 9 days. T-APCs were used as APCs during the

short *in vitro* stimulation before intracellular cytokine staining. Media was exchanged every second day by TC-RPMI containing 25 U/mL IL-2.

Intracellular cytokine staining (ICS)

The presence of TAA-specific T cells was tested by short-term restimulation with the relevant peptides, followed by intracellular cytokine staining. Briefly, T cells were stimulated with peptide-loaded autologous T-APCs at a 1:2 ratio for 5 h in the presence of Brefeldin A (10 µg/mL, Sigma), monensin (10 µg/mL, Sigma), 1 µg/mL anti-CD28/49d (BD) and appropriately diluted phycoerythrin (PE)-labeled anti-CD107a antibody. Before addition to the assay T-APCs were labeled with 2 µM carboxyfluorescein succinimidyl ester (CFSE, Sigma), which allowed their exclusion before analysis. Surface staining for CD45-PerCP, CD3-PacificOrange (Invitrogen), CD8-ECD (Beckman Coulter), CD14-FITC, CD16-FITC, CD19-FITC, and live-dead staining (LIVE/DEAD® Fixable Green Dead Cell Stain Kit**,** Invitrogen) was performed in PBS (NaCl (136mM, Fluka), Na_2HPO_4 (8mM, Roth), KH_2PO_4 (1.5mM, Roth), pH7) for 20 min at room temperature. Subsequently, cells were fixed with 4% formalin (Kantonsapotheke Zurich) and incubated for 5 min at RT with permeabilization buffer (PB: PBS supplemented with 2mM EDTA (Sigma), 2% FCS (PAA Laboratories), 0.05% NaN_3 (Sigma) and 0.1% Saponin (Sigma)). Intracellular staining was performed using IFNγ-APC, TNFα-PECy7 (ebiosciences) and IL2-PacificBlue antibodies in PB for 20 min at room temperature in the dark. Cells were washed once with PB and resuspended in PBS containing 1% formalin. Samples were measured with a CyAn ADP 9 (Beckman Coulter) and data were analyzed using the FlowJo software (TreeStar). Unless stated differently, all antibodies were purchased from BioLegend.

REFERENCES

1. Schreiber, R.D., Old, L.J., and Smyth, M.J. 2011. Cancer immunoediting: integrating immunity's roles in cancer suppression and promotion. *Science* 331:1565-1570.
2. Fridman, W.H., Pages, F., Sautes-Fridman, C., and Galon, J. 2012. The immune contexture in human tumours: impact on clinical outcome. *Nat Rev Cancer* 12:298-306.
3. Vesely, M.D., Kershaw, M.H., Schreiber, R.D., and Smyth, M.J. 2011. Natural innate and adaptive immunity to cancer. *Annu Rev Immunol* 29:235-271.
4. Smyth, M.J., Godfrey, D.I., and Trapani, J.A. 2001. A fresh look at tumor immunosurveillance and immunotherapy. *Nat Immunol* 2:293-299.
5. Mellman, I., Coukos, G., and Dranoff, G. 2011. Cancer immunotherapy comes of age. *Nature* 480:480-489.
6. Moch, H., Gasser, T., Amin, M.B., Torhorst, J., Sauter, G., and Mihatsch, M.J. 2000. Prognostic utility of the recently recommended histologic classification and revised TNM staging system of renal cell carcinoma: a Swiss experience with 588 tumors. *Cancer* 89:604-614.
7. Vickers, M.M., and Heng, D.Y. 2010. Prognostic and predictive biomarkers in renal cell carcinoma. *Target Oncol* 5:85-94.
8. Motzer, R.J., and Bukowski, R.M. 2006. Targeted therapy for metastatic renal cell carcinoma. *Journal of clinical oncology : official journal of the American Society of Clinical Oncology* 24:5601-5608.
9. Itsumi, M., and Tatsugami, K. 2010. Immunotherapy for renal cell carcinoma. *Clin Dev Immunol* 2010:284581.
10. Oehlrich, N., Devitt, G., Linnebacher, M., Schwitalle, Y., Grosskinski, S., Stevanovic, S., and Zoller, M. 2005. Generation of RAGE-1 and MAGE-9 peptide-specific cytotoxic T-lymphocyte lines for transfer in patients with renal cell carcinoma. *Int J Cancer* 117:256-264.
11. Vissers, J.L., De Vries, I.J., Schreurs, M.W., Engelen, L.P., Oosterwijk, E., Figdor, C.G., and Adema, G.J. 1999. The renal cell carcinoma-associated antigen G250 encodes a human leukocyte antigen (HLA)-A2.1-restricted epitope recognized by cytotoxic T lymphocytes. *Cancer Res* 59:5554-5559.
12. Kruger, T., Schoor, O., Lemmel, C., Kraemer, B., Reichle, C., Dengjel, J., Weinschenk, T., Muller, M., Hennenlotter, J., Stenzl, A., et al. 2005. Lessons to be learned from primary renal cell carcinomas: novel tumor antigens and HLA ligands for immunotherapy. *Cancer Immunol Immunother* 54:826-836.
13. Gouttefangeas, C., Stenzl, A., Stevanovic, S., and Rammensee, H.G. 2007. Immunotherapy of renal cell carcinoma. *Cancer Immunol Immunother* 56:117-128.
14. Walter, A., Barysch, M.J., Behnke, S., Dziunycz, P., Schmid, B., Ritter, E., Gnjatic, S., Kristiansen, G., Moch, H., Knuth, A., et al. 2010. Cancer-testis antigens and immunosurveillance in human cutaneous squamous cell and basal cell carcinomas. *Clin Cancer Res* 16:3562-3570.
15. Bolli, M., Schultz-Thater, E., Zajac, P., Guller, U., Feder, C., Sanguedolce, F., Carafa, V., Terracciano, L., Hudolin, T., Spagnoli, G.C., et al. 2005. NY-ESO-1/LAGE-1 coexpression with MAGE-A cancer/testis antigens: a tissue microarray study. *Int J Cancer* 115:960-966.
16. von Boehmer, L., Keller, L., Mortezavi, A., Provenzano, M., Sais, G., Hermanns, T., Sulser, T., Jungbluth, A.A., Old, L.J., Kristiansen, G., et al. 2011. MAGE-C2/CT10 protein expression is an independent predictor of recurrence in prostate cancer. *PLoS One* 6:e21366.
17. Yamanaka, K., Miyake, H., Hara, I., Gohji, K., Arakawa, S., and Kamidono, S. 1998. Expression of MAGE genes in renal cell carcinoma. *Int J Mol Med* 2:57-60.
18. Ringhoffer, M., Muller, C.R., Schenk, A., Kirsche, H., Schmitt, M., Greiner, J., and Gschwend, J.E. 2004. Simultaneous expression of T-cell activating antigens in renal cell carcinoma: implications for specific immunotherapy. *J Urol* 171:2456-2460.
19. Scanlan, M.J., Simpson, A.J., and Old, L.J. 2004. The cancer/testis genes: review, standardization, and commentary. *Cancer Immun* 4:1.
20. Neumann, E., Engelsberg, A., Decker, J., Storkel, S., Jaeger, E., Huber, C., and Seliger, B. 1998. Heterogeneous expression of the tumor-associated antigens RAGE-1, PRAME,

and glycoprotein 75 in human renal cell carcinoma: candidates for T-cell-based immunotherapies? *Cancer Res* 58:4090-4095.
21. Jungbluth, A.A., Chen, Y.T., Stockert, E., Busam, K.J., Kolb, D., Iversen, K., Coplan, K., Williamson, B., Altorki, N., and Old, L.J. 2001. Immunohistochemical analysis of NY-ESO-1 antigen expression in normal and malignant human tissues. *Int J Cancer* 92:856-860.
22. Chen, Y.T., Scanlan, M.J., Sahin, U., Tureci, O., Gure, A.O., Tsang, S., Williamson, B., Stockert, E., Pfreundschuh, M., and Old, L.J. 1997. A testicular antigen aberrantly expressed in human cancers detected by autologous antibody screening. *Proc Natl Acad Sci U S A* 94:1914-1918.
23. Gaugler, B., Brouwenstijn, N., Vantomme, V., Szikora, J.P., Van der Spek, C.W., Patard, J.J., Boon, T., Schrier, P., and Van den Eynde, B.J. 1996. A new gene coding for an antigen recognized by autologous cytolytic T lymphocytes on a human renal carcinoma. *Immunogenetics* 44:323-330.
24. Frew, I.J., and Krek, W. 2008. pVHL: a multipurpose adaptor protein. *Science signaling* 1:pe30.
25. Murakami, Y., Kanda, K., Tsuji, M., Kanayama, H., and Kagawa, S. 1999. MN/CA9 gene expression as a potential biomarker in renal cell carcinoma. *BJU international* 83:743-747.
26. Vissers, J.L., De Vries, I.J., Engelen, L.P., Scharenborg, N.M., Molkenboer, J., Figdor, C.G., Oosterwijk, E., and Adema, G.J. 2002. Renal cell carcinoma-associated antigen G250 encodes a naturally processed epitope presented by human leukocyte antigen-DR molecules to CD4(+) T lymphocytes. *Int J Cancer* 100:441-444.
27. Oosterwijk, E., Debruyne, F.M., and Schalken, J.A. 1995. The use of monoclonal antibody G250 in the therapy of renal-cell carcinoma. *Semin Oncol* 22:34-41.
28. Bleumer, I., Tiemessen, D.M., Oosterwijk-Wakka, J.C., Voller, M.C., De Weijer, K., Mulders, P.F., and Oosterwijk, E. 2007. Preliminary analysis of patients with progressive renal cell carcinoma vaccinated with CA9-peptide-pulsed mature dendritic cells. *J Immunother* 30:116-122.
29. Bauer, S., Oosterwijk-Wakka, J.C., Adrian, N., Oosterwijk, E., Fischer, E., Wuest, T., Stenner, F., Perani, A., Cohen, L., Knuth, A., et al. 2009. Targeted therapy of renal cell carcinoma: synergistic activity of cG250-TNF and IFNg. *Int J Cancer* 125:115-123.
30. Hernandez, J.M., Bui, M.H., Han, K.R., Mukouyama, H., Freitas, D.G., Nguyen, D., Caliliw, R., Shintaku, P.I., Paik, S.H., Tso, C.L., et al. 2003. Novel kidney cancer immunotherapy based on the granulocyte-macrophage colony-stimulating factor and carbonic anhydrase IX fusion gene. *Clin Cancer Res* 9:1906-1916.
31. Schmidt, S.M., Schag, K., Muller, M.R., Weinschenk, T., Appel, S., Schoor, O., Weck, M.M., Grunebach, F., Kanz, L., Stevanovic, S., et al. 2004. Induction of adipophilin-specific cytotoxic T lymphocytes using a novel HLA-A2-binding peptide that mediates tumor cell lysis. *Cancer Res* 64:1164-1170.
32. Schag, K., Schmidt, S.M., Muller, M.R., Weinschenk, T., Appel, S., Weck, M.M., Grunebach, F., Stevanovic, S., Rammensee, H.G., and Brossart, P. 2004. Identification of C-met oncogene as a broadly expressed tumor-associated antigen recognized by cytotoxic T-lymphocytes. *Clin Cancer Res* 10:3658-3666.
33. Weinberg, R.A. 1995. The retinoblastoma protein and cell cycle control. *Cell* 81:323-330.
34. Bartkova, J., Lukas, J., Strauss, M., and Bartek, J. 1994. The PRAD-1/cyclin D1 oncogene product accumulates aberrantly in a subset of colorectal carcinomas. *Int J Cancer* 58:568-573.
35. Zhang, S.Y., Caamano, J., Cooper, F., Guo, X., and Klein-Szanto, A.J. 1994. Immunohistochemistry of cyclin D1 in human breast cancer. *Am J Clin Pathol* 102:695-698.
36. Hedberg, Y., Davoodi, E., Roos, G., Ljungberg, B., and Landberg, G. 1999. Cyclin-D1 expression in human renal-cell carcinoma. *Int J Cancer* 84:268-272.
37. Lin, B.T., Brynes, R.K., Gelb, A.B., McCourty, A., Amin, M.B., and Medeiros, L.J. 1998. Cyclin D1 expression in renal carcinomas and oncocytomas: an immunohistochemical study. *Mod Pathol* 11:1075-1081.
38. Dahinden, C., Ingold, B., Wild, P., Boysen, G., Luu, V.D., Montani, M., Kristiansen, G., Sulser, T., Buhlmann, P., Moch, H., et al. 2010. Mining tissue microarray data to uncover combinations of biomarker expression patterns that improve intermediate staging and

grading of clear cell renal cell cancer. *Clinical cancer research : an official journal of the American Association for Cancer Research* 16:88-98.
39. Odunsi, K., Qian, F., Matsuzaki, J., Mhawech-Fauceglia, P., Andrews, C., Hoffman, E.W., Pan, L., Ritter, G., Villella, J., Thomas, B., et al. 2007. Vaccination with an NY-ESO-1 peptide of HLA class I/II specificities induces integrated humoral and T cell responses in ovarian cancer. *Proc Natl Acad Sci U S A* 104:12837-12842.
40. Boss, C.N., Grunebach, F., Brauer, K., Hantschel, M., Mirakaj, V., Weinschenk, T., Stevanovic, S., Rammensee, H.G., and Brossart, P. 2007. Identification and characterization of T-cell epitopes deduced from RGS5, a novel broadly expressed tumor antigen. *Clin Cancer Res* 13:3347-3355.
41. Wolfel, T., Hauer, M., Schneider, J., Serrano, M., Wolfel, C., Klehmann-Hieb, E., De Plaen, E., Hankeln, T., Meyer zum Buschenfelde, K.H., and Beach, D. 1995. A p16INK4a-insensitive CDK4 mutant targeted by cytolytic T lymphocytes in a human melanoma. *Science* 269:1281-1284.
42. Musgrove, E.A., Caldon, C.E., Barraclough, J., Stone, A., and Sutherland, R.L. 2011. Cyclin D as a therapeutic target in cancer. *Nature reviews. Cancer* 11:558-572.
43. Krause, D.S., and Van Etten, R.A. 2005. Tyrosine kinases as targets for cancer therapy. *The New England journal of medicine* 353:172-187.
44. Kondo, E., Maecker, B., Weihrauch, M.R., Wickenhauser, C., Zeng, W., Nadler, L.M., Schultze, J.L., and von Bergwelt-Baildon, M.S. 2008. Cyclin D1-specific cytotoxic T lymphocytes are present in the repertoire of cancer patients: implications for cancer immunotherapy. *Clin Cancer Res* 14:6574-6579.
45. Dao, T., Korontsvit, T., Zakhaleva, V., Haro, K., Packin, J., and Scheinberg, D.A. 2009. Identification of a human cyclin D1-derived peptide that induces human cytotoxic CD4 T cells. *PLoS One* 4:e6730.
46. Dengjel, J., Decker, P., Schoor, O., Altenberend, F., Weinschenk, T., Rammensee, H.G., and Stevanovic, S. 2004. Identification of a naturally processed cyclin D1 T-helper epitope by a novel combination of HLA class II targeting and differential mass spectrometry. *Eur J Immunol* 34:3644-3651.
47. Wang, M., Sun, L., Qian, J., Han, X., Zhang, L., Lin, P., Cai, Z., and Yi, Q. 2009. Cyclin D1 as a universally expressed mantle cell lymphoma-associated tumor antigen for immunotherapy. *Leukemia : official journal of the Leukemia Society of America, Leukemia Research Fund, U.K* 23:1320-1328.
48. Shi, F.D., Zhang, J.Y., Liu, D., Rearden, A., Elliot, M., Nachtsheim, D., Daniels, T., Casiano, C.A., Heeb, M.J., Chan, E.K., et al. 2005. Preferential humoral immune response in prostate cancer to cellular proteins p90 and p62 in a panel of tumor-associated antigens. *Prostate* 63:252-258.
49. Nuber, N., Curioni-Fontecedro, A., Matter, C., Soldini, D., Tiercy, J.M., von Boehmer, L., Moch, H., Dummer, R., Knuth, A., and van den Broek, M. 2010. Fine analysis of spontaneous MAGE-C1/CT7-specific immunity in melanoma patients. *Proc Natl Acad Sci U S A* 107:15187-15192.

ACKNOWLEDGEMENTS

We thank Maurizio Provenzano and Giovanni Sais (Department of Urology, University Hospital Zurich) for advice in planning the qRT-PCR experiment. This work was supported in part by the Cancer Research Institute/Cancer Vaccine Collaborative, the Hanne Liebermann Foundation, Dr. Leopold and Carmen Ellinger Foundation Zurich, Science Foundation Oncology SFO (31-135792), Swiss National Science Foundation (3238BO, 103145), the Hartmann Müller Foundation Zurich and Alumni Grant University Zurich.

2.2 Tumor-associated macrophages subvert T cell function and correlate with reduced survival in clear cell renal cell carcinoma

Manuscript accepted for publication in OncoImmunology

Authors: Stefanie Regine Dannenmann, Julia Thielicke, Martina Stöckli, Claudia Matter, Lotta von Boehmer, Virginia Cecconi, Thomas Hermanns, Lukas Hefermehl, Peter Hans Schraml, Holger Moch, Alexander Knuth and Maries van den Broek

Contributions: SRD and MvdB designed the experiments and wrote the manuscript. SRD conducted and analyzed all experiments. MS, JT and CM contributed to gene-profiling. VC contributed to cell sorting.

Tumor-associated macrophages subvert T cell function and correlate with reduced survival in clear cell renal cell carcinoma

Stefanie Regine Dannenmann[1], Julia Thielicke[1], Martina Stöckli[1], Claudia Matter[1], Lotta von Boehmer[1], Virginia Cecconi[1], Thomas Hermanns[2], Lukas Hefermehl[2], Peter Hans Schraml[3], Holger Moch[3], Alexander Knuth[1], Maries van den Broek[1,4]
University Hospital Zurich, Departments of [1]Oncology, [2]Urology, and [3]Pathology, Zurich, Switzerland.
[4]Corresponding author: Maries van den Broek, University Hospital Zurich, Department of Oncology, Wagistrasse 14, CH-8592 Schlieren, Switzerland. Tel.: +41 44 556 3134, email: maries@van-den-broek.ch

ABSTRACT

Malignant cells are recognized and controlled by the immune system, however, in patients with clinically apparent cancer immune surveillance failed. To better understand local immunoregulatory processes that impact on disease progression, we correlated intratumoral immunological profiles with survival in patients with primary clear cell renal cell carcinoma (ccRCC). A retrospective analysis of 54 primary ccRCCs for 31 different immune response-related transcripts, revealed a negative correlation of CD68 (tumor-associated macrophages, TAMs) and FoxP3 (regulatory T cells, Tregs) with survival. Subsequent analysis for 12 TAM-related transcripts showed an association of the M2-signature genes CD163, IRF-4 and FN-1 with reduced survival and increased tumor stage, whereas the opposite was the case for the M1-associated gene iNOS.
The M2-signature of TAMs ($CD68^+$) was found to be associated with CD163 expression as determined in prospectively collected fresh ccRCC tissue samples. Upon coculture with autologous tumor cells $CD11b^+$ cells isolated from paired blood samples expressed CD163 and other M2-associated genes, suggesting that the tumor promotes the accumulation of M2 TAMs. Furthermore, the tumor-associated milieu as well as sorted TAMs induced skewing of autologous, blood-derived $CD4^+$ T cells towards a more regulated phenotype as shown by decreased production of effector cytokines, increased production of IL-10 and enhanced expression of the co-inhibitory molecules PD-1 and Tim-3.
Together, our data suggest that ccRCC progressively attracts macrophages and induces their skewing into M2 TAMs that subvert tumor-infiltrating T cells such that regulating functions are increased at the expense of effector functions.

INTRODUCTION

It is well established that the immune system recognizes and can destroy tumor cells and the association between immune infiltration and patient prognosis was described in many different cancers (1). However, the interactions between immune cells and tumor cells are complex and we are only beginning to understand them. According to the current view, cancer and immune cells mutually influence each other, ultimately resulting in escape from immunological control in patients with overt cancer (2). Besides tumor cell-intrinsic escape mechanisms including downregulation of MHC molecules and/or tumor-associated antigens (TAAs), tumors can create an environment, which interferes with immune effector mechanisms. This includes immunosuppressive cytokines such as IL-10 and TGF-β (3, 4) and the generation and recruitment of immunoregulatory cell types such as regulatory T cells (Tregs) and tumor-associated macrophages (TAMs) including myeloid derived suppressor cells (MDSC) (5-7). CD68 is expressed by macrophages and there is evidence from preclinical models that TAMs are tumor-promoting by stimulating angiogenesis, tumor cell proliferation and metastasis, but also because they contribute to subversion of adaptive immune responses (8). TAMs show a remarkable degree of plasticity and it was shown that the conversion of proinflammatory M1 macrophages to so-called alternatively activated M2 macrophages (9) or the preferential accumulation (10) of the latter subtype in tumors is crucial for their tumor-promoting effect. M1 macrophages express the transcription factor IRF-5 (11) and are thought to exert anti-tumoricidal activities because of an IL-12^{high} IL-10^{low} phenotype (5) and high expression of inducible nitric oxide synthetase (iNOS) (12), which results in increased production of NO. M2 macrophages express the transcription factor IRF4 (13) and are characterized by an $IL12^{low}$ $IL10^{high}$ phenotype (5), the expression of the scavenger receptor CD163 (14), the mannose receptor (MR) (15), and increased levels of fibronectin 1 (FN-1) (16).

The clinical outcome of renal cell cancer (RCC) varies considerably, especially in tumors presenting without metastases. The prognosis for localized disease is good with a five-year survival rate of more than 90% after removing the tumor via radical or partial nephrectomy (17). However, due to the lack of symptoms, about one-third present metastatic disease at time of diagnosis, and 25-50% of patients treated for local disease will develop metastasis (18). In the case of metastatic RCC the survival rate drops dramatically with a five-year survival rate of less than 15%. Treatment is difficult due to resistance to radio- and chemotherapy (19).

RCCs are considered immunogenic tumors that are frequently infiltrated by immune cells (20). In contrast to breast and bladder and other cancers (reviewed in(1)), a high number of tumor infiltrating leukocytes (TILs) is associated with poor prognosis in RCC (21). To better understand the local mechanisms that preclude immunological control of clinically apparent RCC, we correlated intratumoral immunological profiles with survival and tumor stage (pT) in patients with primary clear cell renal cell carcinoma (ccRCC), which is the most frequent subtype of RCC.

Furthermore, we investigated the impact of the tumor microenvironment on T cell phenotype and function.

RESULTS

Correlation between the expression of immune response-related transcripts and survival in ccRCC

To better understand the local mechanisms that preclude immunological control of clinically apparent RCC, we correlated intratumoral immunological profiles with survival in 54 patients with primary ccRCC, We retrospectively analyzed the expression of 31 immune response-related transcripts (**Supplementary Table S1A**) by qRT-PCR analysis using a collection of formalin-fixed paraffin-embedded (FFPE) tumor tissue of ccRCC patients with known tumor size and course of disease. Samples of patients, who died of tumor-unrelated causes, were excluded from the analysis (**Supplementary Table S2**). We found no significant correlation using the Cox proportional hazard model between the degree of leukocyte infiltration (Ct values of CD45 normalized to 18S rRNA) and survival (**Fig. 1A**).

Subsequently, we determined transcripts for immune response-related genes after normalization to CD45, which enables the analysis of the infiltrate quality independent of the degree of infiltration. We correlated each of the 33 transcripts with survival using Cox regression analysis and present these data in **Fig. 1A** and **Supplementary Fig. S1**. We excluded the data for LT-α, Arginase 1, BTLA, IL-2 and IL-17 from the analysis because of very low or undetectable expression. Univariate Cox regression analysis revealed a significant correlation of high FoxP3 (Treg) mRNA and of high CD68 (macrophages) mRNA with reduced survival, whereas CD3 transcripts (T cells) did not correlate with patient survival (**Fig. 1A**). We correlated the expression of CD68 transcripts with CD3, CD4 and CD8 transcripts and found no correlation between CD68/CD3 (correlation coefficient -0.082, two-tailed p=0.556) or CD68/CD8 (correlation coefficient -0.031, two-tailed p=0.882), but a significant correlation between CD68/CD4 (correlation coefficient 0.391, two-tailed p=0.003). The latter correlation is a positive one, which presumably reflects the co-existence of macrophages and regulatory T cells. Furthermore, high expression levels of perforin and TNF-α showed a correlation with increased survival, while high expression levels of LT-βR showed a correlation with reduced survival (**Supplementary Fig. S1A**). Since, significance for these 3 genes was only achieved with one of the statistical tests and clearly not with the other test, these genes were not considered to significantly correlate with survival. In the case of CTLA-4 and IL-10 in a few samples no signal was observed, and an estimated value (Ct=40) was set for these samples (**Supplementary Fig. S1A**). When those “no-signal” samples were excluded from the analysis, high expression values of CTLA-4 and IL-10 significantly correlated with reduced survival (**Supplementary Fig. S1B**). Also for other genes

(marked with an asterisk **Supplementary Fig. S1A**) no signal was detected in a few samples, however statistical analysis did not reveal different results when “no-signal” samples were excluded (data not shown).

While correlation of FoxP3 expression and survival just reached the level of significance using univariate Cox regression analysis, the correlation between CD68 mRNA levels and reduced survival was independent of tumor size and patients’ age as assessed by multivariate Cox regression analysis (Fig.1 legend). To validate the qRT-PCR results, we performed immunohistochemical staining for CD68 on seven ccRCC tumor samples and found a clear correlation between CD68 expression measured by qRT-PCR and immunohistochemistry in all seven samples (four examples shown in **Supplementary Fig. S2**).

The expression of M2-associated transcripts correlates with reduced survival in ccRCC

To further investigate the phenotype and impact of TAMs on patient survival, we analyzed the same samples (**Supplementary Table S2**) for another 12 TAM-associated genes (**Supplementary Table S1B and Figure S1C**). We found a significant correlation between low iNOS transcripts and decreased survival and a similar trend for high CD163 transcripts and decreased survival (**Fig. 1B**). Multivariate Cox regression analysis revealed that both correlations are independent of pT and patients’ age (Fig.1 legend). Along the same line, high expression of the M2-associated genes FN-1 and IRF-4 showed a tendency to correlate with reduced survival **(Fig. 1B)**. Furthermore, we observed a positive correlation between transcripts of CD163 and the M2-associated genes MR, IL-10 and FN-1 as well as a negative correlation between CD163 and the M1 marker iNOS (**Fig. 1C**) suggesting that TAMs with an M2-like signature impact on reduced survival of patients with ccRCC.

$CD163^{high}$ tumor-associated macrophages (TAMs) have an M2-phenotype

We further characterized TAMs by flowcytometry in 12 fresh primary ccRCC tumor tissue samples. Tumors from most patients contained a subpopulation of $CD45^{+}CD3^{-}CD19^{-}CD68^{+}CD11b^{+}CD163^{high}$ cells (termed T_2 population hereafter), which was absent in matched blood samples. In blood as well as in tumors we found a P_1 and T_1 population, respectively, both of which were characterized as $CD45^{+}CD3^{-}CD19^{-}CD68^{+}CD11b^{+}CD163^{low}$ (**Fig. 2A**). Both T_1 and T_2 TAMs expressed higher levels of MHC class II than P_1 cells, suggesting that TAMs are activated (**Fig. 2B, Supplementary Fig. S4**). Based on the high expression of CD163 and the mannose receptor (MR), the T_2 population classifies as M2 TAMs. Furthermore, the T_2 but not the T_1 or P_1 population showed increased expression of the programmed death ligand 1 (PD-L1) **(Fig. 2B and Supplementary Fig. S4).** To further strengthen the presumption that CD163 associates with M2 TAMs, we performed qRT-PCR analysis on sorted T_2 TAMs for different M1- and M2-related genes (**Supplementary Table S1B and parts of S1A**). When we compared T_2 and P_1 cells for expression of M2-associated genes, we found a strong increase of FN-1 and IL-10 and even a slight increase of IRF-4 and the transcription factor c-MYC(22) in the T_2

population, whereas the expression of the M1-associated genes IRF-5, iNOS and IL-12 was low (**Fig. 2C**). Except for elevated expression of CD163 and MR, no clear differences of M1 and M2 genes were observed in T_2 compared to T_1 population on the mRNA level (**Supplementary Fig. S5**).

The expression of M2-associated transcripts correlates with tumor progression

RCC patients who develop metastasis, have a poor prognosis with a 5-year survival rate of less than 15% (23). We observed a correlation of short survival with the incidence of metastasis (**Fig. 3A**). Also high levels of transcripts for FoxP3 or CD68 correlated with the incidence of metastasis, whereas CD45 and CD3 expression did not (**Fig. 3B**). A correlation between macrophages and metastasis has been suggested for other cancer types (24). In this context, a role for the paracrine and autocrine axis of the colony-stimulating factor-1 (CSF-1) and the epidermal growth factor (EGF) (25) as well as for the actin-binding protein mammalian enabled (Mena) (26). However, in the cohort of primary ccRCC patients we analysed, we did not find a significant correlation between CSF-1, EGF, their receptors and Mena with survival (**Supplementary Figure S1C**).

We found a significant correlation between low iNOS transcripts and increased tumor stage (pT) and a similar trend for high CD163 transcripts (**Fig. 3C**). These data suggest a progressive accumulation of or conversion to $CD163^{high}$ M2 macrophages at the expense of $iNOS^{high}$ M1 macrophages in ccRCC, which correlates with reduced survival of patients with ccRCC.

ccRCC tumor cells contribute to M1 → M2 conversion of myeloid cells

To investigate whether freshly isolated ccRCC tumor cells can induce tumor-promoting changes in myeloid cells, we sorted P_1 cells from blood and $CD45^-$ cells from simultaneously processed tumor tissue samples and co-incubated P_1 cells with autologous $CD45^-$ cells for 48 h at a 1:3 ratio followed by analysis of P_1 cells. Coculture induced an upregulation of CD163 and MR in blood-derived myeloid cells on the protein level (**Supplementary Fig. S6A**). On the mRNA level a slight increase in the M2-related genes CD163, c-MYC and IL-10 was observed and a strong rise in FN-1 (**Supplementary Fig. S6B**). Furthermore, the M1-associated gene iNOS was induced in two samples while IL-12 was not expressed in two samples and lost in one sample upon coculture with tumor cells. Because we only had sufficient material from a limited number of patients, we could not investigate this phenomenon in more patients.

In summary, the $CD45^+CD3^-CD19^-CD68^+CD11b^+CD163^{high}$ T_2 population, which is found in ccRCC tumors but not in paired blood samples, shows features of tumor-promoting TAMs with an M2-like signature. Our observation that the level of CD163 transcripts in the tumor correlates with reduced survival and increased pT supports this. Furthermore, we showed that tumor cells contribute to M1 → M2 skewing, which is in line with the progressive accumulation of T_2 TAMs in ccRCC.

The ccRCC microenvironment impacts on the phenotype and function of T cells

We noticed a correlation of high transcript levels of FoxP3 and IL-10 with increased tumor stage (**Supplementary Fig. S7**), suggesting a progressive accumulation of Tregs and IL-10 in the tumor. To investigate the impact of the immunoregulatory tumor microenvironment on the phenotype and function of T cells we sorted $CD45RA^-CD4^+$ and $CD45RA^-CD8^+$ T cells from fresh ccRCC (**Supplementary Table S4**) and from paired blood samples. We sorted $CD45RA^-$ (antigen-experienced) T cells because the proportion of antigen-experienced T cells in tumors was much higher than in paired blood samples (**Fig. 4A**) and these T cells have a lower threshold for *in vitro* cytokine production upon stimulation than naïve T cells (27). Levels of transcripts for effector cytokines including TNF-α, IFN-γ, IL-2 and for the cytotoxic effector molecule Granzyme B were higher in tumor-derived $CD4^+$ and $CD8^+$ T cells than in blood-derived $CD4^+$ and $CD8^+$ T cells (**Fig. 4B, C**). At the same time, however, tumor-derived T cells displayed high mRNA levels of immunoregulatory molecules including PD-1, Tim-3 and CTLA-4 and also of the immunosuppressive cytokine IL-10. Furthermore, tumor-derived $CD4^+$ T cells expressed higher levels of the transcription factor FoxP3, IL-17 and the Th2 cytokines IL-4 and IL-13. Only a slight increase in TGF-β was observed in TILs, which may be explained by the fact that TGF-β is mainly regulated post translationally (**Fig. 4B, C**). By flowcytometry we confirmed the activated stage of TIL-derived T cells by the strong expression of the activation marker CD69 and also confirmed the increased expression of PD-1, Tim-3, CTLA-4 and FoxP3 on the protein level (**Fig.5 A and B, Supplementary Fig. S8**). Together these data suggest that ccRCCs are sites with an active immune response, which has features reminiscent of immune regulation or chronic inflammation (28, 29).

To confirm the changed cytokine profile in tumor-derived T cells on the protein level and to investigate the role of the tumor microenvironment on these functional deviations towards a more regulated phenotype, we polyclonally stimulated $CD45RA^-$ antigen-experienced T cells in the presence of the entire tumor digest and compared their cytokine production with that of $CD45RA^-$ T cells from the same source but that were previously sorted. The production of the effector cytokines IFN-γ and IL-2 by sorted $CD4^+$ T cells was higher, whereas the production of the immunoregulatory cytokine IL-10 was lower compared to the same T cells in the presence of their natural tumor environment (**Fig. 6A**). The difference in effector cytokine production between sorted and non-sorted cells was less pronounced for $CD8^+$ T cells, whereas the production of IL-10 was supported by the presence of the tumor (**Fig. 6B**). We detected a very low percentage of IL-17-producing cells that was comparable in sorted and non-sorted cells (**Supplementary Fig. S9**). We conclude that the tumor microenvironment induced skewing towards a more regulated phenotype upon T cell receptor (TCR)-dependent (anti-CD3/CD28-coated beads) as well as–independent (PMA plus ionomycin) stimulation.

M2 TAMs impact on the cytokine profile of $CD4^+$ T cells

TAMs have been described to suppress tumor-specific immunity (30, 31). To investigate whether the T_2 population in the tumor contributes to the immune subversion of tumor-infiltrating antigen-experienced T cells, we stimulated sorted, blood-derived $CD45RA^-CD4^+$ cells with anti-CD3/CD28-coated beads in the presence or absence of autologous, sorted, tumor-derived T_2 cells ($CD45^+CD2^-CD19^-CD11b^+CD163^{high}$) (**Supplementary Fig. S10**). Because of limited availability of material, we could only perform TCR-dependent stimulation of $CD4^+$ T cells. Blood-derived $CD4^+$ T cells produced significantly less IL-2 and significantly more TGF-β, IL-10 and IL-4 upon addition of autologous T_2 TAMs (**Fig. 7A**). The production of the effector cytokines IFN-γ und TNF-α followed the same trend as IL-2, although the effect was not statistically significant. Furthermore, the co-incubation with T_2 TAMs resulted in an upregulation of transcripts for PD-1 and Tim-3 (**Fig. 7B**). No changes in T cell function were observed when T cells were cocultured with the sorted T_1 fraction ($CD45^+CD2^-CD19^-CD11b^+CD163^{low}$) (data not shown). There was a trend towards reduced proliferation of T cells in the presence of the T_2 fraction, however data were not consistent (data not shown). These results indicate that $CD45^+CD2^-CD19^-CD11b^+CD163^{high}$ cells contribute to functional and phenotypic immune subversion of tumor-infiltrating T cells in ccRCC patients.

DISCUSSION

There is growing evidence that the immunoregulatory milieu, which is associated with most tumors, precludes protective anti-tumor immunity and presumably diminishes the efficacy of immunotherapy (32). To better understand local immunoregulatory processes that impact on disease progression, we correlated intratumoral immunological profiles with survival in patients with primary ccRCC. In addition, we performed functional experiments to dissect the mutual influences of tumor cells, TAMs and T cells.

We retrospectively analyzed the transcripts for 31 immune response-related genes in a cohort of 54 primary ccRCC FFPE tumor samples and correlated the expression of each of these genes with survival. In line with the finding that not the degree of leukocyte infiltration but rather leukocyte subtypes, their function and location are relevant to disease outcome (1) we did not observe a correlation of the degree of leukocyte infiltration (CD45) and survival. Data on the impact of tumor infiltrating leukocytes (TILs) on disease outcome in ccRCC are conflicting. Whereas one study showed that an increased frequency of $CD8^+$ T cells correlates with poor prognosis, except when these T cells are proliferating (33), another study shows a correlation of increased Th1 type responses with good prognosis (34). Furthermore, a recent publication showed that increased presence of lymphocytes negatively impacts on overall survival (21). Of all lymphocyte-associated transcripts, only FoxP3, a transcription factor specific for regulatory T

cells (35) correlated with decreased survival, which confirms previously published findings (36, 37). Tregs are a subpopulation of T cells that play an important physiological role in suppressing effector T cell responses to self-antigens thereby preventing autoimmunity (38). Furthermore, Tregs suppress anti-tumor immunity (7, 39). A correlation between high numbers of Treg or a low Teffector/Treg ratio and reduced survival has been shown in several other cancer types including ccRCC (39, 40).

We discovered that increased transcripts for the macrophage marker CD68 correlated significantly with reduced survival in primary ccRCC. Although most studies correlate an increased frequency of TAMs with unfavorable prognosis of patients with breast, prostate, bladder or kidney cancer, some studies with patients suffering from melanoma, stomach and colocrectal cancer find the opposite (summarized in(8)). A possible explanation for these conflicting observations may be the use of the pan-macrophage marker CD68, which recognizes all subsets of this heterogeneous and plastic population (41) and does not differentiate between functionally different M1 and M2 macrophages (42, 43). Pro-inflammatory M1 macrophages are induced by IFN-γ and LPS, whereas alternatively activated, anti-inflammatory M2 macrophages differentiate in the context of IL-4, IL-13 and IL-10 (5). M2 macrophages dampen immune and inflammatory responses to prevent tissue damage in the case of chronic inflammation (44). In the context of tumors, M2 macrophages promote tumor progression, metastasis and immunosuppression (43). For this reason we expanded our retrospective analysis with 12 TAM-associated genes and found a correlation between M1-associated transcripts (iNOS) and prolonged survival as well as an association between M2-associated genes (CD163, FN-1 and IRF-4) and reduced survival. iNOS was correlated before with increased survival of patients with colorectal cancer (45). Furthermore, a correlation between CD163 and reduced survival has been recently observed in different cancers including ccRCC (46, 47). Subsequent analysis of prospectively collected fresh tumor samples showed the presence of two different myeloid fractions in primary ccRCC ($CD11b^+CD68^+CD163^{high}$ cells (T_2 fraction) and $CD11b^+CD68^+CD163^{low}$ cells (T_1 fraction), whereas we only found the $CD11b^+CD68^+CD163^{low}$cells (P_1 fraction) in paired blood samples. The T_2 population expressed high levels of MR, FN-1 and IL-10 and low levels of iNOS, thus uncovering CD163 as a marker for TAMs with an M2-like signature in ccRCC (5, 44). T_2 cells – but not T_1 or P_1 cells – showed increased expression of molecules that are involved in negative immune regulation including PD-L1 and IL-10. We noticed that differences in the CD163 signal between the different fractions were not as pronounced on the mRNA level as seen on the protein level. One explanation for this could be that transcripts of CD163 are less stable than the protein. The high level of MHC class II on the T_2 fraction clearly discriminates them from $CD11b^+$ MHC-$II^{-/low}$ myeloid derived suppressor cells (MDSC) (6, 48).

TAMs can support tumor progression in many ways including the promotion of tumor survival, invasion, metastasis and angiogenesis (8). Our analyses showed a correlation between CD68 transcripts and an increased incidence of metastases. We observed a correlation between high

CD163 levels and high tumor staging (pT) and the opposite for iNOS. This suggests a progressive accumulation of M2 TAMs in ccRCC, which may be due to an increased influx of M2 TAMs (10) or to *in situ* conversion of M1 to M2 macrophages (9, 48, 49). Our data supports the second scenario, since we observed the induction of M2-associated markers on blood-derived myeloid cells after coculture with autologous tumor cells. These findings are in line with another study showing that supernatants of ccRCC tumor cell lines induced the expression of M2 markers in human macrophages (49).

Our observation that transcript levels for CD163 but also for FoxP3 and IL-10 positively correlate with pT, suggests increasing immune regulation during tumor progression (7, 50, 51). Along this line, transcripts for the effector molecules TNF-α and perforin positively correlated with survival whereas the opposite was true for CTLA-4 and IL-10. Functional analysis of TILs confirmed this: although TILs showed an antigen-experienced ($CD45RO^+$) and activated ($CD69^+$, IFN-γ^+, TNF-α^+) phenotype, they expressed higher levels of PD-1, Tim-3, CTLA-4 and IL-10 at the same time, all of which are indicative for immune regulation. The increased expression of PD-1 and Tim-3 was more pronounced in tumor-derived $CD8^+$ T cells, whereas CTLA-4 and FoxP3 expression was more prominent in tumor-derived $CD4^+$ T cells. This suggests that $CD4^+$ and $CD8^+$ T cells may be subject to different mechanisms of immune regulation in the tumor. Especially, the significant increase of the PD-1^+/Tim-3^+ population is indicative for an exhausted T cell phenotype (52) and implies reduced effector function of $CD8^+$ T cells within ccRCCs. The tumor environment itself, or more specifically, TAMs, contribute to the regulated phenotype of T cells because their effector function was partially rescued by sorting $CD4^+$ and $CD8^+$ T cells out of the tumor. The reversed experiment – addition of sorted $CD11b^+CD163^{high}$ cells (T_2 fraction) from primary ccRCC tumor samples to autologous blood-derived $CD4^+$ T cells– confirmed the negative impact of TAMs on T cell effector function.

In conclusion, we found that high infiltration of primary ccRCC by Tregs and M2 TAMs correlates with reduced survival. Furthermore, we showed a progressive accumulation of and/or conversion to M2 macrophages that is supported by tumor cells. M2 TAMs in turn induce skewing of tumor-infiltrating T cells towards a more regulated phenotype at the expense of protective effector function.

FIGURES

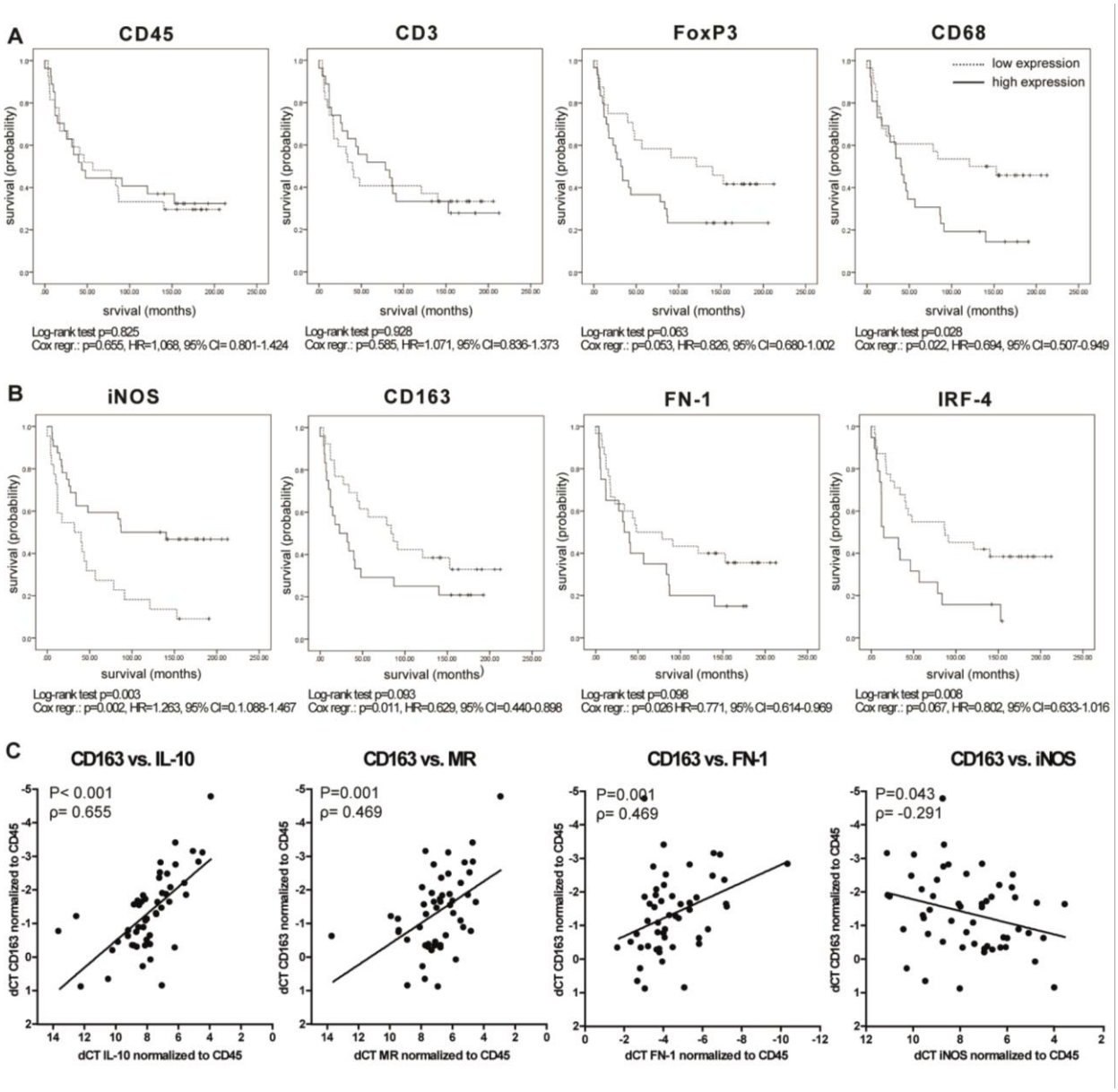

Figure 1: Transcripts of FoxP3, CD68, and genes associated to M2 TAMs inversely correlate with survival in patients with ccRCC

54 ccRCC FFPE tumor samples were subjected to a retrospective qRT-PCR analysis for different immune response-related genes. ΔCt levels of CD45 were calculated by normalization to the endogenous control (18SrRNA), ΔCt levels of all other genes were calculated by normalization to CD45. Survival analysis was performed using the Cox proportional hazard model and, after dichotomizing the data based on the mean-expression level, also with the log-rank test of the Kaplan-Meier estimator. The results of both statistical tests are displayed for selected genes. Patients that were still alive at time of analysis are marked with a tick. Kaplan-Meier survival curves show the relation of gene expression with survival for (A) CD45, CD3, FoxP3 and CD68 and (B) iNOS, CD163, FN-1 and IRF-4. Multivariate Cox regression analysis revealed that the correlation of target gene expression and survival is independent of pT for CD68: p=0.02, HR=0.704, 95% CI 0.520-0.954; iNOS: p=0.011, HR=1.261, 95% CI 1.055-1.506 and CD163 p=0.015, HR=0.645, 95% CI 0.453-0.919, as well as independent of patients' age for CD68: p=0.04, HR=0.720, 95% CI 0.524-0.989; iNOS: p=0.012, HR=1.299, 95% CI 1.060-1.592 and CD163: p=0.013, HR=0.636, 95% CI 0.445-0.909. (C) ΔCt levels of CD163 plotted against ΔCt values of IL10, MR, FN-1 and iNOS. Results of Spearman Rho correlation analysis are depicted in the plots. Each dot represents an individual patient.

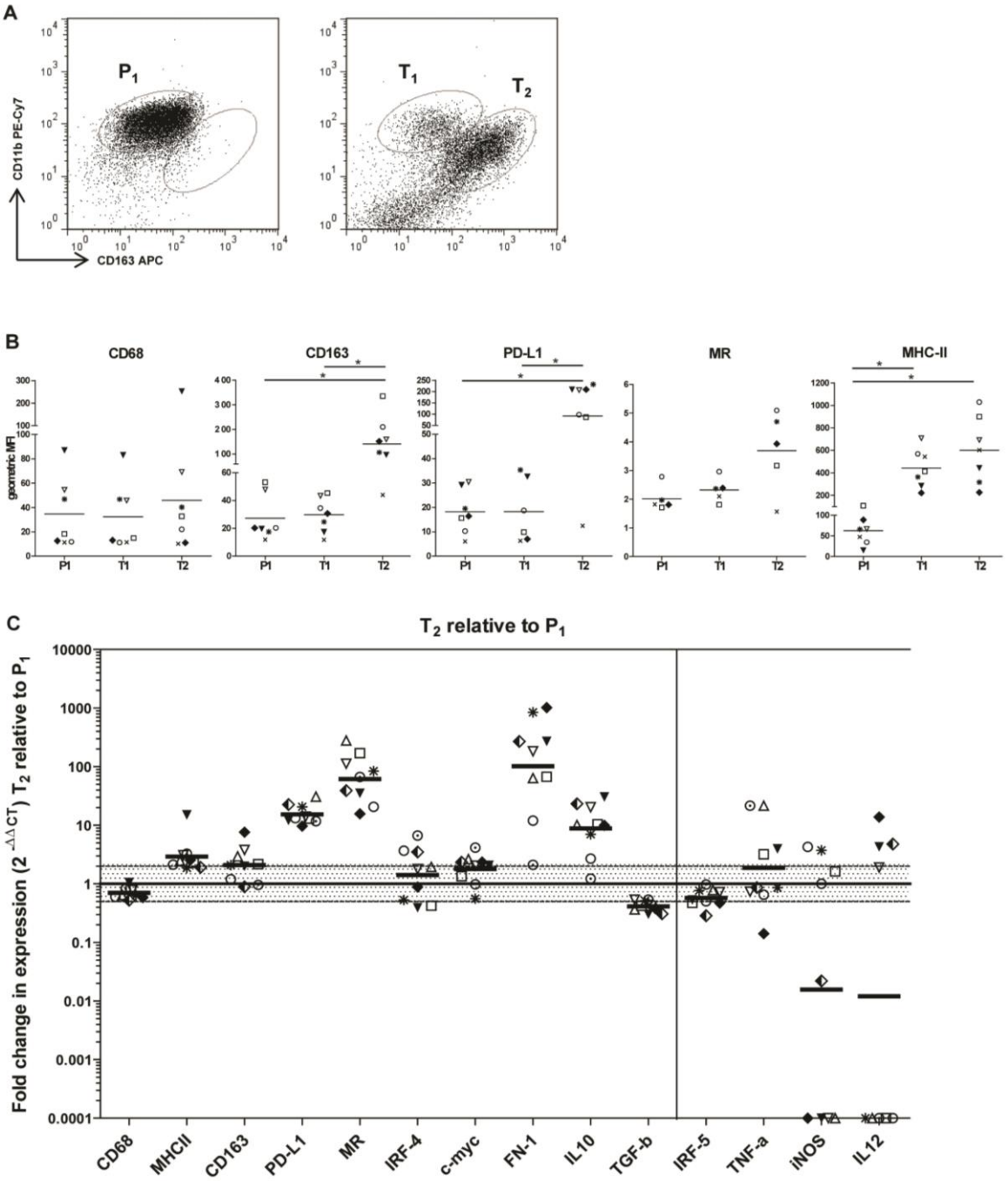

Figure 2: Characterization of tumor-associated myeloid cells in ccRCC

Fresh primary cRCCs and paired blood samples were collected and processed as described under Materials and Methods. (A) Dot plots display staining of PBMC (left histogram) and processed tumor (right histogram) for CD11b and CD163 after gating on $CD45^+$ $CD3^-$ $CD19^-$ cells. P_1, T_1 and T_2 designate individual myeloid populations. The plots show a representative example of one patient. (B) Expression of different macrophage-associated molecules after gating on the populations P_1, T_1 and T_2, displayed as the geometric mean of fluorescence intensity. Each symbol represents an individual patient; means of each group and significant differences (* $p<0.05$) are displayed. (C) qRT-PCR analysis of FACS-sorted P_1 and T_2 fractions. Genes displayed on the left side of the vertical line are related to M2 TAMs, on the right side to M1 TAMs. ΔCT levels were calculated by normalization to the endogenous control PPIA. Results are presented as fold change in expression level of T_2 relative to P_1; the geometric mean of each group is depicted. Fold differences in expression within the shaded area are considered as not significant. Symbols at the 0.0001 line on the y-axis represent samples of which the fold change could not be calculated, since expression was only detected in one of the fractions. Each symbol represents an individual patient in B and C.

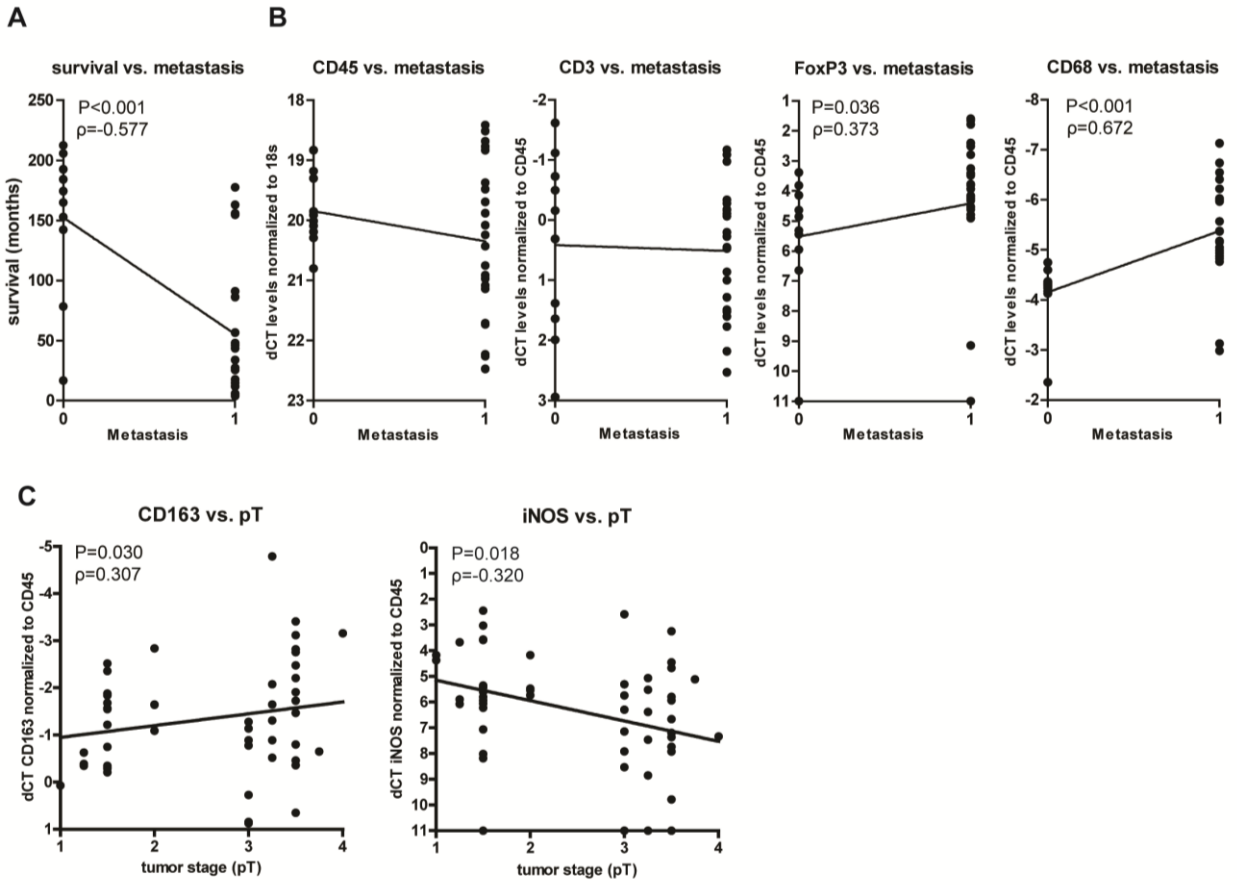

Figure 3: Positive correlation of FoxP3 and CD68 gene expression with the incidence of metastasis and of M2 TAM-associated genes with tumor stage

(A) Survival in months after diagnosis, (B) ΔCt levels of CD45, CD3, FoxP3 and CD68 correlated with the incidence of metastasis (0= patient did not develop metastasis, 1= patient developed metastasis). (C) ΔCT levels of CD163 and iNOS correlated with tumor stage (pT). Each dot represents an individual patient. ΔCt levels of target genes were calculated as described for Fig. 1. Only when correlations are significant, the results of the Spearman Rho correlation test are displayed within the plot. Tumor stage was defined as: 1= pT1, 1.25= pT1a, 1.5=pT1b, 2=pT2, 3=pT3, 3.25=pT3a, 3.5=pT3b, 3.75=pT3c and 4=pT4.

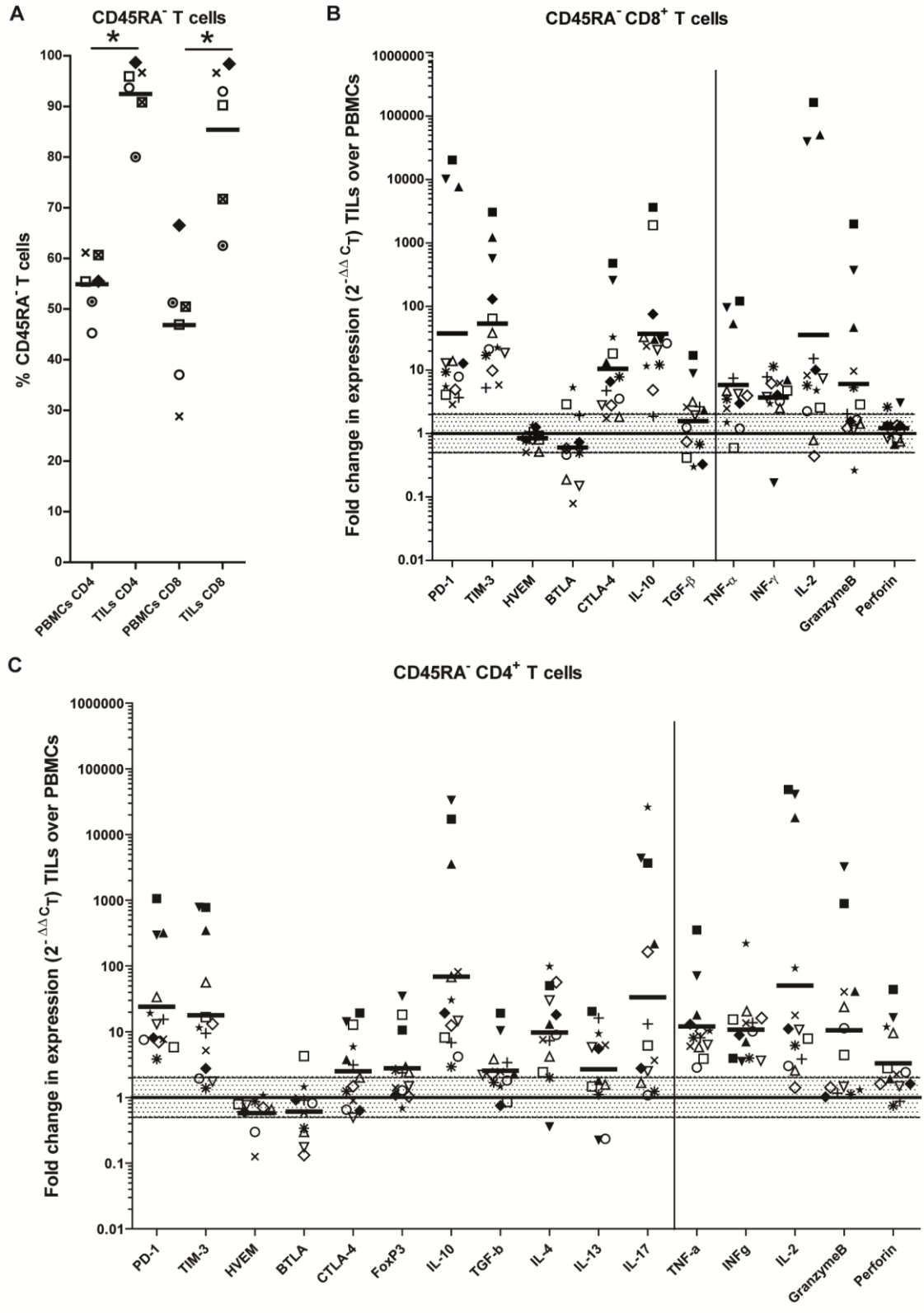

Figure 4: Tumor-derived T cells show an antigen-experienced and regulated phenotype

(A) The percentage of CD45RA$^-$ (antigen-experienced) T cells in blood and tumors of ccRCC patients was determined by flowcytometry; the means of each group and significant differences (* $p<0.05$) are displayed. (B, C) Gene expression analysis was performed by qRT-PCR on FACS-sorted CD45RA$^-$ CD8$^+$ (B) and CD45RA$^-$ CD4$^+$ (C) from blood and tumors of ccRCC patients. Ct values were normalized to the endogenous control PPIA. Results are presented as fold change in expression level of tumor-derived relative to blood-derived T cells; the geometric mean of each group is depicted; fold differences in expression within the shaded area are considered as not significant. Each symbol represents an individual patient.

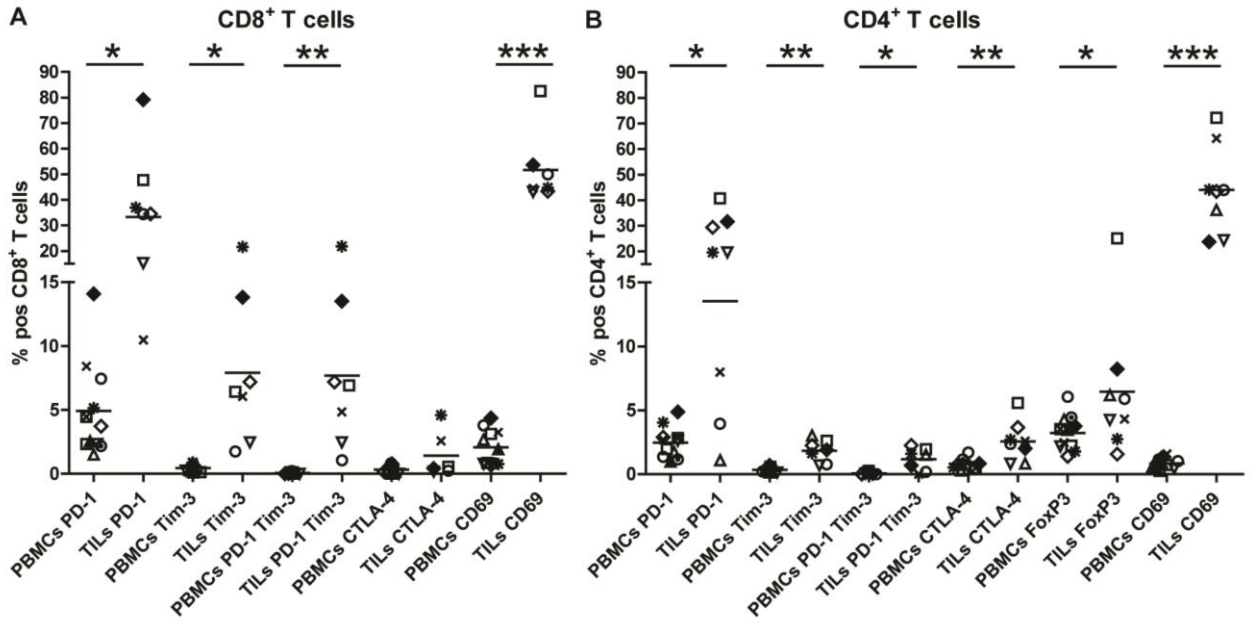

Figure 5: Tumor-derived T cells express higher levels of regulatory molecules than T cells derived from paired blood samples

FACS analysis on tumor- and blood-derived cells after gating on $CD8^+CD45RA^-$ T cells (A) or $CD4^+CD45RA^-$ T cells (B). The graphs display the percentage of cells positive for a particular marker. A representative staining is shown in Supplementary Fig. S4. Each symbol represents an individual patient. The mean of each group and significant differences (* $p<0.05$; ** $p<0.005$; *** $p<0.0005$) are depicted.

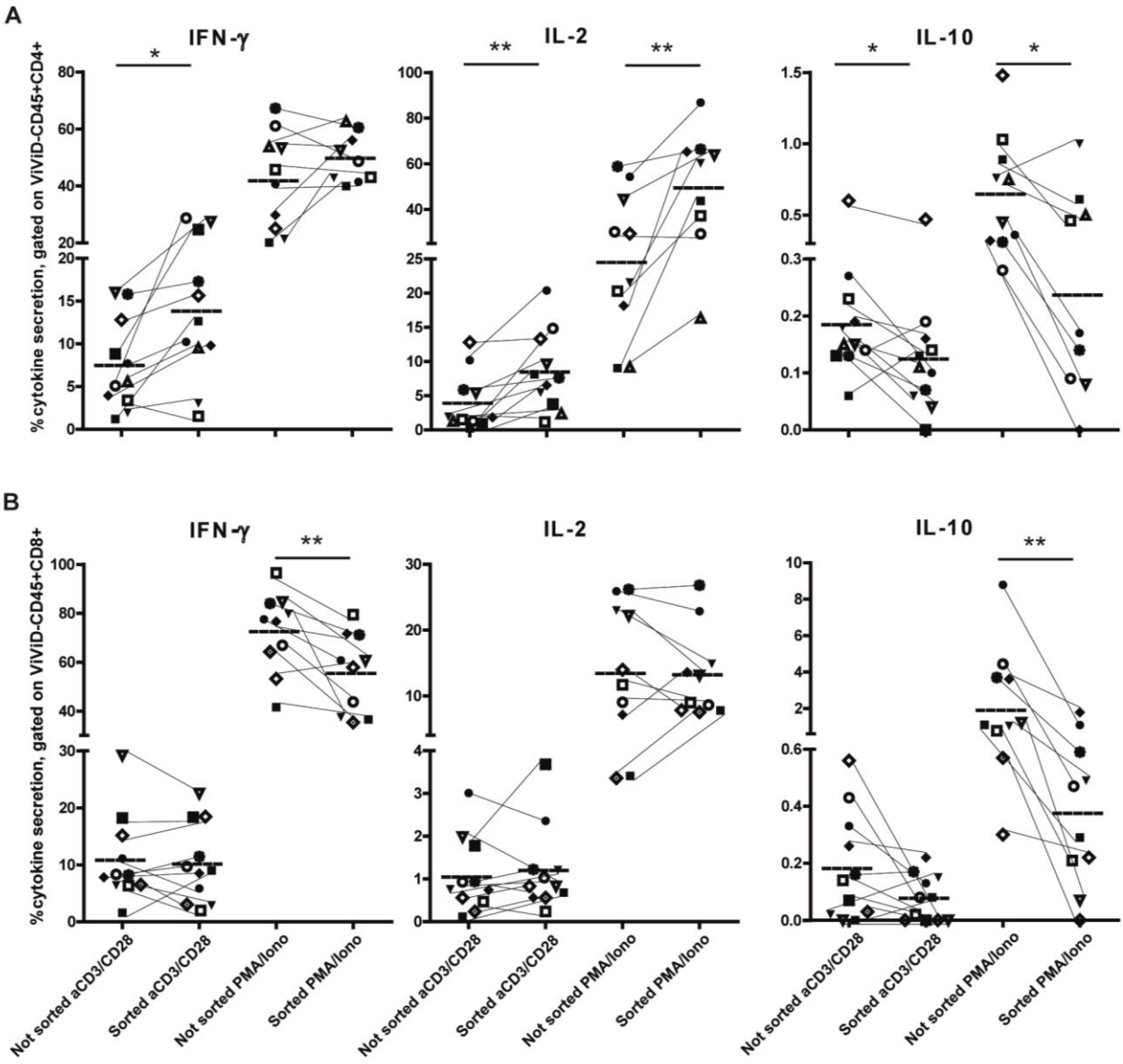

Figure 6: The tumor microenvironment impacts on the cytokine profile of T cells

Intracellular staining for cytokines after 6h *ex vivo* stimulation with anti-CD3/CD28 beads or with PMA + ionomycin in the presence of brefeldin A and monensin. Cells were stimulated within the tumor digest or after sorting of $CD45^+$ $CD4^+$ T cells (A) or $CD45^+$ $CD8^+$ T cells (B) and analyzed after gating on live $CD45^+$ $CD4^+$ T cells (A) or live $CD45^+$ $CD8^+$ T cells (B). Each symbol represents an individual patient. Results of unsorted and sorted T cells from the same patient are connected by a thin line. The mean of each group and significant differences (* $p<0.05$; ** $p<0.005$) are depicted.

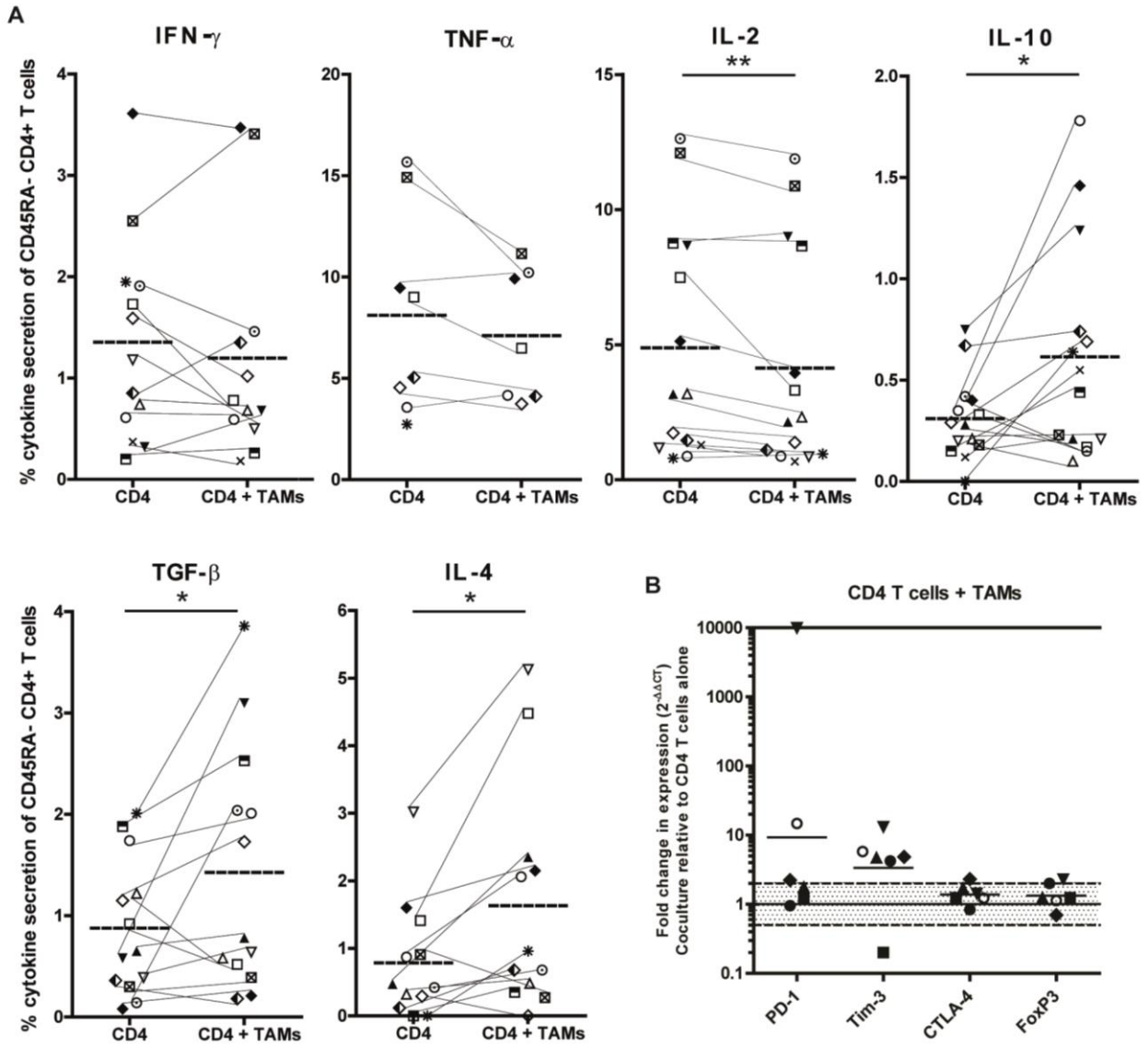

Figure 7: ccRCC-derived M2 TAMs skew T cells towards a more regulated phenotype

Sorted blood-derived $CD4^+$ T cells were cultured for 48 h with or without sorted autologous T_2 cells ($CD45^+CD2^-CD19^-CD11b^+CD163^{high}$) in a ratio of 1:1. (A) Production of cytokines was assessed via ICS after 6h *ex vivo* stimulation with anti-CD3/CD28 beads in the presence of brefeldin A and monensin after gating on live $CD45^+$ $CD11b^-$ $CD4^+$ cells. Results of the same patient are connected by a thin line. The mean of each group and significant differences (* $p<0.05$; ** $p<0.005$) are depicted. (B) The expression of regulatory molecules was assessed by qRT-PCR. ΔCt levels were calculated by normalizing the Ct values of the target genes to the Ct values of CD4. Results are presented as fold change in expression level of $CD4^+$ T cells cocultured with autologous T_2 cells ($CD45^+CD2^-CD19^-CD11b^+CD163^{high}$) relative to $CD4^+$ T cells cultured without. Fold differences in expression within the shaded area are considered as not significant. The symbol at the 10'000 line on the y-axis represents a sample of which fold change could not be calculated, since expression was only detected after coculture. Each symbol represents an individual patient.

SUPPLEMENTARY FIGURES AND TABLES

Supplementary Table S1: Summary of Taq Man Assays used for retrospective screen

	Target	Gene Symbol	Taq Man Assay ID
A	CD45	PTPRC	Hs00236304_m1
	CD3	CD3G	Hs00962186_m1
	CD4	CD4	Hs00181217_m1
	CD8	CD8A	Hs00233520_m1
	CD68	CD68	Hs00154355_m1
	MHC class-I	HLA-C	Hs03044135_m1
	MHC class-II	HLA-DRA	Hs00219575_m1
	CTLA-4	CTLA4	Hs00175480_m1
	FoxP3	FOXP3	Hs01085834_m1
	Tim-3	HAVCR2	Hs00262170_m1
	PD-1	PDCD1	Hs00169472_m1
	PD-L1	CD274	Hs00204257_m1
	BTLA	BTLA	Hs00699198_m1
	HVEM	TNFRSF14	Hs00187058_m1
	CD200	CD200	Hs01033303_m1
	IDO	IDO1	Hs00984148_m1
	Arginase 1	ARG1	Hs00968979_m1
	NKG2D	KLRK1	Hs00183683_m1
	MICA	MICA	Hs00741286_m1
	MICB	MICB	Hs00792952_m1
	IL-10	IL10	Hs00961622_m1
	TGF-b	TGFB1	Hs00998133_m1
	IL-17a	IL17A	Hs00174383_m1
	TNF-a	TNF	Hs00174128_m1
	IFN-g	IFNG	Hs00174143_m1
	IL-2	IL2	Hs00174114_m1
	Perforin	PRF1	Hs00169473_m1
	Granzyme B	GZMB	Hs00188051_m1
	LT-a	LTA	Hs00236874_m1
	LT-b	LTB	Hs00242739_m1
	LT-bR	LTBR	Hs00158922_m1

	Target	Gene Symbol	Taq Man Assay ID
B	iNOS	NOS2	Hs01075529_m1
	CD163	CD163	Hs00174705_m1
	MR (CD206)	MRC1;MRC1L1	Hs00267207_m1
	FN-1	FN1	Hs01549976_m1
	IRF-4	IRF4	Hs01056533_m1
	IRF-5	IRF5	Hs00158114_m1
	IL-12	IL12B	Hs01011518_m1
	EGF	EGF	Hs01099999_m1
	EGFR	EGFR	Hs01076078_m1
	CSF-1	CSF1	Hs00174164_m1
	CSF-1R	CSF1R	Hs00911250_m1
	Mena	ENAH	Hs00403109_m1
C	IL-4	IL4	Hs00174122_m1
	IL-13	IL13	Hs00174379_m1
D	c-MYC	MYC	Hs00905030_m1

Taq Man Assays used for initial screen (A), for TAM-related screen (C), and to further characterize sorted CD4+ T cells (C) and myeloid fractions (D).

Supplementary Table S2: Patients' characteristics of received FFPE material

Histology	**clear cell renal cell carcinoma**	
Patient number	**n=54**	
Age (years)	**40-86 (66.3 ± 7.2)**	
Survival time (months)	**0-213 (80.9 ± 64.2)**	
Pathological Stage	**pT1**	**2**
	pT1a	**3**
	pT1b	**16**
	pT2	**4**
	pT3	**8**
	pT3a	**6**
	pT3b	**13**
	pT3c	**1**
	pT4	**1**

Information is only displayed for those patients who died of tumor-related causes.

A

Perforin

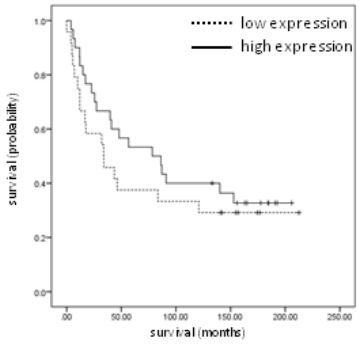

Log-rank test p=0.384
Cox regression: p=0.009, HR=1.550, 95% CI=1.177-2.151

CD4

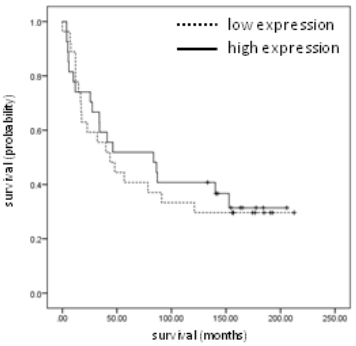

Log-rank test p=0.750
Cox regression: p=0.979, HR=0.933, 95% CI=0.588-1.678

CD8

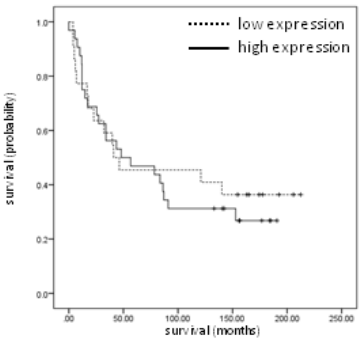

Log-rank test p=0.695
Cox regression: p=0.998, HR=1.000, 95% CI=0.788-1.267

MHC class-I

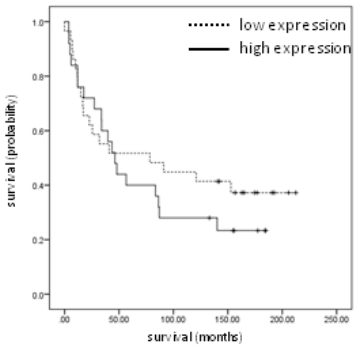

Log-rank test p=0.412
Cox regression: p=0.276, HR=0.885, 95% CI=0.710-1.103

MHC class-II

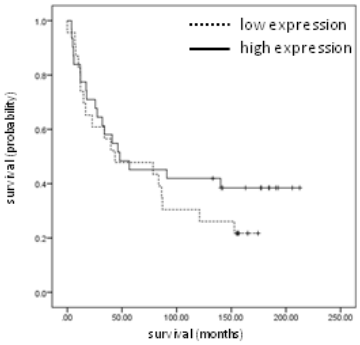

Log-rank test p=0.340
Cox regression: p=0.478 HR=0.899 95% CI=0.670-1.207

IDO

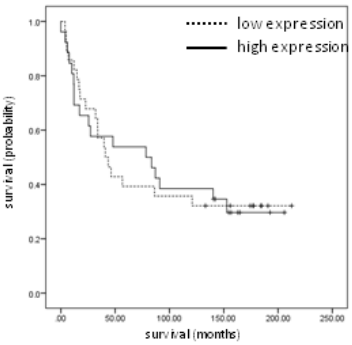

Log-rank test p=0.987
Cox regression: p=0.409, HR=1.077, 95% CI=0.903-1.284

IFN-γ*

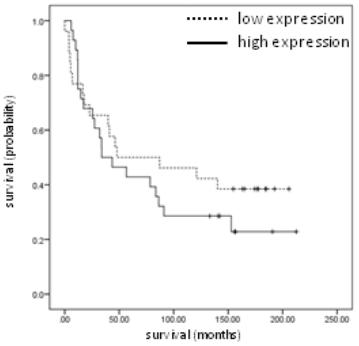

Log-rank test p=0.384
Cox regression: p=0.745, HR=0.973, 95% CI=0.827-1.146

TNF-α*

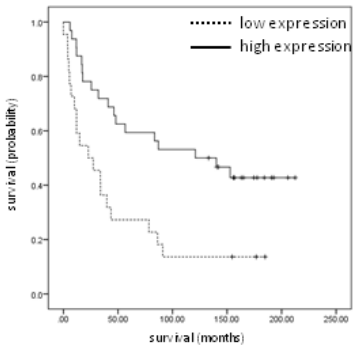

Log-rank test p=0.002
Cox regression: p=0.626, HR=1.035, 95% CI=0.902-1.186

Granzyme B*

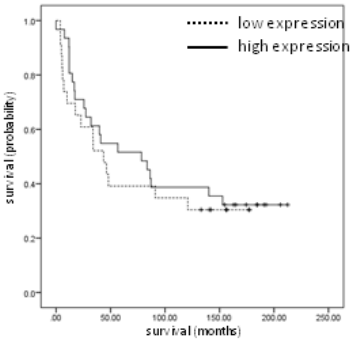

Log-rank test p=0.580
Cox regression: p=0.983, HR=0.998, 95% CI=0.841-1.184

HVEM

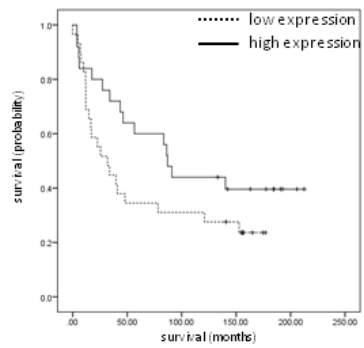

Log-rank test p=0.113
Cox regression: p=0.076, HR=1.380, 95% CI=0.967-1.970

LT-βR

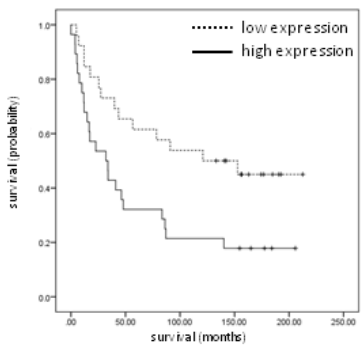

Log-rank test p=0.012
Cox regression: p=0.795, HR=0.963, 95% CI=0.722-1.283

LT-β*

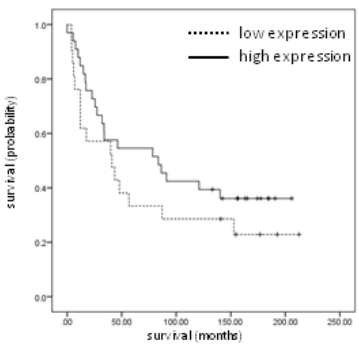

Log-rank test p=0.248
Cox regression: p=0.324, HR=1.129, 95% CI=0.887-1.436

NKG2D

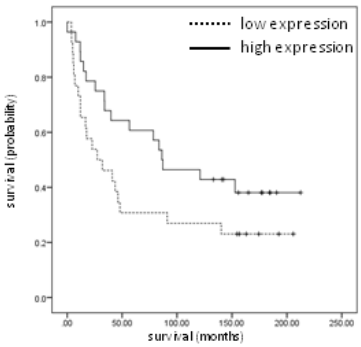

Log-rank test p=0.084
Cox regression: p=0.119, HR=1.337, 95% CI=0.928-1.926

MICA

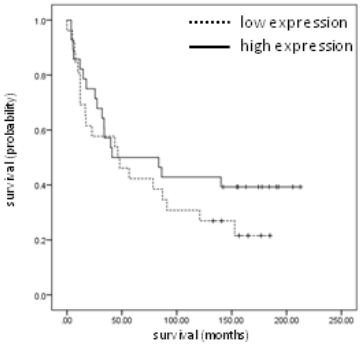

Log-rank test p=0.293
Cox regression: p=0.686, HR=0.949, 95% CI=0.737-1.222

MICB

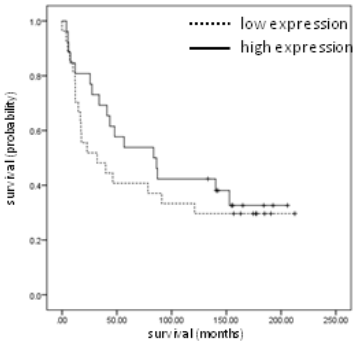

Log-rank test p=0.399
Cox regression: p=0.893, HR=1.011, 95% CI=0.858-1.192

CTLA-4*

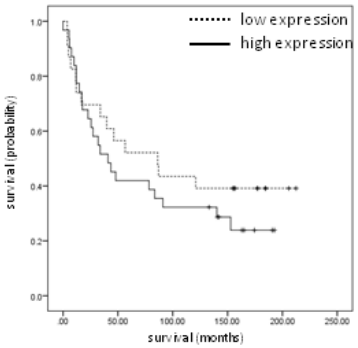

Log-rank test p=0.346
Cox regression: p=0.211, HR=0.923, 95% CI=0.814-1.046

IL-10*

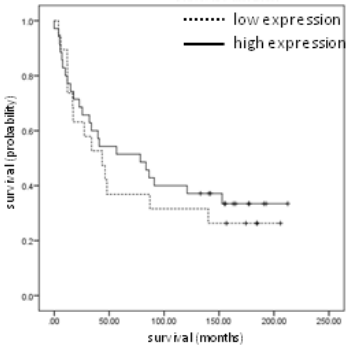

Log-rank test p=0.568
Cox regression: p=0.154, HR=0.871, 95% CI=0.721-1.053

TGF-β

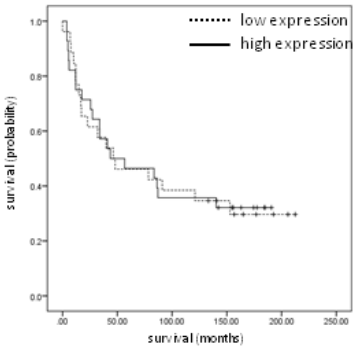

Log-rank test p=0.950
Cox regression: p=0.771, HR=1.054, 95% CI=0.740-1.501

PD-L1

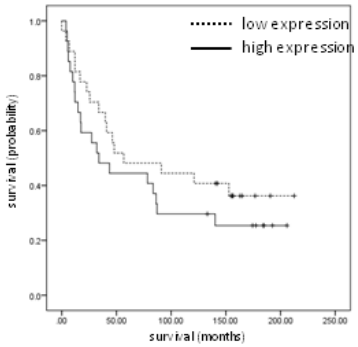

Log-rank test p=0.281
Cox regression: p=0.109, HR=0.820, 95% CI=0.644-1.045

PD-1*

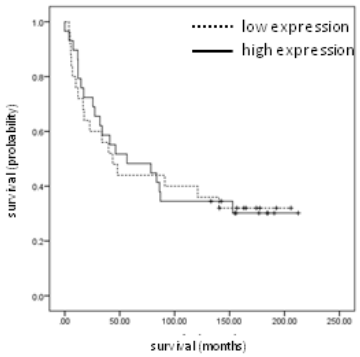

Log-rank test p=0.913
Cox regression: p=0.504, HR=0.952, 95% CI=0.826-1.099

Tim-3*

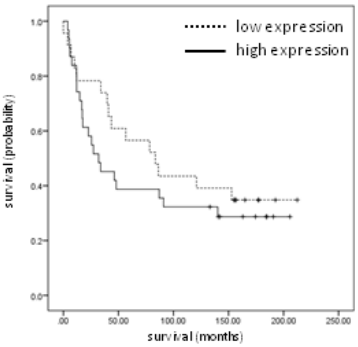

Log-rank test p=0.377
Cox regression: p=0.513, HR=0.947, 95% CI=0.806-1.114

CD200

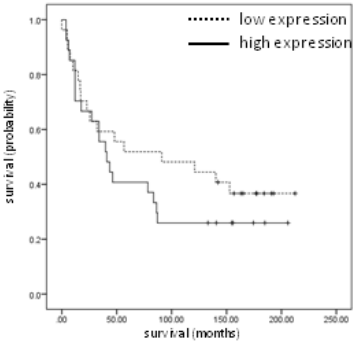

Log-rank test p=0.330
Cox regression: p=0.713, HR=0.968, 95% CI=0.815-1.150

B

CTLA-4

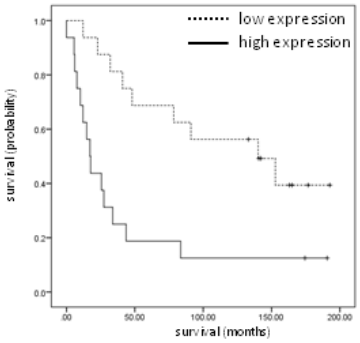

Log-rank test p=0.003
Cox regression: p=0.008, HR=0.556, 95% CI=0.361-0.856

IL-10

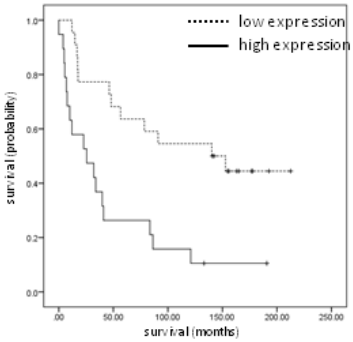

Log-rank test p=0.001
Cox regression: p=0.009, HR=0.588, 95% CI=0.396-0.874

C

MR

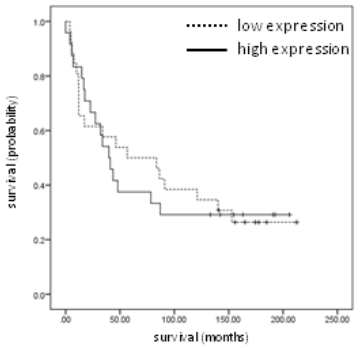

Log-rank test p=0.878
Cox regression: p=0.364, HR=1.109, 95% CI=0.887-1.387

EGF

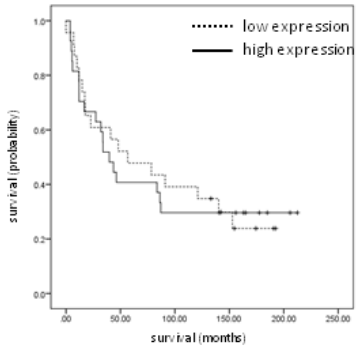

Log-rank test p=0.884
Cox regression: p=0.688 HR=1.027 95% CI=0.902-1.169

Mena

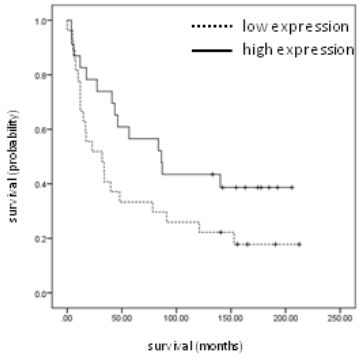

Log-rank test p=0.459
Cox regression: p=0.071, HR=0.771, 95% CI=0.581-1.023

CSF-1

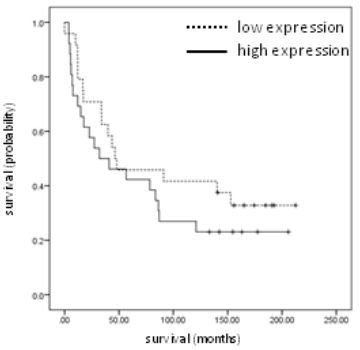

Log-rank test p=0.283
Cox regression: p=0.432, HR=0.860, 95% CI=0.590-1.253

CSF-1R

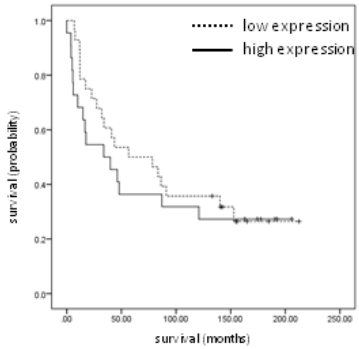

Log-rank test p=0.505
Cox regression: p=0.317, HR=0.816, 95% CI=0.549-1.215

EGF-R

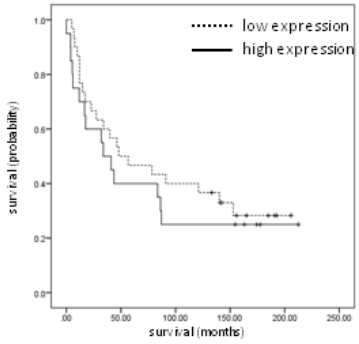

Log-rank test p=0.070
Cox regression: p=0.219, HR=1.18, 95% CI=0.906-1.536

IRF-5

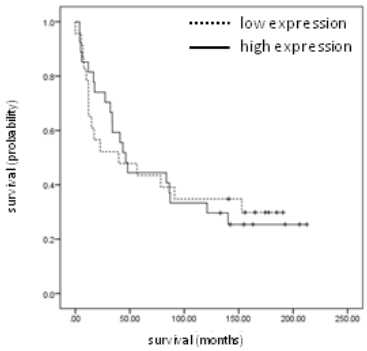

Log-rank test p=0.989
Cox regression: p=0.542, HR=0.882, 95% CI=0.588-1.322

IL-12*

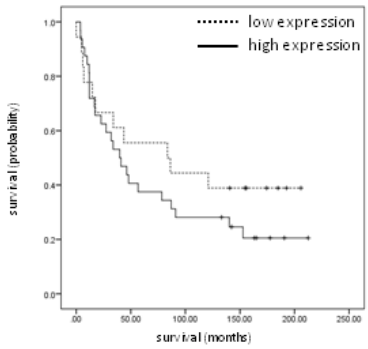

Log-rank test p=0.285
Cox regression: p=0.395, HR=0.959, 95% CI=0.872-1.056

Supplementary Figure S1: Immune profile of ccRCC correlates with survival

54 ccRCC paraffin-embedded tumor samples were subjected to a retrospective qRT-PCR analysis for 43 different immune response-related genes. ΔCt levels of CD45 (A) were calculated by normalization to the endogenous control (18s rRNA), ΔCt levels of all other genes were calculated by normalization to CD45. Transcripts were quantified using original cDNA (A, B) or preamplified cDNA (C). Survival analysis was performed using the Cox proportional hazard model and, after dichotomizing the data based on the mean-expression level, also with the log-rank test of the Kaplan-Meier estimator. Kaplan-Meier curves are shown to represent the relation of the expression of the different target genes with survival and the results of both statistical tests are displayed underneath the plot. Patients that were still alive at time of analysis are marked with a tick. Some genes (marked with an asterisk) were only detected in very low amounts, and in some samples no signal was observed for those genes. Survival analysis was therefore performed once including the no-signal samples by giving an estimated value (Ct=40), and once after excluding the no signal samples from the analysis. The results with or without the no-signal samples were similar for all genes except for IL-10 and CTLA-4. Plots calculated after inclusion of all samples are displayed (A, C), and for CTLA-4 and IL-10 also after exclusion of the no-signal samples (B). Expression of Arginase-1, IL-2, LT-a, BTLA and IL-17 was not detected in the majority of samples and therefore not considered for survival analysis.

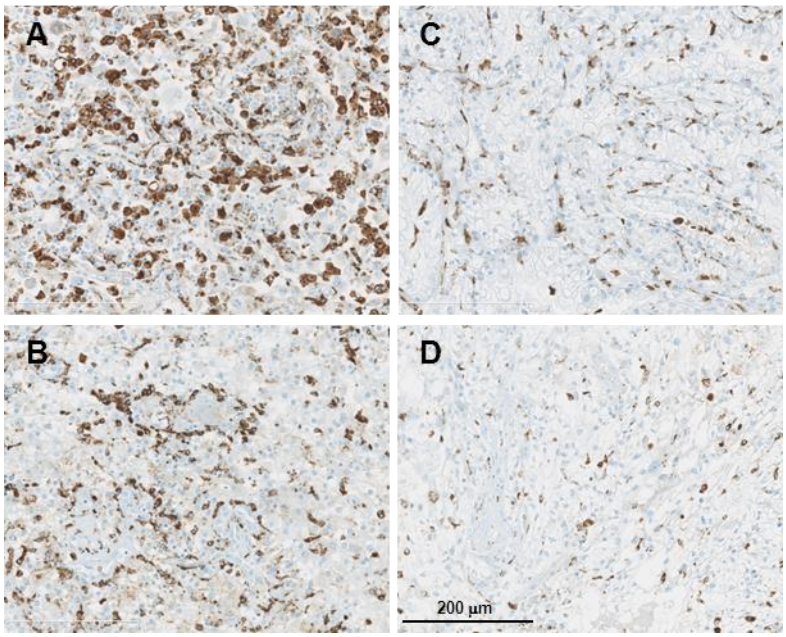

Supplementary Figure S2: Correlation between CD68 expression measured by qRT-PCR and by immunohistochemistry

Tumor sections of selected patients were stained for CD68 by immunohistochemistry (brown staining). Scans of microscopy slides at a magnification of 20x are shown. qRT-PCR analysis of the corresponding paraffin punches normalized to the endogenous control 18SrRNA revealed following ΔCt values (A): 14.07, (B): 14.19, (C): 15.63, (D): 18.47.

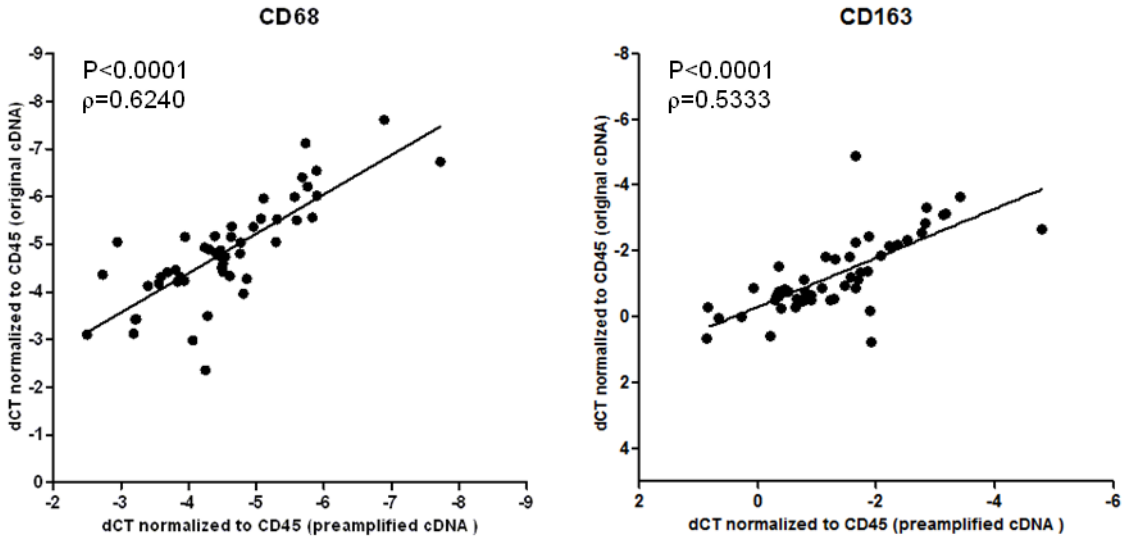

Supplementary Figure S3: ΔCT levels of original cDNA correlate with ΔCT levels of preamplifiedcDNA

cDNA of paraffin-embedded tumor material was preamplified to enable the evaluation of additional genes. The ΔCt levels of the original cDNA were plotted against the ΔCT levels of the preamplified cDNA for CD68 and CD163. ΔCt was calculated by normalizing Ct values to the Ct values of CD45. Each symbol represents an individual sample. Result of Spearman Rho correlation test is displayed in the graph.

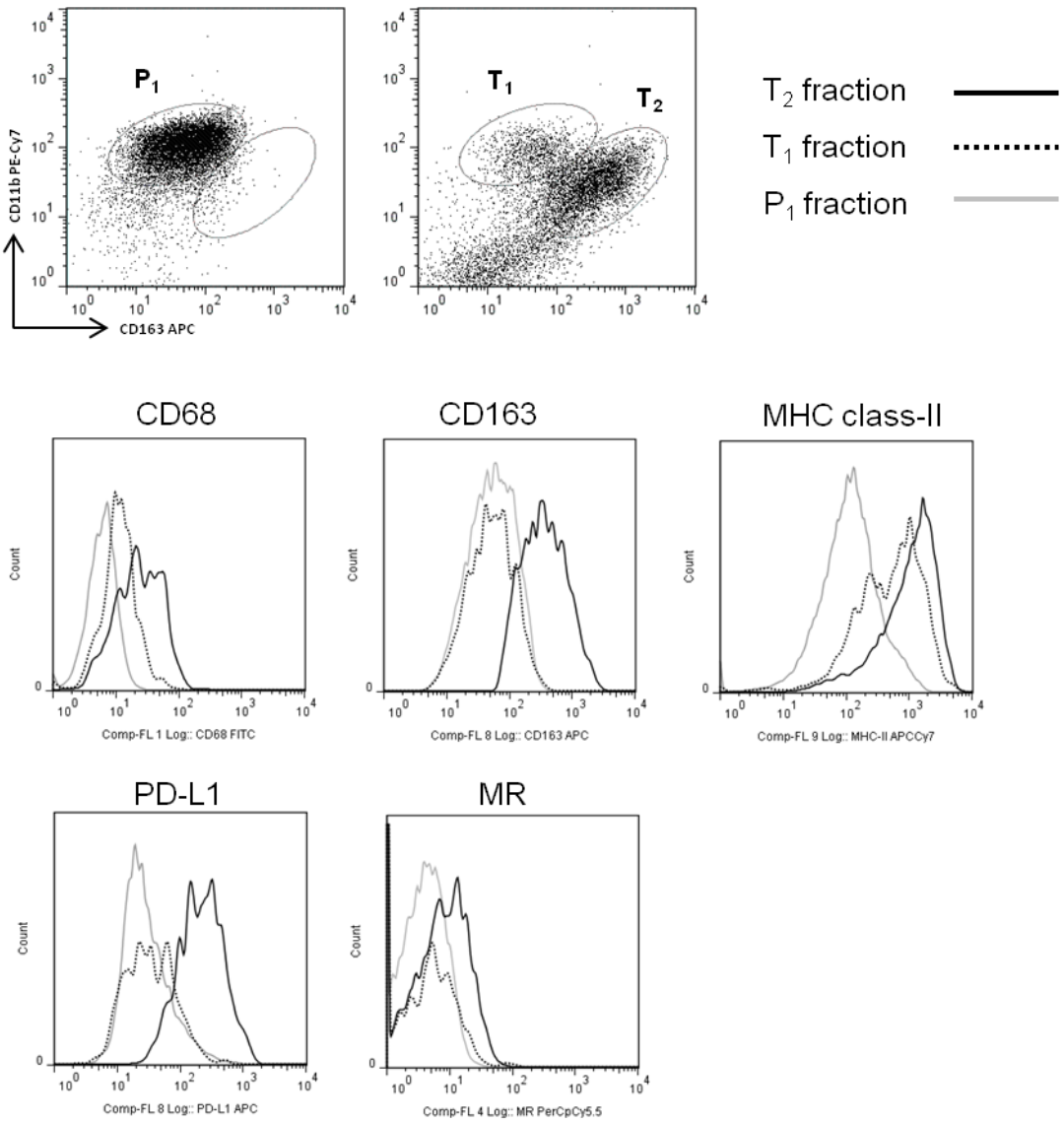

Supplementary Figure S4: Representative staining for regulatory molecules on T_1, T_2 and P_1 myeloid populations

PBMCs and paired TILs were stained and T_1, T_2 and P_1 subpopulations were determined after gating on live $CD45^+CD3^-CD19^-$ cells. Representative dot plots of PBMCs (left) and TILs (right) are shown and histograms of the expression of CD68 (intra-cellular), CD163, PD-L1, MR and MHC class-II after gating on T_1, T_2 and P_1.

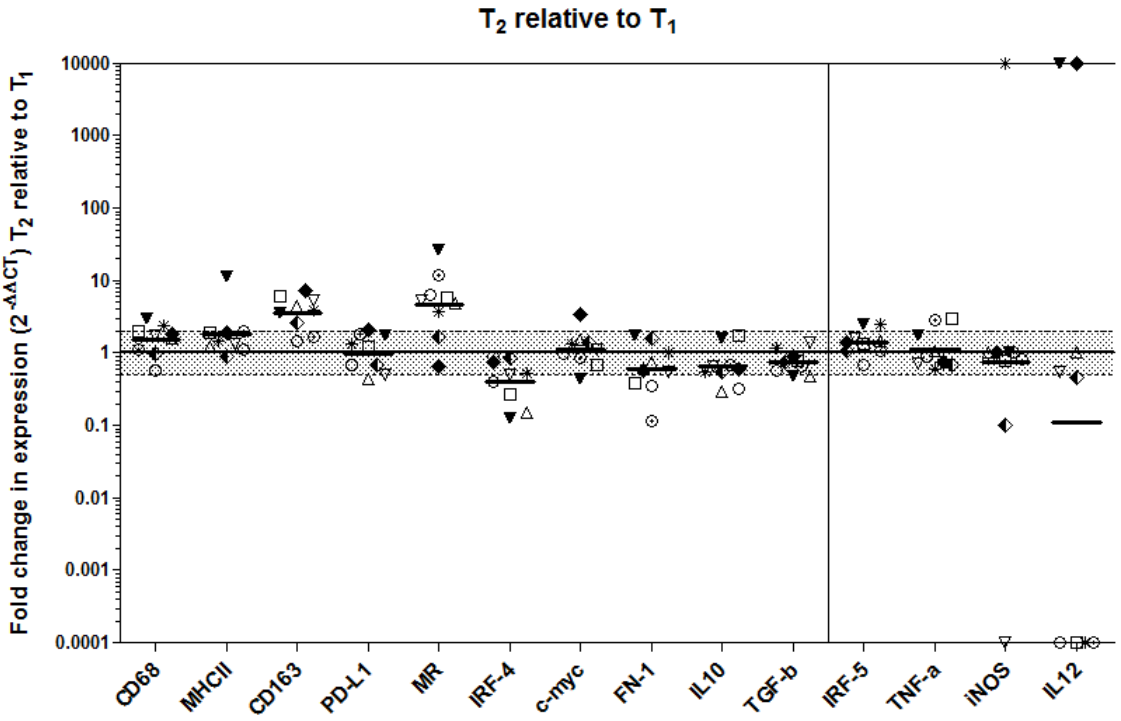

Supplementary Figure S5: Comparison of T_2 and T_1 fraction via qRT-PCR analysis

qRT-PCR analysis of FACS-sorted T_2 and T_1 fractions. Genes displayed on the left side of the vertical line are related to M2 TAMs, on the right side to M1 TAMs. ΔCt levels were calculated by normalizing the Ct values of the target genes to the Ct values of PPIA. Results are presented as fold change in expression level of T_2 relative to T_1. Fold differences in expression within the shaded area are considered as not significant. Symbols at the 10000 or 0.0001 line on the y-axis represent samples of which the fold change could not be calculated, since expression was only detected in one of the fractions. Each symbol represents an individual patient.

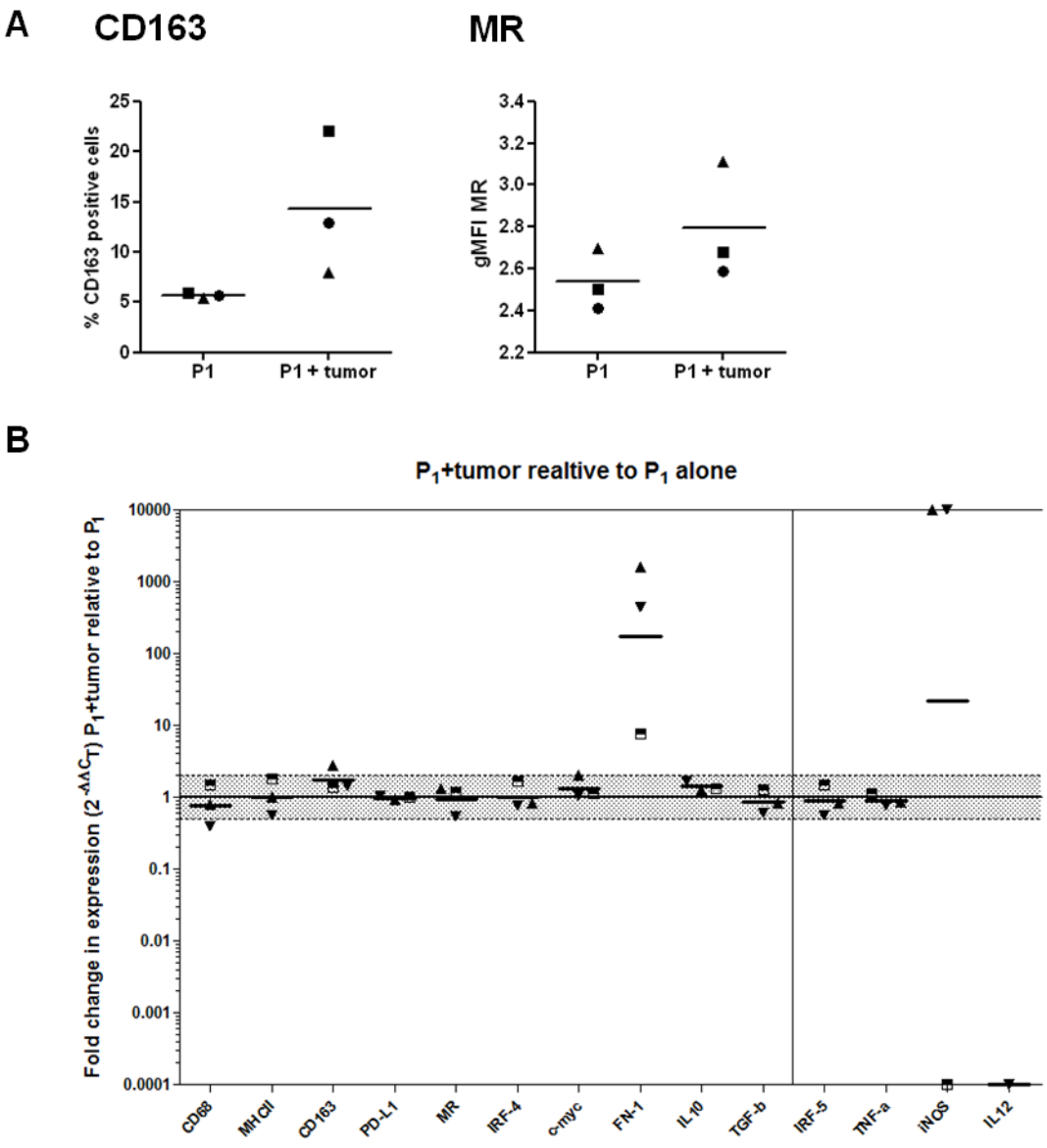

Supplementary Figure S6: Tumor cells promote transition of an M1 to an M2 phenotype

FACS-sorted blood-derived CD11b$^+$ cells were cultured with and without sorted autologous CD45$^-$ tumor cells for 48 h at a 1:3 ratio. (A) Results of FACS staining for different macrophage-associated markers after gating on CD45$^+$CD11b$^+$ cells. (B) qRT-PCR for different M1- and M2-associated genes after preamplification of the cDNA. Genes displayed on the left side of the vertical line are related to M2 TAMs, on the right side to M1 TAMs. ΔCt levels were calculated by normalizing the Ct values of the target genes to the Ct values of CD45. Results are presented as fold change in expression level of CD11b$^+$ cells cocultured with CD45$^-$tumor cells (P_1+tumor) relative to CD11b$^+$ cells cultured without (P_1 alone). Fold differences in expression within the shaded area are considered as not significant. Symbols at the 10000 or 0.0001 line on the y-axis represent samples of which the fold change could not be calculated, since expression was only detected in one of the fractions. Each symbol represents an individual patient. Geometric means of each group are depicted.

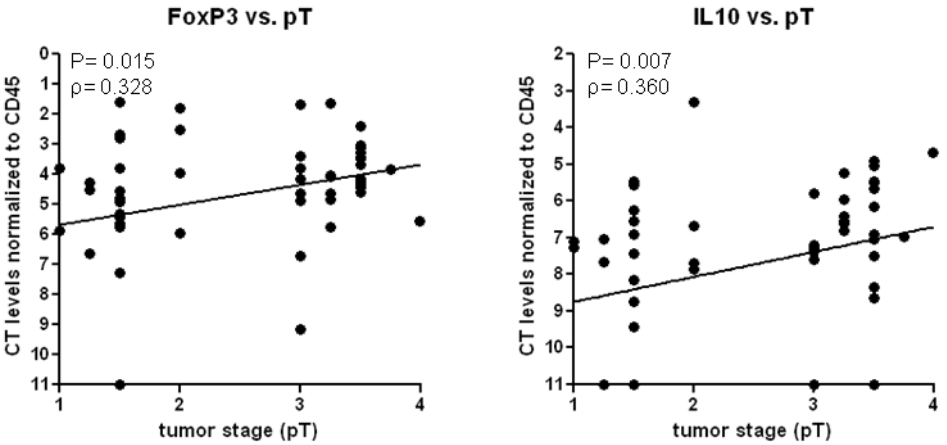

Supplementary Figure S7: Positive correlation of FoxP3 and IL-10 with tumor progression

qRT-PCR was performed on cDNA of FFPE material from ccRCC tumors and gene expression was correlated with tumor stage (pT). Results of Spearman Rho correlation analysis are shown for FoxP3 and IL-10. Each symbol represents an individual patient. ΔCt levels were calculated by normalizing the Ct values of the target genes to the Ct values of CD45. pT was defined as 1= pT1, 1.25= pT1a, 1.5=pT1b, 2=pT2, 3=pT3, 3.25=pT3a, 3.5=pT3b, 3.75=pT3c and 4=pT4.

Supplementary Table S3: Patients' characteristics of fresh tumor material

Histology	**clear cell renal cell carcinoma**	
Patient number	**n=20**	
Age (years)	**37-84 (60.5 ± 11)**	
Pathological Stage	**pT1**	**0**
	pT1a	**9**
	pT1b	**3**
	pT2	**3**
	pT3	**0**
	pT3a	**3**
	pT3b	**2**
	pT3c	**0**
	pT4	**0**

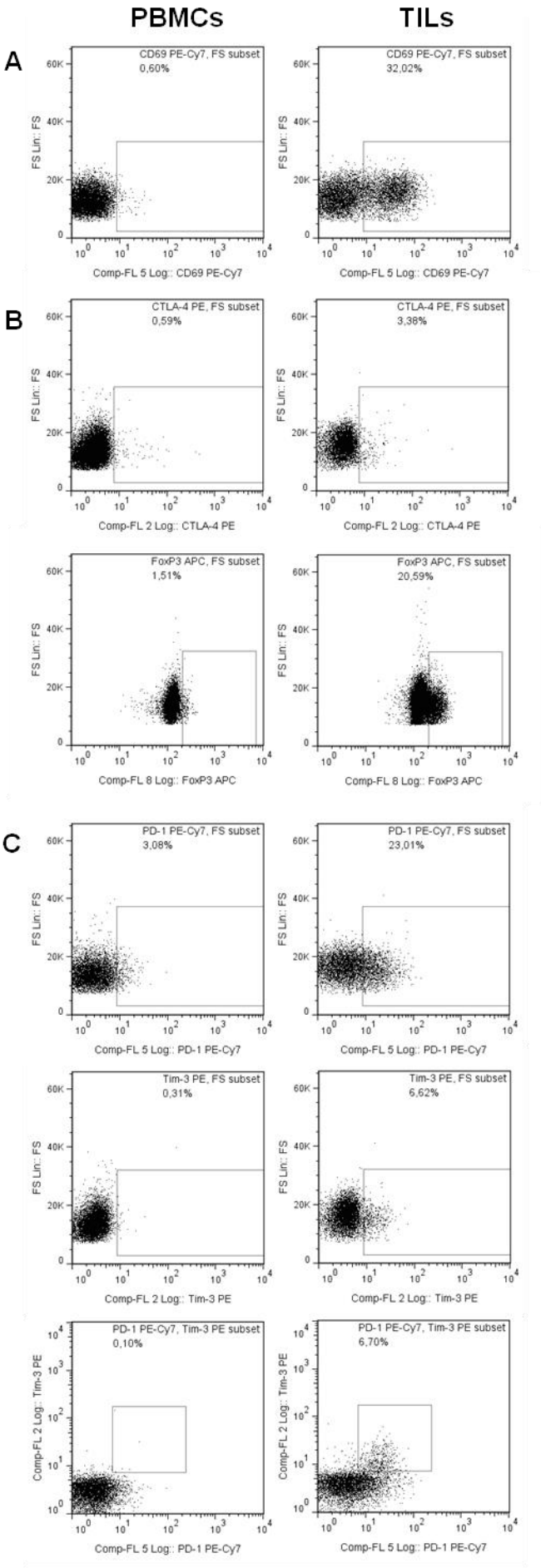

<u>Supplementary Figure S8: Representative staining of co-inhibitory molecules on blood- and tumor-derived T cells</u>

PBMCs and autologous TILs were stained with fluorochrome-labeled antibodies for specific surface markers and their expression is depicted after gating on (A) live $CD45^+CD3^+$ cells, on (B) live $CD45^+CD4^+$ cells or on (C) live $CD45^+CD8^+$ cells.

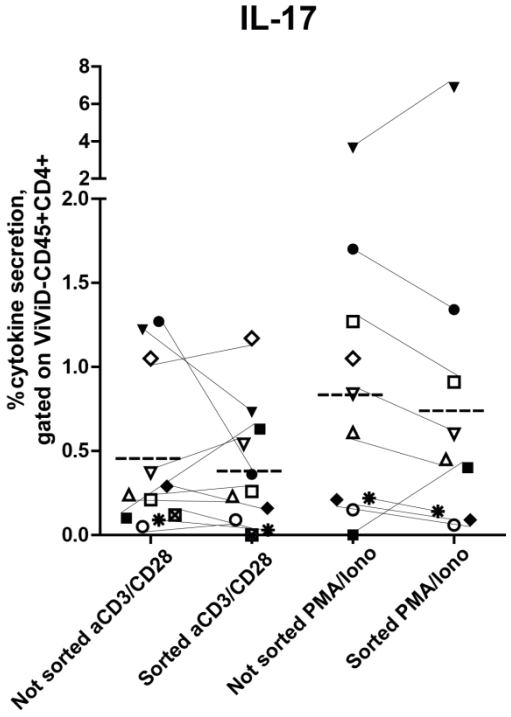

Supplementary Figure S9: The tumor microenvironment does not impact on the capacity of $CD4^+$ T cells to produce IL-17

Intracellular staining for IL-17 after 6h *ex vivo* stimulation with anti-CD3/CD28 beads or with PMA + ionomycin in the presence of brefeldin A and monensin. Cells were stimulated within the tumor digest or after sorting of $CD45^+CD4^+$ T cells and were analysed after gating on live $CD45^+CD4^+$ T cells. Each symbol represents an individual patient and the mean of each group is depicted. Results of unsorted and sorted T cells from the same patient are connected by a thin line.

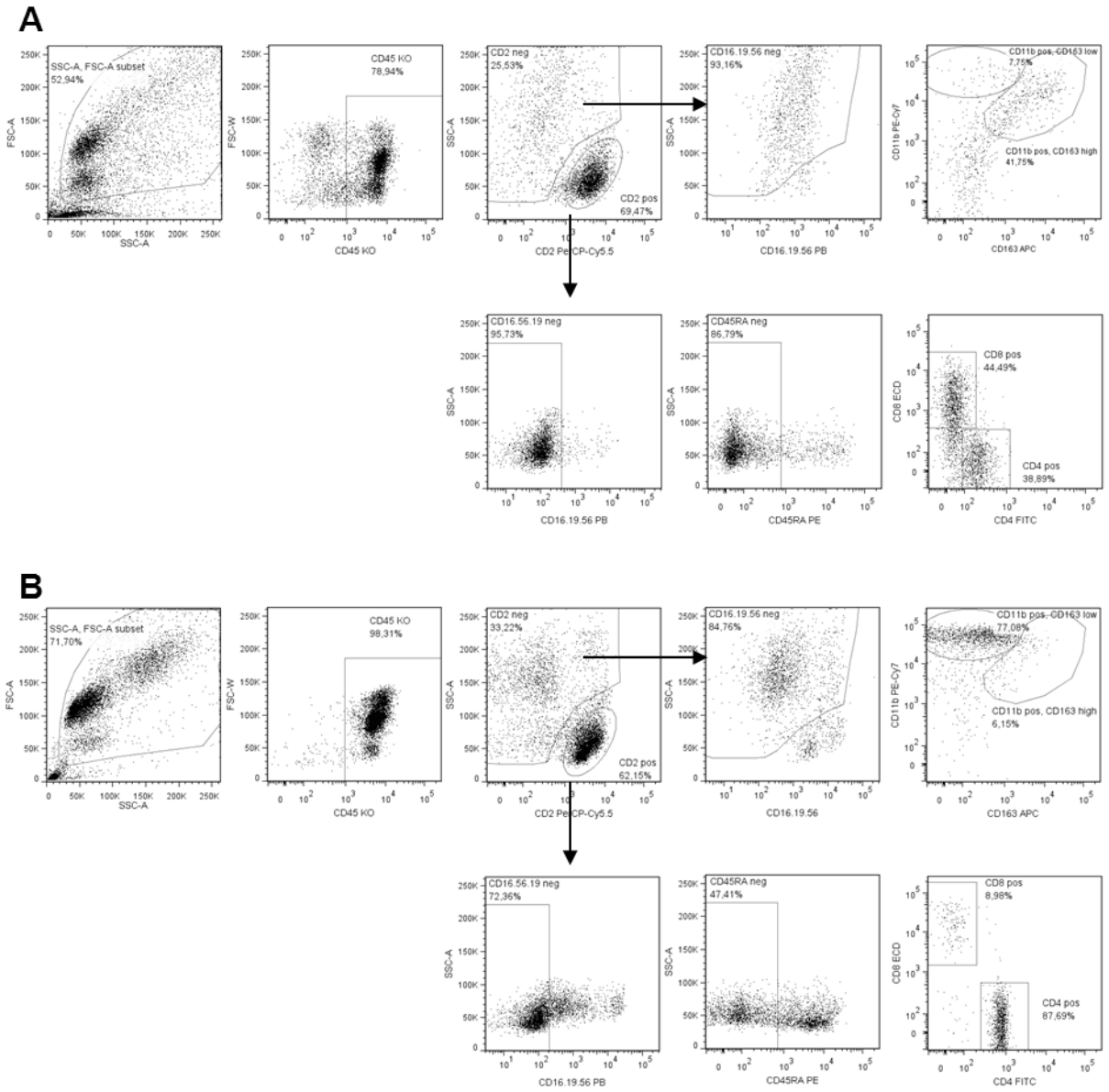

Supplementary Figure S10: Sorting strategy for myeloid cells and T cells from ccRCCs and blood

Sorting strategy for the simultaneous isolation of myeloid cells and T cells from (A) digested ccRCC tumors and (B) autologous PBMCs. After exclusion of cell debris, gates were set on $CD45^+$ cells. For the sorting of T cells gates were set on $CD2^+$ cells, $CD16^-$ $CD19^-$ and $CD56^-$ cells, followed by gating on $CD45RA^-$ cells and finally on either the $CD4^+$ or $CD8^+$ population. For the isolation of myeloid cells gates were set on $CD2^-$ cells, then on $CD16^-$ $CD19^-$ and $CD56^-$ cells, and finally on the $CD11b^+$ $CD163^{low}$ population (P_1 and T_1 fraction) or on the CD11b+$CD163^{high}$ population (T_2 fraction).

MATERIALS AND METHODS

Patient material

(i) Paraffin embedded material: Formalin-fixed, paraffin-embedded material from 60 patients with ccRCC, collected within the years 1993 to 2003 were identified in the archives of the Department of Pathology, University Hospital Zurich. Patients met the same criteria as described above for fresh patient material. The local ethical committee approved this study (KEK ZH Ref. nr, STV38-2005). Six patients died of causes not related to cancer and were excluded from the analysis. A summary of the patients' characteristics can be found in **Supplementary Table S2**.

(ii) Fresh ccRCC tumor samples and blood: 20 renal cancer patients were enrolled in the study. The patients underwent full or partial nephrectomy as part of their standard treatment at the Department of Urology, University Hospital Zurich. Tumor samples and peripheral blood were prospectively collected following informed consent in accordance with the Declaration of Helsinki. The local ethics committee and Swissmedic approved the study (EK-1017). All patients met the following criteria: a) a new renal tumor diagnosis with histological confirmation of a clear cell renal tumor subtype according to the 2004 WHO classification of renal tumors; b) no prior treatment for kidney cancer. A summary of the patients' characteristics can be found in **Supplementary Table S3**. PBMCs were isolated from peripheral whole blood by Ficoll (Ficoll-PaqueTM PLUS; GE Healthcare) density centrifugation. The tumor material was cut into multiple pieces of 2-4 mm^3 and further dissociated with DNase I Type IV (6 U/mL, Sigma) and Collagenase IV (1 mg/mL, Sigma) in DMEM (Gibco) plus Penicillin and Streptomycin (50 U/mL, Gibco) for 1-2 hours at 37 °C. The digested material was afterwards filtered and the obtained single cell suspension and the PBMCs were cryopreserved at -80°C until further analysis.

Flow Cytometry for phenotypical analysis

Surface staining with fluorochrome-conjugated antibodies was performed in PBS (NaCl (136mM, Fluka), Na_2HPO_4 (8mM, Roth), KH2PO4 (1.5mM, Roth), pH7) together with live/dead staining (LIVE/DEAD® Fixable Violet Dead Cell Stain Kit, Invitrogen) for 20 min at room temperature. Intracellular staining for CD68 and FoxP3 was performed according to manufacturer's instructions (eBioscience). Staining was measured with a flow cytometer (CyAn ADP 9, Beckman Coulter) and **data were analyzed with FlowJo software (TreeStar). All antibodies used in this study are listed in the supplementary materials and methods section and were purchased from BioLegend,** BD Biosciences, Beckman Coulter or eBioscience**.**

FACS sorting of T cells and TAMs from TILs and PBMCs

TILs and PBMCs were stained in sorting buffer (SB: PBS containing 2 % pooled human serum (PAA Laboratories) and 6 U/mL DNase I TypeIV (Sigma)) and stained with a mixture of fluorochrome-conjugated antibodies plus live-dead staining (LIVE/DEAD® Fixable Violet Dead Cell Stain Kit, Invitrogen). After staining for 20 min at 4 °C cells were washed and resuspended in

SB. Cells were either gated on $CD45^+CD8^+$ T cells and on $CD45^+CD4^+$ T cells, or in the case of simultaneous sorting of T cells and myeloid cells as shown in the gating strategy (**Supplementary Fig. S10**), and the different populations were sorted using a FACSAria III cell sorter (BD Biosciences).

Polyclonal stimulation and intracellular cytokine staining (ICS)

After sorting, cells were rested overnight in a 96-well round-bottom plate in TC-RPMI (RPMI (Gibco), supplemented with $NaHCO_3$ (2 g/L, Sigma), L-glutamine (2 mM, Sigma), Penicillin and Streptomycin (50 U/mL, Gibco), MEM nonessential amino acids (1X, Gibco), sodium pyruvate (1 mM, Gibco), 10^{-4} M β-mercaptoethanol (Sigma) and 10% pooled human serum) plus DNase I (6 U/mL, Sigma). T cells (at least 10'000 per well) were either cultured alone or with the tumor digest or with TAMs (ratio 1:1). After overnight resting, T cells were stimulated in 96-well plates in the presence or absence of the tumor digest or TAMs with anti-CD3/CD28 Dynabeads (Ratio T cells: beads was 1:3; Invitrogen, Cat. No. 111.41D) or with PMA (50 ng/mL Sigma) plus ionomycin (500 ng/mL, Sigma). Stimulation was performed for 6 h at 37 °C in TC-RPMI supplemented with Brefeldin A (10 µg/mL, Sigma) and DNase I Type IV (6 U/mL, Sigma). Cells were surface stained with a fluorochrome-conjugated antibody cocktail including live-dead staining (LIVE/DEAD® Fixable Violet Dead Cell Stain Kit (ViViD), Invitrogen) in PBS for 20 min at room temperature in the dark. Subsequently, cells were fixed in 4% formalin (Kantonsapotheke Zürich) and permeabilized with permeabilization buffer (PB: PBS supplemented with 2% FCS, 20 mM EDTA, 0.05% NaN_3, and 0.1% Saponin). For intracellular staining, cells were incubated with a mix of fluorescent-conjugated antibodies in PB for 20 min at room temperature in the dark. Cells were washed once with PB and resuspended in PBS containing 1% formalin before analysis by flow cytometry as described before. Antibodies used are listed in the supplementary material and methods section. When stimulation of T cells was performed in presence or absence of the tumor microenvironment cytokine production was measured after gating on ViViD- CD45+ CD14- CD16- CD19- CD8+ or CD4+ T cells, and in presence or absence of TAMs after gating on ViViD- CD45+ CD11b- CD4+ T cells.

RNA isolation

After FACS sorting and after co-culture experiments a portion of the cells (at least 500 cells) was resuspended in TRI Reagent (Ambion) and frozen at -80 °C until RNA isolation. RNA was isolated using a MagMAX™-96 for Microarrays Total RNA isolation kit (AM1839 Ambion) by the No-Spin Procedure according to the manufacturer's instructions. RNA isolation from FFPE material was performed using Trizol as described in the supplementary material and methods section.

Real-time quantitative reverse transcription–polymerase chain reaction (qRT-PCR)

The concentration and purity of RNA was evaluated using the NanoDrop ND-1000 spectrophotometer (NanoDrop Technologies). 500 ng of RNA was reverse transcribed using the high-capacity cDNA Reverse Transcription Kit (Applied Biosystems). The obtained cDNAs were stored at -20 °C until qRT-PCR analysis. Because of limited material, cDNA of sorted cells and paraffin punches was preamplified. Preamplification was performed for 14 cycles according to manufacturer's instructions (TaqMan® PreAmp Master Mix Kit, Applied Biosystems). We tested the correlation of expression analysed on original cDNA with that analysed on preamplified cDNA for selected highly expressed (CD45, CD68, CD163, TNF-α, MHC-II) and lowly expressed genes (iNOS, FoxP3, IL-10, IDO) and found an excellent correlation for all, confirming uniform preamplification for all samples (CD68 and CD163 are shown in **Supplementary Fig. S3**). qRT-PCR was done on a Rotor-Gene Q real-time PCR cycler (Qiagen) using commercially available predeveloped TaqMan reagents with optimized primer and probe concentrations (TaqMan® gene expression assays, Applied Biosystems) (**Supplementary Table S1**).

After an initial hold for 2 min at 50 C and 10 min at 95 C the probes were cycled 45 times at 95 C for 15 sec and at 60 C for 60 sec. All PCR reactions were performed in triplicates. Threshold cycle (Ct) values were determined with the Rotor-Gene Q Series software 1.7. ΔCt values were calculated by normalizing the target mRNA levels to (i) the endogenous control 18S rRNA (Hs03928990_g1), (ii) the endogenous control PPIA (Hs99999904_m1), or (iii) to the levels of CD4 as stated in the figure legends. Immune response-related genes other than CD45 were normalized to CD45. Because there was no correlation between CD45 transcripts and survival (**Fig. 1A**), this normalization will not obscure potential correlations between the expression of other immune response-related genes and survival. In some cases ΔCt levels were expressed as relative to the appropriate control. Therefore $\Delta\Delta$Ct values were determined (Ct target gene-Ct control) and fold change calculated with the formula $2^{-\Delta\Delta Ct}$.Ct values >38 cycles were interpreted such that the gene is not expressed. Fold changes in the range of a fold increase of <2 and a fold decrease of <0.5 was considered as not significant. This range was illustrated as shaded area in the figures.

Statistical analysis

The relationship between the expression of the target genes and patient survival was analysed using a univariate Cox proportional hazard regression model with 95% confidence intervals. Prognostic effect of variables that showed a correlation with survival in univariate analysis was tested for dependence on age at operation and pT by multivariate Cox regression analysis. Furthermore, data was dichotomized based on mean gene expression value of all analysed samples, log-rank test performed and Kaplan-Meier curves generated in which probability of overall survival was plotted over time. Correlations between different parameters were assessed using the Spearman Rho correlation test (IBM SPSS statistics software). Wilcoxon matched-pairs

signed rank test was used to analyse statistical significance between groups (GraphPad Prism Software). The criterion for significance was set at $p \leq 0.05$.

SUPPLEMENTARY MATERIALS AND METHODS

Antibodies used in this study were purchased from BioLegend (BL), BD Biosciences (BD), Beckman Coulter (BC) and eBioscience (eB).

Flow Cytometry for phenotypical analysis

Cells were stained with combinations of following fluorochrome-conjugated antibodies CD4 FITC (BD), Tim-3 PE (BL), CTLA-4 PE (BL), CD8 ECD (BC), CD3 PerCP (BL), PD-1 PE-Cy7 (BL), CD69 PE-Cy7 (BL), CD45RA PacificBlue (eB), CD45 KromeOrange (BC), FoxP3 APC (eB), CD45RA APC (BL), CD25 APC-Cy7 (BD), CD68 FITC (eB), PD-L1 PE (BL), CD14 ECD (BC), MR PerCPCy5.5 (BL), CD11b PE-Cy7 (BL), CD3 PacificBlue (BL)e, CD19 PacificBlue (BL), CD45 KromeOrange (BC), CD163 APC (BL) or PD-L1 APC (BL), HLA-DR APC-Cy7 (BL).

FACS sorting of T cells and TAMs from TILs and PBMCs

(i) Sorting of T cells only: processed tumors or PBMC

Surface staining mix: CD45 PerCP-Cy5.5 (BL), CD8 ECD (BC) and CD4 KromeOrange (BC).

(ii) Sorting of T cells plus TAMs: processed tumors or PBMC

Surface staining mix: CD45 KromeOrange (BC), CD19, CD16, CD56 PacificBlue (all BL), CD8 ECD (BC), CD4 FITC (BD), CD11b PE-Cy7 (BL), CD163 APC (BL), CD2 PerCP-Cy5.5 (BL), and CD45RA PE or PacificBlue (both eB).

Polyclonal stimulation and intracellular cytokine staining (ICS)

(i) Stimulation of T cells in presence or absence of tumor microenvironment

Surface staining mix: CD45 PerCP-Cy5.5 (BL), CD8 ECD (BC), CD4 KromeOrange (BC), CD14, CD16, CD19 PacificBlue (all BL); intracellular staining mix: IFN-γ FITC (BC), IL-17 PE (eB), IL-2 PE-Cy7 (BL), IL10 APC (eB).

(ii) Stimulation of T cells in presence or absence of TAMs

Surface staining mix: CD45 KromeOrange (BC), CD4 FITC (BD), CD11b PacificBlue (BL) with (A) or without TGF-β1 (LAP) PE (BL) (B); intracellular staining mix: (A) IL-4 PE-Cy7 (BL), IL-2 PerCP-Cy5.5 (BL), IL-10 APC (eB), (B) IL17 PE (eB), IFN-γ PE-Cy7 (BL), IL-13 APC (BL), TNF-α PerCPCy5.5 (BL).

RNA isolation from paraffin material

Deparaffinization of the paraffin punches was performed in 300 µL elution buffer (1 M Tris pH 8, 0.5 M EDTA pH 8, 20% SDS (all Ambion), ultrapure water (Sigma)) for 10 min at 95°C while shaking. Samples were subsequently centrifuged (Eppendorf centrifuge 5417R, Omnilab) for 10 min at 14'000 rpm and 4°C and digested with 3 µL of Proteinase K (18 +/- 4 mg/ml, Roche) for 72 hours at 55°C. Thereafter samples were centrifuged for 2 min at 14'000 rpm and 4°C and 250 µL of the obtained supernatants were transferred into new tubes. 750 µL TRIzol LS Reagent (Invitrogen) was added to each sample and tubes were mixed by vortexing. Samples were homogenized by centrifugation for 2 min at 14'000 rpm and 4°C using QIA-shredder columns. RNA purification was performed by phenol and chloroform extractions: 200 µL of chloroform was added to each flow-through, then samples were mixed by inverting the tubes, incubated at room temperature for 5 min until two phases were visible and centrifuged for 15 min at 14'000 rpm and 4°C. The upper aqueous phase containing the RNA was transferred into a new tube, 20 µg glycogen (Invitrogen) was added and the RNA precipitated by adding 0.5 mL isopropanol (99.9% V/V, Kantonsapotheke Zürich). Samples were subsequently incubated for 15 min at room temperature and centrifuged for 20 min at 14'000rpm and 4°C. After removing the supernatant the pellet was washed with 1 mL 75% ethanol (absolute for analysis, Merck), air-dried, dissolved in RNase free water (Sigma) and digested with 80 U/ml DNAse I (New England Biolabs) for 15 min at room temperature followed by an inactivation by 2 mM EDTA (Ambion) for 10 min at 65°C.

REFERENCES

1. Fridman, W.H., Pages, F., Sautes-Fridman, C., and Galon, J. 2012. The immune contexture in human tumours: impact on clinical outcome. *Nat Rev Cancer* 12:298-306.
2. Schreiber, R.D., Old, L.J., and Smyth, M.J. 2011. Cancer immunoediting: integrating immunity's roles in cancer suppression and promotion. *Science* 331:1565-1570.
3. Beck, C., Schreiber, H., and Rowley, D. 2001. Role of TGF-beta in immune-evasion of cancer. *Microsc Res Tech* 52:387-395.
4. Kawamura, K., Bahar, R., Natsume, W., Sakiyama, S., and Tagawa, M. 2002. Secretion of interleukin-10 from murine colon carcinoma cells suppresses systemic antitumor immunity and impairs protective immunity induced against the tumors. *Cancer Gene Ther* 9:109-115.
5. Sica, A., Schioppa, T., Mantovani, A., and Allavena, P. 2006. Tumour-associated macrophages are a distinct M2 polarised population promoting tumour progression: potential targets of anti-cancer therapy. *Eur J Cancer* 42:717-727.
6. Filipazzi, P., Huber, V., and Rivoltini, L. 2012. Phenotype, function and clinical implications of myeloid-derived suppressor cells in cancer patients. *Cancer Immunol Immunother* 61:255-263.
7. Facciabene, A., Motz, G.T., and Coukos, G. 2012. T-Regulatory Cells: Key Players in Tumor Immune Escape and Angiogenesis. *Cancer Res* 72:2162-2171.
8. Lewis, C.E., and Pollard, J.W. 2006. Distinct role of macrophages in different tumor microenvironments. *Cancer Res* 66:605-612.
9. Sica, A., Larghi, P., Mancino, A., Rubino, L., Porta, C., Totaro, M.G., Rimoldi, M., Biswas, S.K., Allavena, P., and Mantovani, A. 2008. Macrophage polarization in tumour progression. *Semin Cancer Biol* 18:349-355.
10. Bailey, C., Negus, R., Morris, A., Ziprin, P., Goldin, R., Allavena, P., Peck, D., and Darzi, A. 2007. Chemokine expression is associated with the accumulation of tumour associated macrophages (TAMs) and progression in human colorectal cancer. *Clin Exp Metastasis* 24:121-130.
11. Krausgruber, T., Saliba, D., Ryzhakov, G., Lanfrancotti, A., Blazek, K., and Udalova, I.A. 2010. IRF5 is required for late-phase TNF secretion by human dendritic cells. *Blood* 115:4421-4430.
12. Keller, R., Geiges, M., and Keist, R. 1990. L-arginine-dependent reactive nitrogen intermediates as mediators of tumor cell killing by activated macrophages. *Cancer Res* 50:1421-1425.
13. Satoh, T., Takeuchi, O., Vandenbon, A., Yasuda, K., Tanaka, Y., Kumagai, Y., Miyake, T., Matsushita, K., Okazaki, T., Saitoh, T., et al. 2010. The Jmjd3-Irf4 axis regulates M2 macrophage polarization and host responses against helminth infection. *Nat Immunol* 11:936-944.
14. Lau, S.K., Chu, P.G., and Weiss, L.M. 2004. CD163: a specific marker of macrophages in paraffin-embedded tissue samples. *Am J Clin Pathol* 122:794-801.
15. Stein, M., Keshav, S., Harris, N., and Gordon, S. 1992. Interleukin 4 potently enhances murine macrophage mannose receptor activity: a marker of alternative immunologic macrophage activation. *J Exp Med* 176:287-292.
16. Martinez, F.O., Gordon, S., Locati, M., and Mantovani, A. 2006. Transcriptional profiling of the human monocyte-to-macrophage differentiation and polarization: new molecules and patterns of gene expression. *J Immunol* 177:7303-7311.
17. Kutikov, A., Egleston, B.L., Wong, Y.N., and Uzzo, R.G. 2010. Evaluating overall survival and competing risks of death in patients with localized renal cell carcinoma using a comprehensive nomogram. *J Clin Oncol* 28:311-317.
18. Vickers, M.M., and Heng, D.Y. 2010. Prognostic and predictive biomarkers in renal cell carcinoma. *Target Oncol* 5:85-94.
19. Motzer, R.J., Bander, N.H., and Nanus, D.M. 1996. Renal-cell carcinoma. *N Engl J Med* 335:865-875.
20. Gouttefangeas, C., Stenzl, A., Stevanovic, S., and Rammensee, H.G. 2007. Immunotherapy of renal cell carcinoma. *Cancer Immunol Immunother* 56:117-128.

21. Morra, L., Rechsteiner, M., Casagrande, S., Duc Luu, V., Santimaria, R., Diener, P.A., Sulser, T., Kristiansen, G., Schraml, P., Moch, H., et al. 2011. Relevance of periostin splice variants in renal cell carcinoma. *Am J Pathol* 179:1513-1521.
22. Pello, O.M., De Pizzol, M., Mirolo, M., Soucek, L., Zammataro, L., Amabile, A., Doni, A., Nebuloni, M., Swigart, L.B., Evan, G.I., et al. 2012. Role of c-MYC in alternative activation of human macrophages and tumor-associated macrophage biology. *Blood* 119:411-421.
23. Mulders, P.F., Brouwers, A.H., Hulsbergen-van der Kaa, C.A., van Lin, E.N., Osanto, S., and de Mulder, P.H. 2008. [Guideline 'Renal cell carcinoma']. *Ned Tijdschr Geneeskd* 152:376-380.
24. Qian, B.Z., and Pollard, J.W. 2010. Macrophage diversity enhances tumor progression and metastasis. *Cell* 141:39-51.
25. Patsialou, A., Wyckoff, J., Wang, Y., Goswami, S., Stanley, E.R., and Condeelis, J.S. 2009. Invasion of human breast cancer cells in vivo requires both paracrine and autocrine loops involving the colony-stimulating factor-1 receptor. *Cancer Res* 69:9498-9506.
26. Gertler, F., and Condeelis, J. 2011. Metastasis: tumor cells becoming MENAcing. *Trends Cell Biol* 21:81-90.
27. Sallusto, F., Geginat, J., and Lanzavecchia, A. 2004. Central memory and effector memory T cell subsets: function, generation, and maintenance. *Annu Rev Immunol* 22:745-763.
28. Wherry, E.J., Ha, S.J., Kaech, S.M., Haining, W.N., Sarkar, S., Kalia, V., Subramaniam, S., Blattman, J.N., Barber, D.L., and Ahmed, R. 2007. Molecular signature of CD8+ T cell exhaustion during chronic viral infection. *Immunity* 27:670-684.
29. Attig, S., Hennenlotter, J., Pawelec, G., Klein, G., Koch, S.D., Pircher, H., Feyerabend, S., Wernet, D., Stenzl, A., Rammensee, H.G., et al. 2009. Simultaneous infiltration of polyfunctional effector and suppressor T cells into renal cell carcinomas. *Cancer Res* 69:8412-8419.
30. Kuang, D.M., Zhao, Q., Peng, C., Xu, J., Zhang, J.P., Wu, C., and Zheng, L. 2009. Activated monocytes in peritumoral stroma of hepatocellular carcinoma foster immune privilege and disease progression through PD-L1. *J Exp Med* 206:1327-1337.
31. Savage, N.D., de Boer, T., Walburg, K.V., Joosten, S.A., van Meijgaarden, K., Geluk, A., and Ottenhoff, T.H. 2008. Human anti-inflammatory macrophages induce Foxp3+ GITR+ CD25+ regulatory T cells, which suppress via membrane-bound TGFbeta-1. *J Immunol* 181:2220-2226.
32. Vasievich, E.A., and Huang, L. 2011. The suppressive tumor microenvironment: a challenge in cancer immunotherapy. *Mol Pharm* 8:635-641.
33. Nakano, O., Sato, M., Naito, Y., Suzuki, K., Orikasa, S., Aizawa, M., Suzuki, Y., Shintaku, I., Nagura, H., and Ohtani, H. 2001. Proliferative activity of intratumoral CD8(+) T-lymphocytes as a prognostic factor in human renal cell carcinoma: clinicopathologic demonstration of antitumor immunity. *Cancer Res* 61:5132-5136.
34. Kondo, T., Nakazawa, H., Ito, F., Hashimoto, Y., Osaka, Y., Futatsuyama, K., Toma, H., and Tanabe, K. 2006. Favorable prognosis of renal cell carcinoma with increased expression of chemokines associated with a Th1-type immune response. *Cancer Sci* 97:780-786.
35. Sakaguchi, S. 2003. The origin of FOXP3-expressing CD4+ regulatory T cells: thymus or periphery. *J Clin Invest* 112:1310-1312.
36. Griffiths, R.W., Elkord, E., Gilham, D.E., Ramani, V., Clarke, N., Stern, P.L., and Hawkins, R.E. 2007. Frequency of regulatory T cells in renal cell carcinoma patients and investigation of correlation with survival. *Cancer Immunol Immunother* 56:1743-1753.
37. Adotevi, O., Pere, H., Ravel, P., Haicheur, N., Badoual, C., Merillon, N., Medioni, J., Peyrard, S., Roncelin, S., Verkarre, V., et al. 2010. A decrease of regulatory T cells correlates with overall survival after sunitinib-based antiangiogenic therapy in metastatic renal cancer patients. *J Immunother* 33:991-998.
38. Hori, S., Takahashi, T., and Sakaguchi, S. 2003. Control of autoimmunity by naturally arising regulatory CD4+ T cells. *Adv Immunol* 81:331-371.
39. Siddiqui, S.A., Frigola, X., Bonne-Annee, S., Mercader, M., Kuntz, S.M., Krambeck, A.E., Sengupta, S., Dong, H., Cheville, J.C., Lohse, C.M., et al. 2007. Tumor-infiltrating Foxp3-CD4+CD25+ T cells predict poor survival in renal cell carcinoma. *Clin Cancer Res* 13:2075-2081.

40. Li, J.F., Chu, Y.W., Wang, G.M., Zhu, T.Y., Rong, R.M., Hou, J., and Xu, M. 2009. The prognostic value of peritumoral regulatory T cells and its correlation with intratumoral cyclooxygenase-2 expression in clear cell renal cell carcinoma. *BJU Int* 103:399-405.
41. Holness, C.L., and Simmons, D.L. 1993. Molecular cloning of CD68, a human macrophage marker related to lysosomal glycoproteins. *Blood* 81:1607-1613.
42. Mills, C.D., Kincaid, K., Alt, J.M., Heilman, M.J., and Hill, A.M. 2000. M-1/M-2 macrophages and the Th1/Th2 paradigm. *J Immunol* 164:6166-6173.
43. Mantovani, A., Sozzani, S., Locati, M., Allavena, P., and Sica, A. 2002. Macrophage polarization: tumor-associated macrophages as a paradigm for polarized M2 mononuclear phagocytes. *Trends Immunol* 23:549-555.
44. Gordon, S., and Martinez, F.O. 2010. Alternative activation of macrophages: mechanism and functions. *Immunity* 32:593-604.
45. Ropponen, K.M., Kellokoski, J.K., Lipponen, P.K., Eskelinen, M.J., Alanne, L., Alhava, E.M., and Kosma, V.M. 2000. Expression of inducible nitric oxide synthase in colorectal cancer and its association with prognosis. *Scand J Gastroenterol* 35:1204-1211.
46. Clear, A.J., Lee, A.M., Calaminici, M., Ramsay, A.G., Morris, K.J., Hallam, S., Kelly, G., Macdougall, F., Lister, T.A., and Gribben, J.G. 2010. Increased angiogenic sprouting in poor prognosis FL is associated with elevated numbers of CD163+ macrophages within the immediate sprouting microenvironment. *Blood* 115:5053-5056.
47. Komohara, Y., Ohnishi, K., Kuratsu, J., and Takeya, M. 2008. Possible involvement of the M2 anti-inflammatory macrophage phenotype in growth of human gliomas. *J Pathol* 216:15-24.
48. Gabrilovich, D.I., Ostrand-Rosenberg, S., and Bronte, V. 2012. Coordinated regulation of myeloid cells by tumours. *Nat Rev Immunol* 12:253-268.
49. Komohara, Y., Hasita, H., Ohnishi, K., Fujiwara, Y., Suzu, S., Eto, M., and Takeya, M. 2011. Macrophage infiltration and its prognostic relevance in clear cell renal cell carcinoma. *Cancer Sci* 102:1424-1431.
50. Sato, T., Terai, M., Tamura, Y., Alexeev, V., Mastrangelo, M.J., and Selvan, S.R. 2011. Interleukin 10 in the tumor microenvironment: a target for anticancer immunotherapy. *Immunol Res* 51:170-182.
51. Daurkin, I., Eruslanov, E., Stoffs, T., Perrin, G.Q., Algood, C., Gilbert, S.M., Rosser, C.J., Su, L.M., Vieweg, J., and Kusmartsev, S. 2011. Tumor-associated macrophages mediate immunosuppression in the renal cancer microenvironment by activating the 15-lipoxygenase-2 pathway. *Cancer Res* 71:6400-6409.
52. Fourcade, J., Sun, Z., Benallaoua, M., Guillaume, P., Luescher, I.F., Sander, C., Kirkwood, J.M., Kuchroo, V., and Zarour, H.M. 2010. Upregulation of Tim-3 and PD-1 expression is associated with tumor antigen-specific CD8+ T cell dysfunction in melanoma patients. *J Exp Med* 207:2175-2186.

ACKNOWLEDGEMENTS

We thank Dr. Giovanni Sais and Prof. Dr. Maurizio Provenzano (Department of Urology, University Hospital Zurich) for help in setting up the qRT-PCR screen, Dr. Claudia Dumrese (Center for Microscopy and Image Analysis, University Zurich) for assistance in FACS sorting and Prof. Dr. Burkhardt Seifert (Division of Biostatistics, University Zurich) for advice in statistical analysis. This work was supported in part by the Cancer Research Institute/Cancer Vaccine Collaborative, the Hanne Liebermann Foundation, Dr. Leopold and Carmen Ellinger Foundation Zurich, Science Foundation Oncology SFO, Swiss National Science Foundation (3238BO, 10314531), the Hartmann Müller Foundation Zurich and Alumni Grant University Zurich.

2.3 Supplemental results

In addition to the results presented in part 2.1 and 2.2 I performed supplemental experiments and analysis that are not included in the manuscripts and are displayed and discussed in the appendix.

2.4 Collaborative projects

I contributed to collaborative projects with Dr. Rowayda Peters (University Hospital Zurich, Department of Oncology, Zurich, Switzerland) and Dr. Natko Nuber (University Hospital Zurich, Department of Oncology, Lab of Tumor immunology, Zurich, Switzerland). My contribution resulted in two co-authorships. The manuscripts are not further discussed in the scope of this thesis. For details please refer to the appendix.

3. DISCUSSION

After a debate on anti-tumor immunity for over more than 150 years it is by now well accepted that the immune system can recognize and destroy tumor cells. The fact that we observed T cell responses towards the TAA Cyclin D1 (CCND1) in the blood of ccRCC patients indicates that also in ccRCC immunosurveillance occurs.

There is growing evidence that analysis of phenotype and functions of T cells in the peripheral blood often do not reflect the situation within tumors. It was for example shown that Melan-A specific T cells in the blood of melanoma patients were able to lyse melanoma cells, whereas Melan-A specific T cells isolated from TILs were functionally impaired (184). When we analyzed T cell responses towards CCND1 in TILs of those patients that showed a CCND1-response in PBMCs we could not detect CCND1-specific T cell responses in TILs of any of the patients tested. One explanation could be the reduced quality of TILs compared to PBMCs. However, it could also well be that T cells within TILs are not able to respond to antigenic stimulation due to the suppressive impact of the tumor microenvironment on T cell function as we observed in the case of polyclonal stimulation experiments. Since we could detect CCND1-specific T cells in TILs via tetramer staining, but not via intracellular cytokine staining, we hypothesize that CCND1-specific cells were present within TILs, but the tumor microenvironment made them unable to respond to antigenic-stimulation.

Hanahan and Weinberg added tumor promoting inflammation and the escape of the tumor from immune attack recently as emerging hallmarks of cancer (185). TAMs are part of the tumor microenvironment and they are known to be involved in many processes leading to tumor progression, such as angiogenesis, metastasis, but also the suppression of anti-tumor immunity (142). Macrophages isolated from lymph nodes of melanoma patients were for example shown to down-regulate the tumor-specific cytotoxicity of T cells and NK cells (186). TAMs have a poor antigen-presenting capacity and produce suppressive mediators like IL-10 and TGF-β that leads to an inhibition of T cell activation and proliferation (143). We observed a significant increase in IL-10 production from T cells when incubated with TAMs, confirming the results of a recently published paper on the immunoregulatory effect of ccRCC-infiltrating TAMs (187). In addition to that, we showed that T cells produce less effector cytokines and increased amounts of Th2 cytokines in the presence of TAMs. While in some studies an increase of FoxP3 and CTLA-4 was detected in T cells upon coculture with TAMs isolated from ccRCC (187), we observed an increase in the immunoregulatory molecules PD-1 and Tim-3. These results suggest that TAMs may use multiple mechanisms to skew T cells into a more regulated phenotype and functional state, favoring escape of ccRCC from the immune control.

It was shown that TAMs are unable to produce IL-12 and therefore induce Tregs instead of triggering a Th1 response (188). M2 macrophage polarization induces the production of a distinct panel of chemokines, such as CCL17, CCL22 and CCL24. The corresponding chemokine receptors CCR4 and CCR3 are expressed on Th2 cells and Tregs, which results in a recruitment of these cells and to an amplification of a Th2 polarized response (189). Furthermore, human monocytes were shown to differentiate into M2-like macrophages in the presence of $CD4^+CD25^+FoxP3^+$ Tregs mediated by Treg-derived IL-10 (190). In accordance with this, we detected a significant correlation between CD68 and FoxP3 mRNA levels in our patient cohort of fresh tumor samples (**Figure D-1**), suggesting a simultaneous accumulation of Tregs and TAMs within ccRCC tumors. Both cell types were shown to negatively impact on patient prognosis in different cancer types (142, 191, 192), what we confirmed for ccRCC. Furthermore CD163 and the M2-like genes FN-1 and IRF-4 correlated with reduced survival in our patient cohort. CD163 was associated before with TAMs bearing a M2-like phenotype and a correlation with reduced survival has been recently observed in different cancers including ccRCC (152, 193, 194).

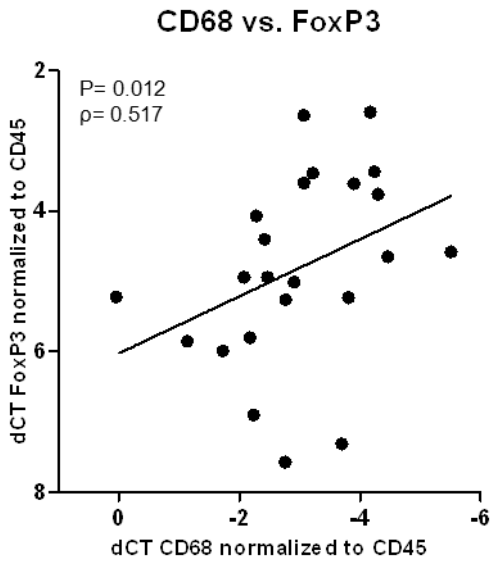

Figure D-1: Correlation of FoxP3 and CD68 mRNA levels in fresh ccRCC tumor samples

qRT-PCR analysis was performed on cDNA of fresh RCCs. Spearman's Rho correlation test revealed a significant correlation between FoxP3 and CD68 mRNA levels.

We observed increased levels of the M1-marker iNOS in small tumors and high levels of the M2-marker CD163 in large tumors. A transition of M1 polarization toward M2 polarization during tumor progression was already suggested by Mantovani and colleagues (112). The observed induction of M2-realted genes in $CD11b^+$ cells when incubated with ccRCC tumor cells support the idea that ccRCC tumor cells directly impact on M1 to M2 polarization (152). It was proposed that the M1 to M2 transition goes in line with the establishment of an immunoregulatory milieu during the immunoediting process leading to tumor immune-escape (112). We detected a

positive correlation of high expression levels of FoxP3 and IL-10 with increased pT indicative for the development of an immunoreguatory milieu during tumor progression. The finding that larger tumors contain more IL-10 than small tumors supports data from a previous study on ccRCC (187).

Based on the results of this thesis we hypothesize the following scenario of immunoregulation during ccRCC development (illustrated in **Figure D-2**):

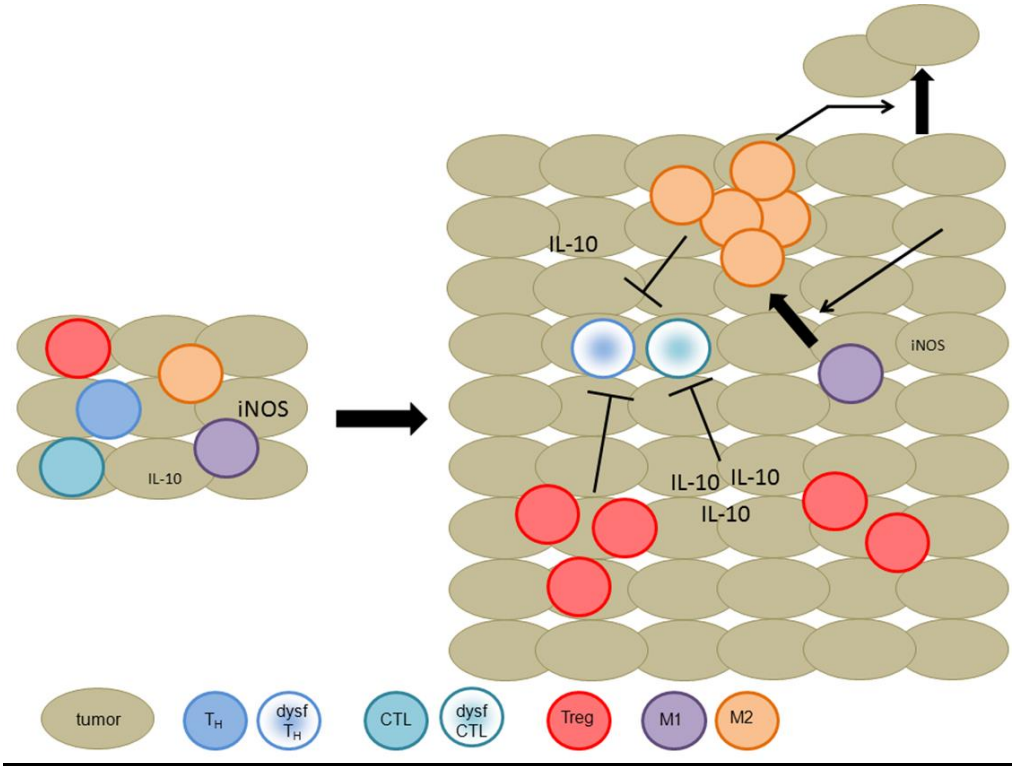

Figure D-2: Immunoregulation in ccRCC

The establishment of an immunoregulatory milieu with increased levels of IL-10 and Tregs goes in line with a switch from M1 macrophages to M2-like macrophages promoting immune escape, tumor progression and metastasis (figure created by Maries van den Broek).

High expression levels of iNOS correlated with reduced tumor stage, suggesting that when macrophages are recruited to developing tumors, TAMs display an M1 phenotype. We detected a low expression level of IL-10 and FoxP3 in small tumors that increased with tumor progression. Additionally, high levels of M2-associated genes correlated with increased tumor stage, suggesting the establishment of an immunoregulatory milieu during tumor progression, which is characterized by elevated levels of IL-10, increased presence of Tregs and a phenotype switch of M1 towards M2 TAMs. Tumor cells at least partially contribute to this switch. Immunosuppressive factors of the tumor microenvironment, including M2 TAMs, impact on the cytokine profile of T cells leading to reduced production of effector cytokines and increased secretion of IL-10. Furthermore we detected an increased expression of immunoregulatory molecules on T cells

from TILs, which is a sign for exhaustion of T cells within tumors. Another hint for the impaired function of T cells might be that we were not able to detect TAA-specific T cell responses in TILs despite the detection of TAA-specific T cell responses in 85% of PBMCS as observed in the case of CCND1. Finally, the increased presence of TAMs also correlated with an increased incidence of metastasis, suggesting an impact of TAMs in promoting ccRCC spread. Significant correlation of high iNOS levels with increased survival time and a significant correlation of CD68 and M2-like markers with reduced survival strengthen the point that TAMs influence disease outcome in ccRCC patients.

Based on the above, different therapeutic tools can be designed to target the immunoregulatory milieu that might improve standard and immunotherapy for ccRCC patients.

Cytokine-based immunotherapy is so far the only treatment option for metastatic ccRCC that was shown to result in few complete responses (195, 196). However, high-dose IL-2 treatment is very toxic, can be only administered to a selected group of patients and in most of the cases the long-term effect is not achieved (197). One explanation for this might be the increased presence of Tregs in ccRCC patients receiving IL-2-based immunotherapy (198). Like activated T cells also Tregs express the IL-2 receptor (IL-2R), therefore not only effector T cells are stimulated to proliferate, but also Tregs. The fact that increased levels of FoxP3, the transcription factor specific for Tregs, correlated with reduced survival, and because of the immunosuppressive functions of Tregs, depletion of these cells might be one possibility to improve anti-tumor immunity and thus patient outcome. Tregs express high levels of CD25, a subunit of the IL-2R on the surface. Targeting CD25 by using depleting mAbs or an IL-2-diphteria toxin fusion protein was shown to enhance anti-tumor immune responses (199, 200). However, no striking effects were observed so far, eventually because the lack of specificity in that also activated T cells express CD25 and might be depleted along the way (201). The IL-2-diphteria toxin fusion protein denileukin diftitox in combination with high dose IL-2 showed promising results in a phase I study of patients with metastatic RCC (202). The use of IL-2/anti-IL-2 immune complexes may increase efficacy and reduce toxicity at the same time (203). Such effects were observed with human IL-2 in complex with the human-IL-2-specific antibody MAB602 in mice, but it still has to be defined whether these complexes have comparable functions in humans. Blocking CTLA-4 is another way to target Tregs and was shown to result in the enhanced recruitment of memory T cells in metastatic melanoma (204). In one study, treatment with the CTLA-4 antibody ipilimumab revealed partial response in 5 of 40 patients with metastatic RCC (205). High dose IL-2 in combination with CTLA-4 blockage revealed promising results in patients with metastatic melanoma (206). Since also high dose IL-2 cytokine therapy shows some effect in ccRCC patients, the combination of high-dose IL-2 with CTLA-4 antibodies might be one strategy to improve outcome of cytokine-based immunotherapy for those patients.

As described before, CTLA-4 is not only expressed on Tregs, but also on effector T cells where its interaction with CD28 on APCs leads to an inhibition of the T cell response. Besides

antibodies blocking CTLA-4, there are other novel immune-modulating antibodies under investigation that target co-stimulatory signals involved in T cell activation. As seen in **Figure D-3** there are several immune checkpoints that can be targeted either with agonistic antibodies stimulating the signaling of activating receptors or with blocking antibodies that suppress the signaling of inhibitory receptors (17). In this study here we saw an increased expression of CTLA-4, PD-1 and also Tim-3 in TILs and thus these molecules might be interesting therapeutic targets in ccRCC.

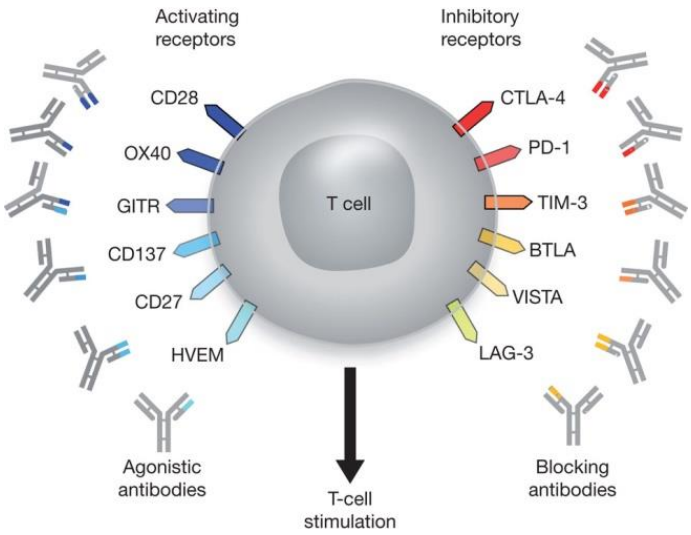

Figure D-3: T cell targets for immunoregulatroy antibody therapy

Summary of activating and inhibitory receptors on activated T cells that can be targeted by antibody-mediated immunotherapy (17).

Our results suggest that macrophages play a central role in the local immunoregulation during ccRCC development and hence targeting TAMs might present a potential strategy to control tumor growth. Unspecific depletion of TAMs can be achieved by for example the administration of bisphosphonate clodronic acid. This treatment reduced microvascular density and tumor growth in a mouse model of RCC (RENCA) (207). Also the monoclonal antibody bevacizumab, known to inhibit VEGF-A, a chemoattractant for macrophages, was shown to block macrophage recruitment in different tumor mouse models thereby inhibiting tumor growth (208, 209).

Depending on their polarization TAMs can either promote tumor progression or tumor rejection via activation or suppression of various subsets of effector and regulatory immune cells. Therefore, instead of macrophage depletion, re-orientation of the tumor-promoting phenotype of TAMs into the anti-tumoral phenotype sounds promising although technically very challenging. Several studies in mice demonstrate that re-polarization of TAMs is possible. Treatment with the M1-associated cytokine IL-12 altered the functional activity of TAMs from a tumor-promoting profile to a proinflammatory profile and inhibited tumor growth in the RENCA mouse model (210, 211). Furthermore, TAMs lacking STAT-6, the mediator of IL-4 and IL-13 signaling, display a M1

phenotype with high levels of NO, leading to spontaneous rejection of mammary carcinoma in mice (212). IL-10 was observed to increase during tumor progression and is known to induce an M2-like phenotype in TAMs. Since IL-10 has many other immunoregulatory functions, like impairing the antigen-presentation capabilities of APCs, thereby inhibiting T cell proliferation (213), neutralizing IL-10 could be another immunotherapeutic strategy to induce M2 to M1 polarization and to increase anti-tumor immunity. In this regard, the combination of CpG and anti-IL10 receptor antibodies was shown to induce a switch from M2 to M1 with a reduction in tumor size (214, 215), and also the inhibition of STAT-3 activity, required for IL-10 biological functions, restored the M1-related functions in TAMs and revealed tumor inhibition (216).
It was shown that PD-1 ligation induces IL-10 production by monocytes leading to an inhibition of $CD4^+$ T cell responses (217). We saw an increased expression of PD-1 on TILs and also elevated levels of PD-L1 on M2 TAMs suggesting that also in ccRCC tumors the impact of TAMs on T cells might be mediated trough PD-1/PD-L1 interactions. Thus, blockade of either PD-1 or PD-L1 might represent one possibility to overcome immunosuppression. Indeed, an antibody blocking PD-1 was recently tested in different cancers in a clinical trial (218) that resulted in an objective response in 27% (9/33) of RCC patients (219).

To date, the clinical evaluation of immunotherapy has mainly focused on single agents that interfere with individual steps in the anti-tumor immune response. However, it is becoming clear that monotherapies are unlikely to be sufficiently effective (220). Instead, targeting of multiple pathways and processes may be necessary. These include (i) the induction of immunogenic cell death through radiotherapy (221) chemotherapy (222), or targeted therapy such as kinase inhibitors (223), plus (ii) improving antigen presentation (224) including upregulation of co-stimulatory signals (24), plus (iii) blocking immune checkpoints of T cell activation, or regulatory cell types.

4. REFERENCES

1. Coley, W.B. 1891. II. Contribution to the Knowledge of Sarcoma. *Ann Surg* 14:199-220.
2. Coley, W.B. 1910. The Treatment of Inoperable Sarcoma by Bacterial Toxins (the Mixed Toxins of the Streptococcus erysipelas and the Bacillus prodigiosus). *Proc R Soc Med* 3:1-48.
3. Ehrlich, P. 1909. Ueber den jetzigen Stand der Karzinomforschung. *Ned Tjdschr Geneeskd* 5:273-290.
4. Burnet, M. 1957. Cancer; a biological approach. I. The processes of control. *Br Med J* 1:779-786.
5. Thomas, L. 1959. Discussion: In Cellular and Humoral Aspects of the Hypersensitive States, H.S. Lawrence, ed. (New York: Hoeber-Harper) 529-532.
6. Stutman, O. 1974. Tumor development after 3-methylcholanthrene in immunologically deficient athymic-nude mice. *Science* 183:534-536.
7. Rygaard, J., and Povlsen, C.O. 1974. The mouse mutant nude does not develop spontaneous tumours. An argument against immunological surveillance. *Acta Pathol Microbiol Scand B Microbiol Immunol* 82:99-106.
8. Old, L.J., and Boyse, E.A. 1964. Immunology of Experimental Tumors. *Annu Rev Med* 15:167-186.
9. Vesely, M.D., Kershaw, M.H., Schreiber, R.D., and Smyth, M.J. 2011. Natural innate and adaptive immunity to cancer. *Annu Rev Immunol* 29:235-271.
10. Dunn, G.P., Koebel, C.M., and Schreiber, R.D. 2006. Interferons, immunity and cancer immunoediting. *Nat Rev Immunol* 6:836-848.
11. Frisch, M., Biggar, R.J., Engels, E.A., and Goedert, J.J. 2001. Association of cancer with AIDS-related immunosuppression in adults. *JAMA* 285:1736-1745.
12. Vajdic, C.M., McDonald, S.P., McCredie, M.R., van Leeuwen, M.T., Stewart, J.H., Law, M., Chapman, J.R., Webster, A.C., Kaldor, J.M., and Grulich, A.E. 2006. Cancer incidence before and after kidney transplantation. *JAMA* 296:2823-2831.
13. Knuth, A., Danowski, B., Oettgen, H.F., and Old, L.J. 1984. T-cell-mediated cytotoxicity against autologous malignant melanoma: analysis with interleukin 2-dependent T-cell cultures. *Proc Natl Acad Sci U S A* 81:3511-3515.
14. Nuber, N., Curioni-Fontecedro, A., Matter, C., Soldini, D., Tiercy, J.M., von Boehmer, L., Moch, H., Dummer, R., Knuth, A., and van den Broek, M. 2010. Fine analysis of spontaneous MAGE-C1/CT7-specific immunity in melanoma patients. *Proc Natl Acad Sci U S A* 107:15187-15192.
15. Clark, W.H., Jr., Elder, D.E., Guerry, D.t., Braitman, L.E., Trock, B.J., Schultz, D., Synnestvedt, M., and Halpern, A.C. 1989. Model predicting survival in stage I melanoma based on tumor progression. *J Natl Cancer Inst* 81:1893-1904.
16. Clemente, C.G., Mihm, M.C., Jr., Bufalino, R., Zurrida, S., Collini, P., and Cascinelli, N. 1996. Prognostic value of tumor infiltrating lymphocytes in the vertical growth phase of primary cutaneous melanoma. *Cancer* 77:1303-1310.
17. Mellman, I., Coukos, G., and Dranoff, G. 2011. Cancer immunotherapy comes of age. *Nature* 480:480-489.
18. Prestwich, R.J., Errington, F., Hatfield, P., Merrick, A.E., Ilett, E.J., Selby, P.J., and Melcher, A.A. 2008. The immune system--is it relevant to cancer development, progression and treatment? *Clin Oncol (R Coll Radiol)* 20:101-112.
19. Gilboa, E. 1999. The makings of a tumor rejection antigen. *Immunity* 11:263-270.
20. Mellman, I., and Steinman, R.M. 2001. Dendritic cells: specialized and regulated antigen processing machines. *Cell* 106:255-258.
21. Trombetta, E.S., and Mellman, I. 2005. Cell biology of antigen processing in vitro and in vivo. *Annu Rev Immunol* 23:975-1028.
22. Steinman, R.M. 2003. Some interfaces of dendritic cell biology. *APMIS* 111:675-697.
23. Palucka, K., and Banchereau, J. 2012. Cancer immunotherapy via dendritic cells. *Nat Rev Cancer* 12:265-277.
24. Chambers, C.A., and Allison, J.P. 1999. Costimulatory regulation of T cell function. *Curr Opin Cell Biol* 11:203-210.
25. Hawiger, D., Inaba, K., Dorsett, Y., Guo, M., Mahnke, K., Rivera, M., Ravetch, J.V., Steinman, R.M., and Nussenzweig, M.C. 2001. Dendritic cells induce peripheral T cell unresponsiveness under steady state conditions in vivo. *J Exp Med* 194:769-779.
26. Probst, H.C., Lagnel, J., Kollias, G., and van den Broek, M. 2003. Inducible transgenic mice reveal resting dendritic cells as potent inducers of CD8+ T cell tolerance. *Immunity* 18:713-720.
27. Darrasse-Jeze, G., Deroubaix, S., Mouquet, H., Victora, G.D., Eisenreich, T., Yao, K.H., Masilamani, R.F., Dustin, M.L., Rudensky, A., Liu, K., et al. 2009. Feedback control of regulatory T cell homeostasis by dendritic cells in vivo. *J Exp Med* 206:1853-1862.

28. Wei, S., Kryczek, I., Zou, L., Daniel, B., Cheng, P., Mottram, P., Curiel, T., Lange, A., and Zou, W. 2005. Plasmacytoid dendritic cells induce CD8+ regulatory T cells in human ovarian carcinoma. *Cancer Res* 65:5020-5026.
29. Derbinski, J., Schulte, A., Kyewski, B., and Klein, L. 2001. Promiscuous gene expression in medullary thymic epithelial cells mirrors the peripheral self. *Nat Immunol* 2:1032-1039.
30. Gotter, J., Brors, B., Hergenhahn, M., and Kyewski, B. 2004. Medullary epithelial cells of the human thymus express a highly diverse selection of tissue-specific genes colocalized in chromosomal clusters. *J Exp Med* 199:155-166.
31. Schoenberger, S.P., Toes, R.E., van der Voort, E.I., Offringa, R., and Melief, C.J. 1998. T-cell help for cytotoxic T lymphocytes is mediated by CD40-CD40L interactions. *Nature* 393:480-483.
32. Smyth, M.J., Godfrey, D.I., and Trapani, J.A. 2001. A fresh look at tumor immunosurveillance and immunotherapy. *Nat Immunol* 2:293-299.
33. Schreiber, R.D., Old, L.J., and Smyth, M.J. 2011. Cancer immunoediting: integrating immunity's roles in cancer suppression and promotion. *Science* 331:1565-1570.
34. Dunn, G.P., Bruce, A.T., Ikeda, H., Old, L.J., and Schreiber, R.D. 2002. Cancer immunoediting: from immunosurveillance to tumor escape. *Nat Immunol* 3:991-998.
35. Dunn, G.P., Old, L.J., and Schreiber, R.D. 2004. The three Es of cancer immunoediting. *Annu Rev Immunol* 22:329-360.
36. Shankaran, V., Ikeda, H., Bruce, A.T., White, J.M., Swanson, P.E., Old, L.J., and Schreiber, R.D. 2001. IFNgamma and lymphocytes prevent primary tumour development and shape tumour immunogenicity. *Nature* 410:1107-1111.
37. Girardi, M., Oppenheim, D.E., Steele, C.R., Lewis, J.M., Glusac, E., Filler, R., Hobby, P., Sutton, B., Tigelaar, R.E., and Hayday, A.C. 2001. Regulation of cutaneous malignancy by gammadelta T cells. *Science* 294:605-609.
38. Smyth, M.J., Thia, K.Y., Street, S.E., Cretney, E., Trapani, J.A., Taniguchi, M., Kawano, T., Pelikan, S.B., Crowe, N.Y., and Godfrey, D.I. 2000. Differential tumor surveillance by natural killer (NK) and NKT cells. *J Exp Med* 191:661-668.
39. Smyth, M.J., Crowe, N.Y., and Godfrey, D.I. 2001. NK cells and NKT cells collaborate in host protection from methylcholanthrene-induced fibrosarcoma. *Int Immunol* 13:459-463.
40. Cosman, D., Mullberg, J., Sutherland, C.L., Chin, W., Armitage, R., Fanslow, W., Kubin, M., and Chalupny, N.J. 2001. ULBPs, novel MHC class I-related molecules, bind to CMV glycoprotein UL16 and stimulate NK cytotoxicity through the NKG2D receptor. *Immunity* 14:123-133.
41. Pende, D., Rivera, P., Marcenaro, S., Chang, C.C., Biassoni, R., Conte, R., Kubin, M., Cosman, D., Ferrone, S., Moretta, L., et al. 2002. Major histocompatibility complex class I-related chain A and UL16-binding protein expression on tumor cell lines of different histotypes: analysis of tumor susceptibility to NKG2D-dependent natural killer cell cytotoxicity. *Cancer Res* 62:6178-6186.
42. Mistry, A.R., and O'Callaghan, C.A. 2007. Regulation of ligands for the activating receptor NKG2D. *Immunology* 121:439-447.
43. Groh, V., Rhinehart, R., Secrist, H., Bauer, S., Grabstein, K.H., and Spies, T. 1999. Broad tumor-associated expression and recognition by tumor-derived gamma delta T cells of MICA and MICB. *Proc Natl Acad Sci U S A* 96:6879-6884.
44. Jinushi, M., Takehara, T., Tatsumi, T., Kanto, T., Groh, V., Spies, T., Kimura, R., Miyagi, T., Mochizuki, K., Sasaki, Y., et al. 2003. Expression and role of MICA and MICB in human hepatocellular carcinomas and their regulation by retinoic acid. *Int J Cancer* 104:354-361.
45. Vetter, C.S., Groh, V., thor Straten, P., Spies, T., Brocker, E.B., and Becker, J.C. 2002. Expression of stress-induced MHC class I related chain molecules on human melanoma. *J Invest Dermatol* 118:600-605.
46. Street, S.E., Trapani, J.A., MacGregor, D., and Smyth, M.J. 2002. Suppression of lymphoma and epithelial malignancies effected by interferon gamma. *J Exp Med* 196:129-134.
47. van den Broek, M.E., Kagi, D., Ossendorp, F., Toes, R., Vamvakas, S., Lutz, W.K., Melief, C.J., Zinkernagel, R.M., and Hengartner, H. 1996. Decreased tumor surveillance in perforin-deficient mice. *J Exp Med* 184:1781-1790.
48. Smyth, M.J., Thia, K.Y., Street, S.E., MacGregor, D., Godfrey, D.I., and Trapani, J.A. 2000. Perforin-mediated cytotoxicity is critical for surveillance of spontaneous lymphoma. *J Exp Med* 192:755-760.
49. Liu, J., Xiang, Z., and Ma, X. 2004. Role of IFN regulatory factor-1 and IL-12 in immunological resistance to pathogenesis of N-methyl-N-nitrosourea-induced T lymphoma. *J Immunol* 173:1184-1193.
50. Rousalova, I., and Krepela, E. 2010. Granzyme B-induced apoptosis in cancer cells and its regulation (review). *Int J Oncol* 37:1361-1378.
51. Boyman, O., and Sprent, J. 2012. The role of interleukin-2 during homeostasis and activation of the immune system. *Nat Rev Immunol* 12:180-190.

52. Koebel, C.M., Vermi, W., Swann, J.B., Zerafa, N., Rodig, S.J., Old, L.J., Smyth, M.J., and Schreiber, R.D. 2007. Adaptive immunity maintains occult cancer in an equilibrium state. *Nature* 450:903-907.
53. Khazaie, K., Prifti, S., Beckhove, P., Griesbach, A., Russell, S., Collins, M., and Schirrmacher, V. 1994. Persistence of dormant tumor cells in the bone marrow of tumor cell-vaccinated mice correlates with long-term immunological protection. *Proc Natl Acad Sci U S A* 91:7430-7434.
54. Feuerer, M., Rocha, M., Bai, L., Umansky, V., Solomayer, E.F., Bastert, G., Diel, I.J., and Schirrmacher, V. 2001. Enrichment of memory T cells and other profound immunological changes in the bone marrow from untreated breast cancer patients. *Int J Cancer* 92:96-105.
55. Schirrmacher, V. 2001. T-cell immunity in the induction and maintenance of a tumour dormant state. *Semin Cancer Biol* 11:285-295.
56. Aguirre-Ghiso, J.A. 2007. Models, mechanisms and clinical evidence for cancer dormancy. *Nat Rev Cancer* 7:834-846.
57. Karrison, T.G., Ferguson, D.J., and Meier, P. 1999. Dormancy of mammary carcinoma after mastectomy. *J Natl Cancer Inst* 91:80-85.
58. MacKie, R.M., Reid, R., and Junor, B. 2003. Fatal melanoma transferred in a donated kidney 16 years after melanoma surgery. *N Engl J Med* 348:567-568.
59. von Boehmer, L., Draenert, A., Jungraithmayr, W., Inci, I., Niklaus, S., Boehler, A., Hofer, M., Stahel, R., Soltermann, A., van den Broek, M., et al. 2012. Immunosuppression and lung cancer of donor origin after bilateral lung transplantation. *Lung Cancer* 76:118-122.
60. Zitvogel, L., Tesniere, A., and Kroemer, G. 2006. Cancer despite immunosurveillance: immunoselection and immunosubversion. *Nat Rev Immunol* 6:715-727.
61. Algarra, I., Cabrera, T., and Garrido, F. 2000. The HLA crossroad in tumor immunology. *Hum Immunol* 61:65-73.
62. Marincola, F.M., Jaffee, E.M., Hicklin, D.J., and Ferrone, S. 2000. Escape of human solid tumors from T-cell recognition: molecular mechanisms and functional significance. *Adv Immunol* 74:181-273.
63. Seliger, B., Maeurer, M.J., and Ferrone, S. 2000. Antigen-processing machinery breakdown and tumor growth. *Immunol Today* 21:455-464.
64. Jager, E., Ringhoffer, M., Altmannsberger, M., Arand, M., Karbach, J., Jager, D., Oesch, F., and Knuth, A. 1997. Immunoselection in vivo: independent loss of MHC class I and melanocyte differentiation antigen expression in metastatic melanoma. *Int J Cancer* 71:142-147.
65. Khong, H.T., Wang, Q.J., and Rosenberg, S.A. 2004. Identification of multiple antigens recognized by tumor-infiltrating lymphocytes from a single patient: tumor escape by antigen loss and loss of MHC expression. *J Immunother* 27:184-190.
66. Stern-Ginossar, N., Gur, C., Biton, M., Horwitz, E., Elboim, M., Stanietsky, N., Mandelboim, M., and Mandelboim, O. 2008. Human microRNAs regulate stress-induced immune responses mediated by the receptor NKG2D. *Nat Immunol* 9:1065-1073.
67. Hinz, S., Trauzold, A., Boenicke, L., Sandberg, C., Beckmann, S., Bayer, E., Walczak, H., Kalthoff, H., and Ungefroren, H. 2000. Bcl-XL protects pancreatic adenocarcinoma cells against CD95- and TRAIL-receptor-mediated apoptosis. *Oncogene* 19:5477-5486.
68. Shin, M.S., Kim, H.S., Lee, S.H., Park, W.S., Kim, S.Y., Park, J.Y., Lee, J.H., Lee, S.K., Lee, S.N., Jung, S.S., et al. 2001. Mutations of tumor necrosis factor-related apoptosis-inducing ligand receptor 1 (TRAIL-R1) and receptor 2 (TRAIL-R2) genes in metastatic breast cancers. *Cancer Res* 61:4942-4946.
69. Li, M.O., Wan, Y.Y., Sanjabi, S., Robertson, A.K., and Flavell, R.A. 2006. Transforming growth factor-beta regulation of immune responses. *Annu Rev Immunol* 24:99-146.
70. Kawamura, K., Bahar, R., Natsume, W., Sakiyama, S., and Tagawa, M. 2002. Secretion of interleukin-10 from murine colon carcinoma cells suppresses systemic antitumor immunity and impairs protective immunity induced against the tumors. *Cancer Gene Ther* 9:109-115.
71. O'Garra, A., Barrat, F.J., Castro, A.G., Vicari, A., and Hawrylowicz, C. 2008. Strategies for use of IL-10 or its antagonists in human disease. *Immunol Rev* 223:114-131.
72. Uyttenhove, C., Pilotte, L., Theate, I., Stroobant, V., Colau, D., Parmentier, N., Boon, T., and Van den Eynde, B.J. 2003. Evidence for a tumoral immune resistance mechanism based on tryptophan degradation by indoleamine 2,3-dioxygenase. *Nat Med* 9:1269-1274.
73. Chambers, C.A., Kuhns, M.S., Egen, J.G., and Allison, J.P. 2001. CTLA-4-mediated inhibition in regulation of T cell responses: mechanisms and manipulation in tumor immunotherapy. *Annu Rev Immunol* 19:565-594.
74. Keir, M.E., Butte, M.J., Freeman, G.J., and Sharpe, A.H. 2008. PD-1 and its ligands in tolerance and immunity. *Annu Rev Immunol* 26:677-704.
75. Greenwald, R.J., Freeman, G.J., and Sharpe, A.H. 2005. The B7 family revisited. *Annu Rev Immunol* 23:515-548.
76. Munn, D.H., Sharma, M.D., and Mellor, A.L. 2004. Ligation of B7-1/B7-2 by human CD4+ T cells triggers indoleamine 2,3-dioxygenase activity in dendritic cells. *J Immunol* 172:4100-4110.

77. Puccetti, P., and Grohmann, U. 2007. IDO and regulatory T cells: a role for reverse signalling and non-canonical NF-kappaB activation. *Nat Rev Immunol* 7:817-823.
78. Saudemont, A., and Quesnel, B. 2004. In a model of tumor dormancy, long-term persistent leukemic cells have increased B7-H1 and B7.1 expression and resist CTL-mediated lysis. *Blood* 104:2124-2133.
79. Fourcade, J., Sun, Z., Benallaoua, M., Guillaume, P., Luescher, I.F., Sander, C., Kirkwood, J.M., Kuchroo, V., and Zarour, H.M. 2010. Upregulation of Tim-3 and PD-1 expression is associated with tumor antigen-specific CD8+ T cell dysfunction in melanoma patients. *J Exp Med* 207:2175-2186.
80. Murphy, K.M., Nelson, C.A., and Sedy, J.R. 2006. Balancing co-stimulation and inhibition with BTLA and HVEM. *Nat Rev Immunol* 6:671-681.
81. Fourcade, J., Sun, Z., Pagliano, O., Guillaume, P., Luescher, I.F., Sander, C., Kirkwood, J.M., Olive, D., Kuchroo, V., and Zarour, H.M. 2012. CD8(+) T cells specific for tumor antigens can be rendered dysfunctional by the tumor microenvironment through upregulation of the inhibitory receptors BTLA and PD-1. *Cancer Res* 72:887-896.
82. Barclay, A.N., Wright, G.J., Brooke, G., and Brown, M.H. 2002. CD200 and membrane protein interactions in the control of myeloid cells. *Trends Immunol* 23:285-290.
83. Gorczynski, R.M., Cattral, M.S., Chen, Z., Hu, J., Lei, J., Min, W.P., Yu, G., and Ni, J. 1999. An immunoadhesin incorporating the molecule OX-2 is a potent immunosuppressant that prolongs allo- and xenograft survival. *J Immunol* 163:1654-1660.
84. Kretz-Rommel, A., and Bowdish, K.S. 2008. Rationale for anti-CD200 immunotherapy in B-CLL and other hematologic malignancies: new concepts in blocking immune suppression. *Expert Opin Biol Ther* 8:5-15.
85. Petermann, K.B., Rozenberg, G.I., Zedek, D., Groben, P., McKinnon, K., Buehler, C., Kim, W.Y., Shields, J.M., Penland, S., Bear, J.E., et al. 2007. CD200 is induced by ERK and is a potential therapeutic target in melanoma. *J Clin Invest* 117:3922-3929.
86. Gorczynski, R.M., Lee, L., and Boudakov, I. 2005. Augmented Induction of CD4+CD25+ Treg using monoclonal antibodies to CD200R. *Transplantation* 79:1180-1183.
87. Gabrilovich, D.I., Ostrand-Rosenberg, S., and Bronte, V. 2012. Coordinated regulation of myeloid cells by tumours. *Nat Rev Immunol* 12:253-268.
88. Sakaguchi, S. 2003. The origin of FOXP3-expressing CD4+ regulatory T cells: thymus or periphery. *J Clin Invest* 112:1310-1312.
89. Huang, B., Pan, P.Y., Li, Q., Sato, A.I., Levy, D.E., Bromberg, J., Divino, C.M., and Chen, S.H. 2006. Gr-1+CD115+ immature myeloid suppressor cells mediate the development of tumor-induced T regulatory cells and T-cell anergy in tumor-bearing host. *Cancer Res* 66:1123-1131.
90. Sakaguchi, S., Wing, K., Onishi, Y., Prieto-Martin, P., and Yamaguchi, T. 2009. Regulatory T cells: how do they suppress immune responses? *Int Immunol* 21:1105-1111.
91. Ralainirina, N., Poli, A., Michel, T., Poos, L., Andres, E., Hentges, F., and Zimmer, J. 2007. Control of NK cell functions by CD4+CD25+ regulatory T cells. *J Leukoc Biol* 81:144-153.
92. Chen, M.L., Pittet, M.J., Gorelik, L., Flavell, R.A., Weissleder, R., von Boehmer, H., and Khazaie, K. 2005. Regulatory T cells suppress tumor-specific CD8 T cell cytotoxicity through TGF-beta signals in vivo. *Proc Natl Acad Sci U S A* 102:419-424.
93. Curiel, T.J. 2007. Tregs and rethinking cancer immunotherapy. *J Clin Invest* 117:1167-1174.
94. Knutson, K.L., and Disis, M.L. 2005. Tumor antigen-specific T helper cells in cancer immunity and immunotherapy. *Cancer Immunol Immunother* 54:721-728.
95. Ostrand-Rosenberg, S. 2008. Immune surveillance: a balance between protumor and antitumor immunity. *Curr Opin Genet Dev* 18:11-18.
96. Yu, H., Pardoll, D., and Jove, R. 2009. STATs in cancer inflammation and immunity: a leading role for STAT3. *Nat Rev Cancer* 9:798-809.
97. Reich, N.C., and Liu, L. 2006. Tracking STAT nuclear traffic. *Nat Rev Immunol* 6:602-612.
98. Takeda, K., and Akira, S. 2000. STAT family of transcription factors in cytokine-mediated biological responses. *Cytokine Growth Factor Rev* 11:199-207.
99. Lee, H., Pal, S.K., Reckamp, K., Figlin, R.A., and Yu, H. 2011. STAT3: a target to enhance antitumor immune response. *Curr Top Microbiol Immunol* 344:41-59.
100. Karin, M., and Greten, F.R. 2005. NF-kappaB: linking inflammation and immunity to cancer development and progression. *Nat Rev Immunol* 5:749-759.
101. Bui, J.D., and Schreiber, R.D. 2007. Cancer immunosurveillance, immunoediting and inflammation: independent or interdependent processes? *Curr Opin Immunol* 19:203-208.
102. El-Serag, H.B., and Rudolph, K.L. 2007. Hepatocellular carcinoma: epidemiology and molecular carcinogenesis. *Gastroenterology* 132:2557-2576.
103. Haybaeck, J., Zeller, N., Wolf, M.J., Weber, A., Wagner, U., Kurrer, M.O., Bremer, J., Iezzi, G., Graf, R., Clavien, P.A., et al. 2009. A lymphotoxin-driven pathway to hepatocellular carcinoma. *Cancer Cell* 16:295-308.

104. Tumanov, A.V., Kuprash, D.V., and Nedospasov, S.A. 2003. The role of lymphotoxin in development and maintenance of secondary lymphoid tissues. *Cytokine Growth Factor Rev* 14:275-288.
105. Summers-DeLuca, L.E., McCarthy, D.D., Cosovic, B., Ward, L.A., Lo, C.C., Scheu, S., Pfeffer, K., and Gommerman, J.L. 2007. Expression of lymphotoxin-alphabeta on antigen-specific T cells is required for DC function. *J Exp Med* 204:1071-1081.
106. Greten, F.R., and Karin, M. 2004. The IKK/NF-kappaB activation pathway-a target for prevention and treatment of cancer. *Cancer Lett* 206:193-199.
107. Langowski, J.L., Zhang, X., Wu, L., Mattson, J.D., Chen, T., Smith, K., Basham, B., McClanahan, T., Kastelein, R.A., and Oft, M. 2006. IL-23 promotes tumour incidence and growth. *Nature* 442:461-465.
108. Moore, R.J., Owens, D.M., Stamp, G., Arnott, C., Burke, F., East, N., Holdsworth, H., Turner, L., Rollins, B., Pasparakis, M., et al. 1999. Mice deficient in tumor necrosis factor-alpha are resistant to skin carcinogenesis. *Nat Med* 5:828-831.
109. Numasaki, M., Fukushi, J., Ono, M., Narula, S.K., Zavodny, P.J., Kudo, T., Robbins, P.D., Tahara, H., and Lotze, M.T. 2003. Interleukin-17 promotes angiogenesis and tumor growth. *Blood* 101:2620-2627.
110. Benchetrit, F., Ciree, A., Vives, V., Warnier, G., Gey, A., Sautes-Fridman, C., Fossiez, F., Haicheur, N., Fridman, W.H., and Tartour, E. 2002. Interleukin-17 inhibits tumor cell growth by means of a T-cell-dependent mechanism. *Blood* 99:2114-2121.
111. Calzascia, T., Pellegrini, M., Hall, H., Sabbagh, L., Ono, N., Elford, A.R., Mak, T.W., and Ohashi, P.S. 2007. TNF-alpha is critical for antitumor but not antiviral T cell immunity in mice. *J Clin Invest* 117:3833-3845.
112. Sica, A., Larghi, P., Mancino, A., Rubino, L., Porta, C., Totaro, M.G., Rimoldi, M., Biswas, S.K., Allavena, P., and Mantovani, A. 2008. Macrophage polarization in tumour progression. *Semin Cancer Biol* 18:349-355.
113. Stein, M., Keshav, S., Harris, N., and Gordon, S. 1992. Interleukin 4 potently enhances murine macrophage mannose receptor activity: a marker of alternative immunologic macrophage activation. *J Exp Med* 176:287-292.
114. Sinha, P., Clements, V.K., and Ostrand-Rosenberg, S. 2005. Interleukin-13-regulated M2 macrophages in combination with myeloid suppressor cells block immune surveillance against metastasis. *Cancer Res* 65:11743-11751.
115. Cua, D.J., and Stohlman, S.A. 1997. In vivo effects of T helper cell type 2 cytokines on macrophage antigen-presenting cell induction of T helper subsets. *J Immunol* 159:5834-5840.
116. Doyle, A.G., Herbein, G., Montaner, L.J., Minty, A.J., Caput, D., Ferrara, P., and Gordon, S. 1994. Interleukin-13 alters the activation state of murine macrophages in vitro: comparison with interleukin-4 and interferon-gamma. *Eur J Immunol* 24:1441-1445.
117. Mills, C.D., Kincaid, K., Alt, J.M., Heilman, M.J., and Hill, A.M. 2000. M-1/M-2 macrophages and the Th1/Th2 paradigm. *J Immunol* 164:6166-6173.
118. Darnell, J.E., Jr., Kerr, I.M., and Stark, G.R. 1994. Jak-STAT pathways and transcriptional activation in response to IFNs and other extracellular signaling proteins. *Science* 264:1415-1421.
119. Trinchieri, G., and Gerosa, F. 1996. Immunoregulation by interleukin-12. *J Leukoc Biol* 59:505-511.
120. Biswas, S.K., and Mantovani, A. 2010. Macrophage plasticity and interaction with lymphocyte subsets: cancer as a paradigm. *Nat Immunol* 11:889-896.
121. MacMicking, J., Xie, Q.W., and Nathan, C. 1997. Nitric oxide and macrophage function. *Annu Rev Immunol* 15:323-350.
122. Krausgruber, T., Saliba, D., Ryzhakov, G., Lanfrancotti, A., Blazek, K., and Udalova, I.A. 2010. IRF5 is required for late-phase TNF secretion by human dendritic cells. *Blood* 115:4421-4430.
123. Takeda, K., Tanaka, T., Shi, W., Matsumoto, M., Minami, M., Kashiwamura, S., Nakanishi, K., Yoshida, N., Kishimoto, T., and Akira, S. 1996. Essential role of Stat6 in IL-4 signalling. *Nature* 380:627-630.
124. Lawrence, T., and Natoli, G. 2011. Transcriptional regulation of macrophage polarization: enabling diversity with identity. *Nat Rev Immunol* 11:750-761.
125. Chang, C.I., Liao, J.C., and Kuo, L. 2001. Macrophage arginase promotes tumor cell growth and suppresses nitric oxide-mediated tumor cytotoxicity. *Cancer Res* 61:1100-1106.
126. Cheng, F., Wang, H.W., Cuenca, A., Huang, M., Ghansah, T., Brayer, J., Kerr, W.G., Takeda, K., Akira, S., Schoenberger, S.P., et al. 2003. A critical role for Stat3 signaling in immune tolerance. *Immunity* 19:425-436.
127. Brayer, J., Cheng, F., Wang, H., Horna, P., Vicente-Suarez, I., Pinilla-Ibarz, J., and Sotomayor, E.M. 2010. Enhanced CD8 T cell cross-presentation by macrophages with targeted disruption of STAT3. *Immunol Lett* 131:126-130.

128. Satoh, T., Takeuchi, O., Vandenbon, A., Yasuda, K., Tanaka, Y., Kumagai, Y., Miyake, T., Matsushita, K., Okazaki, T., Saitoh, T., et al. 2010. The Jmjd3-Irf4 axis regulates M2 macrophage polarization and host responses against helminth infection. *Nat Immunol* 11:936-944.
129. Gordon, S. 2003. Alternative activation of macrophages. *Nat Rev Immunol* 3:23-35.
130. Lin, E.Y., Nguyen, A.V., Russell, R.G., and Pollard, J.W. 2001. Colony-stimulating factor 1 promotes progression of mammary tumors to malignancy. *J Exp Med* 193:727-740.
131. Duyndam, M.C., Hilhorst, M.C., Schluper, H.M., Verheul, H.M., van Diest, P.J., Kraal, G., Pinedo, H.M., and Boven, E. 2002. Vascular endothelial growth factor-165 overexpression stimulates angiogenesis and induces cyst formation and macrophage infiltration in human ovarian cancer xenografts. *Am J Pathol* 160:537-548.
132. Solinas, G., Schiarea, S., Liguori, M., Fabbri, M., Pesce, S., Zammataro, L., Pasqualini, F., Nebuloni, M., Chiabrando, C., Mantovani, A., et al. 2010. Tumor-conditioned macrophages secrete migration-stimulating factor: a new marker for M2-polarization, influencing tumor cell motility. *J Immunol* 185:642-652.
133. Sica, A., Schioppa, T., Mantovani, A., and Allavena, P. 2006. Tumour-associated macrophages are a distinct M2 polarised population promoting tumour progression: potential targets of anti-cancer therapy. *Eur J Cancer* 42:717-727.
134. Lopez, M., Bony, V., Martinache, C., Vincent, F., Chokri, M., Abina, M.A., and Bernard, J. 1996. Tumoricidal potential of human macrophages grown in vitro from blood monocytes. *J Exp Ther Oncol* 1:143-154.
135. Yanagawa, E., Uchida, A., Moore, M., and Micksche, M. 1985. Autologous tumor killing and natural cytotoxic activity of tumor-associated macrophages in cancer patients. *Cancer Immunol Immunother* 19:163-167.
136. Cameron, D.J., and O'Brien, P. 1982. Cytotoxicity of cancer patient's macrophages for tumor cells. *Cancer* 50:498-502.
137. Holness, C.L., and Simmons, D.L. 1993. Molecular cloning of CD68, a human macrophage marker related to lysosomal glycoproteins. *Blood* 81:1607-1613.
138. Lau, S.K., Chu, P.G., and Weiss, L.M. 2004. CD163: a specific marker of macrophages in paraffin-embedded tissue samples. *Am J Clin Pathol* 122:794-801.
139. Allavena, P., Chieppa, M., Bianchi, G., Solinas, G., Fabbri, M., Laskarin, G., and Mantovani, A. 2010. Engagement of the mannose receptor by tumoral mucins activates an immune suppressive phenotype in human tumor-associated macrophages. *Clin Dev Immunol* 2010:547179.
140. Martinez, F.O., Gordon, S., Locati, M., and Mantovani, A. 2006. Transcriptional profiling of the human monocyte-to-macrophage differentiation and polarization: new molecules and patterns of gene expression. *J Immunol* 177:7303-7311.
141. Pello, O.M., De Pizzol, M., Mirolo, M., Soucek, L., Zammataro, L., Amabile, A., Doni, A., Nebuloni, M., Swigart, L.B., Evan, G.I., et al. 2012. Role of c-MYC in alternative activation of human macrophages and tumor-associated macrophage biology. *Blood* 119:411-421.
142. Bingle, L., Brown, N.J., and Lewis, C.E. 2002. The role of tumour-associated macrophages in tumour progression: implications for new anticancer therapies. *J Pathol* 196:254-265.
143. Mantovani, A., Sozzani, S., Locati, M., Allavena, P., and Sica, A. 2002. Macrophage polarization: tumor-associated macrophages as a paradigm for polarized M2 mononuclear phagocytes. *Trends Immunol* 23:549-555.
144. Hagemann, T., and Lawrence, T. 2009. Investigating macrophage and malignant cell interactions in vitro. *Methods Mol Biol* 512:325-332.
145. Condeelis, J., and Pollard, J.W. 2006. Macrophages: obligate partners for tumor cell migration, invasion, and metastasis. *Cell* 124:263-266.
146. Patsialou, A., Wyckoff, J., Wang, Y., Goswami, S., Stanley, E.R., and Condeelis, J.S. 2009. Invasion of human breast cancer cells in vivo requires both paracrine and autocrine loops involving the colony-stimulating factor-1 receptor. *Cancer Res* 69:9498-9506.
147. Denardo, D.G., Brennan, D.J., Rexhepaj, E., Ruffell, B., Shiao, S.L., Madden, S.F., Gallagher, W.M., Wadhwani, N., Keil, S.D., Junaid, S.A., et al. 2011. Leukocyte Complexity Predicts Breast Cancer Survival and Functionally Regulates Response to Chemotherapy. *Cancer Discov* 1:54-67.
148. Wang, W., Wyckoff, J.B., Goswami, S., Wang, Y., Sidani, M., Segall, J.E., and Condeelis, J.S. 2007. Coordinated regulation of pathways for enhanced cell motility and chemotaxis is conserved in rat and mouse mammary tumors. *Cancer Res* 67:3505-3511.
149. Philippar, U., Roussos, E.T., Oser, M., Yamaguchi, H., Kim, H.D., Giampieri, S., Wang, Y., Goswami, S., Wyckoff, J.B., Lauffenburger, D.A., et al. 2008. A Mena invasion isoform potentiates EGF-induced carcinoma cell invasion and metastasis. *Dev Cell* 15:813-828.
150. Di Modugno, F., Bronzi, G., Scanlan, M.J., Del Bello, D., Cascioli, S., Venturo, I., Botti, C., Nicotra, M.R., Mottolese, M., Natali, P.G., et al. 2004. Human Mena protein, a serex-defined antigen overexpressed in breast cancer eliciting both humoral and CD8+ T-cell immune response. *Int J Cancer* 109:909-918.

151. Di Modugno, F., Mottolese, M., Di Benedetto, A., Conidi, A., Novelli, F., Perracchio, L., Venturo, I., Botti, C., Jager, E., Santoni, A., et al. 2006. The cytoskeleton regulatory protein hMena (ENAH) is overexpressed in human benign breast lesions with high risk of transformation and human epidermal growth factor receptor-2-positive/hormonal receptor-negative tumors. *Clin Cancer Res* 12:1470-1478.
152. Komohara, Y., Hasita, H., Ohnishi, K., Fujiwara, Y., Suzu, S., Eto, M., and Takeya, M. 2011. Macrophage infiltration and its prognostic relevance in clear cell renal cell carcinoma. *Cancer Sci* 102:1424-1431.
153. Savage, N.D., de Boer, T., Walburg, K.V., Joosten, S.A., van Meijgaarden, K., Geluk, A., and Ottenhoff, T.H. 2008. Human anti-inflammatory macrophages induce Foxp3+ GITR+ CD25+ regulatory T cells, which suppress via membrane-bound TGFbeta-1. *J Immunol* 181:2220-2226.
154. Lewis, C.E., and Pollard, J.W. 2006. Distinct role of macrophages in different tumor microenvironments. *Cancer Res* 66:605-612.
155. Thoenes, W., Storkel, S., and Rumpelt, H.J. 1986. Histopathology and classification of renal cell tumors (adenomas, oncocytomas and carcinomas). The basic cytological and histopathological elements and their use for diagnostics. *Pathol Res Pract* 181:125-143.
156. Mulders, P.F., Brouwers, A.H., Hulsbergen-van der Kaa, C.A., van Lin, E.N., Osanto, S., and de Mulder, P.H. 2008. [Guideline 'Renal cell carcinoma']. *Ned Tijdschr Geneeskd* 152:376-380.
157. Jemal, A., Siegel, R., Ward, E., Hao, Y., Xu, J., Murray, T., and Thun, M.J. 2008. Cancer statistics, 2008. *CA Cancer J Clin* 58:71-96.
158. Volpe, A., and Patard, J.J. 2010. Prognostic factors in renal cell carcinoma. *World J Urol* 28:319-327.
159. Moch, H., Gasser, T., Amin, M.B., Torhorst, J., Sauter, G., and Mihatsch, M.J. 2000. Prognostic utility of the recently recommended histologic classification and revised TNM staging system of renal cell carcinoma: a Swiss experience with 588 tumors. *Cancer* 89:604-614.
160. Gudbjartsson, T., Hardarson, S., Petursdottir, V., Thoroddsen, A., Magnusson, J., and Einarsson, G.V. 2005. Histological subtyping and nuclear grading of renal cell carcinoma and their implications for survival: a retrospective nation-wide study of 629 patients. *Eur Urol* 48:593-600.
161. Oosterwijk, E., Rathmell, W.K., Junker, K., Brannon, A.R., Pouliot, F., Finley, D.S., Mulders, P.F., Kirkali, Z., Uemura, H., and Belldegrun, A. 2011. Basic research in kidney cancer. *Eur Urol* 60:622-633.
162. Haddad, H., and Rini, B.I. 2012. Current treatment considerations in metastatic renal cell carcinoma. *Curr Treat Options Oncol* 13:212-229.
163. Chow, W.H., Dong, L.M., and Devesa, S.S. 2010. Epidemiology and risk factors for kidney cancer. *Nat Rev Urol* 7:245-257.
164. Parsons, J.K., Schoenberg, M.S., and Carter, H.B. 2001. Incidental renal tumors: casting doubt on the efficacy of early intervention. *Urology* 57:1013-1015.
165. Shuin, T., Kondo, K., Torigoe, S., Kishida, T., Kubota, Y., Hosaka, M., Nagashima, Y., Kitamura, H., Latif, F., Zbar, B., et al. 1994. Frequent somatic mutations and loss of heterozygosity of the von Hippel-Lindau tumor suppressor gene in primary human renal cell carcinomas. *Cancer Res* 54:2852-2855.
166. Kim, W.Y., and Kaelin, W.G. 2004. Role of VHL gene mutation in human cancer. *J Clin Oncol* 22:4991-5004.
167. Kapitsinou, P.P., and Haase, V.H. 2008. The VHL tumor suppressor and HIF: insights from genetic studies in mice. *Cell Death Differ* 15:650-659.
168. van Rooijen, E., Voest, E.E., Logister, I., Bussmann, J., Korving, J., van Eeden, F.J., Giles, R.H., and Schulte-Merker, S. 2010. von Hippel-Lindau tumor suppressor mutants faithfully model pathological hypoxia-driven angiogenesis and vascular retinopathies in zebrafish. *Dis Model Mech* 3:343-353.
169. Janzen, N.K., Kim, H.L., Figlin, R.A., and Belldegrun, A.S. 2003. Surveillance after radical or partial nephrectomy for localized renal cell carcinoma and management of recurrent disease. *Urol Clin North Am* 30:843-852.
170. Motzer, R.J., Bander, N.H., and Nanus, D.M. 1996. Renal-cell carcinoma. *N Engl J Med* 335:865-875.
171. Schrader, A.J., Varga, Z., Hegele, A., Pfoertner, S., Olbert, P., and Hofmann, R. 2006. Second-line strategies for metastatic renal cell carcinoma: classics and novel approaches. *J Cancer Res Clin Oncol* 132:137-149.
172. Escudier, B., Eisen, T., Stadler, W.M., Szczylik, C., Oudard, S., Siebels, M., Negrier, S., Chevreau, C., Solska, E., Desai, A.A., et al. 2007. Sorafenib in advanced clear-cell renal-cell carcinoma. *N Engl J Med* 356:125-134.
173. Motzer, R.J., Michaelson, M.D., Rosenberg, J., Bukowski, R.M., Curti, B.D., George, D.J., Hudes, G.R., Redman, B.G., Margolin, K.A., and Wilding, G. 2007. Sunitinib efficacy against advanced renal cell carcinoma. *J Urol* 178:1883-1887.

174. Ratain, M.J., Eisen, T., Stadler, W.M., Flaherty, K.T., Kaye, S.B., Rosner, G.L., Gore, M., Desai, A.A., Patnaik, A., Xiong, H.Q., et al. 2006. Phase II placebo-controlled randomized discontinuation trial of sorafenib in patients with metastatic renal cell carcinoma. *J Clin Oncol* 24:2505-2512.
175. Motzer, R.J., Michaelson, M.D., Redman, B.G., Hudes, G.R., Wilding, G., Figlin, R.A., Ginsberg, M.S., Kim, S.T., Baum, C.M., DePrimo, S.E., et al. 2006. Activity of SU11248, a multitargeted inhibitor of vascular endothelial growth factor receptor and platelet-derived growth factor receptor, in patients with metastatic renal cell carcinoma. *J Clin Oncol* 24:16-24.
176. Penn, I. 1995. Primary kidney tumors before and after renal transplantation. *Transplantation* 59:480-485.
177. Gouttefangeas, C., Stenzl, A., Stevanovic, S., and Rammensee, H.G. 2007. Immunotherapy of renal cell carcinoma. *Cancer Immunol Immunother* 56:117-128.
178. Balch, C.M., Riley, L.B., Bae, Y.J., Salmeron, M.A., Platsoucas, C.D., von Eschenbach, A., and Itoh, K. 1990. Patterns of human tumor-infiltrating lymphocytes in 120 human cancers. *Arch Surg* 125:200-205.
179. Ritchie, A.W., and deKernion, J.B. 1987. The natural history and clinical features of renal carcinoma. *Semin Nephrol* 7:131-139.
180. Snow, R.M., and Schellhammer, P.F. 1982. Spontaneous regression of metastatic renal cell carcinoma. *Urology* 20:177-181.
181. 1999. Interferon-alpha and survival in metastatic renal carcinoma: early results of a randomised controlled trial. Medical Research Council Renal Cancer Collaborators. *Lancet* 353:14-17.
182. Geiger, C., Nossner, E., Frankenberger, B., Falk, C.S., Pohla, H., and Schendel, D.J. 2009. Harnessing innate and adaptive immunity for adoptive cell therapy of renal cell carcinoma. *J Mol Med (Berl)* 87:595-612.
183. Frankenberger, B., Noessner, E., and Schendel, D.J. 2007. Immune suppression in renal cell carcinoma. *Semin Cancer Biol* 17:330-343.
184. Zippelius, A., Batard, P., Rubio-Godoy, V., Bioley, G., Lienard, D., Lejeune, F., Rimoldi, D., Guillaume, P., Meidenbauer, N., Mackensen, A., et al. 2004. Effector function of human tumor-specific CD8 T cells in melanoma lesions: a state of local functional tolerance. *Cancer Res* 64:2865-2873.
185. Hanahan, D., and Weinberg, R.A. 2011. Hallmarks of cancer: the next generation. *Cell* 144:646-674.
186. Kono, K., Salazar-Onfray, F., Petersson, M., Hansson, J., Masucci, G., Wasserman, K., Nakazawa, T., Anderson, P., and Kiessling, R. 1996. Hydrogen peroxide secreted by tumor-derived macrophages down-modulates signal-transducing zeta molecules and inhibits tumor-specific T cell-and natural killer cell-mediated cytotoxicity. *Eur J Immunol* 26:1308-1313.
187. Daurkin, I., Eruslanov, E., Stoffs, T., Perrin, G.Q., Algood, C., Gilbert, S.M., Rosser, C.J., Su, L.M., Vieweg, J., and Kusmartsev, S. 2011. Tumor-associated macrophages mediate immunosuppression in the renal cancer microenvironment by activating the 15-lipoxygenase-2 pathway. *Cancer Res* 71:6400-6409.
188. Sica, A., Saccani, A., Bottazzi, B., Polentarutti, N., Vecchi, A., van Damme, J., and Mantovani, A. 2000. Autocrine production of IL-10 mediates defective IL-12 production and NF-kappa B activation in tumor-associated macrophages. *J Immunol* 164:762-767.
189. Mantovani, A., Sica, A., Sozzani, S., Allavena, P., Vecchi, A., and Locati, M. 2004. The chemokine system in diverse forms of macrophage activation and polarization. *Trends Immunol* 25:677-686.
190. Tiemessen, M.M., Jagger, A.L., Evans, H.G., van Herwijnen, M.J., John, S., and Taams, L.S. 2007. CD4+CD25+Foxp3+ regulatory T cells induce alternative activation of human monocytes/macrophages. *Proc Natl Acad Sci U S A* 104:19446-19451.
191. Curiel, T.J., Coukos, G., Zou, L., Alvarez, X., Cheng, P., Mottram, P., Evdemon-Hogan, M., Conejo-Garcia, J.R., Zhang, L., Burow, M., et al. 2004. Specific recruitment of regulatory T cells in ovarian carcinoma fosters immune privilege and predicts reduced survival. *Nat Med* 10:942-949.
192. Li, J.F., Chu, Y.W., Wang, G.M., Zhu, T.Y., Rong, R.M., Hou, J., and Xu, M. 2009. The prognostic value of peritumoral regulatory T cells and its correlation with intratumoral cyclooxygenase-2 expression in clear cell renal cell carcinoma. *BJU Int* 103:399-405.
193. Clear, A.J., Lee, A.M., Calaminici, M., Ramsay, A.G., Morris, K.J., Hallam, S., Kelly, G., Macdougall, F., Lister, T.A., and Gribben, J.G. 2010. Increased angiogenic sprouting in poor prognosis FL is associated with elevated numbers of CD163+ macrophages within the immediate sprouting microenvironment. *Blood* 115:5053-5056.
194. Shabo, I., Olsson, H., Sun, X.F., and Svanvik, J. 2009. Expression of the macrophage antigen CD163 in rectal cancer cells is associated with early local recurrence and reduced survival time. *Int J Cancer* 125:1826-1831.
195. Rosenblatt, J., and McDermott, D.F. 2011. Immunotherapy for renal cell carcinoma. *Hematol Oncol Clin North Am* 25:793-812.

196. Fyfe, G., Fisher, R.I., Rosenberg, S.A., Sznol, M., Parkinson, D.R., and Louie, A.C. 1995. Results of treatment of 255 patients with metastatic renal cell carcinoma who received high-dose recombinant interleukin-2 therapy. *J Clin Oncol* 13:688-696.
197. McDermott, D.F. 2009. The application of high-dose interleukin-2 for metastatic renal cell carcinoma. *Med Oncol* 26 Suppl 1:13-17.
198. Jensen, H.K., Donskov, F., Nordsmark, M., Marcussen, N., and von der Maase, H. 2009. Increased intratumoral FOXP3-positive regulatory immune cells during interleukin-2 treatment in metastatic renal cell carcinoma. *Clin Cancer Res* 15:1052-1058.
199. Morse, M.A., Hobeika, A.C., Osada, T., Serra, D., Niedzwiecki, D., Lyerly, H.K., and Clay, T.M. 2008. Depletion of human regulatory T cells specifically enhances antigen-specific immune responses to cancer vaccines. *Blood* 112:610-618.
200. Kudo-Saito, C., Schlom, J., Camphausen, K., Coleman, C.N., and Hodge, J.W. 2005. The requirement of multimodal therapy (vaccine, local tumor radiation, and reduction of suppressor cells) to eliminate established tumors. *Clin Cancer Res* 11:4533-4544.
201. Curtin, J.F., Candolfi, M., Fakhouri, T.M., Liu, C., Alden, A., Edwards, M., Lowenstein, P.R., and Castro, M.G. 2008. Treg depletion inhibits efficacy of cancer immunotherapy: implications for clinical trials. *PLoS One* 3:e1983.
202. Atchison, E., Eklund, J., Martone, B., Wang, L., Gidron, A., Macvicar, G., Rademaker, A., Goolsby, C., Marszalek, L., Kozlowski, J., et al. 2010. A pilot study of denileukin diftitox (DD) in combination with high-dose interleukin-2 (IL-2) for patients with metastatic renal cell carcinoma (RCC). *J Immunother* 33:716-722.
203. Krieg, C., Letourneau, S., Pantaleo, G., and Boyman, O. 2010. Improved IL-2 immunotherapy by selective stimulation of IL-2 receptors on lymphocytes and endothelial cells. *Proc Natl Acad Sci U S A* 107:11906-11911.
204. Hodi, F.S., O'Day, S.J., McDermott, D.F., Weber, R.W., Sosman, J.A., Haanen, J.B., Gonzalez, R., Robert, C., Schadendorf, D., Hassel, J.C., et al. 2010. Improved survival with ipilimumab in patients with metastatic melanoma. *N Engl J Med* 363:711-723.
205. Yang, J.C., Hughes, M., Kammula, U., Royal, R., Sherry, R.M., Topalian, S.L., Suri, K.B., Levy, C., Allen, T., Mavroukakis, S., et al. 2007. Ipilimumab (anti-CTLA4 antibody) causes regression of metastatic renal cell cancer associated with enteritis and hypophysitis. *J Immunother* 30:825-830.
206. Prieto, P.A., Yang, J.C., Sherry, R.M., Hughes, M.S., Kammula, U.S., White, D.E., Levy, C.L., Rosenberg, S.A., and Phan, G.Q. 2012. CTLA-4 blockade with ipilimumab: long-term follow-up of 177 patients with metastatic melanoma. *Clin Cancer Res* 18:2039-2047.
207. Soltau, J., Zirrgiebel, U., Esser, N., Schachtele, C., Totzke, F., Unger, C., Merfort, I., and Drevs, J. 2008. Antitumoral and antiangiogenic efficacy of bisphosphonates in vitro and in a murine RENCA model. *Anticancer Res* 28:933-941.
208. Salnikov, A.V., Heldin, N.E., Stuhr, L.B., Wiig, H., Gerber, H., Reed, R.K., and Rubin, K. 2006. Inhibition of carcinoma cell-derived VEGF reduces inflammatory characteristics in xenograft carcinoma. *Int J Cancer* 119:2795-2802.
209. Roland, C.L., Dineen, S.P., Lynn, K.D., Sullivan, L.A., Dellinger, M.T., Sadegh, L., Sullivan, J.P., Shames, D.S., and Brekken, R.A. 2009. Inhibition of vascular endothelial growth factor reduces angiogenesis and modulates immune cell infiltration of orthotopic breast cancer xenografts. *Mol Cancer Ther* 8:1761-1771.
210. Brunda, M.J., Luistro, L., Warrier, R.R., Wright, R.B., Hubbard, B.R., Murphy, M., Wolf, S.F., and Gately, M.K. 1993. Antitumor and antimetastatic activity of interleukin 12 against murine tumors. *J Exp Med* 178:1223-1230.
211. Hwang, K.S., Cho, W.K., Yoo, J., Yun, H.J., Kim, S., and Im, D.S. 2005. Adenovirus-mediated interleukin-12 gene transfer combined with cytosine deaminase followed by 5-fluorocytosine treatment exerts potent antitumor activity in Renca tumor-bearing mice. *BMC Cancer* 5:51.
212. Ostrand-Rosenberg, S., Grusby, M.J., and Clements, V.K. 2000. Cutting edge: STAT6-deficient mice have enhanced tumor immunity to primary and metastatic mammary carcinoma. *J Immunol* 165:6015-6019.
213. de Waal Malefyt, R., Haanen, J., Spits, H., Roncarolo, M.G., te Velde, A., Figdor, C., Johnson, K., Kastelein, R., Yssel, H., and de Vries, J.E. 1991. Interleukin 10 (IL-10) and viral IL-10 strongly reduce antigen-specific human T cell proliferation by diminishing the antigen-presenting capacity of monocytes via downregulation of class II major histocompatibility complex expression. *J Exp Med* 174:915-924.
214. Guiducci, C., Vicari, A.P., Sangaletti, S., Trinchieri, G., and Colombo, M.P. 2005. Redirecting in vivo elicited tumor infiltrating macrophages and dendritic cells towards tumor rejection. *Cancer Res* 65:3437-3446.
215. Colombo, M.P., and Mantovani, A. 2005. Targeting myelomonocytic cells to revert inflammation-dependent cancer promotion. *Cancer Res* 65:9113-9116.

216. Kortylewski, M., Kujawski, M., Wang, T., Wei, S., Zhang, S., Pilon-Thomas, S., Niu, G., Kay, H., Mule, J., Kerr, W.G., et al. 2005. Inhibiting Stat3 signaling in the hematopoietic system elicits multicomponent antitumor immunity. *Nat Med* 11:1314-1321.
217. Said, E.A., Dupuy, F.P., Trautmann, L., Zhang, Y., Shi, Y., El-Far, M., Hill, B.J., Noto, A., Ancuta, P., Peretz, Y., et al. 2010. Programmed death-1-induced interleukin-10 production by monocytes impairs CD4+ T cell activation during HIV infection. *Nat Med* 16:452-459.
218. Brahmer, J.R., Drake, C.G., Wollner, I., Powderly, J.D., Picus, J., Sharfman, W.H., Stankevich, E., Pons, A., Salay, T.M., McMiller, T.L., et al. 2010. Phase I study of single-agent anti-programmed death-1 (MDX-1106) in refractory solid tumors: safety, clinical activity, pharmacodynamics, and immunologic correlates. *J Clin Oncol* 28:3167-3175.
219. Topalian, S.L., Hodi, F.S., Brahmer, J.R., Gettinger, S.N., Smith, D.C., McDermott, D.F., Powderly, J.D., Carvajal, R.D., Sosman, J.A., Atkins, M.B., et al. 2012. Safety, Activity, and Immune Correlates of Anti-PD-1 Antibody in Cancer. *N Engl J Med*.
220. Vanneman, M., and Dranoff, G. 2012. Combining immunotherapy and targeted therapies in cancer treatment. *Nat Rev Cancer* 12:237-251.
221. Gupta AK, Probst HC, Landshammer A, Vuong V, Muth S, Yagita H, Schwendener R, Pruschy M, , Knuth A, van den Broek M. Radiotherapy promotes tumor-specific CD8+ T cells via DC activation. *In press at The Journal of immunology*.
222. Zitvogel, L., Apetoh, L., Ghiringhelli, F., Andre, F., Tesniere, A., and Kroemer, G. 2008. The anticancer immune response: indispensable for therapeutic success? *J Clin Invest* 118:1991-2001.
223. Farsaci, B., Higgins, J.P., and Hodge, J.W. 2012. Consequence of dose scheduling of sunitinib on host immune response elements and vaccine combination therapy. *Int J Cancer* 130:1948-1959.
224. Steinman, R.M., and Mellman, I. 2004. Immunotherapy: bewitched, bothered, and bewildered no more. *Science* 305:197-200.

5. APPENDIX

5.1 Functional differences of peripheral and local T cells in patients with ccRCC

Despite detection of Cyclin D1 (CCND1)-specific $CD8^+$ T cells in PBMCs and corresponding TILs of ccRCC patients (results part 2.1) we only observed T cell responses towards CCND1-peptide simulation in PBMCs but not in TILs. Therefore, we were not able to compare TAA-specific responses of PBMCs and TILs. To at least enable a comparison of the function of TILs and PBMCs to some extent, we decided to stimulate isolated T cells polyclonally instead of antigen-specifically. In this regard, we FACS sorted $CD45RA^-$ T cells from PBMCs and autologous TILs and assessed their cytokine profile after TCR-dependent and -independent *ex-vivo* polyclonal stimulation using anti-CD3/CD28 beads and PMA plus ionomycin respectively (**Figure A-1**). These assays were performed on the same patient material that was used for functional studies in results part 2.2.

$CD8^+$ TILs secreted significantly less TNF-α than $CD8^+$ PBMCs after TCR-dependent stimulation and showed a tendency to secrete less IL-2 and IFN-γ after both stimulation procedures. Furthermore, $CD8^+$ TILs produced significantly more IL-10, and there was a trend towards increased secretion of TGF-β after TCR-dependent and -independent stimulation. In the same line $CD4^+$ TILs also produced less IL-2 after TCR-independent stimulation compared to $CD4^+$ PBMCs and more IL-10 after both stimulation methods. However, significantly more IFN-γ was produced by $CD4^+$ TILs after both stimulation procedures and also significantly more TNF-α after TCR-dependent stimulation. Attig et al. also reported that T cells from ccRCC TILs are able to respond to both TCR-dependent and -independent stimulations and they noted that TILs produced more effector and also more regulatory cytokines than corresponding PBMCs (1). The observation in our study that $CD4^+$ TILs show an increased secretion of effector cytokines IFN-γ and TNF-α, but a reduced production of IL-2, suggests that $CD4^+$ TILs are in general able to respond to stimulations, however don't exert the complete repertoire of all effector cytokines needed for a proper anti-tumor immune response. IL-2 produced by $CD4^+$ T cell is for example required for expansion and survival of $CD8^+$ T cells (2). From these results we conclude that the function of T cells infiltrating ccRCC tumors differs to some extent from T cells in the periphery. $CD8^+$ TILs were not able to secrete as much of the effector cytokines as PBMCs, and also $CD4^+$ TILs produced less IL-2. Both $CD4^+$ and $CD8^+$ TILs produced more of the regulatory cytokine IL-10 thereby contributing to the immunosuppressive milieu in ccRCC tumors. Even though the production of IL-10 is more linked to $CD4^+$ T cells, and Tregs (3) it was shown that also $CD8^+$ T cells are a source of IL-10 within tumors (1, 4).

Furthermore, when comparing the phenotype of T cells from TILs and corresponding PBMCs in regard to the expression of regulatory molecules we observed a difference towards a more

regulated phenotype of TILs (**Figure 4 and 5 in results 2.2**). While we saw an increased expression of TGF-β, IL-17, IL-4, IL-13 and also of IL-2 on the mRNA level of sorted non-stimulated $CD4^+$ TILs compared to PBMCs (**Figure 4 in results 2.2**), they did not secrete more of these cytokines after polyclonal stimulations compared to PBMCs (**Figure A-1**). While mRNA analysis was possible *ex-vivo* directly after FACS sorting, T cells had to be cultured for stimulation experiments. T cells after culture might not reflect the exact situation as observed directly after FACS sorting what might explain the discrepancy between mRNA and protein levels (5). However, that T cells express high levels of cytokines on the mRNA level, but are not able to produce the cytokine on the protein level was observed before for self-reactive T cells, and it was suggested that translation is limited due to posttranscriptional silencing (6). The fact that we observed an increased secretion of TGF-β and IL-4 when $CD4^+$ T cells were stimulated in presence of the tumor microenvironment and TAMs (**Figure 6 and 7 in results 2.2**), might as well suggest that the disconnect in mRNA and protein level observed in our study is due to an altered behavior of T cells when cultured and stimulated isolated from the tumor microenvironment since then they are not under the influence of immunoregulatory mediators like TAMs anymore.

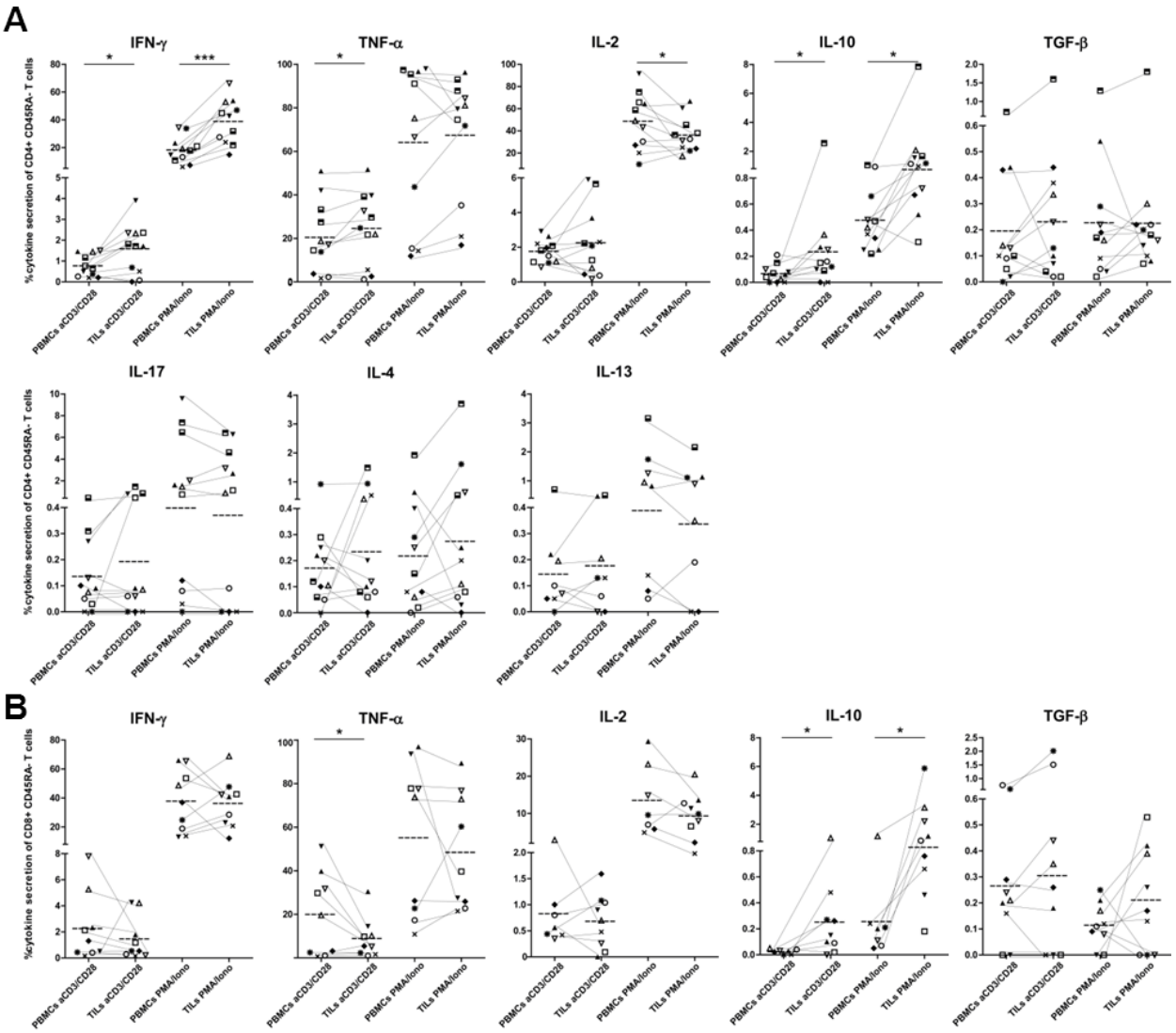

Figure A-1: Cytokine profile differs between T cells from PBMCs and TILs

Intracellular staining for cytokines is shown for ViViD$^-$CD45RA$^-$CD4$^+$ T cells (A) and ViViD$^-$ CD45RA$^-$CD8$^+$ T cells (B). Each symbol represents an individual patient. Results of PBMCs and TILs from the same patient are connected by a thin line. Wilcoxon matched-pairs signed rank test was used to analyze statistical significance between groups (GraphPad Prism Software). Means of each group and significant differences are depicted (* $p<0.05$; ** $p<0.005$).
Methodological details can be found in materials and methods section of results part 2.2. Shortly T cells were FACS sorted from TILs and PBMCs of the same patient and *ex-vivo* stimulated with anti-CD3/CD28 Dynabeads (ratio T cells:beads 1:3) or with PMA plus ionomycin for 6 h at 37 °C in the presence of Brefeldin A. Subsequently, cells were surface stained with a pooled fluorochrom-conjugated antibody cocktail (CD4$^+$ T cells: CD45 KromeOrange, CD4 FITC, with (a1) or without TGF-β PE (a2), and CD8$^+$ T cells: CD45 KromeOrange, CD8 ECD (b)) including live-dead staining (LIVE/DEAD® Fixable Violet Dead Cell Stain Kit (ViViD), Invitrogen) in PBS for 20 min at room temperature in the dark. Intracellular staining was performed with a mix of fluorescent-conjugated antibodies (IL-2 PerCPCy5.5, IL-10 APC, IFN-γ Alexa700 (a1); IL17 PE, IL4 PECy7, IL13 APC, TNF-α PerCPCy5.5 (a2); TNF-α PerCPCy5.5, IL-2 PECy7, IL-10 APC, IFN-γ Alexa700 (b)) in permeabilization buffer for 20 min at room temperature in the dark.

REFERENCES

1. Attig, S., Hennenlotter, J., Pawelec, G., Klein, G., Koch, S.D., Pircher, H., Feyerabend, S., Wernet, D., Stenzl, A., Rammensee, H.G., et al. 2009. Simultaneous infiltration of polyfunctional effector and suppressor T cells into renal cell carcinomas. *Cancer Res* 69:8412-8419.
2. Wilson, E.B., and Livingstone, A.M. 2008. Cutting edge: CD4+ T cell-derived IL-2 is essential for help-dependent primary CD8+ T cell responses. *J Immunol* 181:7445-7448.
3. Sato, T., Terai, M., Tamura, Y., Alexeev, V., Mastrangelo, M.J., and Selvan, S.R. 2011. Interleukin 10 in the tumor microenvironment: a target for anticancer immunotherapy. *Immunol Res* 51:170-182.
4. Wei, S., Kryczek, I., Zou, L., Daniel, B., Cheng, P., Mottram, P., Curiel, T., Lange, A., and Zou, W. 2005. Plasmacytoid dendritic cells induce CD8+ regulatory T cells in human ovarian carcinoma. *Cancer Res* 65:5020-5026.
5. Nakagomi, H., Pisa, P., Pisa, E.K., Yamamoto, Y., Halapi, E., Backlin, K., Juhlin, C., and Kiessling, R. 1995. Lack of interleukin-2 (IL-2) expression and selective expression of IL-10 mRNA in human renal cell carcinoma. *Int J Cancer* 63:366-371.
6. Villarino, A.V., Katzman, S.D., Gallo, E., Miller, O., Jiang, S., McManus, M.T., and Abbas, A.K. 2011. Posttranscriptional silencing of effector cytokine mRNA underlies the anergic phenotype of self-reactive T cells. *Immunity* 34:50-60.

5.2 Correlation of immune response-related genes in ccRCC tumor material

Recent efforts have made progress in using formalin-fixed paraffin-embedded (FFPE) tissues for molecular analysis, enabling studies on enormous archives of existing specimens (1), especially in regard to long-term patient survival. Quantitative real-time PCR (qRT-PCR), using TaqMan® Gene expression assays, is a sensitive, accurate and highly reproducible method to study gene expression in FFPE material (2-4). Furthermore, qRT-PCR precisely determines cell density and cytokine gene profile in the tumor microenvironment (5). Based on these findings, we performed a retrospective qRT-PCR screen, using TaqMan® Gene expression assays for 43 different target genes related to tumor immunology (**Supplemental Table S1A, B in results 2.2**) on FFPE material of ccRCCs from 54 patients (**Supplemental Table S2 in results 2.2)**. To receive sufficient template for complete analyses cDNA had to be preamplified prior to qRT-PCR performance. Preamplification of cDNA was introduced before as a suitable method for amplification of limited cDNA of FFPE material (6). Significant correlation of mRNA levels from non-preamplified cDNA and preamplified cDNA confirmed that preamplification was carried out uniformly among all samples (**Supplementary Figure S3 in results 2.2**). Correlations between the expression levels of different target genes were analyzed using the Spearman's Rho correlation test. **Table A-1 A and B** summarizes the results of the Spearman's Rho correlation test on data received from an initial qRT-PCR screen on non-preamplified cDNA and **Table A-2 A and B** the results on data from the additional screen on preamplified cDNA.

Expression levels of the pan-macrophage marker CD68 correlated significantly with genes of an inflammatory signature including LT-βR, MHC-class II, MHC-class I, CD4, HVEM (**Table A-1**) and also IRF-5 (**Table A-2**). Furthermore, CD68 expression levels also correlated with the type 2 response-related gene TGF-β (**Table A-1**) and also FN-1 (**Table A-2**). Together with the fact that enhanced CD68 mRNA levels strongly correlate with increased incidence of metastasis and reduced survival (**Figure 3B and 1A in results 2.2**), $CD68^+$ TAMs seem to mediate tumor-promoting inflammation in the case of ccRCC.

Despite being a marker for M1 macrophages, for iNOS and the production of NO multiple data was published, on the one hand providing evidence for a pro-apoptotic role and a relation with favorable prognosis, and on the other hand providing evidence for a role in tumor promotion (7). Here the levels of iNOS negatively correlate with the M2-related genes IL-10 (**Table A-1**) and CD163 (**Table A-2**) and show an association with the inflammation-related genes LT-βR and HVEM (**Table A-1**). Together with the observation that increased levels of iNOS correlate with prolonged survival and low tumor stage (**Figure 1B and 3C in results 2.2**), we suggest that iNOS is indeed a marker for M1 TAMs in ccRCC, where it has an effector function in anti-tumor immunity.

Another molecule found on antigen-presenting cells with dual roles in anti-tumor immunity is HVEM. By binding the receptor LIGHT it promotes T cell effector functions and by binding the

BTLA receptor inhibition of T cell responses (8). We observed a negative correlation of HVEM with the M2-related genes IL-10 and CD163 and a positive correlation with the inflammation-related genes LT-βR and iNOS (**Table A-1**). Accordingly, increased mRNA levels of HVEM showed a tendency to correlate with increased survival (**Supplementary Figure S1A in results 2.2**). Furthermore, no difference in the inhibitory receptor BTLA in T cells from PBMCs and TILs was observed (**Figure 4 in results 2.2**) suggesting that the anti-tumor effects of HVEM are prominent in ccRCC.

An association of Th1 type responses and favorable prognosis was observed in many cancer types including ccRCC (9, 10). Th1 cells can drive classical activation of M1 macrophages by producing IFN-γ. M1 macrophages start to express cytokines and chemokines, including IL-12, CXCL9 and CXCL10 leading to the recruitment of Th1 cells and the amplification of a type 1 response (11, 12). In this line, we could correlate increased expression levels of the M1 marker iNOS with prolonged survival (**Figure 1B in results 2.2**) and in the same tumor samples also a similar trend for the expression levels of the effector cytokines TNF-α and perforin (**Supplementary Figure S1A in results 2.2**).

On the other hand we observed a significant correlation of FoxP3 with reduced survival (**Figure 1A in results 2.2**) as already published for different cancer types including ccRCC (9, 13, 14). A similar trend we also observed for CTLA-4 and IL-10 (**Supplementary Figure S1B in results 2.2**). We found FoxP3 and IL-10 transcript levels increased in late-stage tumors (**Supplementary Figure S7 in results 2.2)**. In this line, **Table A-2** illustrates that IL-10 transcript levels correlate with the M2 markers CD163 and MR and show a tendency to negatively correlate with inflammation-related genes such as HVEM, LT-βR and the M1-signature genes iNOS (**Table A-1**) and IRF-5 (**Table A-2**). Furthermore, FoxP3 positively correlates with CTLA-4, PD-1, PD-L1 and CD200 and to some extend also with Tim-3 (**Table A-1**), all molecules known to have a role in dampening T cell responses.

We found a significant correlation of CD163 expression with other M2-associated genes like IL-10, MR and FN-1 (**Table A-2**) and on the other hand, a significant negative correlation with CD3, the Th1 cytokine IFN-γ (**Table A-1**) and the M1 marker iNOS (**Table A-2**). These findings and the fact that CD163 shows an association with reduced survival and increased pT (**Figure 1B and 3C in results 2.2**) suggest that CD163 expression levels are indeed a sign of tumor-promoting M2 TAMs in ccRCC.

A positive feedback loop between tumor cells and TAMs, involving EGF, CSF-1, their receptors and Mena, was suggested to promote metastasis (15). To test whether this mechanism plays a role in ccRCC, we also included those genes in the survival and correlation analysis. After normalization to the levels of CD45, we found a significant correlation of the macrophage-associated genes EGF and CSF1R with CD68 (**Table A-2**). It was more problematic to analyze the tumor-associated genes EGFR and CSF-1 and Mena, because we lacked a control gene that would normalize to the amount of tumor cells. When normalized for PPIA or CD45, a correlation

was observed toward increased levels of Mena and reduced survival (**Supplementary Figure S1C in results 2.2**). Furthermore, PPIA-normalized levels of Mena correlated with increased levels of CSF1-R and CD163, as well as with reduced levels of IL12 (**Table A-2**), supporting the idea that Mena is involved in M2 TAM-mediated promotion of metastasis. Because of the lack of a suitable normalization control, the results are not definite and it is not possible to draw any conclusions in whether this pathway plays a role in TAM-mediated metastasis in ccRCC.

In summary we found that in tumor samples of ccRCC patients transcripts related to Th1 cells followed a similar expression pattern than transcripts related to M1 TAMs. Expression levels of these genes negatively correlated with transcripts related to Th2, inhibitory molecules and M2 TAMs. In combination with the fact that we observed a significant positive correlation of the M1 marker iNOS and patient survival and the opposite for FoxP3 and M2-related genes, suggests that Th1 responses and M1 TAMs are important for anti-tumor immune responses in ccRCC patients, while Th2 responses, inhibitory molecules and M2 TAMs negatively impact on that. Hence, immunotherapy for ccRCC should be designed to stimulate Th1 responses and M1 TAMs, and ideally simultaneously suppress Th2 responses, inhibitory molecules and M2 TAMs.

Table A-1A: Summary of correlations between target genes of the initial qRT-PCR screen on non-preamplified cDNA

	IL10	IFNγ	TNFα	LTβ	MICA	PD1	PDL1	FoxP3	CTLA4	IDO	Perf.	GranB	iNOS	MICB	Tim3	TGFβ	LTβR	MHCII	MHCI	CD200	NKG2D	CD8	CD3	CD4	CD163	CD68	HVEM
IL10									(x)				x				x		x	x					xx		x
IFNγ						xx		x	(x)											x	xx		xx		x		
TNFα				(x)			x			x	x				x			x									
LTβ		(x)	(x)		(x)			xx																			
MICA				(x)			xx	x			x		x			xx	xx	xx	x					xx		xx	xx
PD1		xx						xx			x	x				x	xx				xx	xx	xx		x		xx
PDL1				x	xx			xx	xx				x	xx	xx	x	xx		x					xx				
FoxP3		x		xx	x	xx	xx		xx				x	x	x	(x)	(x)		x	xx		x	x	xx				
CTLA4							xx	xx						x														
IDO			x								x	xx																
Perf.			x		x	xx				x		xx	x															
GranB						x				xx	xx										x							
iNOS	x				x		x									(x)	x										x	
MICB							xx	x									xx		xx	x					x		x	
Tim3			x				xx	x	x									xx									x	
TGFβ					xx		x										xx	xx	xx	xx						xx	xx	
LTβR	x				xx		xx						x	xx	xx	xx		xx	xx	xx						xx	xx	
MHCII			x		xx			x			x				xx	xx	xx									xx	xx	
MHCI	x				x		x	x						xx		xx	xx			xx					x	xx	xx	
CD200	x							xx						x		xx	xx									x	x	
NKG2D		xx				xx					xx	x										xx						
CD8		xx				xx		x			x										xx		xx		x			
CD3		xx				xx		x			x										xx	xx			x			
CD4					xx		xx	xx						x		xx	xx	xx	x							xx	xx	
CD163	xx	xx				x												x		x			x				x	x
CD68					xx		xx			(x)						xx	xx	xx	x	x							xx	
HVEM	x				xx		xx						x	x	x	xx		xx	xx	x						xx		

Summary of correlations between target gene expression levels within FFPE ccRCC samples are shown after normalization to the Ct values of CD45. Correlations were statistically analyzed using the Spearman's Rho correlation test. Tendencies ($p<0.1$) are marked with (x), significant correlations with x ($p<0.05$) and with xx ($p<0.01$), inverse tendencies and correlations are highlighted in red.

Table A-2A: Summary of correlations between target genes of the supplemental qRT-PCR analysis on preamplified cDNA

	CD68	MHC-II	CD163	MR	IRF-4	FN-1	IL-10	IRF-5	TNF-α	iNOS	IL-12	EGF	CSF-1R	CSF-1	CSF-1(PPIA)	EGFR	EGFR(PPIA)	Mena	Mena(PPIA)
CD68		xx				xx		xx	(x)			xx	xx		xx	xx	(x)	xx	
MHC-II	xx				x			xx					xx		xx	xx	x	x	
CD163				xx		xx	xx			x			xx		(x)				x
MR			xx				xx				x		x	xx				x	
IRF-4		x																	
FN-1	xx		xx									x		xx		xx		xx	
IL-10			xx	xx								x		x	xx			x	
IRF-5	xx	xx				xx	x		xx			xx	x	x	xx	xx		xx	
TNF-α								xx							x				
iNOS			x				(x)									x			
IL-12					x														xx
EGF	xx					xx	x	xx							xx	xx		x	
CSF-1R	xx	xx	xx	x		xx	x	x										xx	x
CSF-1		xx		x		xx	x	x							xx	xx		xx	
CSF-1(PPIA)	xx	xx	(x)				xx	xx	x			xx		xx		x		xx	
EGFR	xx	xx				xx		xx		x		xx		xx	x		xx	xx	
EGFR(PPIA)	(x)	x						xx		(x)						xx			
Mena	xx	x		x		xx		xx				x	xx	xx	xx	xx			xx
Mena(PPIA)			x								xx		x					xx	

Summary of correlations between target gene expression levels within FFPE ccRCC samples are shown after normalization to the Ct values of CD45 or, when mentioned, to PPIA. Correlations were statistically analyzed using the Spearman's Rho correlation test. Tendencies ($p<0.1$) are marked with (x), significant correlations with x ($p<0.05$) and with xx ($p<0.01$), inverse tendencies and correlations are highlighted in red.

Table A-1B: Statistical values of correlations between target genes of the initial qRT-PCR screen on non-preamplified cDNA

			IL10	IFNg	TNFa	LTb	MICA	PD1	PDL1	FoxP3	CTLA4	IDO	Perforin	GranzymeB	iNOS	MICB
Spearman's rho	IL10	Correlation Coefficient	1,000	-,117	-,160	,040	-,134	-,065	,019	,197	,258	-,158	-,217	-,022	-.316*	,037
		Sig. (2-tailed)		,399	,248	,773	,333	,638	,893	,154	,059	,255	,115	,877	,020	,790
		N	54	54	54	54	54	54	54	54	54	54	54	54	54	54
	IFNg	Correlation Coefficient	-,117	1,000	-,045	,244	,041	.644**	,188	.303*	,243	,017	,170	,197	-,225	,047
		Sig. (2-tailed)	,399		,746	,076	,770	,000	,173	,026	,077	,903	,219	,153	,102	,733
		N	54	54	54	54	54	54	54	54	54	54	54	54	54	54
	TNFa	Correlation Coefficient	-,160	-,045	1,000	,238	,226	-,092	,164	-,053	,075	.297*	.312*	,137	,006	,164
		Sig. (2-tailed)	,248	,746		,083	,101	,507	,235	,704	,587	,029	,022	,323	,966	,237
		N	54	54	54	54	54	54	54	54	54	54	54	54	54	54
	LTb	Correlation Coefficient	,040	,244	,238	1,000	,249	,220	.278*	.417**	,217	-,025	,191	-,002	,181	,000
		Sig. (2-tailed)	,773	,076	,083		,069	,111	,042	,002	,114	,860	,167	,990	,190	,997
		N	54	54	54	54	54	54	54	54	54	54	54	54	54	54
	MICA	Correlation Coefficient	-,134	,041	,226	,249	1,000	,031	.450**	.293*	,150	-,016	.295*	,118	.270*	,174
		Sig. (2-tailed)	,333	,770	,101	,069		,824	,001	,031	,280	,911	,030	,397	,048	,209
		N	54	54	54	54	54	54	54	54	54	54	54	54	54	54
	PD1	Correlation Coefficient	-,065	.644**	-,092	,220	,031	1,000	,140	.467**	,040	,034	.311*	.299*	-,127	,062
		Sig. (2-tailed)	,638	,000	,507	,111	,824		,312	,000	,773	,809	,022	,028	,360	,654
		N	54	54	54	54	54	54	54	54	54	54	54	54	54	54
	PDL1	Correlation Coefficient	,019	,188	,164	.278*	.450**	,140	1,000	.523**	.403**	,183	,195	,137	.296*	.373**
		Sig. (2-tailed)	,893	,173	,235	,042	,001	,312		,000	,003	,186	,157	,325	,030	,005
		N	54	54	54	54	54	54	54	54	54	54	54	54	54	54
	FoxP3	Correlation Coefficient	,197	.303*	-,053	.417**	.293*	.467**	.523**	1,000	.399**	,137	,060	,046	,076	.311*
		Sig. (2-tailed)	,154	,026	,704	,002	,031	,000	,000		,003	,324	,667	,739	,585	,022
		N	54	54	54	54	54	54	54	54	54	54	54	54	54	54
	CTLA4	Correlation Coefficient	,258	,243	,075	,217	,150	,040	.403**	.399**	1,000	,149	-,145	,205	,088	,203
		Sig. (2-tailed)	,059	,077	,587	,114	,280	,773	,003	,003		,283	,296	,138	,527	,141
		N	54	54	54	54	54	54	54	54	54	54	54	54	54	54
	IDO	Correlation Coefficient	-,158	,017	.297*	-,025	-,016	,034	,183	,137	,149	1,000	.322*	.360**	-,021	,219
		Sig. (2-tailed)	,255	,903	,029	,860	,911	,809	,186	,324	,283		,018	,008	,881	,111
		N	54	54	54	54	54	54	54	54	54	54	54	54	54	54
	Perforin	Correlation Coefficient	-,217	,170	.312*	,191	.295*	.311*	,195	,060	-,145	.322*	1,000	.547**	,097	,138
		Sig. (2-tailed)	,115	,219	,022	,167	,030	,022	,157	,667	,296	,018		,000	,484	,320
		N	54	54	54	54	54	54	54	54	54	54	54	54	54	54
	GranzymeB	Correlation Coefficient	-,022	,197	,137	-,002	,118	.299*	,137	,046	,205	.360**	.547**	1,000	,030	,130
		Sig. (2-tailed)	,877	,153	,323	,990	,397	,028	,325	,739	,138	,008	,000		,831	,350
		N	54	54	54	54	54	54	54	54	54	54	54	54	54	54
	iNOS	Correlation Coefficient	-.316*	-,225	,006	,181	.270*	-,127	.296*	,076	,088	-,021	,097	,030	1,000	,199
		Sig. (2-tailed)	,020	,102	,966	,190	,048	,360	,030	,585	,527	,881	,484	,831		,149
		N	54	54	54	54	54	54	54	54	54	54	54	54	54	54
	MICB	Correlation Coefficient	,037	,047	,164	,000	,174	,062	.373**	.311*	,203	,219	,138	,130	,199	1,000
		Sig. (2-tailed)	,790	,733	,237	,997	,209	,654	,005	,022	,141	,111	,320	,350	,149	
		N	54	54	54	54	54	54	54	54	54	54	54	54	54	54
	Tim3	Correlation Coefficient	-,075	,030	.321*	,220	,206	,149	.353**	.318*	.306*	,105	,196	,180	,180	,165
		Sig. (2-tailed)	,589	,831	,018	,110	,134	,283	,009	,019	,024	,452	,155	,194	,194	,233
		N	54	54	54	54	54	54	54	54	54	54	54	54	54	54
	TGFb	Correlation Coefficient	-,207	,055	,113	,061	.557**	,217	.302*	,262	-,037	-,085	,115	-,106	,260	,193
		Sig. (2-tailed)	,134	,691	,418	,662	,000	,114	,026	,056	,788	,543	,406	,447	,058	,161
		N	54	54	54	54	54	54	54	54	54	54	54	54	54	54
	LTbR	Correlation Coefficient	-.306*	-,113	,203	,105	.603**	-,008	.393**	,249	-,068	,001	,076	-,101	.296*	.364**
		Sig. (2-tailed)	,024	,417	,141	,450	,000	,952	,003	,070	,623	,996	,583	,467	,030	,007
		N	54	54	54	54	54	54	54	54	54	54	54	54	54	54
	MHCII	Correlation Coefficient	-,101	-,077	.345*	,217	.539**	-,011	,245	,017	,096	,005	.285*	-,037	,068	-,100
		Sig. (2-tailed)	,467	,581	,011	,116	,000	,938	,075	,905	,491	,971	,036	,791	,624	,474
		N	54	54	54	54	54	54	54	54	54	54	54	54	54	54
	MHCI	Correlation Coefficient	-.290*	,100	,072	,016	.305*	,257	.311*	.308*	-,256	-,044	,165	-,116	,042	.370**
		Sig. (2-tailed)	,033	,471	,603	,907	,025	,061	,022	,024	,062	,754	,234	,405	,763	,006
		N	54	54	54	54	54	54	54	54	54	54	54	54	54	54
	CD200	Correlation Coefficient	-.301*	,100	-,068	-,153	,258	,261	,153	.360**	-,160	,072	,014	-,180	,051	.281*
		Sig. (2-tailed)	,027	,472	,624	,269	,060	,057	,269	,007	,248	,603	,919	,192	,716	,040
		N	54	54	54	54	54	54	54	54	54	54	54	54	54	54
	NKG2D	Correlation Coefficient	,033	.407**	-,035	,225	-,267	.546**	-,157	,122	-,151	,025	.424**	.277*	-,009	-,026
		Sig. (2-tailed)	,814	,002	,801	,102	,051	,000	,256	,378	,277	,860	,001	,043	,951	,851
		N	54	54	54	54	54	54	54	54	54	54	54	54	54	54
	CD8	Correlation Coefficient	-,172	.607**	-,129	,219	-,147	.763**	,053	.328*	,016	-,068	.288*	,154	,021	,039
		Sig. (2-tailed)	,212	,000	,353	,111	,288	,000	,704	,015	,911	,627	,035	,265	,878	,780
		N	54	54	54	54	54	54	54	54	54	54	54	54	54	54
	CD3	Correlation Coefficient	-,178	.613**	-,133	,131	-,222	.721**	-,066	.294*	-,157	-,002	.280*	,263	-,135	,111
		Sig. (2-tailed)	,197	,000	,339	,346	,106	,000	,637	,031	,256	,991	,040	,055	,329	,425
		N	54	54	54	54	54	54	54	54	54	54	54	54	54	54
	CD4	Correlation Coefficient	,029	,052	,188	,234	.498**	,204	.360**	.351**	,022	,201	,251	,052	,214	.333*
		Sig. (2-tailed)	,833	,709	,173	,088	,000	,138	,008	,009	,872	,145	,067	,710	,120	,014
		N	54	54	54	54	54	54	54	54	54	54	54	54	54	54
	CD163	Correlation Coefficient	.415**	-.381**	-,068	-,219	,029	-.320*	-,056	-,063	,120	,056	-,094	-,064	,084	-,113
		Sig. (2-tailed)	,002	,004	,625	,111	,836	,018	,687	,649	,389	,689	,499	,647	,548	,416
		N	54	54	54	54	54	54	54	54	54	54	54	54	54	54
	CD68	Correlation Coefficient	-,157	,061	,154	-,024	.435**	,019	,150	,169	-,020	-,219	,165	-,180	-,099	,154
		Sig. (2-tailed)	,257	,661	,267	,862	,001	,894	,281	,223	,887	,112	,233	,194	,477	,265
		N	54	54	54	54	54	54	54	54	54	54	54	54	54	54
	HVEM	Correlation Coefficient	-.344*	-,034	,256	,246	.502**	,054	.453**	,201	-,043	,047	,253	-,047	.334*	.328*
		Sig. (2-tailed)	,011	,809	,062	,073	,000	,697	,001	,144	,758	,734	,064	,735	,013	,015
		N	54	54	54	54	54	54	54	54	54	54	54	54	54	54

*. Correlation is significant at the 0.05 level (2-tailed).

**. Correlation is significant at the 0.01 level (2-tailed).

			Tim3	TGFb	LTbR	MHCII	MHCI	CD200	NKG2D	CD8	CD3	CD4	CD163	CD68	HVEM
Spearman's rho	IL10	Correlation Coefficient	-,075	-,207	-,306*	-,101	-,290*	-,301*	,033	-,172	-,178	,029	,415**	-,157	-,344*
		Sig. (2-tailed)	,589	,134	,024	,467	,033	,027	,814	,212	,197	,833	,002	,257	,011
		N	54	54	54	54	54	54	54	54	54	54	54	54	54
	IFNg	Correlation Coefficient	,030	,055	-,113	-,077	,100	,100	,407**	,607**	,613**	,052	-,381**	,061	-,034
		Sig. (2-tailed)	,831	,691	,417	,581	,471	,472	,002	,000	,000	,709	,004	,661	,809
		N	54	54	54	54	54	54	54	54	54	54	54	54	54
	TNFa	Correlation Coefficient	,321*	,113	,203	,345*	,072	-,068	-,035	-,129	-,133	,188	-,068	,154	,256
		Sig. (2-tailed)	,018	,418	,141	,011	,603	,624	,801	,353	,339	,173	,625	,267	,062
		N	54	54	54	54	54	54	54	54	54	54	54	54	54
	LTb	Correlation Coefficient	,220	,061	,105	,217	,016	-,153	,225	,219	,131	,234	-,219	-,024	,246
		Sig. (2-tailed)	,110	,662	,450	,116	,907	,269	,102	,111	,346	,088	,111	,862	,073
		N	54	54	54	54	54	54	54	54	54	54	54	54	54
	MICA	Correlation Coefficient	,206	,557**	,603**	,539**	,305*	,258	-,267	-,147	-,222	,498**	,029	,435**	,502**
		Sig. (2-tailed)	,134	,000	,000	,000	,025	,060	,051	,288	,106	,000	,836	,001	,000
		N	54	54	54	54	54	54	54	54	54	54	54	54	54
	PD1	Correlation Coefficient	,149	,217	-,008	-,011	,257	,261	,546**	,763**	,721**	,204	-,320*	,019	,054
		Sig. (2-tailed)	,283	,114	,952	,938	,061	,057	,000	,000	,000	,138	,018	,894	,697
		N	54	54	54	54	54	54	54	54	54	54	54	54	54
	PDL1	Correlation Coefficient	,353**	,302*	,393**	,245	,311*	,153	-,157	,053	-,066	,360**	-,056	,150	,453**
		Sig. (2-tailed)	,009	,026	,003	,075	,022	,269	,256	,704	,637	,008	,687	,281	,001
		N	54	54	54	54	54	54	54	54	54	54	54	54	54
	FoxP3	Correlation Coefficient	,318*	,262	,249	,017	,308*	,360**	,122	,328*	,294*	,351**	-,063	,169	,201
		Sig. (2-tailed)	,019	,056	,070	,905	,024	,007	,378	,015	,031	,009	,649	,223	,144
		N	54	54	54	54	54	54	54	54	54	54	54	54	54
	CTLA4	Correlation Coefficient	,306*	-,037	-,068	,096	-,256	-,160	-,151	,016	-,157	,022	,120	-,020	-,043
		Sig. (2-tailed)	,024	,788	,623	,491	,062	,248	,277	,911	,256	,872	,389	,887	,758
		N	54	54	54	54	54	54	54	54	54	54	54	54	54
	IDO	Correlation Coefficient	,105	-,085	,001	,005	-,044	,072	,025	-,068	-,002	,201	,056	-,219	,047
		Sig. (2-tailed)	,452	,543	,996	,971	,754	,603	,860	,627	,991	,145	,689	,112	,734
		N	54	54	54	54	54	54	54	54	54	54	54	54	54
	Perforin	Correlation Coefficient	,196	,115	,076	,285*	,165	,014	,424**	,288*	,280*	,251	-,094	,165	,253
		Sig. (2-tailed)	,155	,406	,583	,036	,234	,919	,001	,035	,040	,067	,499	,233	,064
		N	54	54	54	54	54	54	54	54	54	54	54	54	54
	GranzymeB	Correlation Coefficient	,180	-,106	-,101	-,037	-,116	-,180	,277*	,154	,263	,052	-,064	-,180	-,047
		Sig. (2-tailed)	,194	,447	,467	,791	,405	,192	,043	,265	,055	,710	,647	,194	,735
		N	54	54	54	54	54	54	54	54	54	54	54	54	54
	iNOS	Correlation Coefficient	,180	,260	,296*	,068	,042	,051	-,009	,021	-,135	,214	,084	-,099	,334*
		Sig. (2-tailed)	,194	,058	,030	,624	,763	,716	,951	,878	,329	,120	,548	,477	,013
		N	54	54	54	54	54	54	54	54	54	54	54	54	54
	MICB	Correlation Coefficient	,165	,193	,364**	-,100	,370**	,281*	-,026	,039	,111	,333*	-,113	,154	,328*
		Sig. (2-tailed)	,233	,161	,007	,474	,006	,040	,851	,780	,425	,014	,416	,265	,015
		N	54	54	54	54	54	54	54	54	54	54	54	54	54
	Tim3	Correlation Coefficient	1,000	,118	,156	,379**	,114	,018	-,013	,124	,028	,136	-,136	,188	,278*
		Sig. (2-tailed)		,394	,261	,005	,411	,896	,928	,371	,839	,328	,328	,174	,042
		N	54	54	54	54	54	54	54	54	54	54	54	54	54
	TGFb	Correlation Coefficient	,118	1,000	,671**	,364**	,513**	,430**	-,065	,164	,013	,418**	-,085	,574**	,521**
		Sig. (2-tailed)	,394		,000	,007	,000	,001	,641	,237	,926	,002	,541	,000	,000
		N	54	54	54	54	54	54	54	54	54	54	54	54	54
	LTbR	Correlation Coefficient	,156	,671**	1,000	,355**	,566**	,501**	-,189	-,064	-,049	,521**	-,029	,595**	,672**
		Sig. (2-tailed)	,261	,000		,008	,000	,000	,172	,648	,726	,000	,835	,000	,000
		N	54	54	54	54	54	54	54	54	54	54	54	54	54
	MHCII	Correlation Coefficient	,379**	,364**	,355**	1,000	,161	-,066	-,177	-,112	-,228	,434**	-,032	,510**	,468**
		Sig. (2-tailed)	,005	,007	,008		,245	,637	,200	,420	,097	,001	,821	,000	,000
		N	54	54	54	54	54	54	54	54	54	54	54	54	54
	MHCI	Correlation Coefficient	,114	,513**	,566**	,161	1,000	,657**	,127	,204	,257	,401**	-,317*	,485**	,546**
		Sig. (2-tailed)	,411	,000	,000	,245		,000	,360	,138	,061	,003	,020	,000	,000
		N	54	54	54	54	54	54	54	54	54	54	54	54	54
	CD200	Correlation Coefficient	,018	,430**	,501**	-,066	,657**	1,000	-,030	,157	,194	,276*	-,105	,343*	,291*
		Sig. (2-tailed)	,896	,001	,000	,637	,000		,828	,257	,160	,043	,451	,011	,033
		N	54	54	54	54	54	54	54	54	54	54	54	54	54
	NKG2D	Correlation Coefficient	-,013	-,065	-,189	-,177	,127	-,030	1,000	,674**	,705**	,086	-,090	-,167	-,057
		Sig. (2-tailed)	,928	,641	,172	,200	,360	,828		,000	,000	,535	,520	,226	,681
		N	54	54	54	54	54	54	54	54	54	54	54	54	54
	CD8	Correlation Coefficient	,124	,164	-,064	-,112	,204	,157	,674**	1,000	,726**	-,030	-,330*	-,031	,022
		Sig. (2-tailed)	,371	,237	,648	,420	,138	,257	,000		,000	,827	,015	,822	,873
		N	54	54	54	54	54	54	54	54	54	54	54	54	54
	CD3	Correlation Coefficient	,028	,013	-,049	-,228	,257	,194	,705**	,726**	1,000	,107	-,461**	-,082	,047
		Sig. (2-tailed)	,839	,926	,726	,097	,061	,160	,000	,000		,441	,000	,556	,738
		N	54	54	54	54	54	54	54	54	54	54	54	54	54
	CD4	Correlation Coefficient	,136	,418**	,521**	,434**	,401**	,276*	,086	-,030	,107	1,000	,195	,391**	,399**
		Sig. (2-tailed)	,328	,002	,000	,001	,003	,043	,535	,827	,441		,159	,003	,003
		N	54	54	54	54	54	54	54	54	54	54	54	54	54
	CD163	Correlation Coefficient	-,136	-,085	-,029	-,032	-,317*	-,105	-,090	-,330*	-,461**	,195	1,000	-,029	-,331*
		Sig. (2-tailed)	,328	,541	,835	,821	,020	,451	,520	,015	,000	,159		,835	,015
		N	54	54	54	54	54	54	54	54	54	54	54	54	54
	CD68	Correlation Coefficient	,188	,574**	,595**	,510**	,485**	,343*	-,167	-,031	-,082	,391**	-,029	1,000	,450**
		Sig. (2-tailed)	,174	,000	,000	,000	,000	,011	,226	,822	,556	,003	,835		,001
		N	54	54	54	54	54	54	54	54	54	54	54	54	54
	HVEM	Correlation Coefficient	,278*	,521**	,672**	,468**	,546**	,291*	-,057	,022	,047	,399**	-,331*	,450**	1,000
		Sig. (2-tailed)	,042	,000	,000	,000	,000	,033	,681	,873	,738	,003	,015	,001	
		N	54	54	54	54	54	54	54	54	54	54	54	54	54

Statistical values of correlations between target gene expression levels within FFPE ccRCC samples are shown after normalization to the Ct values of CD45. Correlations were statistically analyzed using the Spearman's Rho correlation test.

Table A-2B: Statistical values of correlations between target genes of the supplemental qRT-PCR analysis on preamplified cDNA

			CD68	MHCII	CD163	MR	IRF4	FN1	IL10	IRF5	TNFa	iNOS
Spearman's rho	CD68	Correlation Coefficient	1.000	.470**	.086	-.011	-.112	.393**	-.091	.563**	.276	.112
		Sig. (2-tailed)		.001	.551	.941	.440	.005	.529	.000	.052	.438
		N	50	50	50	50	50	50	50	50	50	50
	MHCII	Correlation Coefficient	.470**	1.000	-.009	.169	-.305*	.229	-.041	.366**	.147	.106
		Sig. (2-tailed)	.001		.949	.241	.031	.109	.777	.009	.309	.465
		N	50	50	50	50	50	50	50	50	50	50
	CD163	Correlation Coefficient	.086	-.009	1.000	.461**	-.049	.385**	.671**	-.179	-.102	-.279*
		Sig. (2-tailed)	.551	.949		.001	.735	.006	.000	.215	.482	.050
		N	50	50	50	50	50	50	50	50	50	50
	MR	Correlation Coefficient	-.011	.169	.461**	1.000	-.235	.197	.403**	.005	-.268	.209
		Sig. (2-tailed)	.941	.241	.001		.101	.170	.004	.975	.059	.146
		N	50	50	50	50	50	50	50	50	50	50
	IRF4	Correlation Coefficient	-.112	-.305*	-.049	-.235	1.000	.088	-.102	-.034	.203	-.068
		Sig. (2-tailed)	.440	.031	.735	.101		.542	.481	.814	.158	.640
		N	50	50	50	50	50	50	50	50	50	50
	FN1	Correlation Coefficient	.393**	.229	.385**	.197	.088	1.000	.098	.275	-.004	.102
		Sig. (2-tailed)	.005	.109	.006	.170	.542		.498	.053	.978	.479
		N	50	50	50	50	50	50	50	50	50	50
	IL10	Correlation Coefficient	-.091	-.041	.671**	.403**	-.102	.098	1.000	-.321*	-.164	-.237
		Sig. (2-tailed)	.529	.777	.000	.004	.481	.498		.023	.256	.097
		N	50	50	50	50	50	50	50	50	50	50
	IRF5	Correlation Coefficient	.563**	.366**	-.179	.005	-.034	.275	-.321*	1.000	.404**	.144
		Sig. (2-tailed)	.000	.009	.215	.975	.814	.053	.023		.004	.318
		N	50	50	50	50	50	50	50	50	50	50
	TNFa	Correlation Coefficient	.276	.147	-.102	-.268	.203	-.004	-.164	.404**	1.000	-.019
		Sig. (2-tailed)	.052	.309	.482	.059	.158	.978	.256	.004		.895
		N	50	50	50	50	50	50	50	50	50	50
	iNOS	Correlation Coefficient	.112	.106	-.279*	.209	-.068	.102	-.237	.144	-.019	1.000
		Sig. (2-tailed)	.438	.465	.050	.146	.640	.479	.097	.318	.895	
		N	50	50	50	50	50	50	50	50	50	50
	IL12	Correlation Coefficient	.122	.177	-.109	-.087	.319*	.094	.024	-.032	.189	-.093
		Sig. (2-tailed)	.398	.220	.451	.548	.024	.516	.869	.826	.189	.519
		N	50	50	50	50	50	50	50	50	50	50
	EGF	Correlation Coefficient	.408**	.211	-.150	-.227	-.020	.361*	-.313*	.428**	.214	.199
		Sig. (2-tailed)	.003	.142	.300	.113	.890	.010	.027	.002	.135	.167
		N	50	50	50	50	50	50	50	50	50	50
	CSF1R	Correlation Coefficient	.410**	.517**	.467**	.341*	-.228	.275	.154	.303*	.089	-.032
		Sig. (2-tailed)	.003	.000	.001	.015	.111	.054	.284	.032	.540	.825
		N	50	50	50	50	50	50	50	50	50	50
	CSF1	Correlation Coefficient	.023	.031	.220	.307*	-.088	.384**	.294*	.305*	-.016	.084
		Sig. (2-tailed)	.874	.830	.124	.030	.541	.006	.038	.031	.915	.563
		N	50	50	50	50	50	50	50	50	50	50
	CSF1_PPIA	Correlation Coefficient	-.523**	-.432**	.272	.157	-.025	-.205	.475**	-.401**	-.332*	-.143
		Sig. (2-tailed)	.000	.002	.056	.276	.862	.152	.000	.004	.018	.323
		N	50	50	50	50	50	50	50	50	50	50
	EGFR	Correlation Coefficient	.509**	.455**	-.083	.097	-.075	.511**	-.184	.686**	.223	.303*
		Sig. (2-tailed)	.000	.001	.564	.504	.605	.000	.201	.000	.119	.033
		N	50	50	50	50	50	50	50	50	50	50
	EGFR_PPIA	Correlation Coefficient	.259	.290*	-.100	-.061	-.136	.184	-.116	.409**	.201	.250
		Sig. (2-tailed)	.069	.041	.490	.676	.347	.202	.423	.003	.161	.079
		N	50	50	50	50	50	50	50	50	50	50
	Mena	Correlation Coefficient	.461**	.282*	.198	.321*	-.115	.497**	-.009	.537**	.095	.100
		Sig. (2-tailed)	.001	.048	.168	.023	.426	.000	.951	.000	.511	.490
		N	50	50	50	50	50	50	50	50	50	50
	Mena_PPIA	Correlation Coefficient	.007	-.107	.286*	.132	-.053	.088	.199	.082	-.034	-0.101
		Sig. (2-tailed)	.963	.460	.044	.360	.713	.543	.166	.571	.813	.484
		N	50	50	50	50	50	50	50	50	50	50

*. Correlation is significant at the 0.05 level (2-tailed).
**. Correlation is significant at the 0.01 level (2-tailed).

			IL12	EGF	CSF1R	CSF1	CSF1_PPIA	EGFR	EGFR_PPIA	Mena	Mena_PPIA
Spearman's rho	CD68	Correlation Coefficient	.122	.408**	.410**	.023	-.523**	.509**	.259	.461**	.007
		Sig. (2-tailed)	.398	.003	.003	.874	.000	.000	.069	.001	.963
		N	50	50	50	50	50	50	50	50	50
	MHCII	Correlation Coefficient	.177	.211	.517**	.031	-.432**	.455**	.290*	.282*	-.107
		Sig. (2-tailed)	.220	.142	.000	.830	.002	.001	.041	.048	.460
		N	50	50	50	50	50	50	50	50	50
	CD163	Correlation Coefficient	-.109	-.150	.467**	.220	.272	-.083	-.100	.198	.286*
		Sig. (2-tailed)	.451	.300	.001	.124	.056	.564	.490	.168	.044
		N	50	50	50	50	50	50	50	50	50
	MR	Correlation Coefficient	-.087	-.227	.341*	.307*	.157	.097	-.061	.321*	.132
		Sig. (2-tailed)	.548	.113	.015	.030	.276	.504	.676	.023	.360
		N	50	50	50	50	50	50	50	50	50
	IRF4	Correlation Coefficient	.319*	-.020	-.228	-.088	-.025	-.075	-.136	-.115	-.053
		Sig. (2-tailed)	.024	.890	.111	.541	.862	.605	.347	.426	.713
		N	50	50	50	50	50	50	50	50	50
	FN1	Correlation Coefficient	.094	.361*	.275	.384**	-.205	.511**	.184	.497**	.088
		Sig. (2-tailed)	.516	.010	.054	.006	.152	.000	.202	.000	.543
		N	50	50	50	50	50	50	50	50	50
	IL10	Correlation Coefficient	.024	-.313*	.154	.294*	.475**	-.184	-.116	-.009	.199
		Sig. (2-tailed)	.869	.027	.284	.038	.000	.201	.423	.951	.166
		N	50	50	50	50	50	50	50	50	50
	IRF5	Correlation Coefficient	-.032	.428**	.303*	.305*	-.401**	.686**	.409**	.537**	.082
		Sig. (2-tailed)	.826	.002	.032	.031	.004	.000	.003	.000	.571
		N	50	50	50	50	50	50	50	50	50
	TNFa	Correlation Coefficient	.189	.214	.089	-.016	-.332*	.223	.201	.095	-.034
		Sig. (2-tailed)	.189	.135	.540	.915	.018	.119	.161	.511	.813
		N	50	50	50	50	50	50	50	50	50
	iNOS	Correlation Coefficient	-.093	.199	-.032	.084	-.143	.303*	.250	.100	-.101
		Sig. (2-tailed)	.519	.167	.825	.563	.323	.033	.079	.490	.484
		N	50	50	50	50	50	50	50	50	50
	IL12	Correlation Coefficient	1.000	.003	-.191	-.020	-.153	.082	-.050	-.202	-.444**
		Sig. (2-tailed)		.983	.183	.890	.288	.573	.731	.160	.001
		N	50	50	50	50	50	50	50	50	50
	EGF	Correlation Coefficient	.003	1.000	.126	.089	-.430**	.369**	.099	.319*	-.077
		Sig. (2-tailed)	.983		.384	.537	.002	.008	.494	.024	.595
		N	50	50	50	50	50	50	50	50	50
	CSF1R	Correlation Coefficient	-.191	.126	1.000	.204	-.196	.241	.096	.477**	.287*
		Sig. (2-tailed)	.183	.384		.155	.172	.092	.508	.000	.043
		N	50	50	50	50	50	50	50	50	50
	CSF1	Correlation Coefficient	-.020	.089	.204	1.000	.428**	.398**	.181	.416**	.226
		Sig. (2-tailed)	.890	.537	.155		.002	.004	.208	.003	.114
		N	50	50	50	50	50	50	50	50	50
	CSF1_PPIA	Correlation Coefficient	-.153	-.430**	-.196	.428**	1.000	-.329*	-.008	-.412**	.052
		Sig. (2-tailed)	.288	.002	.172	.002		.019	.955	.003	.720
		N	50	50	50	50	50	50	50	50	50
	EGFR	Correlation Coefficient	.082	.369**	.241	.398**	-.329*	1.000	.751**	.565**	-.017
		Sig. (2-tailed)	.573	.008	.092	.004	.019		.000	.000	.906
		N	50	50	50	50	50	50	50	50	50
	EGFR_PPIA	Correlation Coefficient	-.050	.099	.096	.181	-.008	.751**	1.000	.182	.046
		Sig. (2-tailed)	.731	.494	.508	.208	.955	.000		.205	.752
		N	50	50	50	50	50	50	50	50	50
	Mena	Correlation Coefficient	-.202	.319*	.477**	.416**	-.412**	.565**	.182	1.000	.595**
		Sig. (2-tailed)	.160	.024	.000	.003	.003	.000	.205		.000
		N	50	50	50	50	50	50	50	50	50
	Mena_PPIA	Correlation Coefficient	-.444**	-.077	.287*	.226	.052	-.017	.046	.595**	1.000
		Sig. (2-tailed)	.001	.595	.043	.114	.720	.906	.752	.000	
		N	50	50	50	50	50	50	50	50	50

*. Correlation is significant at the 0.05 level (2-tailed).
**. Correlation is significant at the 0.01 level (2-tailed).

Statistical values of correlations between target gene expression levels within FFPE ccRCCs are shown after normalization to the Ct values of CD45 or, when mentioned, to PPIA. Correlations were statistically analyzed using the Spearman's Rho correlation test.

REFERENCES

1. Huang, W.Y., Sheehy, T.M., Moore, L.E., Hsing, A.W., and Purdue, M.P. 2010. Simultaneous recovery of DNA and RNA from formalin-fixed paraffin-embedded tissue and application in epidemiologic studies. Cancer Epidemiol Biomarkers Prev 19:973-977.
2. Mocellin, S., Rossi, C.R., Pilati, P., Nitti, D., and Marincola, F.M. 2003. Quantitative real-time PCR: a powerful ally in cancer research. Trends Mol Med 9:189-195.
3. Sheils, O.M., O'Leary, J.J., and Sweeney, E.C. 2000. Assessment of ret/PTC-1 rearrangements in neoplastic thyroid tissue using TaqMan RT-PCR. J Pathol 192:32-36.
4. Macabeo-Ong, M., Ginzinger, D.G., Dekker, N., McMillan, A., Regezi, J.A., Wong, D.T., and Jordan, R.C. 2002. Effect of duration of fixation on quantitative reverse transcription polymerase chain reaction analyses. Mod Pathol 15:979-987.
5. Mocellin, S., Provenzano, M., Rossi, C.R., Pilati, P., Nitti, D., and Lise, M. 2003. Use of quantitative real-time PCR to determine immune cell density and cytokine gene profile in the tumor microenvironment. J Immunol Methods 280:1-11.
6. Li, J., Smyth, P., Cahill, S., Denning, K., Flavin, R., Aherne, S., Pirotta, M., Guenther, S.M., O'Leary, J.J., and Sheils, O. 2008. Improved RNA quality and TaqMan Pre-amplification method (PreAmp) to enhance expression analysis from formalin fixed paraffin embedded (FFPE) materials. BMC Biotechnol 8:10.
7. Weigert, A., and Brune, B. 2008. Nitric oxide, apoptosis and macrophage polarization during tumor progression. Nitric Oxide 19:95-102.
8. Murphy, K.M., Nelson, C.A., and Sedy, J.R. 2006. Balancing co-stimulation and inhibition with BTLA and HVEM. Nat Rev Immunol 6:671-681.
9. Fridman, W.H., Pages, F., Sautes-Fridman, C., and Galon, J. 2012. The immune contexture in human tumours: impact on clinical outcome. Nat Rev Cancer 12:298-306.
10. Kondo, T., Nakazawa, H., Ito, F., Hashimoto, Y., Osaka, Y., Futatsuyama, K., Toma, H., and Tanabe, K. 2006. Favorable prognosis of renal cell carcinoma with increased expression of chemokines associated with a Th1-type immune response. Cancer Sci 97:780-786.
11. Gordon, S., and Taylor, P.R. 2005. Monocyte and macrophage heterogeneity. Nat Rev Immunol 5:953-964.
12. Mantovani, A., Sica, A., Sozzani, S., Allavena, P., Vecchi, A., and Locati, M. 2004. The chemokine system in diverse forms of macrophage activation and polarization. Trends Immunol 25:677-686.
13. Curiel, T.J., Coukos, G., Zou, L., Alvarez, X., Cheng, P., Mottram, P., Evdemon-Hogan, M., Conejo-Garcia, J.R., Zhang, L., Burow, M., et al. 2004. Specific recruitment of regulatory T cells in ovarian carcinoma fosters immune privilege and predicts reduced survival. Nat Med 10:942-949.
14. Li, J.F., Chu, Y.W., Wang, G.M., Zhu, T.Y., Rong, R.M., Hou, J., and Xu, M. 2009. The prognostic value of peritumoral regulatory T cells and its correlation with intratumoral cyclooxygenase-2 expression in clear cell renal cell carcinoma. BJU Int 103:399-405.
15. Patsialou, A., Wyckoff, J., Wang, Y., Goswami, S., Stanley, E.R., and Condeelis, J.S. 2009. Invasion of human breast cancer cells in vivo requires both paracrine and autocrine loops involving the colony-stimulating factor-1 receptor. Cancer Res 69:9498-9506.

5.3 Efficient generation of multipotent mesenchymal stem cells from umbilical cord blood in stroma-free liquid culture

Manuscript published in PLOS one, December 2010, Volume 5, Issue 12, e15689

Authors: Rowayda Peters, Monika J. Wolf, Maries van den Broek, Mario Nuvolone, Stefanie Dannenmann, Bruno Stieger, RetoRapold, Daniel Konrad, Arnold Rubin, Joseph R. Bertino, Adriano Aguzzi, Mathias Heikenwalder and Alexander K. Knuth

Contributions: SRD provided data for Figure 2.

OPEN ACCESS Freely available online

PLoS one

Efficient Generation of Multipotent Mesenchymal Stem Cells from Umbilical Cord Blood in Stroma-Free Liquid Culture

Rowayda Peters[1*9], Monika J. Wolf[2,9], Maries van den Broek[1], Mario Nuvolone[2,6], Stefanie Dannenmann[1], Bruno Stieger[3], Reto Rapold[4], Daniel Konrad[4], Arnold Rubin[5], Joseph R. Bertino[5], Adriano Aguzzi[2], Mathias Heikenwalder[2,7], Alexander K. Knuth[1]

1 Clinic of Oncology, University Hospital of Zurich, Zurich, Switzerland, **2** Department of Pathology, Institute of Neuropathology, University Hospital of Zurich, Zurich, Switzerland, **3** Department of Medicine, Institutes of Clinical Pharmacology and Toxicology, University Hospital of Zurich, Zurich, Switzerland, **4** Division of Diabetology und Endocrinology, University Children's Hospital, Zurich, Switzerland, **5** Department of Medicine, The Cancer Institute of New Jersey, Robert Wood Johnson Medical School, University of Medicine and Dentistry, New Brunswick, New Jersey, United States of America, **6** Department of Internal Medicine, Amyloid Center, Fondazione IRCCS Policlinico San Matteo, University of Pavia, Pavia, Italy, **7** Institute of Virology, Technische Universität München/Helmholtz Zentrum München, München, Germany

Abstract

Background: Haematopoiesis is sustained by haematopoietic (HSC) and mesenchymal stem cells (MSC). HSC are the precursors for blood cells, whereas marrow, stroma, bone, cartilage, muscle and connective tissues derive from MSC. The generation of MSC from umbilical cord blood (UCB) is possible, but with low and unpredictable success. Here we describe a novel, robust stroma-free dual cell culture system for long-term expansion of primitive UCB-derived MSC.

Methods and Findings: UCB-derived mononuclear cells (MNC) or selected $CD34^+$ cells were grown in liquid culture in the presence of serum and cytokines. Out of 32 different culture conditions that have been tested for the efficient expansion of HSC, we identified one condition (DMEM, pooled human AB serum, Flt-3 ligand, SCF, MGDF and IL-6; further denoted as D7) which, besides supporting HSC expansion, successfully enabled long-term expansion of stromal/MSC from 8 out of 8 UCB units (5 MNC-derived and 3 $CD34^+$ selected cells). Expanded MSC displayed a fibroblast-like morphology, expressed several stromal/MSC-related antigens (CD105, CD73, CD29, CD44, CD133 and Nestin) but were negative for haematopoietic cell markers (CD45, CD34 and CD14). MSC stemness phenotype and their differentiation capacity *in vitro* before and after high dilution were preserved throughout long-term culture. Even at passage 24 cells remained $Nestin^+$, $CD133^+$ and >95% were positive for CD105, CD73, CD29 and CD44 with the capacity to differentiate into mesodermal lineages. Similarly we show that UCB derived MSC express pluripotency stem cell markers despite differences in cell confluency and culture passages. Further, we generated MSC from peripheral blood (PB) MNC of 8 healthy volunteers. In all cases, the resulting MSC expressed MSC-related antigens and showed the capacity to form CFU-F colonies.

Conclusions: This novel stroma-free liquid culture overcomes the existing limitation in obtaining MSC from UCB and PB enabling so far unmet therapeutic applications, which might substantially affect clinical practice.

Citation: Peters R, Wolf MJ, van den Broek M, Nuvolone M, Dannenmann S, et al. (2010) Efficient Generation of Multipotent Mesenchymal Stem Cells from Umbilical Cord Blood in Stroma-Free Liquid Culture. PLoS ONE 5(12): e15689. doi:10.1371/journal.pone.0015689

Editor: Toshi Shioda, Massachusetts General Hospital, United States of America

Received August 7, 2010; **Accepted** November 20, 2010; **Published** December 30, 2010

Funding: This work was supported by Prof. Dr. Max-Cloëtta, the Oncosuisse (OCS 02113-08-2007) (M.H.), the Roche Research Foundation (M.J.W.), Atlantic Philanthropies, Cancer Research Institute and Stiftung für Forschung der Onkologie (SFO). M.N. was partly supported by an investigator fellowship of Collegio Ghislieri, Pavia, Italy. A.A. was supported by an Advanced Grant of the European Research Council and by a generous grant of the Novartis Research Foundation. The funders had no role in study design, data collection and analysis, decision to publish, or preparation of the manuscript.

Competing Interests: The authors have declared that no competing interests exist.

* E-mail: rowayda.peters@gmail.com

9 These authors contributed equally to this work.

Introduction

In recent years, mesenchymal stem cells (MSC) received considerable attention as a potential source of cell-based therapies and as a cell type that supports the engraftment of haematopoietic stem cells (HSC) [1,2]. The usual source of MSC is the bone marrow (BM), which is not easy to obtain from healthy donors as well as umbilical cord blood (UCB). The advantages of UCB as the source of MSC are the availability of units [3,4] and the primitive nature of UCB-derived MSC [5,6,7].

BM- and UCB-derived MSC are presumably highly similar precursors as they share the following features: (*i*) capacity of self-renewal [8], (*ii*) multipotency, allowing *in vitro* differentiation into mesenchymal tissues (bone, cartilage, tendon, muscle, adipose tissue, stroma) and possibly non-mesenchymal tissues (neuronal, endothelial and hepatic) [9,10,11], (*iii*) formation of colonies of fibroblastic cells (CFU-F) [12], (*iv*) expression of MSC markers (CD29, CD44, CD73, CD105) and lack of haematopoietic markers (CD14, CD34, CD45) [4,13] and (*v*) migration to inflammatory sites, stimulation of proliferation/differentiation of

resident progenitor cells and promotion of recovery of injured cells through growth factor secretion and matrix remodeling [14,15,16].

Although the frequency of MSC referred here as undifferentiated cells is much higher in BM (0.001–0.1%) than in UCB (0.00003%) and some reports have even doubted the presence of MSC in UCB [17,10,4,18,19], UCB-derived MSC have a better potential to expand and can give rise to up to 10^{15} cells [17,4]. However, the scarcity of MSC in UCB and the lack of a robust protocol to reproducibly expand MSC from UCB units have hampered clinical applications [17,4,20,19]. It can not be excluded that the low numbers of MSC in cord blood actually derive from placental MSC that were released into cord blood due to mechanical stress during UCB isolation procedure. Several studies reported that MSC can be isolated and established from only 20–63% of the cord blood units [3,8,21], questioning the feasibility of MSC isolation and cultivation from UCB.

Here, we describe a novel, simple and reproducible method, which is based on stroma-free liquid culture, to expand substantial numbers of multipotent MSC from only a small number of UCB-derived mononuclear cells (MNC). This method allows an extensive expansion of non-adherent HSC plus a marked increase in adherent MSC. MSC produced *in vitro* by this novel culture method maintain their stem cell properties of self-renewal and multi-lineage differentiation for a long-time (up to passage 24), even following cryopreservation.

Methods

Ethics Statement

All experimental work presented in this study has been approved by the local institutional review board.

Umbilical cord blood sample collection and cell processing

UCB from full-term deliveries was obtained from the Department of Gynaecology at the University Hospital of Zurich with the approval of the local ethical committee (Beschlussmitteilung der Ethikkommission, UniversitätsSpital Zürich, and StV 30/2006). A written informed consent was obtained and the blood was processed within 24 h. Briefly, UCB was diluted with an equal volume of PBS layered onto Lymphoprep^{TM} (Axis-Shield, UK) and centrifuged for 30 min at room temperature at 1′800 rpm. Mononuclear cells (MNC) were collected and washed twice with PBS. Aliquots containing 1.0×10^7 cells were cryopreserved in FBS and 10% DMSO at a fixed cooling rate (1°C/min) and stored at −80°C.

Cytokines

Recombinant human stem cell factor (SCF), interleukin 6 (IL-6), FMS-like tyrosine kinase 3 (Flt-3) ligand, epidermal growth factor (EGF), basic fibroblast growth factor (FGF-β), hepatocyte growth factor (HGF) and Oncostatin M (OSM) were purchased from R&D Systems (Europe). Megakaryocyte growth and development factor (MGDF) was a gift from Kirin (Gunma, Japan).

Cell selection

UCB $CD34^+$ cells were positively selected using autoMACS $CD34^+$ magnetic beads (Miltenyi Biotec, Bergisch Gladbach, Germany). The separation technique was performed according to the manufacturer's instructions. The purity of $CD34^+$ cells selected from 3 UCB units ranged between 90–92.7% as determined by flow cytometry.

Stroma-free long-term cultures

Cryopreserved MNC were thawed and cultured for the expansion of HSC in Dulbecco's Modified Eagle's Medium (DMEM, Gibco, Europe) in the presence of 10% pooled human AB serum (Cat. No. 100–512, SLI, UK) in 24-well plates. For expansion, freshly thawed UCB-derived MNC were seeded at a concentration of $1–3\times10^5$/ml. SCF and Flt-3 were used at 25 ng/ml, MGDF at 10 ng/ml and IL-6 at 20 ng/ml. Flt-3, SCF and MGDF were added on day 0 to initiate the cultures and IL-6 was added on day 7-10 (Table 1, Table S 1). UCB cultures were grown at 37°C in humidified 5% CO_2 in air. The cells were fed with fresh media every 3 days. For selected $CD34^+$ cells, 50′000–250′000 cells/ml were obtained from 3 UCB units and were cultured in condition D7 as described above.

Culture of UCB-derived MSC during HSC expansion

On day 14, expanded UCB-derived non-adherent cells, referred to as HSC, were removed from the 24-well plates. The remaining

Table 1. Thirty two different culture conditions tested for the expansion of human umbilical cord blood (UCB) derived hematopoietic precursor cells.

Cytokine Cocktail (CC)	Plasma* 2%	Plasma* 8%	Serum* 10%	FCS 10%	Culture Type
CC1	RPMI	RPMI	RPMI	RPMI	A1-A4
CC1	DMEM	DMEM	DMEM	DMEM	A5-A8
CC2	RPMI	RPMI	RPMI	RPMI	B1-B4
CC2	DMEM	DMEM	DMEM •	DMEM	B5-B8
CC3	RPMI	RPMI	RPMI	RPMI	C1-C4
CC3	DMEM	DMEM	DMEM •	DMEM	C5-C8
CC4	RPMI	RPMI	RPMI	RPMI •	D1-D4
CC4	DMEM	DMEM	DMEM ▲	DMEM	D5-D8

*Plasma and serum are derived from human blood group AB. FCS: fetal calf serum.
CC1 = SCF (10 ng/ml) + IL-3 + IL-6 (100 ng/ml) + IL-1β (3 ng/ml) + EPO (1 U/ml), [25].
CC2 = Flt-3 (50 ng/ml) + MGDF (10 ng/ml), [26].
CC3 = Flt-3 (50 ng/ml) + MGDF (10 ng/ml) + IL-6 (10 ng/ml) + SCF (50 ng/ml), [27].
CC4 = Flt-3 (25 ng/ml) + SCF (25 ng/ml) + MGDF (10 ng/ml) + IL-6 (20 ng/ml), modification of [27].
▲D7 (CC4 + DMEM + 10% serum) maintained long-term expansion of UCB HSC over 7 months.
•B7 (CC2 + DMEM + 10% serum), C7 (CC3 + DMEM + 10% serum) and D4 (CC4 + RPMI +10% FCS) maintained short- term expansion for 6 weeks.
doi:10.1371/journal.pone.0015689.t001

adherent cells, referred to as stromal/MSC, were washed with PBS and thereafter either enriched in culture medium containing 10% fetal bovine serum (FBS; Sera Laboratories International, UK) in DMEM (Sigma-Aldrich Company Ltd, UK), supplemented with 2 mmol/l L-glutamine, 50 IU/ml penicillin, 50 µg/ml streptomycin (Gibco BRLR Life Technologies Ltd, UK), 10 ng/ml FGF-β and 20 ng/ml EGF or in MesenCult and added supplements (StemCell Technologies, Europe) in the presence of 5 ng/ml FGF-β (Table 1, Table S1, Fig. S1). The cultures were maintained at 37°C in a humidified atmosphere containing 5% CO_2. The medium was changed twice weekly. When adherent cells increased in number after 2 weeks, they were passaged, counted and transferred to a 25 cm^2 flask for further expansion. The procedure until passage (P) 1 of stromal/MSC takes 28 days.

CFU-F assay

The colony forming unit fibroblast assay (CFU-F) was first performed after the first passage at day 28 and also later during expansion. MSC (10′000/25 cm^2 tissue flask) were either cultured in 10% FBS in DMEM supplemented with 2 mmol/l L-glutamine, 50 IU/ml penicillin, 50 µg/ml streptomycin and 10 ng/ml FGF-β and 20 ng/ml EGF or in MesenCult and added supplements in the presence of 5 ng/ml FGF-β. CFU-F count was determined at day 14 and a coherent group of ≥10 cells was counted as one colony. After P10, CFU-F count was determined at day 8 instead of day 11 to avoid the overlap between colonies due to a rapid increase in cell division.

Differentiation of MSC

Cultured cells were harvested with 0.5% trypsin-EDTA (Invitrogen AG, Switzerland). Cells at passages 4 or 5, or when the expression of the haematopoietic markers CD45, CD34 and CD14 was ≤1.5%, were seeded in 25 cm^2 tissue culture flasks. MSC were stimulated to differentiate into adipocytes (fat), osteoblasts (bone) and hepatocytes (liver) as follows. At 80% confluence, the cells were treated in adipogenic differentiation medium (Stem Cell Technologies, Europe). The medium was changed twice weekly for 3 weeks. For differentiation into osteoblasts, 3×10^4 cells were incubated in MACSR NH OsteoDiff medium, according to the manufacturer's instructions (Miltenyi Biotec, Germany). The medium was changed every 3 days. To induce hepatogenic differentiation, cells were treated at 80% confluence with differentiation medium, containing DMEM supplemented with 20 ng/ml HGF, 0.5 mM dexamethasone, 50 mg/ml ITS premix, 2 mmol/l L-glutamine and 50 IU/ml penicillin and 50 µg/ml streptomycin for 14 days followed by maturation thereafter. Maturation medium contained the same reagents as differentiation medium except HGF, which was replaced with OSM (20 ng/ml) (10). Medium changes were carried out twice weekly and differentiation into hepatogenic, adipogenic and osteogenic cells was assessed by flow cytometry and real-time PCR at day 10 and 21 and by immunohistochemistry at day 28.

Isolation of adipocytes from human fat tissue

One g of tissue (obtained from a healthy volunteer following the approval of the local ethical committee [Beschlussmitteilung der Ethikkommission, UniversitätsSpital Zürich, EK 647]) was cut into small pieces. The tissue was digested in 10 ml Krebs-Ringer phosphate-HEPES buffer containing 4% fatty acid-free BSA and 1 mg/ml of type I collagenase (Worthington). Digestion was performed in a gyratory water bath at 180 rpm for 45–50 min at 37°C. At the end of the incubation, contents of the vial were filtered through a 250 µm nylon filter (Nitex) into a 50 ml polypropylene conical tube. The filter was rinsed with 10 ml Krebs-Ringer phosphate-HEPES buffer containing 1% BSA (KRB 1%). The filtrate was centrifuged at room temperature at 1′000 rpm for 2 min to float the white adipocytes. Adipocytes were transferred into a 50 ml tube and washed by addition of 10 ml KRB 1% BSA followed by centrifugation for 2 min at 1′000 rpm. Fluid and possible erythrocytes in the pellet were aspirated, the same amount of buffer was added and the tube was slightly shaken. Washing was repeated three times and cells were suspended in 1.5 ml.

Phenotypic analysis

(I) Flow cytometry. To phenotypically characterize MSC, cells were surface stained with monoclonal antibodies specific for CD45, CD34, CD14, CD73, CD105, CD44, CD29, CD133, (HLA)-ABC (MHC class I cell surface receptor), HLA-DR (MHC class II cell surface receptor) and Nestin. Additionally, cells were stained intracellularly for cytokeratin18 (CK18), PPARγ and osteopontin (OPN) after fixation and permeabilization (Perm Buffer II, BD Phosflow, Europe), according to the manufacturer's instructions. All stainings were performed at 4°C for 30 min. The following cell lines were used as positive controls for differentiated cells: Huh7 for hepatocytes, CRL-11372 for osteoblasts and human adipose tissue for adipocytes and undifferentiated MSC were used as negative control. All antibodies were obtained from BD Biosciences (Europe) except CD133 (Miltenyi Biotec GmbH, Germany), and PPARγ and OPN (Santa Cruz Biotechnology, Germany). Appropriate isotype-matched, nonreactive fluorochrome-conjugated antibodies were used as controls. Cells were stained and analyzed as described previously [22,23,24] using a FACS Calibur flow cytometer (BD Biosciences) and data were analyzed using CellQuest Pro software.

(II) Real-time PCR. Total RNA was isolated from 2×10^6 MSC-derived cells using RNeasy kit (Qiagen), according to the manufacturer's instructions. The quantity and quality of the RNA was determined spectroscopically using a nanodrop (Thermo Scientific). Purified RNA was DNase treated and subsequently reversely transcribed into cDNA using Quantitect Reverse Transcription Kit (Qiagen) according to the manufacturer's protocol.

For mRNA expression analysis real-time PCR was performed using Fast Start SYBR Green Master Rox (Roche). Primers were custom made by Microsynth (Switzerland). The following primers were used for the evaluation of human cytokeratin 14, cytokeratin 18, albumin, osteopontin, alkaline phosphatase, igfbp2, pparγ2, lpl, nestin, oct3/4, nanog, sox2 and rex1 mRNA expression:

ck14 fwd: 5′-GGG CGG CCT GTC TGT CTC-3′; ck14 rev: 5′-AGG CGG TCA TTG AGG TTC TG-3′; ck18 fwd: 5′-CCC GCT ACG CCC TAC AGA-3′; ck18 rev: 5′-GCG GGT GGT GGT CTT TTG-3′; albumin fwd: 5′-GCT GCC ATG GAG ATC TGC TTG A-3′; albumin rev: 5′- GCA AGT CAG CAG GCA TCT CAT C-3′; osteopontin-fwd: 5′-CTC CAT TGA CTC GAA CGA CTC-3′; osteopontin-rev: 5′-CAG GTC TGC GAA ACT TCT TAG AT-3′, alpl-fwd: 5′-CAC CCA CGT CGA TTG CAT CT-3′; alpl-rev: 5′-TAG CCA CGT TGG TGT TGA GC-3′; pparγ2-fwd: 5′-CCT ATT GAC CCA GAA AGC GAT T-3′; pparγ2-rev: 5′-CAT TAC GGA GAG ATC CAC GGA-3′; igfbp2-fwd: 5′-GAC AAT GGC GAT GAC CAC TCA-3′; igfbp2-rev: 5′-GCT CCT TCA TAC CCG ACT TGA-3′; lpl-fwd: 5′-TCA TTC CCG GAG TAG CAG AGT-3′; lpl-rev: 5′-GGC CAC AAG TTT TGG CAC C-3′; nestin-fwd: 5′-GGC GCA CCT CAA GAT GTC C-3′; nestin-rev: 5′-CTT GGG GTC CTG AAA GCT G-3′, oct3/4-fwd: 5′-CCC TCG TGC AGG CCC GAA AG-3′; oct3/4-rev: 5′-AAG CTG CTG GGC GAT GTG GC-3′; nanog-fwd: 5′-CCT TGG CTG CCG TCT CTG GCT-3′; nanog-rev: 5′-AGC AAA GCC TCC CAA TCC

CAA-3′; sox2-fwd: 5′-AGG GGG AAA GTA GTT TGC TGC CT-3′; sox2-rev: 5′-TGC CGC CGC CGA TGA TTG TT-3′; rex1-fwd: 5′-AGG CCA GTC CAG AAT ACC AG-3′; rex1-rev: 5′-TAG GTA TCC GTC AGG GAA GC-3′.

Real-time PCR was performed on an ABI PRISM 7700 Sequence Detection System (Applied Biosystems). The mRNA expression level for each gene was normalized against 18S rRNA (Applied Biosystems). Data was generated and analyzed using SDS 2.3 and RQ manager 1.2 software.

(III) Immunohistochemistry. Differentiation to adipocytes was recognized by the accumulation of lipid-containing vacuoles stained with Oil red O (Miltenyi Biotec GmbH). Differentiation into osteoblasts is characterized by alkaline phosphatase activity, which was demonstrated using Fast BCIP/NBT as a substrate (Sigma, Europe).

(IV) Immunocytochemistry. Differentiation into hepatocyte-like cells was confirmed by staining for intracellular albumin. For this purpose, cytospin slides were prepared from the MSC cultures, were fixed for 30 min in cold methanol at 4°C and were incubated for one hr with FITC-conjugated polyclonal rabbit antibody against human albumin. Before and after incubation, slides were washed with PBS. Cytospins were prepared from expanded stromal/MSC from one UCB at P7, P13 and P24. These were stained with CD133, Nestin, CD45, and mouse isotype control antibodies at the routine pathology laboratory. In addition, cytospins were prepared from expanded UCB MNC at week 6 in stroma-free liquid culture and from control cells obtained from BD Biosciences Europe, (Cat. No. 340991) and were stained with CD34 monoclonal antibody. Positive staining was demonstrated with peroxidase reaction and the staining was repeated twice.

(V) Transmission electron microscopy. Adherent stromal/MSC cultures were fixed with 3% glutaraldehyde in PBS for 40 min. Subsequently, the culture was washed three times with PBS prior to post fixation with 2% OsO_4 in PBS for 30 min. Cells were rinsed three times with nanopure water and dehydrated in a sequence of increasing ethanol/water mixtures for 30 min each, 70%, 96%, 100% and 100% water-free ethanol (twice). Embedding was carried out with 33% and 50% Epon in ethanol for 2 hrs each, 75% Epon in ethanol over night and 100% Epon for 2 hrs before polymerization at 60°C for 48 hrs. Thin sections were stained with aqueous uranyl acetate 2% and Reynolds lead citrate and imaged in a Phillips CM 12 transmission electron microscope (FEI, Eindhoven, Netherlands) using a Gatan CCD camera (1k×1k) and digital micrograph acquisition software (Gatan GmbH, Munich, Germany).

(VI) Peripheral blood (PB) MNC preparation and stroma-free liquid culture. PB-MNC were obtained from 8 healthy volunteers. The expansion procedure was carried out as described for UCB (see above). Freshly thawed PB-derived MNC were seeded in culture condition D7 at a concentration of 1×10^6/ml. The stromal/adherent cells generated in D7 were either enriched in culture medium containing DMEM, supplemented with 2 mmol/l L-glutamine, 50 IU/ml penicillin, 50 µg/ml streptomycin + different concentrations of FBS (10%, 15% and 20%) or + 10% pooled human AB serum, in the presence of 5 or 10 ng/ml FGF-β and 5, 10 or 20 ng/ml EGF or in MesenCult + supplements ±5 and 10 ng/ml FGF-β. The cultures were maintained at 37°C in a humidified atmosphere containing 5% CO_2.

Results

Generation of UCB-derived MSC during HSC expansion

Unexpectedly, the stroma-free liquid culture, which was initiated to establish culture conditions to expand HSC from freshly thawed MNC, also generated fibroblast-like cells, which we tentatively term UCB-derived MSC (UCB-MSC). Isolation of MSC rested on their classic adhesion on tissue culture plastic. We systematically tested 32 different culture conditions to expand HSC from various independent UCB units. We used various combinations of growth factors, cytokine cocktails [25,26,27], protein sources (FBS, pooled human AB serum or plasma) at different concentrations and basic culture media (Table 1, Fig. S1). Only 4 out of 32 conditions supported the expansion of HSC and 3 of those 4 conditions maintained HSC expansion only temporarily (up to 6 weeks), whereas only condition D7 (Table 1, Fig. 1A) allowed long-term expansion of HSC (Fig S2). To our surprise, condition D7 also allowed another population of adherent fibroblast-like cells to expand at the same time during HSC expansion (Fig. 1B, Table S1, Table S2). We confirmed this for five independent UCB units. Condition D7 consists of DMEM containing Flt-3 ligand, SCF, MGDF, IL-6 and 10% pooled human AB serum. SCF, Flt-3 and MGDF were added on day 0 and IL-6 was added on day 7 or 10.

The total cell count as well as the number of HSC and colony forming cells (CFC) increased in all 3 UCB units tested (Table S2). In addition, after removing non-adherent cells (HSC) during d14 of culture, we reproducibly observed a population of adherent stromal cells, which appeared to fulfill all criteria of MSC as described below (Fig. 1B). Thus, two different stem cell populations, HSC and MSC, can simultaneously expand from UCB in this novel, stroma-free liquid cell culture (D7) (Fig. 1A, 1C).

At day 28 of culture, adherent spindle-shaped cells were further amplified in MesenCult or in DMEM (Fig. 1B). Fourteen days later, we removed expanded HSC and cultured stromal MSC in MesenCult or in DMEM. Another 14 days later, the cultures that were generated from three independent UCB contained 8′000, 10′000 and 7′300 cells, some with MSC morphology. The cells were passaged for the first time (P1) and were transferred to 25 cm^2 flasks for expansion. A steady increase in total MSC counts was observed following repeated passages with a higher expansion capacity when a lower number of MSC were plated (80–400 cells/cm^2). Between P2 and P10, a range of 2.1–800 fold increase in total cell count (mean ± SD: 300±210) was obtained under cultivation with MesenCult, whereas the increase was 6.7–96.4 fold under cultivation with DMEM (51.8±31.4). When seeded at a density of >800 cells/cm^2, cells expanded 8–92 fold in MesenCult and 6.7–70 fold in DMEM (Table S2). We therefore continued to use MesenCult for *in vitro* expansion of UCB-derived MSC (Fig. 1C). Between P11 and P18, the number of the adherent MSC increased 260–1070 fold (617±206.3) and because of the increased growth rate, cells reached confluency of >80% already by 11 days (Fig. 1D). For this reason, we determined the CFU-F count on day 8 instead of the usual day 11.

Furthermore, we validated condition D7 using HSC ($CD34^+$) isolated from 3 independent UCB units. Adherent stromal/MSC were generated in cultures from all selected $CD34^+$ samples. These stromal cells were visible by d7 in culture condition D7 and increased extensively by d14 and were thereafter expanded in MesenCult + supplements +5 ng/ml FGF-β (Figs. 1E and 1F). The expansion protocol proved successful in 8 out of 8 independent UCB units tested.

Electron microscopy of cultured cells showed ultrastructural features of MSC. Mitochondria, vacuoles and filaments were present and Weibel-Palade bodies, which are characteristic for endothelial cells, were absent (Fig. 1G). The morphology of UCB-derived MSC appeared to be similar to that of BM-derived MSC [12].

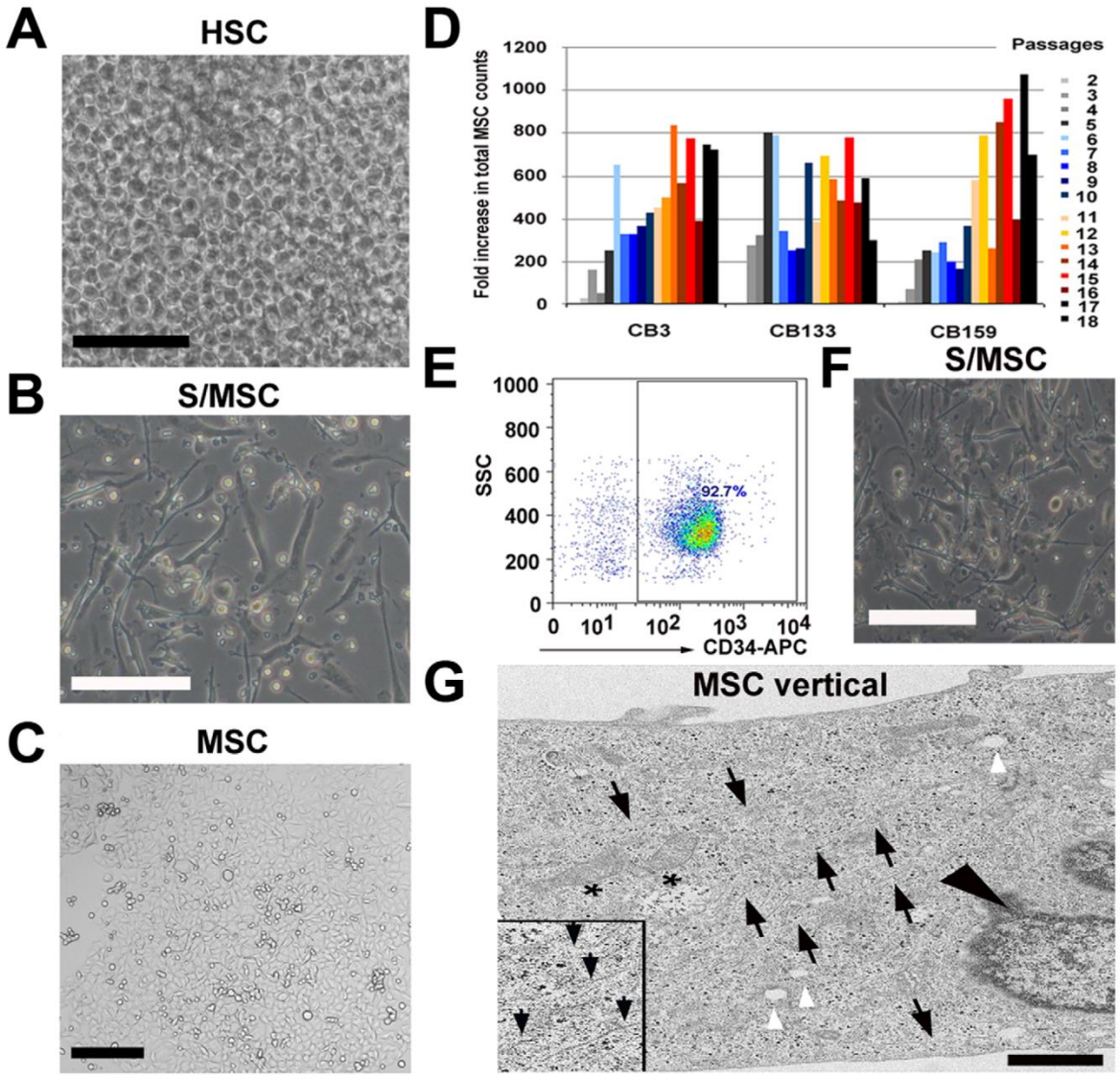

Figure 1. Umbilical cord blood stromal/adherent MSC generated during the expansion of haematopoietic stem cells in stroma-free liquid culture. (A) Confluent growth of HSC from cultured UCB-derived MNC after 14 days expansion under stroma-free culture condition D7. Viable cell count was determined weekly (scale bar: 150 μm). (B) Adherent stromal cells after removal of non-adherent haematopoietic cells and further cultivation in MesenCult with added supplements and 5 ng/ml FGF-β for an additional 14 days (scale bar: 150 μm). (C) Morphology of expanded UCB-derived MSC after 165 days/P11 in culture. After passage 1, cells were transferred from 24-well plate to 25 cm^2 culture flasks and plated at a density of 80–400 cells/cm^2 in MesenCult with added supplements and 5 ng/ml FGF-β. At 80% confluency, the cells were passaged again (scale bar: 100 μm). (D) Total MSC counts of 3 independent human cord blood units (CB3, CB133, CB159) performed from P2 through P18. Different colors depict different passages (2–18). Fold increase was measured by dividing the total MSC count by the starting cell number, which was 10′000 cells/25 cm^2 tissue flask. (E) Percentage $CD34^+$ selected cells using autoMACS $CD34^+$ magnetic beads as determined by flow cytometry. (F) Adherent stromal cells generated from $CD34^+$ selected cells expanded in D7 culture condition for 14 days. Non-adherent haematopoietic cells were removed and adherent cells were cultivated in MesenCult with added supplements and 5 ng/ml FGF-β for an additional 14 days (scale bar: 150 μm). (G) Electron microscopy (EM; vertical section) of a stromal/MSC at 198 days/P14 in culture. White arrowheads point to vacuoles and black arrowhead depicts the nucleus. Asterisks show irregular mitochondria and black arrows point to various filaments (inset, black arrows) characteristic for stromal cells. Black dots within the cytoplasm represent ribosomes (scale bar: 1 μm).
doi:10.1371/journal.pone.0015689.g001

Phenotypic analysis of MSC and formation of CFU-F colonies

We further determined the phenotype of UCB-derived MSC at 80% confluency by flow cytometry analysis. At P3-P4, possible contamination with haematopoietic cells ($CD45^+CD34^+CD14^+$) was no longer detectable by flow cytometry analysis and 10% of all cells expressed the stem-cell marker CD133. More than 95% of UCB-derived MSC expressed typical MSC proteins CD44, CD29,

CD73, CD105 and were also positive for human leukocyte antigen (HLA)-ABC (MHC class I cell surface receptor) but negative for HLA-DR (MHC class II cell surface receptor). This profile remained stable at P4, P7 and P11 (Fig. 2A, B, and C), even as late as passages P13, P18 and P24 (Fig. 2D and E). In addition, the cell population was positive for Nestin (>95%) as determined by flow cytometry analysis (Fig. 2E). The stemness phenotype of UCB stromal/MSC did not change at different confluences [28]. Figure 2D and E display the results of a side-by-side screen of marker profiles of UCB-MSC that were grown in confluent (>95%) vs. sub-confluent (50%) cultures analyzed at passage 24. Immunocytochemistry staining of cytospins prepared from sub-confluent (P7 and P13) and confluent cultures at P24 confirmed the flow cytometry data. Expanded MSC were Nestin positive (range, mean ± SD: 95–98%, 96.3±1.24), $CD133^+$ (6–11%, 9.0±2.16), $CD45^-$ (Fig. 2F) and $mIgG^-$ (data not shown). Stromal/MSC derived from $CD34^+$ selected cells had a similar phenotype; cells were negative for haematopoietic markers and positive for MSC markers (Fig. 2G).

The capacity to form CFU-F colonies is a crucial feature of MSC, and we found that the adherent, MSC-like cells generated large and small CFU-F colonies in MesenCult that was supplemented with 5 ng/ml FGF-β or in DMEM supplemented with 2 mmol/l L-glutamine, 50 IU/ml penicillin, 50 mg/ml streptomycin, 10 ng/ml FGF-β and 20 ng/ml EGF (Fig. 3A). Plating of $1–3\times10^5$ MNC/ml after P1 or during HSC expansion resulted in 19–51 CFU-F colonies (mean: 36) in MesenCult and in 28–142 CFU-F colonies (mean: 79.3) in DMEM. With increasing purity of MSC the number of CFU-F increased: we obtained 50–859 (mean ± SD: 372±212.4) CFU-F from a 10^4 MSC at P2–P10 and 380–788 (mean ± SD: 569 SD ±135) at P11–P18. Also at later passages, we obtained more CFU-F colonies in MesenCult than in DMEM (Table S2). Plating of 50′000–250′000 selected $CD34^+$ cells/ml (mean: 136′700) generated 8–19 CFU-F colonies (mean: 12) during HSC expansion (d28) (Fig. 3B). In addition, secondary colonies were formed when outgrowing cells were harvested and replated following high dilution (<10 cells) at early and late passages, P7 and P24, respectively (Fig. 3C and 3D).

Multilineage differentiation of UCB-derived MSC

To test whether multilineage differentiation of UCB-derived MSC is possible, we induced differentiation of MSC into osteoblast, adipocyte and hepatocytes (Fig. 3E to K, Fig. 4, Fig. S3, Fig. S4,). Differentiation under osteogenic conditions at P4 and P11 resulted in the generation of spindle shaped cells, which progressively flattened and broadened (day 10 of differentiation is shown in Fig. 4A, left panel). High levels of alkaline phosphatase protein (ALPL) expression and increased cell spreading suggested an osteogenic differentiation (Fig. 4B, left panel). Further, analysis by real-time PCR was in line with flow cytometry analysis and immunocytochemical protein expression data (Fig. 4B and D left panel). MSC cultivated under osteogenic stimuli expressed osteopontin (OPN) and ALPL which are characteristic for osteoblasts (Fig. 4C left panel and Fig. S3A). OPN expression was further confirmed by flow cytometry analysis (Fig. 4D, left panel). Undifferentiated MSC were used as a negative control and did not express significant levels of ALPL or OPN. In contrast, the osteoblast cell line CRL-11372 expressed ALPL and OPN (Fig. 4C left panel and Fig. S3A). When MSC were tested for their potential to differentiate into adipocytes at P4 and P11, morphologic changes in the cells as well as the formation of neutral lipid vacuoles were noticeable as early as day 7 after induction (Fig. 4A, right panel). At day 21, a reduction in nuclear size and accumulation of lipid vacuoles within and around the cells was visualized by staining with Oil red O (Fig. 4B, right panel). Real-time PCR to quantify mRNA expression of genes characteristic for adipocytes revealed that differentiated MSC indeed transcribed adipogenic genes such as Igfbp2, LPL, and PPARγ, similar to a positive control (human adipose tissue) (Fig. 4C, right panel and Fig. S3B and C). We confirmed the expression of PPARγ at protein level using flow cytometry (Fig. 4D, right panel). Importantly, undifferentiated MSC expressed low level of Igfbp2 and LPL but did not express PPARγ. These data confirm that UCB-MSC can differentiate into adipocytes. UCB-derived stromal/MSC passaged in sub-confluent and confluent culture maintained their initial marker profile (see above) and their ability to differentiate as well. At P24, UCB-derived stromal/MSC obtained from confluent culture (Fig. 3E) generated after high dilution could be induced towards osteogenic and adipogenic lineages *in vitro* as demonstrated by ALPL expression (Fig. 3F) and accumulation of lipid vacuoles, respectively (Fig. 3I). Further analysis by real-time PCR confirmed osteogenic (Fig. 3G and H) and adipogenic differentiation (Fig. 3J and K).

Expression of pluripotency markers in MSC

We have furthermore analyzed the expression of pluripotency markers (e.g. found in embryonic stem cells) such as Nestin, Oct3/4, Nanog, Rex1 and Sox2 in cultures of MSC (Fig. S5A). Nestin was highly expressed in early MSC cultures and its expression remained at high levels until passage 23. Oct3/4 and Nanog showed an increase in the expression over time in sub-confluent MSC cultures, however in confluent cultures both were weakly expressed through all passages.

Rex1 and Sox2 showed strongly increasing expression levels in sub-confluent cultures between P4 and P14, for confluent cultures a slight increase in gene expression was found between P5 and P23. Altogether, we observed increasing expression levels over time for almost all genes tested with a stronger increase seen in sub-confluent cultures compared to confluent cultures, which appear to reach a steady expression level of pluripotency markers around pP17/18.

In addition, we studied the expression of the osteoblast marker osteopontin (Fig. S5B). We found a strong increase in osteopontin expression in sub-confluent MSC cultures between P4 and P14 and a moderate increase of this marker in confluent cultures over time.

Potential clinical use of UCB-derived MSC

We evaluated the practical implications of the novel methodology developed in the present study. This was conducted in regards to reproducibility, costs, time for generation of MSC, volume of UCB required and the proportion of UCB donations (Fig. S6 and Table S3).

The results show that a small number of MNC or a small volume of UCB can generate an adequate number of stromal/MSC for transplantation of a 70 kg individual ($>100\times10^6$) (Fig. S5, [29]). Importantly, all cytokines needed to expand MSC from UCB and PB with the culture condition D7 are commercially available under "good manufacturing practice" (GMP) grade.

Generation of MSC from peripheral blood

Further, we tested the expansion potential of our novel culture protocol using other sources than UCB. PB MNC were obtained from 8 healthy volunteers. Unlike the expansion of UCB MSC, MSC derived from PB MNC were expanded only when culture condition D7 was replaced gradually at d14 by MesenCult and not by DMEM. A volume of 250 µl out of the total 1 ml volume of culture condition D7 was replaced twice weekly, by addition of

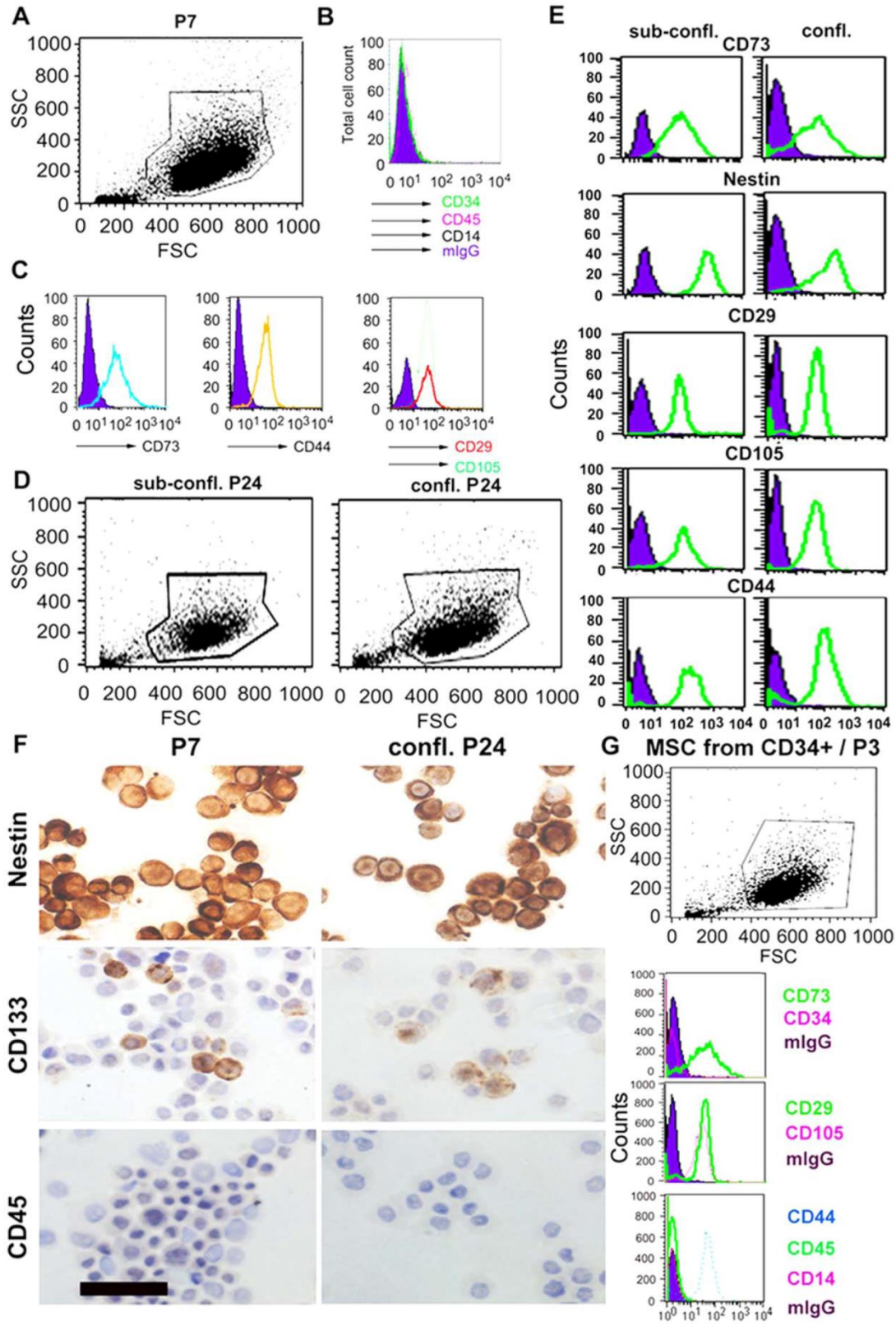
A
P7
SSC
FSC
B
Total cell count
CD34
CD45
CD14
mIgG
C
Counts
CD73
CD44
CD29
CD105
D
sub-confl. P24
confl. P24
SSC
FSC
E
sub-confl.
confl.
CD73
Nestin
CD29
CD105
CD44
Counts
F
P7
confl. P24
Nestin
CD133
CD45
G
MSC from CD34+ / P3
SSC
FSC
CD73
CD34
mIgG
CD29
CD105
mIgG
CD44
CD45
CD14
mIgG
Counts

Figure 2. Phenotype of UCB stromal/MSC during long-term culture as analyzed by flow cytometry and immunocytochemistry. Flow cytometric analysis of UCB-derived stromal/MSC cultivated in MesenCult medium with added supplements and 5 ng/ml FGF-β. (A) FSC/SSC plot of MSC at P7. Gate for live cells is indicated. (B) No expression of the haematopoietic markers CD34, CD45 or CD14 on UCB-derived MSC (open histograms). The filled histogram represents the isotype control. (C) Expression of the stromal/MSC markers CD73, CD44, CD29 and CD105 (open histograms). The filled histograms represent isotype controls. (D) FSC/SSC plot of MSC. Sub-confluent vs confluent cultures at P24. Gates for live cells are indicated. (E) Expression of MSC markers (open histograms) at P24 by cells phenotyped at sub-confluent vs. confluent cultures. The filled histograms represent isotype controls. (F) Immunocytochemistry of stromal/MSC prepared from P7 and from confluent culture at P24. Positive peroxidase staining was seen with Nestin and CD133 but not with CD45. (G) Shows cell scatter and phenotype of stromal/MSC obtained from selected $CD34^+$ cells at P3. Stromal/MSC were positive for CD73, CD29, CD105 and CD44 (open histograms) and negative for haematopoietic cell markers CD34, CD45 and CD14. The filled histograms represent isotype controls.
doi:10.1371/journal.pone.0015689.g002

MesenCult and MesenCult supplements plus 5 ng/ml FGF-β until the first passage at d28. None of the culture conditions tested with either DMEM plus different concentrations of serum and cytokines or MesenCult plus MesenCult supplements alone or with > FGF-β at higher concentration (10 ng/ml) allowed the expansion of MSC derived PB MNC (data not shown). Confluent growth of stromal/MSC bearing MSC immature phenotype and the capacity to form CFU-F colonies were obtained from all PB samples (Fig. 5A, B and C).

Discussion

In recent years, some successful attempts have been made to expand MSC from UCB [4]. However, none of these attempts provided a reproducible protocol to expand MSC, which are rarely found in UCB. In this study, we developed a novel, simple and reliable method which is based on stroma-free liquid culture to expand extensive numbers of multipotent MSC from only a small number of cryopreserved UCB- and PB-derived MNC or $CD34^+$ cells. The stroma-free liquid culture referred to as condition D7 maintained the balance between an extensive expansion of HSC and the simultaneous generation of stromal adherent MSC. Therefore, D7 was adopted to establish MSC in all the cultures obtained from UCB or PB. Maintenance of this balance depended on the presence of serum (10% pooled human AB serum), on the combination and the concentration of cytokines (Flt-3, SCF, MGDF, IL-6), the timing of exposure to those and on the culture medium (DMEM) used. Cultivation of MSC in the presence of cytokines and serum found in D7 and in MesenCult did not affect their stemness. Instead, adherent stromal cells were viable and expanded extensively during d7 to d14 of HSC expansion and continued after in MesenCult. In addition to MSC, growth factors and serum maintained long-term expansion of HSC for several months from fetal liver [24] and cord blood ([27]; Peters et al., 2010, unpublished observations). Similarly, cultures of MSC reported using the classical plastic adherent technique always included either serum [17] or serum plus cytokines (such as FGF-β and FGF-α) [9].

In this regard, it is of interest that the use of commercial serum-free media containing low serum (1%) resulted in fewer numbers of stromal cells and/or rapid differentiation of stem cells with lower numbers of HSC and stromal cells (Peters et al., 2010, unpublished observation). The total cell count increased using other culture conditions that were reported previously [25,26,27], but the maintenance of HSC ($CD34^+$) was only short-term and there was no evidence for concomitant expansion of stromal/MSC. The method developed in the present study to cultivate MNC or $CD34^+$ cells in culture condition D7 in stroma-free liquid culture proved very effective. We confirmed the generation of stromal/MSC in 8 out of 8 independent UCB units, 5 MNC-derived and 3 from selected $CD34^+$ cells (Table S3). Of note, the success rate for isolating stromal/MSC during HSC expansion in D7 was 100%.

It is also possible that MSC are derived from HSC when selected $CD34^+$ cells were cultured in D7. A more homogeneous population of $CD34^+$ cells might be obtained by cell sorting to investigate whether those cells generate $CD34^-$ cells *in vitro* in D7 culture condition. Previously, we have observed the generation of $CD34^-$ cells after 4 to 6 week during long-term culture of fetal liver. Upon flow cytometry analysis these cells appeared as FSC^{low}, $CD34^-$ and $lineage^-$ following the *in vitro* expansion of total cell population (Peters et al., 2010, unpublished observations). Stromal/MSC generated in D7 had a better expansion potential and higher success rate in MesenCult medium (100%) than in DMEM (75%) (Table S3). In MesenCult, expanded cells continued to increase in numbers; showed remarkably little scatter difference in their MSC profiles among samples and among passages; maintained their identity in confluent cultures and their phenotypic profile as well as their differentiation capacity up to the highest passage number we tested in this study, passage 24. In DMEM, the expansion of stromal/MSC after P1 continued in 3 of 4 samples. The expansion potential between P2–P6 was lower in DMEM than MesenCult. After P6, cells increased in size, some detached even when cultures were sub-confluent and cultures needed longer time to reach confluency, >25 days compared to 14 days before P6 (data not shown). In the newly discovered D7 culture condition, a small number of adherent cells, accounting for 5–10% of total expanded cells, were generated every week during UCB expansion. Interestingly, this was also achieved with human PB-derived MNC. Although cultivating PB-derived MNC up to d14 was efficient and reproducible, replacing condition D7 by MesenCult or DMEM for additional 14 days was not. The expansion of stromal adherent cells after d14 decreased and the cultures detached within 48–72 hrs. Unlike UCB, MSC derived from PB MNC were maintained and expanded only when condition D7 was replaced gradually by MesenCult.

It is possible that PB MSC expansion requires the participation of haematopoietic growth factors added as well as the growth factors produced by accompanying haematopoietic cells present in the MNC culture. To maintain their expansion potential PB MNC have to be cultivated in culture condition D7, plus MesenCult and 5 ng/ml FGF-β [30]. In line with these findings, it has been shown that PB-derived MNC and CFU-F differ from BM-derived ones. Both PB-derived MNC as well as PB-derived CFU-F colonies have different growth factors requirements from BM [31,30].

Adherent cells had the characteristics of stromal cells, the capacity to form CFU-F colonies and were capable of growing into a pure population of MSC when expanded under appropriate culture condition (D7). Besides the generation of CFU-F colonies, genuine MSC must be able to differentiate into different mesenchymal (bone, cartilage, tendon, muscle, adipose tissue, stroma) and possibly into non-mesenchymal tissues (neuronal, endothelial and hepatic) [9,10,11] similar to what has been described for MSC from UCB and bone marrow [32,33].

While exogenous IL-6 was not required for initiating UCB cultures, in particular not for MSC culture, in which IL-6 is

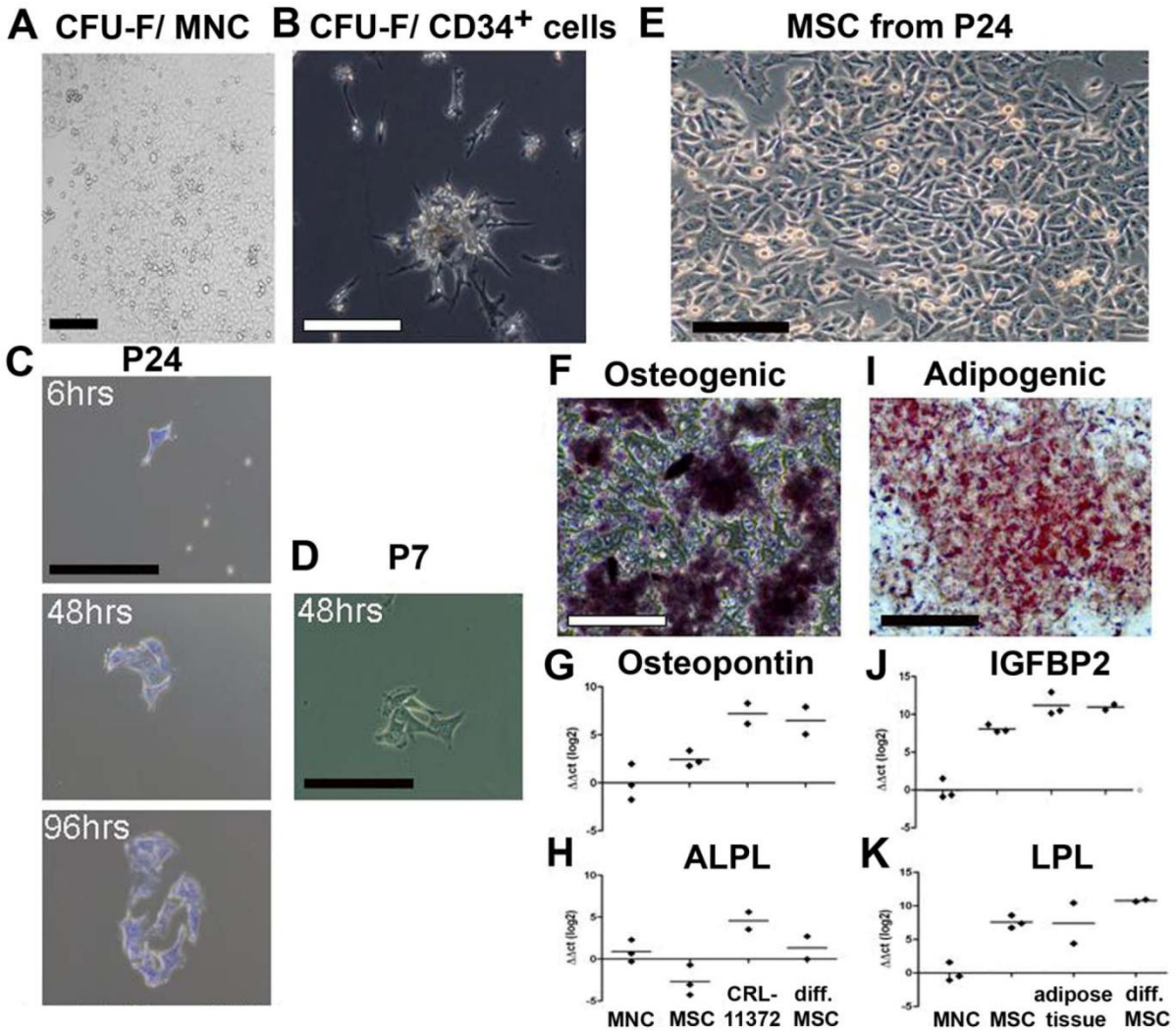

Figure 3. CFU-F colony formation and multilineage differentiation of expanded MSC during long-term culture and following high dilution. (A) Formation of CFU-fibroblast colonies (CFU-F). CFU-F colonies generated from UCB MNC-derived MSC generated large and small CFU-F colonies in MesenCult medium with added supplements and 5 ng/ml FGF-β (scale bar: 150 μm). (B) A CFU-F colony generated from selected $CD34^+$ cells derived MSC (d28) (scale bar: 250 μm). (C) Formation of a CFU-F colony following high dilution of outgrowing colonies obtained from confluent culture at P24. One cell adhered after 6 hrs then a small colony formed after 48 hrs and increased in size at 96 hrs stained with Crystal Violet. (D) A CFU-F colony formed 48 hrs after high dilution of outgrowing colonies from sub-confluent culture at P7. (E) A light microscopy of the confluent culture generated at high dilution of stromal/MSC from P24 (scale bar: 150 μm). (F) Osteogenic differentiation of stromal/MSC generated at high dilution stained with alkaline phosphatase at d10 post differentiation (scale bar: 200 μm). (G–H) Real-time PCR for mRNA expression of tissue-specific genes confirms the osteogenic differentiation of UCB-derived MSC as demonstrated by the expression of osteopontin mRNA (G) and ALPL (H). (I) Adipogenic differentiation of stromal/MSC generated at high dilution following Oil red O staining of lipid vacuoles at d21 post differentiation (scale bar: 200 μm). (J–K) Real-time PCR confirms adipogenic differentiation by the expression of Igfbp2 mRNA (J) and LPL mRNA (K). Human cell line CRL-11372 for osteoblasts and human adipose tissue were used as positive controls. UCB-derived MNC and undifferentiated UCB-derived MSC were used as negative controls. All values were normalized to 18S rRNA. Symbols represent individual samples. Horizontal bars depict the average value. $\Delta\Delta C_t$ values are depicted in a log 2 scale.
doi:10.1371/journal.pone.0015689.g003

secreted by MSC themselves, the addition of IL-6 at 7 to 10 days later was necessary to enhance long-term expansion of both HSC and MSC [34,35,36]. The absence of IL-6 after d7 to d10 during culture in D7 had no short-term effect on HSC expansion but was detrimental for the growth, isolation and expansion of MSC (Peters et al., 2010, unpublished observation). In the presence of IL-6, adherent stromal cells increased and formed a confluent cell layer by d14 (Figs. 1B and 1F). Removal of IL-6 for 24–48 hrs from cultures of cord blood and PB resulted in cell death. Cells detached quickly and MSC isolation and/or expansion were no longer possible.

Consistent with these results, a recent study demonstrated that IL-6 inhibited the expansion of white blood cells, but supported the expansion of $CD34^+$ cells [34]. We observed by flow cytometry

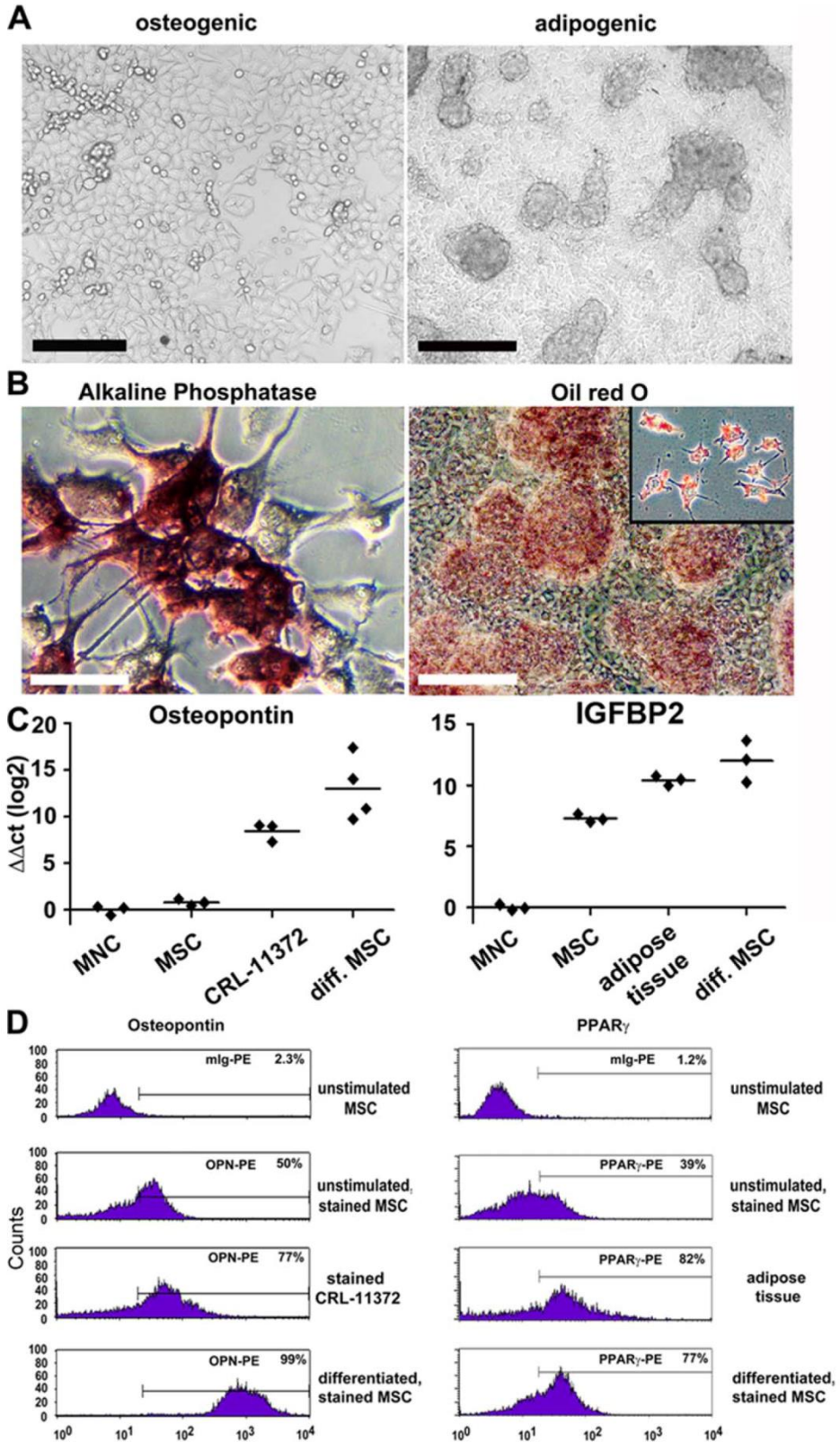
A
osteogenic
adipogenic
B
Alkaline Phosphatase
Oil red O
C
Osteopontin
ΔΔct (log2)
MNC
MSC
CRL-11372
diff. MSC
IGFBP2
MNC
MSC
adipose tissue
diff. MSC
D
Osteopontin
PPARγ
Counts
mIg-PE 2.3%
unstimulated MSC
mIg-PE 1.2%
unstimulated MSC
OPN-PE 50%
unstimulated, stained MSC
PPARγ-PE 39%
unstimulated, stained MSC
OPN-PE 77%
stained CRL-11372
PPARγ-PE 82%
adipose tissue
OPN-PE 99%
differentiated, stained MSC
PPARγ-PE 77%
differentiated, stained MSC

Figure 4. *In vitro* multi-lineage differentiation of UCB-derived MSC into osteoblast- and adipocytes following appropriate induction conditions. (A) Light microscopy of unstained MSC cultures differentiated into osteoblasts (left), adipocytes (right) at 10 and 21 days after differentiation, respectively (scale bar: 200 μm). (B) Osteogenic differentiation was confirmed by alkaline phosphatase activity at d10 post differentiation (left) and adipogenic differentiation by Oil red O staining of lipid vacuoles at d21 post differentiation (right) (scale bar: 200 μm). The inset shows higher magnification of adipocytes stained with Oil red O. (C) Real-time PCR for the mRNA expression of tissue-specific genes confirms the differentiation of UCB-derived MSC. Osteogenic differentiation is demonstrated by the expression of osteopontin mRNA (left) and adipogenic differentiation by the expression of Igfbp2 (right). The osteoblast cell line CRL-11372 and human adipose tissue were used as positive controls. UCB-derived MNC and undifferentiated UCB-derived MSC were used as negative controls. All values were normalized to 18S rRNA. Symbols represent individual samples. Horizontal bars depict the average value. $\Delta\Delta C_t$ values are depicted in a log 2 scale. (D) Flow cytometry confirms the protein expression of tissue-specific genes. Osteogenic differentiation was confirmed by staining at day 10 for osteopontin (left) and adipogenic differentiation by staining at d21 for PPARγ (right). Human cell lines (osteoblast: CRL-11372; hepatocyte: Huh7) and human adipose tissue were used as positive controls. UCB MNC and undifferentiated UCB-derived MSC were used as negative controls.
doi:10.1371/journal.pone.0015689.g004

and immunocytochemistry analyses that cultures from early passages (P3 and P7) and late passages (P11, P13, P18 and P24) expressed the CD133 antigen. CD133 has been found to be restricted to stem cells in normal adult tissues [37] and is expressed by non-committed early progenitors of blood cells and endothelial cells [38], nonmalignant neural progenitors, but also by tumor-initiating stem cells in the brain [39]. Recent studies by Tondreau and colleagues showed that selected $CD133^+$ cells from human PB give rise to MSC [40]. In our report, cells expressing CD133, which constitute approximately 10% of total cells in culture, were most likely responsible for maintaining the integrity of MSC as shown by the Nestin expression which characterizes the undifferentiated stem cells state [41,42], the capacity to form colonies in high dilution and the multi-differentiation capacity towards mesodermal lineages. Similarly, $CD133^+$ cells might have been responsible for generating stromal/MSC in cultures initiated with selected $CD34^+$ cells, in line with published reports where a subpopulation of $CD34^+$ cells was characterized by flow cytometry as $CD34^+/CD133^+$ [41,43,44]. Further studies will have to indicate whether $CD133^+$ cells are the responsible for MSC formation in culture. If this is the case, selection of $CD133^+$ could provide an alternative to MSC selection by adherence to tissue culture plastic.

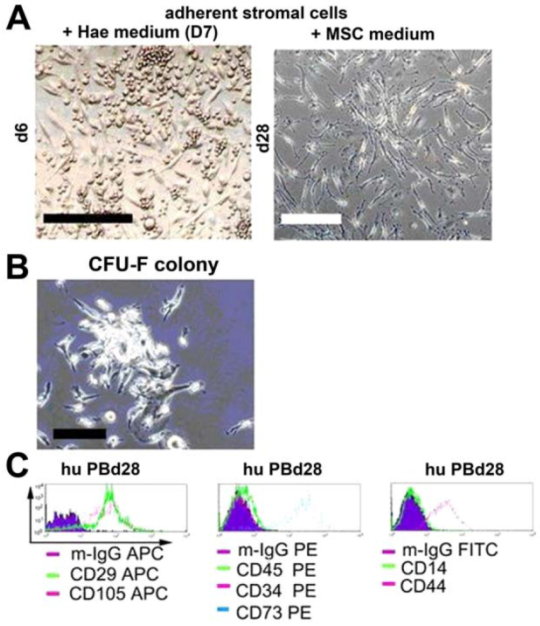

Figure 5. CFU-F colonies of MSC and surface expression of various mesenchymal stem cell markers expressed by MSC generated from steady state PB. Stromal/adherent MSC could be generated from steady state peripheral blood (obtained from 8/8 healthy donors) during the expansion of haematopoietic stem cell in stroma-free liquid culture at day 6 (A, left panel). A confluent growth of stromal adherent cells was obtained at day 28 (A, right panel) (scale bar: 200 μm). (B) A CFU-F colony generated from PB stromal/MSC after P1 (day 28) (scale bar: 100 μm). (C) Flow cytometric analysis of PB-derived stromal/MSC at d28 were positive for stromal/MSC markers CD29, CD105, CD73, CD44 and negative for haematopoietic markers CD45, CD34, CD14. The filled histograms represent isotype controls, respectively.
doi:10.1371/journal.pone.0015689.g005

Furthermore, it is highly unlikely that the herewith accomplished generation of stromal/MSC could be a consequence of a possible contamination with MNC (<8–10%) during the selection procedure of $CD34^+$ cells (see also Table S3): The contaminant MNC population (4′000 to 25′000 MNC) present during the selection of $CD34^+$ cells is very unlikely to form a confluent culture of stromal adherent cells because this number is insufficient to initiate mesenchymal stem cell culture. It was shown previously, that MSC cultures were initiated from 50′000 and $1–3\times10^6$ MNC/ml [11,18] as well was investigated in the herewith presented study: Here we show that at least $1\times10^5–3\times10^5$/ml MNC are required to initiate the stromal adherent cell cultures.

Unlike BM-derived MSC, the growth rate of UCB-derived MSC increased with the time in culture indicating a primitive nature [32,45]. After P11 there was an increase in proliferation rate reaching 205% in total cell count and 153% in CFU-F count. These cells displayed a stable phenotype and retained their potential for differentiation. In the BM, it was reported that senescence of MSC occurred as early as at P11 (47). That was not the case with UCB when MSC were cultured in D7 and thereafter in MesenCult + MesenCult supplements +5 ng/ml FGF-β. The difference is most likely related to the primitive nature of UCB MSC. Alternatively, this might simply be due to the isolation technique which involves the plastic adherence of stromal cells in DMEM + serum. In our hands, senescence of UCB MSC occurred early when MSC were cultured in DMEM + serum ± FGF-β, following 14 days culture in D7.

In the present study, we were able to amplify considerable numbers of multipotent MSC from $1\text{-}3\times10^5$ MNC in 5 out of 5 independent UCB samples during HSC expansion in stroma-free liquid culture. We observed the presence of those adherent stromal cells in additional 15 out of 15 UCB units during HSC expansion cultures, but we did not process those any further. MSC frequency increased during HSC expansion. This indicates that the combination of elements of early growth factors, serum and medium used to promote the expansion of HSC also promoted the expansion of stromal/MSC. In the present study, no direct

comparison was made to evaluate the isolation/cultivation efficiency of UCB MSC under the herewith described culture condition D7 or the classical plastic adherence technique. During the course of establishing MSC from cord blood, we tested 4 independent units of UCB using plastic adherence of MSC. We established adherent MSC only from 1 out of 4 units tested (Peters et al., 2010, unpublished observation), in line with previous reports [3,8,21]. In addition to its efficiency and reproducibility, culture condition D7 has additional advantages compared to the classical plastic adherence method: (*i*) culture condition D7 is quicker in initiating stromal/adherent cells; (*ii*) work with culture condition D7 is less laborious, requires a small number of MNC and is less time consuming; (*iii*) culture condition D7 allows many passages and it initiates rare MSC from all UCB and furthermore, from all PB samples.

UCB MSC expressed the pluripotency markers such as Nestin, Sox2, Rex1, Oct3/4 and Nanog analyzed by real-time PCR in confluent and sub-confluent cultures during early, intermediate and late passages up to P23. Gene up-regulation detected for Nestin, Sox2, and Rex1 was the highest in sub-confluent cultures (P5 to P14). Upregulation of Oct3/4 and Nanog reached the maximum level in sub-confluent cultures by P14 but remained weak throughout late and confluent passages. These results are in agreement with the data presented here demonstrating that UCB derived MSC maintained: a) a stable phenotype, b) multi-differential capacity and c) cell stemness despite differences in cell confluency and culture passages. Similarly, cell confluence did not alter the differentiation potential of the osteopointin gene during long-term culture in sub-confluent vs confluent cultures as determined by real-time PCR analysis.

Recently a growing interest in MSC has evolved due to their ease of culture expansion, immunomodulatory activity and differentiation potential. The clinical spectrum of potential therapeutic application includes many diseases such as steroid refractory graft versus host disease, multiple sclerosis, diabetes mellitus, etc. [46,47]. UCB/MSC have already been used as a potential stem cell therapy in many clinical trials, an ongoing area of development in many clinical and biotechnology institutes worldwide [48,4,49,50,51]. Despite the clinical need for UCB MSC to treat different diseases, no reproducible method for *in vitro* expansion has been published up to date [52]. The methodology presented here provides the means to isolate the very rare population of MSC from blood. Therefore, we recommend the use of this culture strategy to initiate MSC from various tissues starting with D7 culture condition. D7 promotes the expansion of rare stromal adherent cells and potentially facilitate their successful isolation and expansion, e.g. D7 could be used to isolate MSC from other sources such as fetal MSC from maternal blood during normal and abnormal pregnancy.

We evaluated the practical implications of the novel methodology developed in the present study. We show that at P4, $>100\times10^6$ MSC could be generated from only 0.5×10^6 MNC or 23 µl UCB, for transplantation of a 70 kg individual (Fig. S6). The benefits of using this novel technology are (a) to reduce time and costs in preparing MNC, (b) to save a large volume of this valuable source of stem cells (UCB) during MNC preparation and (c) to increase the success rate in generating MSC, which we could show to be 100% in our hands.

We have validated our novel culture protocol using other sources. To our surprise, multipotent MSC were successfully generated from human PB obtained from 8 out of 8 healthy volunteers. This cell population may constitute a unique and sufficiently easy, accessible source of autologous cells with future clinical implications.

Supporting Information

Figure S1 A step by step procedure for the generation of MSC during HSC expansion in stroma-free liquid culture.
(DOC)

Figure S2 Immuno-peroxidase staining of expanded UCB HSC ($CD34^+$) at week 6 during stroma-free liquid culture. (**A**) Control cells obtained from BD Biosciences, show a mixture of stained $CD34^+$ cells (3%) and unstained MNC (97%) (scale bar: 150 µm). (**B**) Expanded MNC showing the increase in $CD34^+$ cell population at week 6 in D7 culture condition (scale bar: 150 µm).
(DOC)

Figure S3 Real-time PCR analysis of MSC differentiated from UBC. mRNA expression analysis of genes characteristic for particular cell types (e.g. osteoblasts, adipocytes and hepatocytes) was performed with UBC-derived MSC differentiated in various culture conditions (e.g. osteogenic, adipogenic, hepatogenic). (**A**) ALPL mRNA expression for osteoblasts, (**B**) LPL and (**C**) PPAR mRNA expression for adipocytes and (**D**) CK14 and (**E**) CK18 for hepatocytes was performed. All values were normalized to 18S rRNA. Symbols represent individual samples. Horizontal bars depict the average value. $\Delta\Delta C_t$ values are shown in a log 2 scale. CRL-11372: Human osteoblast cell line. Huh7: Human hepatoma cell line. Adipose tissue: human adipose tissue.
(DOC)

Figure S4 Differentiation of UCB-derived stromal/MSC into hepatocyte like cells following appropriate induction condition. Under hepatogenic culture conditions, MSC developed the typical cuboidal morphology of hepatocyte-like cells within 14 days and further matured by day 28 in the presence of oncostatin M (**A**). Hepatocyte differentiation was further confirmed by immunofluorescence staining for albumin at day 28 (**B**) and by real-time PCR that revealed expression of hepatocyte-specific genes such as albumin, CK14 and CK18 (**C**, and Supplementary **Fig 3D and E**). Further, the expression of CK18 was confirmed by flow cytometry (**D**).
(DOC)

Figure S5 Expression of pluripotency markers in UCB derived MSC. (**A**) Real-time PCR for the mRNA expression of pluripotency markers confirms the undifferentiated state of MSC in different passages of sub-confluent and confluent cultures. UCB-derived MNC were used as a negative control. All values were normalized to 18S rRNA. Symbols represent individual samples. Horizontal bars depict the average value. $\Delta\Delta C_t$ values are depicted in a log 2 scale. (**B**) Expression of the osteogenic marker osteopontin is found in MSC in different passages of sub-confluent and confluent cultures. UCB-derived MNC were used as a negative control. All values were normalized to 18S rRNA. Symbols represent individual samples. Horizontal bars depict the average value. $\Delta\Delta C_t$ values are depicted in a log 2 scale.
(DOC)

Figure S6 Potential clinical use of UCB-derived stromal/MSC.
(DOC)

Table S1 Appropriate culture conditions for expansion of HSC and MSC.
(DOC)

Table S2 Long-term expansion of MSC from 3 UCB units tested.
(DOC)

Table S3 Percentage success rate obtained for generating stromal/MSC from UCB in D7 culture condition.
(DOC)

Acknowledgments

We acknowledge Prof. Roland Zimmermann, Dr. Konstantin Dedes and Dr. Franziska Krähenmann at the Department of Obstetrics, University Hospital Zürich for providing cord blood samples. Special thanks to Prof. Roger Strair (Department of Haematology, Cancer Institute of New Jersey, Robert Wood Johnson Medical School, University of Medicine and Dentistry, New Jersey) for his input in establishing a culture condition that supports hematopoietic and mesenchymal stem cell expansion. We are very grateful to Prof. Wolfgang Wagner at the Stem Cell Biology and Cellular Engineering, RWTH Aachen Medical School, Germany, for helpful advice and critical reading of the manuscript. We also would like to thank Mrs. Silvia Behnke, Labor für In-Situ-Techniken, Institut für Klinische Pathologie, University Hospital of Zurich for carrying out immunocytochemistry. Our thanks go to Dr. Andres Kaech at the Center for Microscopy and Image Analysis, University Hospital of Zurich for carrying out EM of cultured MSC.

Author Contributions

Conceived and designed the experiments: RP MJW MvdB MN BS AR JRB AA MH AKK. Performed the experiments: RP MJW MvdB MN RR DK. Analyzed the data: RP MJW MN KD AA MH AKK. Contributed reagents/materials/analysis tools: RP MN MH AA AKK. Wrote the paper: RP MJW MvdB MN MH AKK.

References

1. Kulterer B, Friedl G, Jandrositz A, Sanchez-Cabo F, Prokesch A, et al. (2007) Gene expression profiling of human mesenchymal stem cells derived from bone marrow during expansion and osteoblast differentiation. BMC Genomics 8: 70.
2. Bron D, De Bruyn C, Balasse H, Ley P, De Hemptinne D, et al. (2008) [Cord blood: from bench to bedside]. Bull Cancer 95: 314–319.
3. Bieback K, Kern S, Kluter H, Eichler H (2004) Critical parameters for the isolation of mesenchymal stem cells from umbilical cord blood. Stem Cells 22: 625–634.
4. Pozzi S, Lisini D, Podesta M, Bernardo ME, Sessarego N, et al. (2006) Donor multipotent mesenchymal stromal cells may engraft in pediatric patients given either cord blood or bone marrow transplantation. Exp Hematol 34: 934–942.
5. Rocha V, Sanz G, Gluckman E (2004) Umbilical cord blood transplantation. Curr Opin Hematol 11: 375–385.
6. Hough R, Cooper N, Veys P (2009) Allogeneic haemopoietic stem cell transplantation in children: what alternative donor should we choose when no matched sibling is available? Br J Haematol 147: 593–613.
7. Oda M, Isoyama K, Ito E, Inoue M, Tsuchida M, et al. (2009) Survival after cord blood transplantation from unrelated donor as a second hematopoietic stem cell transplantation for recurrent pediatric acute myeloid leukemia. Int J Hematol 89: 374–382.
8. Kern S, Eichler H, Stoeve J, Kluter H, Bieback K (2006) Comparative analysis of mesenchymal stem cells from bone marrow, umbilical cord blood, or adipose tissue. Stem Cells 24: 1294–1301.
9. Schwartz RE, Reyes M, Koodie L, Jiang Y, Blackstad M, et al. (2002) Multipotent adult progenitor cells from bone marrow differentiate into functional hepatocyte-like cells. J Clin Invest 109: 1291–1302.
10. Lee OK, Kuo TK, Chen WM, Lee KD, Hsieh SL, et al. (2004) Isolation of multipotent mesenchymal stem cells from umbilical cord blood. Blood 103: 1669–1675.
11. Wagner W, Wein F, Seckinger A, Frankhauser M, Wirkner U, et al. (2005) Comparative characteristics of mesenchymal stem cells from human bone marrow, adipose tissue, and umbilical cord blood. Exp Hematol 33: 1402–1416.
12. Castro-Malaspina H, Gay RE, Resnick G, Kapoor N, Meyers P, et al. (1980) Characterization of human bone marrow fibroblast colony-forming cells (CFU-F) and their progeny. Blood 56: 289–301.
13. Rojewski M, Weber B, Schrezenmeier H (2008) Phenotypic Characterization of Mesenchymal Stem Cells from Various Tissues. Transfusion Medicine and Hemotherapy 35: 168–184.
14. Hematti P (2008) Role of mesenchymal stromal cells in solid organ transplantation. Transplant Rev (Orlando) 22: 262–273.
15. Valtieri M, Sorrentino A (2008) The mesenchymal stromal cell contribution to homeostasis. J Cell Physiol 217: 296–300.
16. Cho KA, Ju SY, Cho SJ, Jung YJ, Woo SY, et al. (2009) Mesenchymal stem cells showed the highest potential for the regeneration of injured liver tissue compared with other subpopulations of the bone marrow. Cell Biol Int 33: 772–777.
17. Wexler SA, Donaldson C, Denning-Kendall P, Rice C, Bradley B, et al. (2003) Adult bone marrow is a rich source of human mesenchymal 'stem' cells but umbilical cord and mobilized adult blood are not. Br J Haematol 121: 368–374.
18. Perdikogianni C, Dimitriou H, Stiakaki E, Martimianaki G, Kalmanti M (2008) Could cord blood be a source of mesenchymal stromal cells for clinical use? Cytotherapy 10: 452–459.
19. Solves P, Mirabet V, Planelles D, Carbonell-Uberos F, Roig R (2008) Influence of volume reduction and cryopreservation methodologies on quality of thawed umbilical cord blood units for transplantation. Cryobiology 56: 152–158.
20. Stieger B, Peters R, Sidler MA, Meier PJ (2006) Hepatocyte transplantation: potential of hepatocyte progenitor cells and bone marrow derived stem cells. Swiss Med Wkly 136: 552–556.
21. Rebelatto CK, Aguiar AM, Moretao MP, Senegaglia AC, Hansen P, et al. (2008) Dissimilar differentiation of mesenchymal stem cells from bone marrow, umbilical cord blood, and adipose tissue. Exp Biol Med (Maywood) 233: 901–913.
22. Perey L, Peters R, Pampallona S, Schneider P, Gross N, et al. (1998) Extensive phenotypic analysis of CD34 subsets in successive collections of mobilized peripheral blood progenitors. Br J Haematol 103: 618–629.
23. Peters R, Leyvraz S, Perey L (1998) Apoptotic regulation in primitive hematopoietic precursors. Blood 92: 2041–2052.
24. Peters R, Leyvraz S, Faes-Van't Hull E, Jaunin P, Gerber S, et al. (2002) Long-term ex vivo expansion of human fetal liver primitive haematopoietic progenitor cells in stroma-free cultures. Br J Haematol 119: 792–802.
25. Brugger W, Heimfeld S, Berenson RJ, Mertelsmann R, Kanz L (1995) Reconstitution of hematopoiesis after high-dose chemotherapy by autologous progenitor cells generated ex vivo. N Engl J Med 333: 283–287.
26. Piacibello W, Sanavio F, Garetto L, Severino A, Bergandi D, et al. (1997) Extensive amplification and self-renewal of human primitive hematopoietic stem cells from cord blood. Blood 89: 2644–2653.
27. Piacibello W, Sanavio F, Severino A, Dane A, Gammaitoni L, et al. (1999) Engraftment in nonobese diabetic severe combined immunodeficient mice of human CD34(+) cord blood cells after ex vivo expansion: evidence for the amplification and self-renewal of repopulating stem cells. Blood 93: 3736–3749.
28. Semenov OV, Koestenbauer S, Riegel M, Zech N, Zimmermann R, et al. (2010) Multipotent mesenchymal stem cells from human placenta: critical parameters for isolation and maintenance of stemness after isolation. Am J Obstet Gynecol 202: 193 e191–193 e113.
29. Fang B, Song Y, Li N, Li J, Han Q, et al. (2009) Mesenchymal stem cells for the treatment of refractory pure red cell aplasia after major ABO-incompatible hematopoietic stem cell transplantation. Annals of Hematology 88: 261–266.
30. He Q, Wan C, Li G (2007) Concise review: multipotent mesenchymal stromal cells in blood. Stem Cells 25: 69–77.
31. Friedenstein AJ, Latzinik NV, Gorskaya Yu F, Luria EA, Moskvina IL (1992) Bone marrow stromal colony formation requires stimulation by haemopoietic cells. Bone Miner 18: 199–213.
32. Mareschi K, Biasin E, Piacibello W, Aglietta M, Madon E, et al. (2001) Isolation of human mesenchymal stem cells: bone marrow versus umbilical cord blood. Haematologica 86: 1099–1100.
33. Bonab MM, Alimoghaddam K, Talebian F, Ghaffari SH, Ghavamzadeh A, et al. (2006) Aging of mesenchymal stem cell in vitro. BMC Cell Biol 7: 14.
34. Yao CL, Chu IM, Hsieh TB, Hwang SM (2004) A systematic strategy to optimize ex vivo expansion medium for human hematopoietic stem cells derived from umbilical cord blood mononuclear cells. Exp Hematol 32: 720–727.
35. Liu CH, Hwang SM (2005) Cytokine interactions in mesenchymal stem cells from cord blood. Cytokine 32: 270–279.
36. Novotny NM, Markel TA, Crisostomo PR, Meldrum DR (2008) Differential IL-6 and VEGF secretion in adult and neonatal mesenchymal stem cells: role of NFkB. Cytokine 43: 215–219.
37. Florek M, Haase M, Marzesco AM, Freund D, Ehninger G, et al. (2005) Prominin-1/CD133, a neural and hematopoietic stem cell marker, is expressed in adult human differentiated cells and certain types of kidney cancer. Cell Tissue Res 319: 15–26.
38. Loges S, Fehse B, Brockmann MA, Lamszus K, Butzal M, et al. (2004) Identification of the adult human hemangioblast. Stem Cells Dev 13: 229–242.
39. Singh SK, Hawkins C, Clarke ID, Squire JA, Bayani J, et al. (2004) Identification of human brain tumour initiating cells. Nature 432: 396–401.
40. Tondreau T, Meuleman N, Delforge A, Dejeneffe M, Leroy R, et al. (2005) Mesenchymal stem cells derived from CD133-positive cells in mobilized peripheral blood and cord blood: proliferation, Oct4 expression, and plasticity. Stem Cells 23: 1105–1112.
41. Salven P, Mustjoki S, Alitalo R, Alitalo K, Rafii S (2003) VEGFR-3 and CD133 identify a population of CD34+ lymphatic/vascular endothelial precursor cells. Blood 101: 168–172.

42. Poloni A, Rosini V, Mondini E, Maurizi G, Mancini S, et al. (2008) Characterization and expansion of mesenchymal progenitor cells from first-trimester chorionic villi of human placenta. Cytotherapy 10: 690–697.
43. Baal N, Reisinger K, Jahr H, Bohle RM, Liang O, et al. (2004) Expression of transcription factor Oct-4 and other embryonic genes in CD133 positive cells from human umbilical cord blood. Thromb Haemost 92: 767–775.
44. Nguyen VA, Furhapter C, Obexer P, Stossel H, Romani N, et al. (2009) Endothelial cells from cord blood CD133+CD34+ progenitors share phenotypic, functional and gene expression profile similarities with lymphatics. J Cell Mol Med 13: 522–534.
45. Fehrer C, Lepperdinger G (2005) Mesenchymal stem cell aging. Exp Gerontol 40: 926–930.
46. Sensebe L, Krampera M, Schrezenmeier H, Bourin P, Giordano R (2009) Mesenchymal stem cells for clinical application. Vox Sang 98: 93–107.
47. Wagner W, Ho AD, Zenke M (2010) Different facets of aging in human mesenchymal stem cells. Tissue Eng Part B Rev 16: 445–453.
48. Aguayo-Mazzucato C, Bonner-Weir S (2010) Stem cell therapy for type 1 diabetes mellitus. Nat Rev Endocrinol 6: 139–148.
49. Harris DT (2008) Cord blood stem cells: a review of potential neurological applications. Stem Cell Rev 4: 269–274.
50. Macmillan ML, Blazar BR, DeFor TE, Wagner JE (2009) Transplantation of ex-vivo culture-expanded parental haploidentical mesenchymal stem cells to promote engraftment in pediatric recipients of unrelated donor umbilical cord blood: results of a phase I-II clinical trial. Bone Marrow Transplant 43: 447–454.
51. Sueblinvong V, Weiss DJ (2009) Cell therapy approaches for lung diseases: current status. Curr Opin Pharmacol 9: 268–273.
52. Zeddou M, Briquet A, Relic B, Josse C, Malaise MG, et al. (2010) The umbilical cord matrix is a better source of mesenchymal stem cells (MSC) than the umbilical cord blood. Cell Biol Int 34: 693–701.

5.4 MAGE-C1/CT7 spontaneously triggers a $CD4^+$ T cell response in multiple myeloma patients

Manuscript accepted for publication in Leukemia

Authors: Natko Nuber, Alessandra Curioni-Fontecedro, Stefanie Regine Dannenmann, Claudia Matter, Lotta von Boehmer, Djordje Atanackovic, Alexander Knuth and Maries van den Broek

Contributions: SRD provided data for Figure 2.

Leukemia (2013), 1–3

www.nature.com/leu

LETTER TO THE EDITOR

MAGE-C1/CT7 spontaneously triggers a CD4$^+$ T-cell response in multiple myeloma patients

Leukemia advance online publication, 22 February 2013; doi:10.1038/leu.2013.31

Multiple myeloma (MM), a B-cell malignancy with accumulation of clonal, malignant plasma cells in the bone marrow, is the second most common haematological malignancy affecting over 20 000 patients each year in the United States.[1] Although, allogeneic bone marrow transplantation is still performed at the expense of a significant treatment-related toxicity, the graft-versus-myeloma effect has demonstrated that MM cells can be eliminated by effector T cells, and moreover that this results in higher remission rates and even cures.[2] By targeting antigens that are exclusively expressed by MM cells, the efficiency and safety of myeloma-specific immunotherapy can be drastically improved.[3] Among the currently known tumour antigens, cancer-testis (CT) antigens represent one of the most relevant groups for the development of cancer immunotherapy because of their restricted expression in germ line and cancer tissues and their broad immunogenicity.[4] Naturally occurring immune responses against CT antigens, that is,

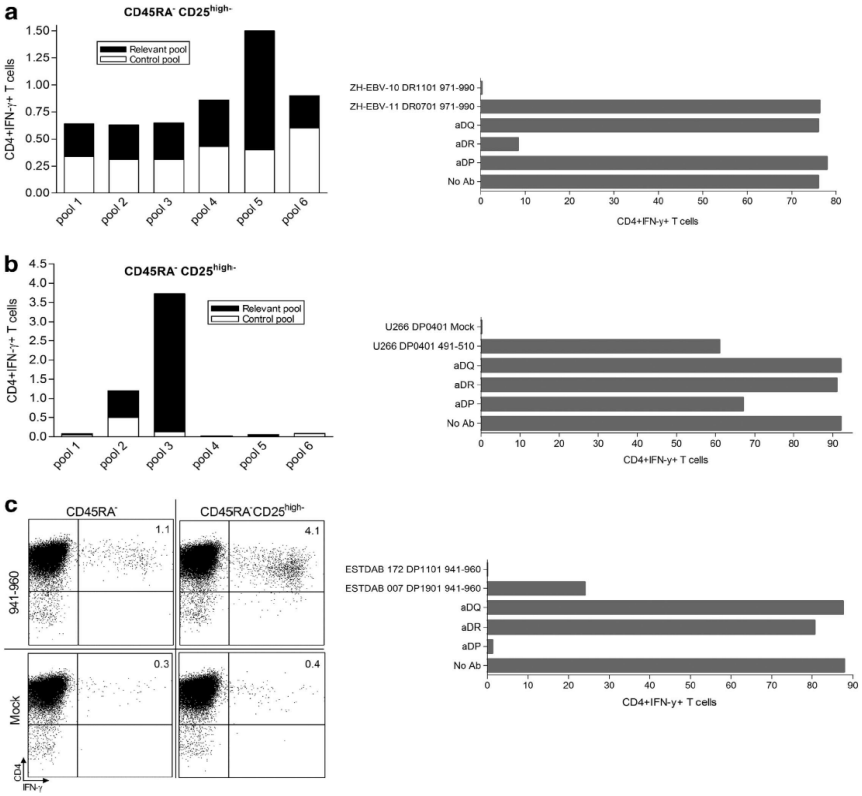

Figure 1. *In vitro* stimulation of sorted CD45RA$^-$CD25$^{high+/-}$ CD4$^+$ T cells and definition of restriction elements. CD4$^+$CD45RA$^-$ and CD4$^+$CD45RA$^-$CD25^{high-} fractions were sequentially sorted out of CD8$^+$ T-cell-depleted peripheral blood mononuclear cells (PBMCs) from three CT7$^+$ MM patients and stimulated with the CD4$^-$CD8$^-$ APC fraction pulsed with either peptide pools (ZH-259; (**a**) left and ZH-590; (**b**) left) or previously identified peptide aa 941–960 for ZH-683 (**c**, left). On days 18–21, cells were harvested and rechallenged using autologous T cell-antigen presenting cells (T-APCs) pulsed with the relevant pool/peptide and a control pool/peptide. Interferon (IFN)-γ was measured in a standard intracellular cytokine stain (ICS) assay. To define restriction elements and minimal epitopes CT7-specific CD4$^+$ T-cell clones were stimulated with the relevant peptide in the presence of blocking antibodies to HLA-DR, HLA-DP or HLA-DQ. Partially matched cell lines pulsed with cognate peptides were used to define the exact restriction allele (**a**–**c**, right). One representative experimental replicate out of three is shown.

Accepted article preview online 1 February 2013

NY-ESO-1 and MAGE-A family of antigens have been previously described in MM patients.[5] These responses were found frequently and often correlated with disease burden.

MAGE-C1/CT7 is the most frequently expressed CT antigen in MM lesions being found in >50% of cases.[6,7] We have described previously that CT7 is able to elicit a specific humoral immune response in a proportion of stages I–III MM patients.[8] Although, the presence of CT7-specific T cells in bone marrow of MM patients has been described, this study did not discriminate between $CD4^+$ and $CD8^+$ T-cell responses, nor did it identify epitopes or exclude the possibility of *in vitro* priming.[9] To assess the presence of a specific memory T-cell response, we analysed naturally occurring CT7-specific $CD4^+$ T cells in peripheral blood mononuclear cell from 18 MM patients with $CT7^+$ bone marrow lesions by *in vitro* stimulation with pools of 20-mer overlapping peptides (10 aa overlap) spanning the entire CT7 sequence. All samples have been taken from patients after they have signed a written consent form according to the Declaration of Helsinki. *In vitro* stimulation assays were performed with fluorescence-activated cell sorted $CD45RA^-$ (memory) $CD4^+$ T-cell fraction from $CD8^+$ T-cell-depleted peripheral blood mononuclear cell to exclude the possibility that the detected $CD4^+$ T cells resulted from *in vitro* primed naive cells. Methods and materials used in this study are analogous to the ones used in our previous study.[10] In addition, to assess whether T regulatory cells (Tregs) preclude the functional detection of CT7-specific $CD4^+$ T-cell responses in MM patients, the $CD45RA^-CD4^+$ T-cell fraction was either depleted of $CD25^{high}$ Treg cells by further sorting or left alone. We detected CT7-specific memory $CD4^+$ T cells in 3 out of 18 MM patients (Figures 1a and b, left panels; patients ZH-259 and ZH-590, respectively). Only one patient (ZH-683; Figure 1c, left panel) showed a detectable CT7-specific $CD4^+$ T-cell response in the presence of Tregs. These results show that Tregs control $CD4^+$ CT7-specific T-cell responses in MM, which is in agreement with our previous findings in melanoma patients.[10] Furthermore, our data suggest that the immunogenicity of tumour-associated antigens may often be underestimated when tested without depleting Treg. Several reports have described a correlation between increased Treg numbers and disease burden in MM patients.[11,12] In addition, a study using mouse models demonstrated that the use of low-dose cyclophosphamide acts by selectively inducing apoptosis of Tregs, which in turn resulted in prolonged disease-free survival of tumour-bearing mice.[13]

From the three patients with CT7-specific T-cell response, we could see that at the time of blood collection, patient ZH-590 had active disease (initial Stage III based on International Staging System (ISS) and III on Durie Salmon staging system (DSS)), patient ZH-259 had a stable disease with partial remission (initial stage I on ISS and III on DSS) and patient ZH-683 had progressive disease (initial stage I on ISS and III on DSS). Previously published report found naturally occurring MAGE-A-specific $CD4^+$ T-cell response predominantly in monoclonal gammopathy of undetermined significance (MGUS) patients.[14] One reason for this discrepancy could be that CT7 is prominently expressed in later stages of MM while MAGE-A is expressed consistently throughout MGUS and MM.[7] The unavailability of peripheral blood samples from MGUS patients precludes any further conclusions.

Single interferon-γ-producing cells were single cell sorted on a FACSAria machine (BD, San Jose, CA, USA) from three CT7-specific $CD4^+$ T-cell cultures (patients ZH-259, ZH-590 and ZH-683; Figures 1a–c left panels) to obtain monoclonal T-cell lines, which enabled the determination of the minimal epitope plus the restriction element. Using blocking monoclonal antibodies, we found that the $CD4^+$ T-cell clone isolated from patient ZH-259 was restricted by human leukocyte antigen (HLA)-DR (Figure 1a right panel), whereas the $CD4^+$ T-cell clones isolated from patients ZH-590 and ZH-683 were restricted by HLA-DP (Figures 1b and c, right panels). HLA-typing for the relevant major

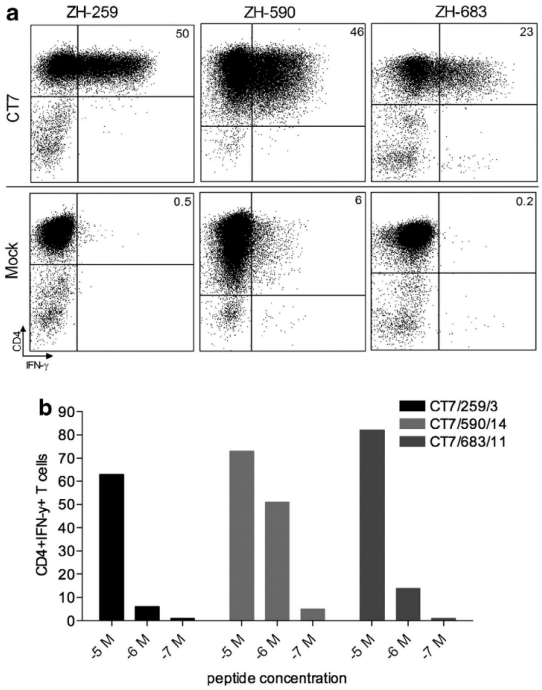

Figure 2. CT7-specific $CD4^+$ T-cell clones recognize naturally processed antigen. CT7-specific $CD4^+$ T-cell clones from ZH-683, ZH-590 and ZH-259 were incubated with autologous mature dendritic cells pulsed with 10 μg/ml recombinant CT7 protein or irrelevant RAB38 protein for 16 h followed by interferon (IFN)-γ ICS. One representative experimental replicate out of two is shown (**a**). Partially matched cell lines, as in Figures 1 (a–c, right), pulsed with titrated amounts cognate peptides were used to measure the exact peptide affinity of CT7-specific CD4 T-cell clones (**b**).

histocompatibility complex class II molecules was performed by single specific primer - PCR (SSP-PCR) with following results: ZH-259: HLA-DRB1*0701/1101; ZH-590: HLA-DPB1*0401/0401; ZH-683: HLA-DPB1*1901/1101. Subsequent experiments using a HLA-DRB1*0701/1101 partially matched B-LCL cell lines pulsed with single 20mer CT7 peptides from the original peptide pool 5 (Figure 1a, left panel) revealed that HLA-DRB1*0701 is the restriction allele and peptide spanning aa 971–990 (DDSYVFVNTLDLTSEGCLSD) to be solely recognized when clone from patient ZH-259 was used (Figure 1a, right panel). $CD4^+$ T-cell clone obtained from patient ZH-590 recognized peptide aa 491–510 (LLSLFQSSPECTQSTFEGFP) in the context of HLA-DP*0401 (Figure 1b, right panel) and clone from ZH-683 recognized peptide aa 941–960 (RYTGYFPVIFRKAREFIEIL) in the context of HLA-DPB1*1901 (Figure 1c, right panel). Two of the above-mentioned epitopes (aa 941–960 and aa 971–990) are located inside the MAGE homology region, one (aa 491–510) is in the region containing repetitive sequences.

To demonstrate that CT7-specific $CD4^+$ T-cell clones recognize naturally processed CT7, we pulsed monocyte-derived mature dendritic cells (DCs) from the same patients with recombinant CT7 protein produced as previously described.[8] All three clones (CT7/259/2; CT7/590/7; CT7/683/9) recognized CT7-pulsed DC, thus demonstrating that the peptides recognized by the $CD4^+$ T-cell clones contain naturally processed epitopes (Figure 2a). Peptide affinity was measured in a classic titration assay demonstrating

that all three clones have a low to intermediate affinity for their respective 20mer peptide (Figure 2b).

High number of overlapping pooled peptides resulting from the large CT7 size (1142 aa) proved to be an inadequate antigen delivery system to analyse CT7-specific $CD8^+$ T cells especially when the patient's material is limited.[10] However, since described CT7-specific $CD4^+$ T-cell responses are clearly of Th1 type it is probable that a Cytotoxic T-Lymphocyte (CTL) response would ensue. Recently, a study identified CT7-specific, HLA-A2 restricted $CD8^+$ T cells, in peripheral blood mononuclear cell from healthy donors. These $CD8^+$ T cells were able to recognize $CT7^+$ MM cell line albeit they have not been confirmed in MM patients.[15] Interestingly, the three patients with CT7-specific $CD4^+$ T-cell response had a, previously described, CT7-specific humoral immune response[8] giving further evidence that there is a broad immune response towards CT7 in MM patients and that CT7-specific $CD4^+$ T cells in MM perform their classical helper role in promoting an anti-tumour immune response.

Taken together these findings show, for the first time, that MM patients develop T-cell immune responses towards CT7, which is the most frequently expressed CT antigen in MM. Therefore, targeting CT7 with simultaneous use of immune suppression antagonists is of great promise for MM immunotherapy.

CONFLICT OF INTEREST

The authors declare no conflict of interest.

ACKNOWLEDGEMENTS

We thank the following associations for support: the Cancer Research Institute/Ludwig Institute for Cancer Research/Cancer Vaccine Collaborative/Atlantic Philanthropies, the Terry Fox Foundation, the Hanne Liebermann Foundation, the Zürcher Krebsliga, and the Hartmann Müller Foundation. We thank JM Tiercy from University Hospital Geneva, Switzerland for kind help with HLA typing.

N Nuber[1,3,4], A Curioni-Fontecedro[1,3], SR Dannenmann[1], C Matter[1], L von Boehmer[2], D Atanackovic[2], A Knuth[1] and M van den Broek[1]

[1]*Department of Oncology, University Hospital Zurich, Zurich, Switzerland and*

[2]*Department of Oncology and Hematology and Department of Stem Cell Transplantation, University Medical Center Hamburg-Eppendorf, Hamburg, Germany*

E-mail: natko.nuber@unibas.ch

[3]*These authors contributed equally to this work.*

[4]*Present address; Department of Biomedicine, University of Basel, Switzerland.*

REFERENCES

1 Jemal A, Siegel R, Ward E, Hao Y, Xu J, Thun MJ. Cancer statistics, 2009. *CA Cancer J Clin* 2009; **59**: 225–249.

2 Lokhorst HM, Wu KL, Verdonck LF, Laterveer LL, Van de Donk NWCJ, van Oers MHJ *et al.* The occurrence of graft-versus-host disease is the major predictive factor for response to donor lymphocyte infusions in multiple myeloma. *Blood* 2004; **103**: 4362–4364.

3 Atanackovic D, Arfsten J, Cao Y, Gnjatic S, Schnieders F, Bartels K *et al.* Cancer-testis antigens are commonly expressed in multiple myeloma and induce systemic immunity following allogeneic stem cell transplantation. *Blood* 2007; **109**: 1103–1112.

4 Caballero OL, Chen YT. Cancer/testis (CT) antigens: potential targets for immunotherapy. *Cancer Sci* 2009; **100**: 2014–2021.

5 Goodyear O, Piper K, Khan N, Starczynski J, Mahendra P, Pratt G *et al.* CD8+ T cells specific for cancer germline gene antigens are found in many patients with multiple myeloma, and their frequency correlates with disease burden. *Blood* 2005; **106**: 4217–4224.

6 Tinguely M, Jenni B, Knights A, Lopes B, Korol D, Rousson V *et al.* MAGE-C1/CT-7 expression in plasma cell myeloma: sub-cellular localization impacts on clinical outcome. *Cancer Sci* 2008; **99**: 720–725.

7 Jungbluth AA, Ely S, DiLiberto M, Niesvizky R, Williamson B, Frosina D *et al.* The cancer-testis antigens CT7 (MAGE-C1) and MAGE-A3/6 are commonly expressed in multiple myeloma and correlate with plasma-cell proliferation. *Blood* 2005; **106**: 167–174.

8 Curioni-Fontecedro A, Knights AJ, Tinguely M, Nuber N, Schneider C, Thomson CW *et al.* MAGE-C1/CT7 is the dominant cancer-testis antigen targeted by humoral immune responses in patients with multiple myeloma. *Leukemia* 2008; **22**: 1646–1648.

9 Lendvai N, Gnjatic S, Ritter E, Mangone M, Austin W, Reyner K *et al.* Cellular immune responses against CT7 (MAGE-C1) and humoral responses against other cancer-testis antigens in multiple myeloma patients. *Cancer Immun* 2010; **10**: 4.

10 Nuber N, Curioni-Fontecedro A, Matter C, Soldini D, Tiercy JM, von Boehmer L *et al.* Fine analysis of spontaneous MAGE-C1/CT7-specific immunity in melanoma patients. *Proc Natl Acad Sci USA* 2010; **107**: 15187–15192.

11 Beyer M, Kochanek M, Giese T, Endl E, Weihrauch MR, Knolle PA *et al. In vivo* peripheral expansion of naive CD4+CD25high FoxP3+ regulatory T cells in patients with multiple myeloma. *Blood* 2006; **107**: 3940–3949.

12 Feyler S, von Lilienfeld-Toal M, Jarmin S, Marles L, Rawstron A, Ashcroft AJ *et al.* CD4(+)CD25(+)FoxP3(+) regulatory T cells are increased whilst CD3(+)CD4(−)CD8(−)alphabetaTCR(+) double negative T cells are decreased in the peripheral blood of patients with multiple myeloma which correlates with disease burden. *Br J Haematol* 2009; **144**: 686–695.

13 Sharabi A, Laronne-Bar-On A, Meshorer A, Haran-Ghera N. Chemoimmunotherapy reduces the progression of multiple myeloma in a mouse model. *Cancer Prev Res (Phila)* 2010; **3**: 1265–1276.

14 Goodyear OC, Pratt G, McLarnon A, Cook M, Piper K, Moss P. Differential pattern of CD4+ and CD8+ T-cell immunity to MAGE-A1/A2/A3 in patients with monoclonal gammopathy of undetermined significance (MGUS) and multiple myeloma. *Blood* 2008; **112**: 3362–3372.

15 Anderson Jr. LD, Cook DR, Yamamoto TN, Berger C, Maloney DG, Riddell SR. Identification of MAGE-C1 (CT-7) epitopes for T-cell therapy of multiple myeloma. *Cancer Immunol Immunother* 2011; **60**: 985–997.

6. ACKNOWLEDGEMENTS

First of all I would like to thank my supervisor Prof. Maries van den Broek for her guidance, help and support during my entire PhD studies, as well as for sharing her valuable knowledge, ideas and skills. I am very thankful to Prof. Alexander Knuth for giving me the opportunity to work in the lab and for his advice.

Furthermore, I am grateful to all my labmembers for the fantastic working atmosphere, as well as for all their help and friendship. Especially I would like to thank Claudia Matter and Alexandro Landshammer for excellent technical support, Virginia Cecconi for assistance in FACS sorting, Ali Bransi for help in preparing the Cylcin D1 manuscript and Lotta von Boehmer for organizing patient information.

I am very thankful to the members of my PhD Committee: Prof. Christoph Renner, Prof. Roland Wenger and Prof. Alfred Zippelius for the supervision and fruitful discussions.

I would like to express my thanks to all our collaborators without their support many aspects of this thesis would not have been possible:

- All the patients, willing to take part in this study
- Thomas Hermanns and Lukas Hefermehl from the department of Urology, USZ, for the recruitment of patients into the study and the organization of blood sampling
- Prof. Holger Moch, Peter Schraml and Martina Storz from the department of Pathology, USZ, for providing me with tumor material
- Prof. Maurizio Provenzano and Giovanni Sais from the department of Urology, USZ, for their advice in planning the qRT-PCR experiments
- Claudia Dumrese of the FACS Core Facility, UZH, for assistance in FACS sorting
- Prof. Stefan Stevanovic from the Department of Immunology, University of Tuebingen, for providing me with different peptides and for the idea of including CCND1 in the qRT-PCR screen
- Prof. Burkhardt Seifert from the Division of Biostatistics, UZH, for advice in statistical analysis

Finally, I would like to thank my parents, sisters, grandparents, friends and Alex for their support, encouragement and patients. Thank you, for letting me know I can always count on you!

7. CURRICULUM VITAE

Personal Information

Name: Stefanie Regine DANNENMANN
Date of birth: 15.01.1982
Nationality: German

Education

09/2007 - 2012 **PhD student**, University Hospital Zurich, Department of Oncology, Laboratory of Tumor Immunology, group Maries van den Broek
Enrolled in the Cancer Research PhD- Program of ETH and University Zurich
PhD thesis: Regulation of tumor-specific immunity in human clear cell renal cell carcinoma

09/2005 - 06/2007: **Graduate studies**, Jacobs University Bremen, Germany
Master of Science in Molecular Biology, June 2007
Master's thesis: Role of cathepsin V in the nucleus of HaCaT keratinocytes

10/2001 - 09/2005: **Undergraduate studies**, University of Applied Sciences Furtwangen, Abteilung Villingen-Schwenningen, Germany
Bachelor of Engineering in Biotechnology, October 2005
Bachelor's thesis: Evaluation of PTD-fusion-proteins for the functional validation of proteins in celllines and platelets

09/1998 - 06/2001: **High School**, Theodor Heuss Gymnasium, Aalen, Germany
Abitur, June 2001

Publications

- **Dannenmann SR**, Bransi A, Matter C, Hermanns T, von Boehmer L, Stevanovic S, Schraml PH, Moch H, Knuth A, van den Broek M, Spontaneous peripheral T cell response towards the tumor-associated antigen Cyclin D1 (CCND1) in patients with clear cell renal cell carcinoma. *Manuscript in preparation*.

- **Dannenmann SR**, Thielicke J, Stöckli M, Matter C, von Boehmer L, Cecconi V, Hermanns T, Hefermehl L, Schraml PH, Moch H, Knuth A, van den Broek M, Tumor-associated macrophages subvert T cell function and correlate with reduced survival in clear cell renal cell carcinoma. *Manuscript accepted for publication in OncoImmunology*.

- Nuber N, Curioni-Fontecedro A, **Dannenmann SR**, Matter C, von Boehmer L, Atanackovic D., Knuth A, van den Broek M, MAGE-C1/CT7 spontaneously triggers a CD4+ T cell response in multiple myeloma patients. *Manuscript accepted for publication in Leukemia.*

- Peters R, Wolf MJ, van den Broek M, Nuvolone M, **Dannenmann S**, Stieger B, Rapold R, Konrad D, Rubin A, Bertino JR, Aguzzi A, Heikenwalder M, Knuth AK, Efficient generation of multipotent mesenchymal stem cells from umbilical cord blood in stroma-free liquid culture. *PLoS One. 2010, 5(12):e15689.*

- Nazor J, **Dannenmann S**, Adjei RO, Fordjour YB, Ghampson IT, Blanusa M, Roccatano D, Schwaneberg U, Laboratory evolution of P450 BM3 for mediated electron transfer yielding an activity-improved and reductase-independent variant. *Protein Eng Des Sel. 2008, 21(1):29-35.*

- Büth H, Luigi Buttigieg P, Ostafe R, Rehders M, **Dannenmann SR**, Schaschke N, Stark HJ, Boukamp P, Brix K, Cathepsin B is essential for regeneration of scratch-wounded normal human epidermal keratinocytes. *Eur J Cell Biol. 2007, 86 (11-12):747-61.*

- Geiger H, Schleimer D, Nattamai KJ, **Dannenmann SR**, Davies SM, Weiss BD, Mutagenic potential of temozolomide in bone marrow cells in vivo. *Blood, 2006, 107 (7): 3010-1.*